SCUOLA DI DOTTORATO
UNIVERSITÀ DEGLI STUDI DI MILANO-BICOCCA

Department of Biotechnology and Bioscience
PhD program in Biology e Biotechnology; Cycle XXXI

Role of Tel1/ATM in protecting abnormal replication forks and signaling short telomeres

Tutor:

Prof. Michela CLERICI

Coordinator:

Prof. Paola BRANDUARDI

PhD thesis of:

Luca
MENIN
Registration number:
737357

Academic year 2017-2018

INDEX

INDEX

ABSTRACT.....6

LIST OF PUBLICATIONS.....10

INTRODUCTION.....12

1 - Genome instability and cancer onset: a tight connection.....13

2 - Cellular response to DNA damage.....15

2.1 - The DNA damage checkpoint.....17

2.1.1 - Tel1-dependent checkpoint activation.....18

2.1.2 - Mec1-dependent checkpoint activation.....20

2.1.3 - Checkpoint mediators and the activation of effector kinases.....22

2.2 - Repair of DNA double-strand breaks.....24

2.2.1 - Non-Homologous End Joining (NHEJ).....24

2.2.2 - Homologous Recombination (HR).....25

2.2.3 - DNA end resection: a crucial step in the HR dependent repair of DSB.....28

3 - Maintenance of replication fork stability upon replication stress.....33

3.1 - The S-phase checkpoint.....33

3.2 - Replication fork reversal in eukaryotes.....37

3.3 - DNA end resection at stalled replication fork.....38

4 - Camptothecin, a DNA Topoisomerase I Inhibitor.....40

4.1 - Repair of Topoisomerase I-mediated DNA Damage.....42

5 - Telomeres and genome stability.....45

5.1 - Telomere structure and telomeric proteins.....46

5.2 - Capping of Chromosome Ends.....48

5.3 - Telomerase and the “End replication problem”.....50

5.4 - Telomere recombination.....53

6 - Replicative senescence and cancer.....54

RESULTS.....58

Tel1/ATM prevents degradation of replication forks that reverse after topoisomerase poisoning.....59

Tel1 specifically supports resistance to camptothecin.....62

Tel1 counteracts the activation of a Mec1-dependent checkpoint in CPT.....67

The lack of Mrc1 suppresses the sensitivity to CPT of *tel1Δ* cells 69

The lack of Mrc1 DNA replication function relieves hypersensitivity and checkpoint hyperactivation of CPT-treated *tel1Δ* cells 71

Tel1 counteracts Mre11-mediated degradation of CPT-induced reversed forks 74

Mrc1-dependent fork reversal triggers fork degradation in CPT-treated *tel1Δ* cells 76

Tel1/ATM contributes to replicative senescence in the absence of telomerase by signaling to the checkpoint 80

tel1Δ and *TEL1-hy184* alleles exert opposite effect on the onset of replicative senescence in telomerase-negative cells 81

Early senescence in *TEL1-hy184* cells is triggered by the activation of a DNA damage checkpoint that depends on Rad9 and only partially on Mec1 85

TEL1-hy184 does not increase ssDNA generation at telomeres 88

Tel1-hy184 binds telomeric DNA ends more robustly than wild type Tel1 93

TEL1-hy184 N-terminal mutations are responsible for early senescence 95

Tel1 kinase activity is required to induce senescence while it is dispensable for telomere processing 98

DISCUSSION 102

MATERIALS AND METHODS 112

Yeast and bacterial strains 113

Yeast strains and plasmids 113

E. coli strain 116

Growth media 116

S. cerevisiae media 116

E. coli media 117

Conservation and storage of *S. cerevisiae* and *E. coli* strains 117

Synchronization of yeast cells 118

Synchronization of yeast cells with α-factor 118

Synchronization of yeast cells with nocodazole 118

Molecular biology techniques 118

Transformation of *E. coli* DH5α cells 118

Transformation of *S. cerevisiae* cells 118

Plasmid DNA extraction from *E. coli*: minipreps with QIAGEN columns 119

Extraction of yeast genomic DNA (Teeny yeast DNA preps) 119
Polymerase Chain Reaction (PCR) 119
Agarose gel electrophoresis 120
DNA extraction from agarose gel (paper strip method) 121
Southern blot analysis of telomere length 121
In-Gel Hybridization for the visualization of G-tail 121
Southern blot analysis of DSB end resection 121
Chromatin ImmunoPrecipitation (ChIP) analysis 122
EM analysis of reversed forks 123
Total protein extracts 124
SDS-PAGE and Western blot analysis 124
Immunoprecipitation and kinase assay 125
Other techniques 125
Senescence assay 125
FACS analysis of DNA content 125
Drop test 126
REFERENCES 128
APPENDIX 148

ABSTRACT

Eukaryotic cells prevent genomic instability, one of the hallmarks of cancer cells, by activating a complex network of safeguard pathways called DNA Damage Response (DDR). This response ensures fast and efficient repair of DNA lesions that can be caused by both exogenous agents and cellular metabolism. *Saccharomyces cerevisiae* Mec1 and Tel1 protein kinases, orthologs of human ATR and ATM, play a central role in the DDR. These proteins recognize DNA lesions and activate a checkpoint cascade which coordinates DNA damage repair with cell cycle progression. Mec1 has a key role in response to all types of DNA damage, since it is activated by the presence of single-stranded DNA (ssDNA). On the contrary, the role of Tel1 is secondary compared to that of Mec1 and particularly evident in the presence of DNA Double-Strand Breaks (DSBs), one of the most cytotoxic forms of DNA lesions. DSBs can be repaired by Homologous Recombination (HR), which requires the degradation of 5'-ended strands of the break (resection) to generate 3'-ssDNA tails, which are needed for the invasion of a homologous DNA molecule and for the subsequent repair. Resection is a two-step process, whose initiation is promoted by the MRX complex (Mre11-Rad50-Xrs2) together with Sae2 protein, while the generation of extended ssDNA requires Exo1 nuclease or the Sgs1 helicase in collaboration with the Dna2 endonuclease. Tel1 contributes to DSB repair by promoting resection initiation together with MRX/Sae2. Despite Tel1 functions in DDR, *tel1Δ* cells do not lose viability after treatment with genotoxic agents like methyl methane sulphonate, hydroxyurea or phleomycin. However, it has recently been observed that the absence of Tel1 confers a moderate but reproducible sensitivity to camptothecin (CPT), an inhibitor of type I DNA topoisomerases. CPT traps yeast Top1 topoisomerase on DNA, thus stabilizing the intermediate Top1-DNA cleavage complex (Top1cc) which is characterized by a DNA Single-Strand Break (SSB). If Top1cc is not promptly removed, its collision with the replication or transcription apparatus can lead to the formation of a DSB. Since CPT derivatives are currently used in chemotherapy and several solid tumors are characterized by alterations in ATM function, understanding the molecular basis of

tel1Δ mutant sensitivity to CPT is relevant for the development of anti-cancer therapies based on combined treatments with CPT derivatives and ATM inhibitors.

In addition, Tel1 is important for the maintenance of telomeres, the nucleoprotein complexes that protect the natural ends of linear chromosomes from fusion and degradation events. Telomeres consist of short and repetitive G-rich sequences added to chromosome ends by a reverse transcriptase called telomerase. Tel1 promotes the recruitment of telomerase and therefore telomere homeostasis. Telomerase is inactivated in most human tissues, which undergo progressive telomere shortening. When telomeres become critically short, a block of cell division, known as replicative senescence, limits cell proliferation, thus acting as a cancer-suppressor mechanism. Senescence is triggered by the accumulation of ssDNA at telomeres and by the activation of a checkpoint response governed by Mec1/ATR and Tel1/ATM. While Mec1/ATR is known to block cell division in the presence of extended ssDNA, the molecular mechanism by which Tel1/ATM triggers senescence is still unclear.

During my PhD I have managed two different projects with the aim to shed light into the molecular mechanisms that involve Tel1 in response to CPT and in the induction of replicative senescence. Regarding the first project, I discovered that the role of Tel1 in response to CPT-induced DNA damage is based on its kinase activity and it is not correlated with the regulation of DNA end resection and DSB repair, which do not require this kinase activity. In both yeast and mammals, CPT induces replication fork reversal, which has been proposed to stabilize stalled replication forks, thus providing time for the repair of CPT-induced lesions and supporting replication restart. *tel1*Δ cells have a reduced amount of CPT-induced reversed forks compared to wild type cells. The lack of Mre11 nuclease activity restores wild-type levels of reversed forks in CPT-treated *tel1Δ* cells, without affecting fork reversal in wild-type cells. Moreover, Mrc1 inactivation prevents fork reversal in wild-type, *tel1Δ*, and *mre11* nuclease-deficient cells and relieves the hypersensitivity of *tel1Δ* cells to CPT. Altogether, these data

indicate that Tel1 stabilizes Mrc1-dependent reversed forks generated in the presence of CPT by counteracting Mre11 nucleolytic activity at these structures.

During the last year of my PhD I have focused my attention on the study of the role of Tel1/ATM in the induction of senescence. For this purpose, I took advantage of telomerase-deficient yeast cells, which are considered a reliable model of replicative senescence, and the *TEL1-hy184* allele, previously identified because it was able to suppress the checkpoint defects of Mec1-deficient cells. Upon telomerase inactivation, Tel1-hy184 accelerates senescence compared to wild type Tel1, while the lack of Tel1 was found to delay senescence. The enhanced senescence in telomerase-negative *TEL1-hy184* cells depends on the activation of a checkpoint that is completely Rad9-dependent and only partially dependent on Mec1. Furthermore, Tel1-hy184 does not appear to increase ssDNA at DNA ends, suggesting that Tel1 induces replicative senescence by directly contributing to checkpoint signaling at dysfunctional telomeres. Taken together, the results that I have obtained during my PhD allow to better understand the functions of Tel1/ATM in the maintenance of genome stability.

LIST OF PUBLICATIONS

1. **Tel1/ATM contributes to replicative senescence in the absence of telomerase by signaling to the checkpoint. MENIN Luca**, MAESTRINI Giorgia, LONGHESE Maria Pia and CLERICI Michela. [IN PREPARATION]

2. **Uncoupling Sae2 functions in downregulation of Tel1 and Rad53 signaling activities.** COLOMBO Chiara Vittoria, **MENIN Luca**, RANIERI Riccardo, CLERICI Michela and LONGHESE Maria Pia [SUBMITTED to Genetics]

3. **Tel1/ATM prevents degradation of replication forks that reverse after topoisomerase poisoning. MENIN Luca**, URSICH Sebastian, TROVESI Camilla, ZELLWEGER Ralph, LOPES Massimo, LONGHESE Maria Pia and CLERICI Michela. EMBO reports. Jul;19(7). 2018 pii: e45535. [DOI: 10.15252/embr.201745535]

4. **Alkaline Denaturing Southern Blot Analysis to Monitor Double-Strand Break Processing.** COLOMBO Chiara Vittoria, **MENIN Luca**, CLERICI Michela. Methods Mol Biol. 2018 1672:131-145. [DOI: 10.1007/978-1-4939-7306-4_11]

5. **The RNA binding protein Npl3 promotes resection of DNA double-strand breaks by regulating the levels of Exo1.** COLOMBO Chiara Vittoria*, TROVESI Camilla*, **MENIN Luca**, LONGHESE Maria Pia, CLERICI Michela. Nucleic Acids Res. 2017 Jun 20;45(11):6530-6545. [DOI: 10.1093/nar/gkx347]

6. **Sae2 Function at DNA Double-Strand Breaks Is Bypassed by Dampening Tel1 or Rad53 Activity.** GOBBINI Elisa*, VILLA Matteo*, GNUGNOLI Marco, **MENIN Luca**, CLERICI Michela, LONGHESE Maria Pia. PLoS Genet. 2015 Nov 19;11(11):e1005685. [DOI: 10.1371/journal.pgen.1005685]

*These two authors contributed equally to the work

INTRODUCTION

1 - Genome instability and cancer onset: a tight connection

The faithful transmission of genetic information from one cell to its daughters is fundamental for the survival of organisms. To achieve such faithful transmission, cells must ensure an accurate DNA replication and subsequent precise chromosome segregation. Errors in these essential processes are lethal for unicellular organisms and may lead to cancer development in multicellular organisms[1]. Cancer is a disease characterized by an abnormal cellular growth. The World Health Organization (WHO) has estimated that, in 2012, cancer was responsible for 8.8 million death worldwide with respect to 14 million new cases, approximately. In addition, it has estimated that in 2010, the economic cost for cancer treatment was around 1.16 trillion dollars[2]. From these data, it comes to light that cancer is both an economical and medical problem whose resolution is far from being found. So, in the last twenty years, cancer has become a central issue for biological, medical and clinical research.

In 2011, Hanahan and Weinberg defined that tumour cells share at least ten common traits that were called "hallmarks of cancer cells"[3] (*Figure 1*). This way to rationalize such a complex disease creates new chances for a combined therapeutic approach that has the objective to interfere with one or more of these features. Among them, genomic instability was defined as an enabling characteristic. In fact, while all the hallmarks are acquired during a multi-step transformation process, genome instability seems to be the engine of tumour progression.

Genome instability is the result of mutational events at different levels, from point mutations to chromosome rearrangements. In most cases, these alterations arise as the consequence of damaged DNA, left unrepaired or repaired in the wrong way. Also dysfunctions at telomere region, the ribonucleoprotein structures that protect the end of linear chromosomes, are an important source of chromosomal instability commonly found in human carcinomas[4] (*see section 5*). Thus, cells need to recognize and repair

DNA alterations in order to survive and transmit a complete and undamaged genome to the offspring. To achieve this accuracy, cells have evolved a complex cellular response, named DNA damage response (DDR), orchestrated by specialized surveillance mechanisms. Loss of function mutations in genes involved in DNA damage response are responsible for hereditary tumours like breast cancer or colon-rectal cancer[5]. In addition, rare monogenic syndrome due to mutations in DDR genes, like Bloom syndrome, Werner syndrome or Ataxia Telangectasia, are characterized by an increased incidence of cancer[5,6]. These observations are consistent with the "mutator hypothesis", which states that mutations in genes of the DDR drive tumour development by increasing the spontaneous mutational rate. So the understanding of the molecular basis of the maintenance of genome integrity is of high importance in term of cancer therapies.

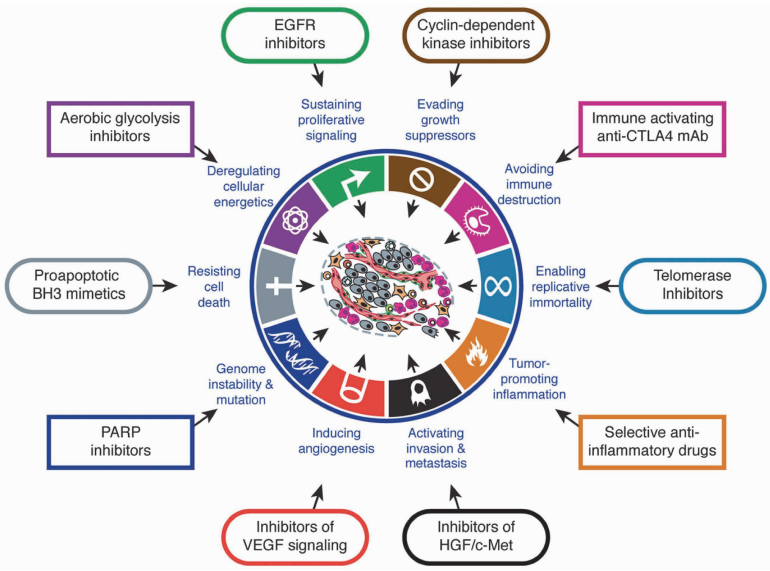

Figure 1 - Representation of the hallmarks of cancer and drugs that interfere with each of the acquired capability (Hanahan and Weinberg 2011).

Nowadays, the best approach against cancer remains chemotherapy and radiotherapy, that have the objective to increase genome instability in dividing cells. Anyway, side effects are the main negative features of these treatments. Recently, the concept of synthetic lethality has exploited to increase cancer therapies efficacy[7]. Genetically, a

synthetic lethal interaction between two genes occurs when the perturbation of either gene alone has no phenotypic effect while the alteration of both genes simultaneously results in loss of viability. In the context of tumour, the synthetic lethality is based on the concept of "oncogene addiction", by which tumours cells rely their viability on a specific pathway. Exploiting this route, different genes have been used as target for synthetic lethal therapies[8]. One of the best result of these studies are the PARP inhibitors that are used to inactivate a specific DNA repair pathway, the Base Excision Repair (BER), in cells that have altered the homologous recombination (HR) repair pathway due to mutations in BRCA1 and/or BRCA2 genes[7,8] associated with breast and ovarian cancer. Alternatively, synthetic lethal approaches, or system based on negative genetic interaction, can be used also to increase the cytotoxicity of existing therapeutic agents[7].

Given the importance of DDR in maintaining genome stability and the correlation of loss of this function with human pathology and cancer, scientists have taken advantage of the extreme conservation of these mechanisms to use model organisms like the budding yeast, *Saccharomyces cerevisiae*[9] to identify the genes and uncover the molecular events at the basis of the DNA damage response in eukaryotes.

2 - Cellular response to DNA damage

DNA is subjected to endogenous and exogenous insults. It has been estimated that human DNA is prone to 10^5 lesions *per* cell *per* day[10]. The heart of the cellular defence against DNA injuries is formed by a variety of DNA repair mechanisms each with their own damage specificity[11]. Together, they are able to remove the majority of injuries from the genome. The simplest solution that emerged in evolution is the direct reversal of lesions by specialized activities, such as photolyases that selectively reverse UV-induced DNA damage[12]. Photolyases are not conserved into the mammalian branch and mammals can rely on a more complex mechanism to remove UV injuries: nucleotide excision repair (NER) which removes a broad spectrum of single-strand lesions that

cause local helix-destabilization[13]. Moreover, bases with small chemical alterations that do not strongly disturb the DNA double-helix structure are substrates for Base Excision Repair (BER) [14]. This damage is targeted by lesion-specific DNA glycosylases that both recognize and remove the damaged base from the sugar-phosphate backbone[14]. The resulting abasic (AP) site is incised by AP-endonucleases and the single nucleotide gap is filled-in by BER-specific DNA polymerase and finally sealed by a specific ligase complex[14].

However, DNA double-strand breaks (DSBs), which occur when the phosphate backbone of two complementary strands is broken simultaneously, are the most dangerous DNA lesion. In fact, failure in repairing them can lead to loss of genetic information, chromosome rearrangements and, as a consequence, genome instability. DSBs can arise from both endogenous and exogenous insults[15–17]. For example, the replication process can induce the formation of DSBs *per se* and in the presence of replication stress (*see section 3*). In principle, each situation that causes the block of the replication fork could give rise to DSBs following the release of the replisome from the DNA (an event also known as replication fork collapse)[15]. Moreover, the interference between transcription and replication machineries represents a major source of endogenous replication stress and collision between the RNA polymerase and the DNA polymerase have been demonstrated to induce ectopic recombination via DSB intermediates[15]. Outside replication stress, some chemical agents like reactive oxygen species (ROS) and other products of cellular metabolism can interact with DNA and create DSBs directly or indirectly. Furthermore, the exposition to other exogenous chemicals, like ionizing radiation or radiomimetic drugs (like bleomycin and phleomycin) can induce DNA breaks directly or indirectly by the formation of clustered nicks, oxidized bases and abasic sites[16].

Interestingly, even if DSBs pose a serious threat to genomic stability, there are physiological processes that need the formation of programmed site-specific DSBs[17]. This is the case of VDJ recombination and class switch in lymphocytes[16,17]. Moreover,

during the meiotic process, self-induced DSBs made by the highly conserved topoisomerase-like protein Spo11, guarantee meiotic recombination[17].

As discussed in the following paragraph, the tight control of DSB metabolism/processing and repair is achieved through a complex and highly conserved DNA damage response (DDR)[18,19] based on a phosphorylation cascade, named DNA damage or DNA replication checkpoint, that halts cell cycle, promotes DNA repair and activates specific transcriptional responses[18].

2.1 - The DNA damage checkpoint

The ability to deal with spontaneous or environmentally induced DNA damage is based on the capability to recognize the presence of an even single lesion inside a million bases length genome. Cells have a sophisticated mechanism called DNA damage checkpoint (DDC)[20] whose activation results in cell-cycle arrest, activation of specific transcriptional programs, support and control of repair processes and, if the damage persists, activation of specific cellular responses that end with the activation of apoptotic or senescence programs[18,20]. In both yeast and mammals, the DNA damage checkpoint activation is dependent on the activity of specific proteins that can be divided in three main classes: sensor, mediators and effectors (*Table 1*). Sensor proteins identify and signal potentially harmful lesions by activating mediator proteins that, in turn, complete the activation of the checkpoint by recruiting and activating effector proteins[18,19].

Saccharomyces cerevisiae	*Schizosaccharomyces pombe*	*Homo sapiens*	Function
Mec1	Rad3	ATR	Checkpoint signaling kinase
Ddc2	Rad26	ATRIP	Mec1/ATR binding partner
Tel1	Tel1	ATM	Checkpoint signaling kinase
Mre11-Rad50-Xrs2	Rad32-Rad50-Nbs1	MRE11-RAD50-NBS1	MRX/MRN complex DSB repair Tel1/ATM activator
Rad53	Cds1	CHK2	Checkpoint effector kinase
Chk1	Chk1	CHK1	Checkpoint effector kinase
Ddc1-Rad17-Mec3	Rad9-Rad1-Hus1	RAD9-RAD1-HUS1	9-1-1 complex Mec1/ATR activator
RFC-Rad24	RFC-Rad17	RFC-RAD17	9-1-1 clamp loader
RFC-Ctf18- Dcc1-Ctf8	RFC-Ctf18- Dcc1-Ctf8	RFC-CTF18-DCC1-CTF8	RFC-Ctf18 complex checkpoint mediator
Dpb11	Rad4	TOPBP1	Replication initiation Mec1/ATR activator
Dna2	Dna2	DNA2	Okazaki fragment processing DSB repair Mec1/ATR activator
Rad9	Crb2	53BP1, BRCA1	Checkpoint mediator Rad53/Dun1 activator
Mrc1	Mrc1	CLASPIN	Checkpoint mediator Rad53 activator
Sgs1	Rqh1	BLM, WRN	Rad53 activator

Table 1 - DNA damage checkpoint factors from yeast to human (Adapted from Pardo et al., 2017).

2.1.1 - Tel1-dependent checkpoint activation

One of the first protein complex recruited to a DNA break is the highly conserved MRX/MRN complex (Mre11-Rad50-Xrs2 in yeast; MRE11-RAD50-NBS1 in mammals)[21]. The Mre11 subunit has, in its N-terminal region, five phosphodiesterase motifs that are essential for its nuclease activities and the Xrs2/NBS1 binding site. In the C-terminal domain, there are two DNA binding sites and the interaction region with Rad50[22]. Mre11 binds preferentially some DNA structures like dsDNA with 3'overhangs, hairpins and Y shaped DNA structures containing both ssDNA and dsDNA[22]. In addition to checkpoint activation, the MRX/MRN complex is implicated in multiple eukaryotic functions, all fundamental for the maintenance of genome integrity and mainly related to the response to DSBs. These functions include: DSB repair, telomere maintenance, meiotic recombination and, during DNA replication, response to stalled replication forks and resolution of DNA hairpins[23–25]. MRX/MRN complex has a wide spectrum of biochemical abilities: DNA binding by multiple subunits and tethering of DNA molecules through interactions between MRX/MRN complexes, incision of the DNA phosphodiester backbone through its single-stranded endonuclease activity and ATP hydrolysis. Thanks to its numerous abilities, the MRX/MRN complex is a key component of the immediate early response to DNA damage, and it is involved in a cross-talk between the repair and the checkpoint machinery[22].

Rad50 is an ATPase belonging to the ABC ATPase superfamily[26]. Its N-terminus and C-terminus contain walker A and walker B motifs that can associate together through the folding of two central coiled-coil domains[26]. The two coiled-coil domains are separated by a "hinge region" that contains a zinc-hook composed by a CXXC motif. One Zn^{2+} atom can be coordinated with the cysteine of two different CXXC motifs. This interaction allows the dimerization between two Rad50 molecules belonging to different MRX complexes[27]. The dimerization of Rad50 is responsible and essential for maintaining two DNA ends tethered.

In both yeast and mammals, Xrs2/NBS1 exerts a regulatory function for the MRX/MRN complex[22]. It physically interacts with Mre11 and is responsible for the correct

localization of the complex in the nucleus[28,29]. In addition, Xrs2/NBS1 stimulates the activity of both Mre11 and Rad50 by promoting the DNA binding activity of the complex and supporting the nuclease activity of Mre11[30,31]. Xrs2 and NBS1 share domains organization[22] with the binding site of Mre11 and the interaction site with Tel1/ATM kinase at the C-terminus. This is particularly important in term of checkpoint activation. In fact, the MRX/MRN complex is required for the complete activation of the checkpoint kinase Tel1/ATM[32].

In yeast, Tel1 is a member of the phosphoinositide 3-kinase-related protein kinase (PIKK) family and its mammalian ortholog is called ATM (Ataxia Telangectasia Mutated)[33]. Loss of function mutations in ATM are related to a rare recessive disease named Ataxia Telangiectasia (AT). Symptoms of the AT are ataxia, impaired body movements and telangiectasia. In addition, AT patients show high risk of developing tumours, like lymphomas and leukemia, and premature aging[34,35]. The PIKK enzymes are large proteins (321 kDa in the case of Tel1) with a characteristic domains organization that presents N-terminal HEAT repeats followed by a C-terminal kinase domain[36] (*Figure 2*). The kinase domain is preceded by the FRAP-ATM-TRRAP (FAT) domain, followed by the PIKK-regulatory domain (PRD) and by the FAT-C-terminal (FATC) domain. All these domains participate together in the regulation of the kinase activity by mediating protein-protein interactions and/or by structural changes[36,37].

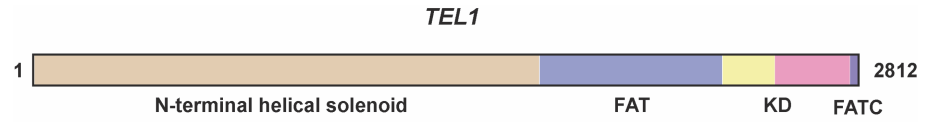

Figure 2 - Schematic representation of the structural organization of the Tel1 Protein.

Tel1/ATM is primarily activated by DSBs and the full activation of ATM depends on phosphorylation events[19,38,39]. ATM is predominantly nuclear and exists as a noncovalent homodimer. A recent structural study conducted on *S. pombe* Tel1 has revealed that, in the homodimer conformation, HEAT N-terminal repeats fold in an helical solenoid that packs against the FAT and kinase domains inhibiting, by steric

hindrance, the binding of substrates and regulators[40]. At least in mammals, following DNA damage, autophosphorylation of ATM on serine 1981 causes the monomerization and the activation of the kinase[41]. Even though the signals that activate ATM are not fully understood, studies in both yeast and mammals have clarified the mechanism of Tel1/ATM recruitment and some aspects of its activation. A central role in Tel1/ATM activation is played by the MRX/MRN complex. One of the strongest evidence comes from the finding that hypomorphic mutations in *MRE11* gene give rise to a very rare syndrome, clinically indistinguishable from AT, called AT-like disorder (ATLD). ATLD cells show a reduced level of ATM activation following DSBs, indicating a relationship between ATM activation and the MRN complex[41]. In the regulation of Tel1/ATM, the MRX/MRN complex plays different roles. First, it is responsible for the correct recruitment of the kinase at the damaged site. This happens through the interaction between Tel1 and the C-terminal region of Xrs2/NBS1[32,42]. In fact, yeast *xrs2-11* mutants, lacking Xrs2 C-terminus, show impaired Tel1 recruitment to DSB[32]. In addition, as ATM exists as an inactive dimer, it has been proposed that the MRN complex stimulates the shift between inactive dimers to active monomers[42]. Studies in yeast have demonstrated that the MRX binding to specific DNA structures (like DNA-protein adducts) formed after genotoxic treatments has a stimulatory effect on Tel1[38]. Moreover, in both yeast and mammals there are evidences that the stimulation of Tel1/ATM activity is independent of the nuclease activity of MRX/MRN[32,38,41].

In summary, once a DSB has been occurred, the MRX/MRN complex binds to the damaged extremity of the broken DNA. Here, MRX/MRN is able to recruit and activate Tel1/ATM by Xrs2/NBS1 interaction. Once activated, Tel1/ATM phosphorylates different substrates in order to support the propagation of checkpoint signal (*Figure 4*).

2.1.2 - Mec1-dependent checkpoint activation

Another player in checkpoint activation in response to DSBs is Mec1/ATR kinase. Together with Tel1, Mec1/ATR belongs to the PIKKs kinase family. Mec1/ATR signals the presence of ssDNA and so it is mainly activated by replication stress, but its

activation can be promoted also by DSBs. In fact, yeast Mec1 can be recruited to an HO-induced DSB, whereas ATR foci can form after IR treatment[43,44]. In both yeast and mammals, recruitment of Mec1/ATR at the DSB sites requires the presence of ssDNA, coated by a highly conserved protein complex named Replication Protein A (RPA). This ssDNA-RPA is usually generated by repair processes, like DNA end resection[45] (*see section 2.2.3*) and Mec1/ATR recognition of ssDNA-RPA depends on Ddc2/ATRIP[45].

Although ssDNA-RPA might be sufficient for Mec1/ATR localization to the site of damage, studies in budding yeast have demonstrated that two other proteins contribute to Mec1 activation: Ddc1 and Dpb11[46]. Ddc1 forms a heterotrimeric complex, together with Mec3 and Rad17. This complex is conserved in vertebrate cells and is named 9-1-1. The Loading of this complex onto DNA at the edge of ss/ds-DNA junctions requires the clamp loader formed by the proteins Rfc2-5 and Rad24. The Ddc1 subunit of the clamp physically interacts with Mec1 and is responsible for its activation[47]. In mammalian cells, another key player in ATR activation is the topoisomerase binding protein 1, TopBP1[48]. TopBP1-mediated activation of ATR is conserved also in *S. cerevisiae.* After the phosphorylation of Ddc1 by Mec1, Ddc1 recruits the TopBP1 ortholog Dpb11 at the site of the lesion[49]. Therefore, these evidences suggest that following a DNA damage, the ssDNA generated by the repair pathways can recruit Mec1-Ddc2 by physical interaction with RPA. The region between ssDNA and dsDNA recruits the 9-1-1 clamp that sustains Mec1 activation through Ddc1. At the same time, phosphorylated Ddc1 recruits Dpb11 that, in turn, can support Mec1 activation (*Figure 4*).

Although Mec1 and Tel1 play some overlapping functions, they do not respond equally to different types of DNA damage and they have not redundant functions. In fact, *TEL1* gene deletion increases the sensitivity of *mec1* mutants to DNA damaging agents[50]. Moreover, high levels of Tel1 can suppress both cell lethality and hypersensitivity to DNA damaging agents of *mec1Δ* strains, indicating that an excess of Tel1 can bypass both the essential and the DNA damage response function of Mec1[51].

2.1.3 - Checkpoint mediators and the activation of effector kinases

The DNA damage checkpoint cascade leads to the activation of the two evolutionary conserved effector serine threonine kinases Rad53/CHK2 and Chk1/CHK1 which undergo phosphorylation in response to DNA damage in a Mec1/ATR- and Tel1/ATM-dependent manner[51,52] (*Figure 4*). In yeast, the principal effector kinase is Rad53[18,53] which belongs to the Chk2 family of ser/thr kinases. Structurally, at the N-terminus Chk2-like kinases show an SQ/TQ cluster domain (SCD) which is composed by a series of serine or threonine residues followed by glutamine that is the consensus sequence for Tel1/ATM and Mec1/ATR kinases. Following the SCD domain, the forkhead-associated domain (FHA) is responsible for protein-protein interactions binding phospho-threonine residues. In *S. cerevisiae*, while Chk1 is required only for the DNA damage G_2/M checkpoint, Rad53 is essential for the proper response to DNA damage in all cell cycle phases and to replication blocks[54,55]. On the contrary, in human cells CHK1 appears to be the principal effector for the DNA replication checkpoint, while CHK2 is mainly involved in the response to DSBs[56,57]. The divergent specialization of these proteins in different eukaryotic systems may depend on the presence of DNA damage-specific or S-phase-specific mediators, Rad9 and Mrc1, which link the DNA damage-sensing functions with the downstream effectors allowing their phosphorylation. Both adaptors can recruit the checkpoint kinase Rad53, via their FHA domains, to trigger its activation. Rad9 and Mrc1 have partially redundant roles and simultaneous deletion of both *RAD9* and *MRC1* gene phenocopies a *rad53* mutant[58].

The principal *S. cerevisiae* mediator in response to DNA damage, is Rad9 that acts as a scaffold protein and promotes Mec1-Rad53 interaction and Mec1-mediated Rad53 phosphorylation[59,60]. In particular, once Mec1 and Tel1 become activated by DNA damage, they phosphorylate Rad9 in its SCD domain[59]. This event creates a docking site for the FHA domains of Rad53 recruiting the kinase in close proximity to Mec1 and Tel1. The Rad9-mediated recruitment has two important effects on Rad53 activation. First, it allows Mec1 and Tel1 to phosphorylate Rad53 in its SCD domain, activating the

kinase. Second, it recruits other Rad53 molecules by either Rad9 interaction or Rad53 interaction. This increase in Rad53 local concentration promotes Rad53 autophosphorylation *in trans*. Once hyperphosphorylated (at more than twenty residues), Rad53 is fully active and is released from Rad9 in an ATP dependent manner[61]. Rad9 also contributes to Chk1 activation with a mechanism involving its N-terminal portion, which is not required for Rad53 activation[62]. So, phosphorylation of Rad53 kinase by Mec1 and Tel1 leads to its activation and subsequent autophosphorylation. The resulting hyperphosphorylated Rad53 is frequently used as an experimental marker for monitoring the DNA damage response activation.

Rad9 counterpart in response to replication stress is Mrc1 (Mediator of replication checkpoint protein 1), which has two function in S-phase: activates the S-phase checkpoint (*see section 3.1*) and also actively promotes DNA replication[58,63–65]. Mrc1 (ortholog of vertebrate Claspin) interacts with Tof1 (ortholog of vertebrate Timeless) and Csm3 (ortholog of vertebrate Tipin) and associates with chromatin during S-phase. Mrc1-Tof1-Csm3 complex localize to replication forks[65,66] and during normal S-phase Mrc1 promotes efficient replication coupling the helicase and the polymerase activity of the replisome[67,68]. Upon encountering a replication block, Mrc1 and Tof1 promote the formation of a stable pausing complex at the stalled fork. Deletion of either *MRC1* or *TOF1* gene is sufficient to uncouple the replisome from the replication fork in the presence of damage[64]. Mrc1 associates with several replication proteins including Cdc45[64], the minichromosome maintenance protein helicase complex (MCM)[66], and the GINS complex[69,70]. Mrc1 also interacts with DNA polymerase epsilon (Polε)[71], which itself has been implicated in DNA replication stress signaling[72]. Mrc1 is phosphorylated in a Mec1- and Rad53-dependent manner[58] and contains multiple SQ/TQ sites. Mutation of all 17 SQ/TQ sites of Mrc1 (*mrc1^{AQ}* mutant) successfully abrogates only the checkpoint function of Mrc1. This means that the role of Mrc1 in mediating the checkpoint replication stress response is separable from its role in DNA replication[65]. Moreover, the SQ/TQ residues of Mrc1 are essential for its role in the replication

checkpoint but not in DNA replication itself, strengthening the idea that Mrc1 activates Rad53 in a fashion similar to that of other mediator proteins[65].

Once activated, both Chk1/CHK1 and Rad53/CHK2 can phosphorylate different substrates activating different cellular responses in both yeast and mammal. One of the most important events following checkpoint activation is the block of the cell cycle. This avoids that cells divide with damaged DNA or in the presence of unreplicated DNA. In this context, cell cycle can be blocked at G_1/S transition or at G_2/M transition. Moreover, the effector proteins can promote other important cellular responses like the activation of specific repair pathways, the induction of apoptosis or senescence (*see section 6*) and the stimulation of specific transcriptional responses[73–75].

2.2 - Repair of DNA double-strand breaks

As anticipated, DSBs are the most cytotoxic lesion that living cells must face. Defects or failures in repairing this type of lesions result in detrimental chromosome rearrangements that can increase genome instability. Eukaryotic cells repair DBSs mainly by two highly conserved mechanisms: Non-Homologous End Joining (NHEJ) and Homologous Recombination (HR). These two pathways are mutual exclusive. In fact, when a DSB is channelled towards the HR pathway, NHEJ is completely inhibited. The interplay between HR and NHEJ is influenced by the cell cycle stage at which the damage has occurred and more and more molecular details are emerging about this regulation[76,77].

2.2.1 - Non-Homologous End Joining (NHEJ)

The repair of DSBs by the NHEJ consists in the re-joining of the two broken DNA ends. Mechanistically, the process can be divided in three key steps: binding of specific factors to DNA ends, processing of broken strands and relegation.

In both yeast and mammals, the main DNA binding factor is the highly conserved Ku complex, a heterodimer composed by Ku70 and Ku80 proteins[78–80] which has a sequence independent high affinity for DNA ends[80]. Yeast cells deleted for Ku70 or Ku80

are completely defective in NHEJ even if they do not show any obvious sensitivity to genotoxic agents. In order to re-join two DNA ends, the extremities of the break have to be held in close proximity by the MRX complex and in particular by two Rad50 molecules[78,79]. Most of DSBs have incompatible DNA ends, like DNA-protein adducts or mismatching overhangs, that preclude direct ligation. In these cases, the two DNA ends cannot be simply re-joined together but need to be firstly processed to became compatible. Different proteins take part in this process and in yeast, the most characterized NHEJ endonuclease is Rad27 (ortholog of human FEN1). Importantly, the activities of these proteins at DNA termini lead to the loss of DNA tracts. This is a key concept in NHEJ mediated repair. In fact, since no homology directed repair steps is envisaged, this processing of DNA ends results in different modifications of the initial sequence. Thus, the NHEJ mechanism is a mutagenic repair process. At the end, once the DNA ends have been processed, in yeast the ligation is carried out by the DNA ligase IV together with Lif1 which is recruited at DSBs by a direct interaction with the Xrs2 subunit of the MRX complex.

2.2.2 - Homologous Recombination (HR)

The Homologous Recombination process could be defined as the repair of a DSB using homologous sequences. Depending on which kind of homologous sequence is used as template, the HR process can lead to different genetic consequences. For example, if sister chromatids are used for repair, this results in sister chromatid exchange that is the more precise way to repair DSBs. Furthermore, the use of homologous chromosome for HR may result in the loss of heterozygosity (LHO). In addition, if the recombination occurs between ectopic positions the HR process leads to deletions, duplications, inversion and translocations. All these events are associated with cancer. For these reasons, HR can be seen as a two-side coin: on one hand, it is an error free process for the repair of DSBs because it uses the information on a homologous donor. On the other, if not controlled, it can generate genetic alterations that are associated with genetic instability.

Currently, different models of HR have been described: the double-strand break repair model (DSBR), the synthesis-dependent strand annealing (SDSA) and the break induce replication (BIR) (*Figure 3*)[81]. These three models differ each other for the repair outcomes but share some key steps: i) nucleolytic processing of the extremity of the DSB to obtain ssDNA (DNA end resection); ii) formation of a recombinase ssDNA filament; iii) strand invasion and/or Holliday junction(s) creation; iv) DNA synthesis. v) resolution of the Holliday junction(s) and completion of the repair process.

Once a DSB is created, in order to be channelled toward the HR repair pathway, the DNA ends are subjected to a complex processing that has the goal to create ssDNA. This processing is known as DNA end resection and the molecular details will be described in section 2.2.3. The resulting ssDNA can be highly unstable and subjected to degradation. For this reason, in both yeast and mammals, the ssDNA created during resection is rapidly coated by the RPA complex[81,82]. Nevertheless, the so formed RPA-ssDNA is not able to invade the intact donor DNA. In fact, the strand-invasion reaction is catalysed by the Rad51 recombinase. Rad51 assembles on ssDNA to form a right-handed helical polymer, the pre-synaptic Rad51 filament, that can span thousands of base pairs. Anyway, Rad51 is not able to displace RPA from ssDNA because of the higher affinity for ssDNA and the higher concentration of the RPA complex respect to the one of Rad51[83]. For this reason, in both yeast and mammals, the exchange between RPA and Rad51 requires other proteins known as mediators. Whereas the most important mediator in yeast is Rad52[81,84], in mammals is BRCA2 and its loss of function mutations are associated with ovarian and breast cancer[85]. Once the pre-synaptic Rad51 filament has been assembled, the invasion of the intact DNA molecule occurs. From studies conducted in *E. coli*, it is plausible that the homology search process occurs by random collisions between the Rad51 filament and the donor DNA; although this process is likely more complex in mammalian cells. Once the interaction is stable, there is the formation of the synaptic complex. The Rad51-filament invasion induces the displacement of the same-polarity strand. This event creates a structure, known as D-

loop, that is extremely important for DNA synthesis. At this point, different ways to conclude the HR repair exist (*Figure 3*). The first model proposed was the double-strand break repair model (DSBR), in which the D-loop anneals with the other 3'-OH strand on the damaged molecule that was not engaged by the strand invasion process. This primes a second round of DNA replication and results in the formation of four-way DNA intermediates known as Holliday junctions (HJs). In order to complete the repair process, different nucleases and helicases have been implicated in the HJs resolution. HJs can be resolved by the action of two protein complexes: the yeast Mus81-Mms4 and Slx1-Slx4 complexes, orthologs of the human SLX1-SLX4-MUS81-EME1 complex, and the STR complex composed by Sgs1, TopIII and Rmi1 and their human orthologs BLM, TOP3α and RMI1/2[86,87]. In the first case, HJs are resolved by an endonucleolytic cleavage. This way of resolution induces the formation of both crossover (CO) and non-crossover products (NCO). In the second case, the concerted work of the Sgs1/BLM helicase and topoisomerase activity of Top1III/TOP3α generates only non-crossover products.

The Synthesis Dependent Strand Annealing (SDSA) model of HR was generated in order to justify the higher number of NCO products against the CO events. The SDSA model proposes that the 3'-OH strand invades the homologous donor forming the D-loop that, after limited DNA synthesis is displaced. If DNA synthesis has elongated enough the invading strand to allow the re-annealing with the damaged molecule, the repair process is concluded by fill-in synthesis and ligation. Consequently, only NCO products are generated.

The last model of Homologous Recombination repair is the break induced replication (BIR). BIR is a recombination-dependent replication process that results in nonreciprocal transfer of DNA from the donor to the recipient chromosome. During BIR only a single strand of one DSB end invades the homologous duplex and starts replication. This induces the migration of the D-loop. As far as the replication continues,

using donor as template, the invading strand serves as template for the lagging-strand replication process.

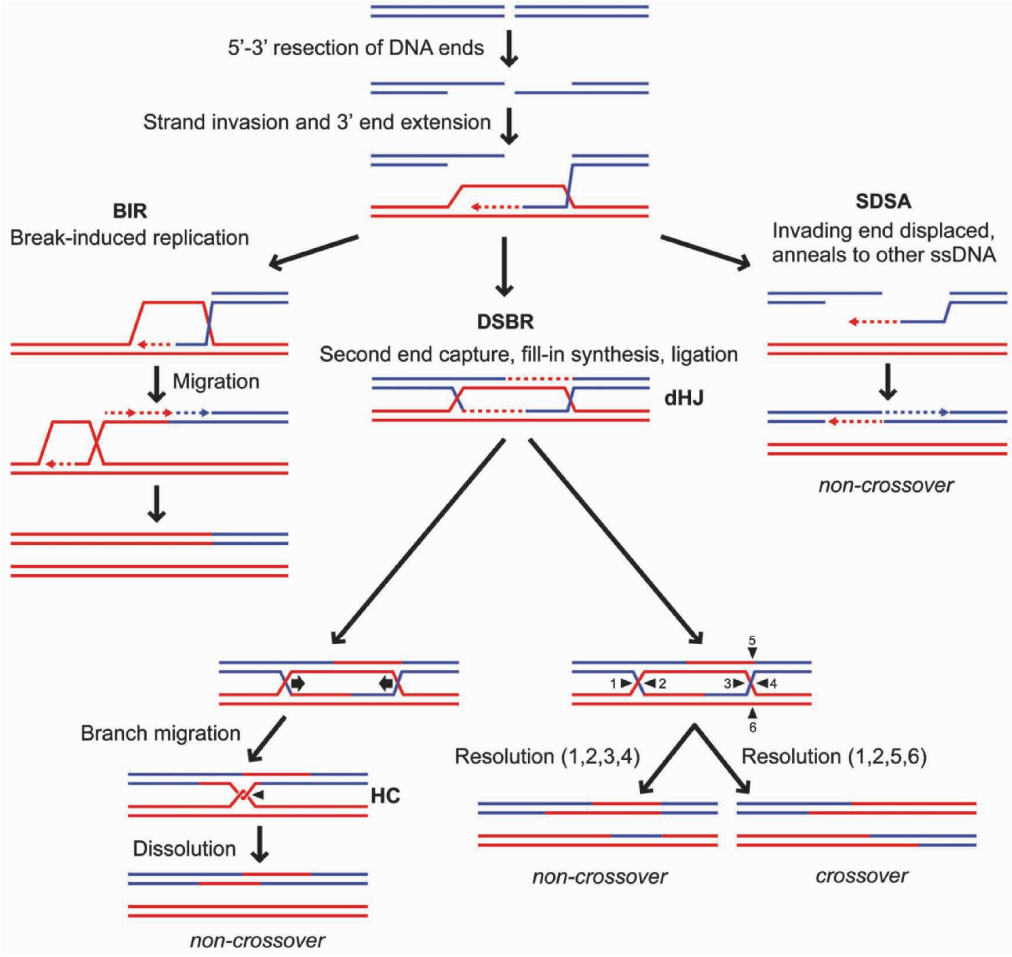

Figure 3 - Models for homology-dependent DSB repair. Homologous recombination repair of a DSB is initiated by 5' to 3' resection of DNA ends. The resulting 3' strand invades the homologous donor template (red). The strand invasion induces the displacement of the same polarity strand of the donor. This generates the displacement loop (D-loop) and leading strand DNA synthesis starts (Symington et al., 2014). See the text for the details.

2.2.3 - DNA end resection: a crucial step in the HR dependent repair of DSB

The HR mediated repair of a DSB starts with the nucleolytic degradation of both 5' ends of the break in order to create long stretches of ssDNA important for the strand invasion

step of HR. This process, named resection, involves the action of different proteins with different enzymatic activities that are well conserved throughout evolution (*Figure 4*). According to the current model, DSB resection is a bidirectional two-step process. In the first step, named "short-range" resection, the MRX/MRN complex is recruited at DSB ends where, together with Sae2/CtIP, catalyses an endonucleolytic cleavage 50-300 nucleotides away from the DSB. This endonucleolytic activity is dispensable in the presence of DSBs with "clean ends", like the one generated by endonucleases[82]. On the contrary, when the DSB termini are blocked by proteins, the endonucleolytic activity of Mre11 becomes essential for a correct HR-mediated repair[83,88]. Moreover, Mre11 has a exonuclease activity with 3' to 5' polarity[89,90]. This opposite polarity with respect to the one required for resection has created debate about the *in vivo* role of Mre11 enzymatic activity. A two-step mechanism of Mre11 has thus been proposed: Mre11 makes the initial ssDNA nick via its endonuclease activity and then digests toward the DSB end through its 3-5' exonuclease activity to produce 3' ssDNA tails[91].

The enzymatic activity of Mre11 is influenced by Rad50 ATPase. Rad50 associates with two α-helices of Mre11 located near the nuclease domain[82,92]. ATP binding and hydrolysis catalyse by Rad50 induces conformational changes in both Mre11 and Rad50. In fact, in the presence of ATP, Mre11 and Rad50 adopt a closed conformation, in which Rad50 head domains dimerize and occlude the nuclease active site of Mre11[90]. ATP hydrolysis induces the disengagement of Rad50 dimer and DNA melting, so Mre11 active sites can access DNA to initiate DSB resection[83,90]. In other words, ATP hydrolysis can switch from a "closed" MRX/MRN complex, where the nuclease action of Mre11 is inhibited, thus favouring the functions of the complex in checkpoint activation and in NHEJ repair, to an "open" MRX/MRN complex that promotes HR repair by initiating DSB resection. In both yeast and mammals, Sae2/CtIP protein has been implicated in the support of MRX/MRN complex function in DSB resection[91,93,94]. Different CDKs phosphorylation sites have been mapped on Sae2. In particular, Sae2 Ser-267 must be phosphorylated to allow resection both *in vivo* and *in vitro*[88,95]. Moreover, a

biochemical study by Cannavo and Cejka, demonstrated that Sae2 activates the endonuclease activity of Mre11[96]. Additional roles of Sae2 have been identified in end tethering, in Ku/MRX removal after DSB formation and in checkpoint activation[97–100].

Thus, the MRX/MRN complex, together with Sae2/CtIP, is responsible for a limited nucleolytic degradation that provides an entry site for the exonucleases Dna2 and Exo1 that act in two parallel pathways[101]. Once recruited, Exo1 and Dna2, with the help of the helicase Sgs1/BLM, degrade DNA in 5'-3' direction creating long stretches of ssDNA. This is the second phase of the resection process and it is known as "long range resection" (until 2-4 Kb of ssDNA in yeast). Exo1 is a member of the XPG family of nucleases. Since yeast Exo1 exerts its nuclease activity starting from dsDNA, no helicase activity is required for DNA unwinding. On the contrary, in both yeast and mammals, the helicase activity of Sgs1/BLM is necessary for creating the right substrate for Dna2/DNA2 which is a bifunctional helicase-nuclease protein responsible for removing DNA flaps arising during lagging strand synthesis.

Once a DSB is subjected to nucleolytic degradation its fate is sealed. In fact, DNA end resection channels DSB repair to HR preventing NHEJ[82]. Therefore, the resection process must be strictly controlled. In fact, if resection takes place in G_1 phase of the cell cycle, when only the homologous chromosome is available, the chances of an incorrect repair will increase because the recombination will happen between two non-homologous sequences. Furthermore, resection must be controlled also in the S/G_2 phase of the cell cycle as an excessive generation of ssDNA could be detrimental for genome stability in particular during DNA replication (*see section 3.3*). In fact, an excessive resection can induce the destabilization of DNA polymerase and the inability to complete DNA replication[102].

The first level of regulation relies in the activity of the CDK-cyclin complexes, CDK1 in yeast[101,103,104]. Sae2 (on Ser267) and Dna2 show S-phase specific phosphorylations and are targets of Cdc28-mediated regulation of end resection[95,105]. Other resection factors have been found to be phosphorylated by CDK, like the MRN complex, RPA and EXO1.

So, cell cycle stage controls the efficiency of DSB resection. Another level of resection control relies on the Ku complex. In both yeast and mammals, it has been proposed a model in witch Ku binding to DNA ends hides them from Exo1[106,107]. In order to resection to take place, the activity of Sae2-MRX induces the displacement of the Ku complex from the DNA allowing Exo1 to initiate resection. In yeast, DSB resection is also inhibited by the checkpoint protein Rad9[108]. Rad9 is recruited to damaged DNA in two different ways. One dependent on chromatin modifications and the other dependent on the interaction with Dpb11. In fact, Rad9 is able to interact with a methylated lysine on histone H3 (H3-K79), and with the serine 129 on histone H2A after it has been phosphorylated by Tel1 and Mec1[108]. Several lines of evidence indicate that Rad9 acts as a barrier toward end processing enzymes by restricting the access of Sgs1-Dna2[108,109]. The human structural and functional ortholog of Rad9 in DSB resection is 53BP1. As Rad9, 53BP1 inhibits DNA end resection in the G_1-phase of the cell cycle[110]. In particular, 53BP1 inhibits BRCA1-CtIP mediated resection by recruiting RIF1 at DSB sites[111,112].

Also the DNA damage checkpoint (*Figure 4*) is involved in resection regulation. In fact, in both yeast and mammals, Mec1/ATR and Tel1/ATM, regulate the formation of ssDNA upon DSB creation. In yeast, deletion of *MEC1* accelerates DSB resection, whereas the presence of the hypermorphic allele *mec1-ad* impairs the process[43,113]. Resection in *mec1Δ* cells is not as efficient as in *rad9Δ* cells, suggesting that Mec1 can also positively regulate DNA resection. Mec1 can influence DSB resection at least in three ways: i) by inducing Rad53 phosphorylation and activation, that, in turn, inhibits Exo1[114]; ii) by promoting the binding of Rad9 through H2A-S129 phosphorylation, thus inhibiting resection; iii) by phosphorylation of different targets like Sae2, favoring the process[115]. On the contrary, the lack of Tel1 only slightly reduces the efficiency of resection[116]. Thus, checkpoint activation and DSB resection are two interconnected processes.

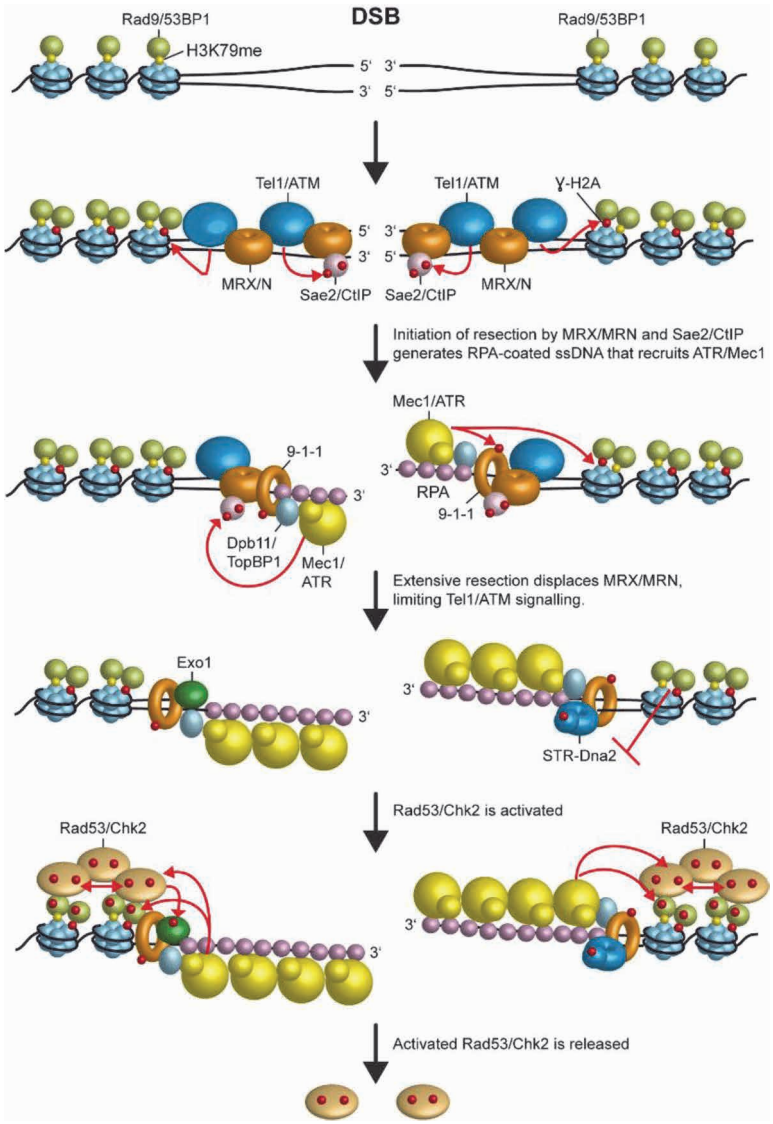

Figure 4 - Interplays between checkpoint and DSB resection. Recognition of the DSB by MRX/MRN complex leads to recruitment of Tel1/ATM, which phosphorylates histone H2A (γH2A). MRX/MRN and Sae2/CtIP start the resection process. Long range resection is carried out by Exo1, Sgs1-Top3-Rmi (STR) and Dna2. The ssDNA tails obtained are coated by the RPA complex. RPA-ssDNA recruits the Mec1-Ddc2/ATR-ATRIP complex. Tel1/ATM, acting on the MRX/MRN complex, promotes DSB resection, which activates Mec1/ATR and concomitantly inhibits Tel1/ATM signaling. Once recruited to the DSB, Mec1/ATR regulates the generation of 3'-ended ssDNA by phosphorylating Sae2/CtIP and histone H2A. γH2A induces the recruitment of Rad9 that inhibits STR-Dna2 dependent resection. Furthermore, Mec1 activates the downstream checkpoint kinase Rad53/Chk2 by phosphorylating Rad9 and Rad53/Chk2 itself. Moreover, phosphorylated Rad9/53BP1 promotes activation of Rad53/Chk2 by allowing its in-trans autophosphorylation. Activated Rad53 is then released from DNA and can regulate both DSB processing by phosphorylating and inhibiting Exo1 and its specific targets in the checkpoint cascade. (Gobbini et al., 2013).

3 - Maintenance of replication fork stability upon replication stress

DNA replication stress can be defined as the transient slowing or stalling of replication forks in response to a variety of situations like hard-to-replicate genomic regions, DNA lesions or the presence of DNA replication inhibitors[117,118]. Replication fork arrest can be artificially induced by genotoxic agents such as hydroxyurea (HU), ultraviolet radiations, methyl methane sulfonate (MMS), camptothecin (CPT) and inter strand crosslinking agents such as mitomycin C. These agents induce fork arrest or collapse at much higher rate than endogenous agents and, for this reason, can be used in basic research to characterize the cellular response to replication stress.

Usually, fork stalling is a transient event that does not cause replisome dissociation[119]. Moreover, the limited extent of ssDNA regions at forks, usually, are insufficient to generate enough signals to promote checkpoint activation[120]. This is not the case in cells treated with DNA synthesis inhibitors, where the large number of stalled forks characterized by ssDNA regions with an average size of 300 nucleotides elicits a robust checkpoint response[120]. Occasionally, the replisome might dissociate from stalled forks, thus causing fork collapse which often generates extensive ssDNA regions (partially due to the nucleolitic processing of nascent chains), four-branched DNA structures resembling recombination intermediates (reversed forks), and DNA breaks[120]. Fork collapse seems to occur when forks hit obstacles that cannot be efficiently removed (such as DNA-protein complexes), when the template is damaged by interstrand crosslinking agents or when forks run off at DNA breaks or telomeres. Further, stalled forks collapse when the checkpoint response is defective, due to the inability in maintaining a stable association between the replisome and the forks[121].

3.1 - The S-phase checkpoint

DNA replication is a very complex process, that needs to occur accurately, rapidly, and only once per cell cycle to prevent genome abnormalities/instability and deleterious

loss of genetic information. Replication forks must maintain their integrity in order to be able to finish chromosome replication accurately when conditions that halt them are eliminated[122,123]. For these reasons, eukaryotic cells activate the S-phase checkpoint (or "replication checkpoint") which shares most of the factors of the DNA damage checkpoint, detects the replication problems and coordinates a global response to maintain genome integrity[124,125]. The S-phase checkpoint activation depends on Mec1/ATR and is activated mainly by extensive ssDNA tracts. If at DSB the ssDNA is provided by the resection process, following HU treatment that blocks DNA replication, yeast cells accumulate short tracts of ssDNA at the replication forks probably because the MCM (minichromosome maintenance complex) helicase complex continues DNA unwinding, although uncoupled from DNA synthesis[66,126]. The checkpoint response during S-phase is depicted schematically in *Figure 5*. RPA binds the ssDNA and triggers the recruitment of Mec1/ATR. Anyway, fully activation of Mec1/ATR requires Dpb11/TopBP1 and the action of the 9-1-1 complex. Since Dpb11/TopBP1 and 9-1-1 complex require ssDNA/dsDNA junction to be recruited onto DNA, the uncoupling of replicative helicases and polymerases cannot fully justify checkpoint activation. The observation that DNA replication continues at a stalled fork through the synthesis and elongation of new primers creating ssDNA/dsDNA junction, solved the problem[127]. Then Mec1 phosphorylates Mrc1 which transduces the signal from Mec1 to the effector kinase Rad53[58]. This model fits perfectly with agents that stall replication fork. Anyway, other genotoxic treatments could block DNA replication without a significant uncoupling between helicases and polymerases because of the stalling of the helicases and not of the replisome. In these cases, active fork remodelling and DNA processing, such as resection and/or fork reversal (*see section 3.2*), generate ssDNA activating Mec1/ATR. Moreover, other situations in which double-strand breaks or single-strand breaks occur in the proximity of DNA replication origin can create ssDNA by activating homologous recombination-mediated repair. Many studies have been performed with the aim to identify the targets of the S-phase checkpoint, but to date the whole view

seems to be yet incomplete. In general, once S-phase checkpoint is activated, it exerts four main functions to promote cell survival to replication stress (*Figure 5*). First, it induces cell cycle arrest. In yeast, this is achieved by the stabilization of the securin Pds1, required for sister chromatids cohesion[128,129]. Anyway, delaying mitosis in *mec1* or *rad53* mutants does not suppress their strong sensitivity to HU, indicating that this checkpoint function is not essential for cell viability after replication stress[129]. Second, the replication checkpoint regulates dNTPs level, increasing dNTPs synthesis in both yeast and mammals. As too much or too little dNTPs can be mutagenic[130], cells need to tightly control ribonucleotide reductase (RNR) activity in order to synthetize just enough dNTPs for efficient chromosome replication. The *RNR* genes are regulated by a repressor known as Crt1 (constitutive *RNR3* transcription), which is inhibited by Dun1 kinase in response to checkpoint activation, leading to increased expression of *RNR* gene[131]. Furthermore, RNR is also post-translationally regulated by the S-phase checkpoint. In fact, the budding yeast *MEC1* and *RAD53* genes are essential for cell viability even in the absence of exogenous sources of replication stress or DNA damage. Mutation of *SML1* gene was found to suppress the lethality of *mec1Δ* or *rad53Δ*, as increases the expression of *RNR* genes[132,133]. The Sml1 protein (phosphorylated by Mec1 and Rad53) represents a direct inhibitor of RNR that must be degraded in each round of the cell cycle when budding yeast cells enter S-phase, and is also degraded in response to DNA damage and replication defects[133].

Third, activation of S-phase checkpoint inhibits late origin firing. As defective replication forks are a potential source of chromosome instability, delaying the firing of new origins in response to replication defects will allow the cell to avoid the accumulation of more defective forks. Rad53 phosphorylates two factors that play a key role during the initiation of replication at each origin: the Dbf4 subunit of the Cdc7 kinase, and the Sld3 protein[134–136]. Inhibition of these factors prevents the activation of the replicative DNA helicase at origins and so blocks the establishment of DNA replication forks. Once the source of stress is overcome, checkpoint is inactivated and the previously silenced

origins can give rise to new forks that will aid the completion of chromosome replication.

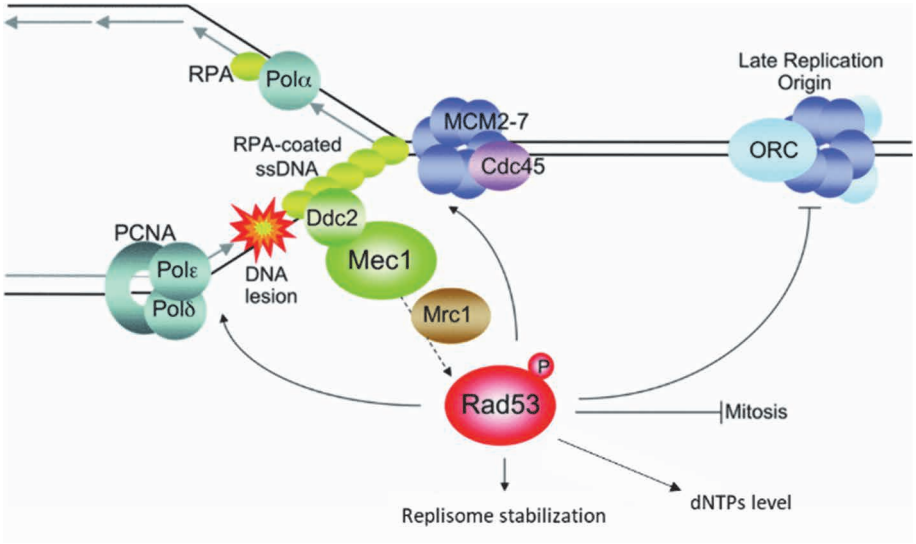

Figure 5 - Schematic illustration of the S-phase checkpoint response. When replication forks hit DNA lesions or stall because of dNTP deprivation, the helicase and the polymerases may uncouple, exposing regions of ssDNA that cause the activation of the checkpoint response. Rad53 stabilizes DNA replication forks, inhibits firing of late origins, activates gene expression and prevents entry into mitosis and unscheduled recombination. (Adapted from Segurado and Tercero, 2009)

Lastly, S-phase checkpoint supports replisome stabilization. For example, checkpoint-dependent phosphorylation of the Polα polymerase seems to be important to stabilize the replisome[137,138]. This is one of the still debated functions of the Mec1/ATR mediated checkpoint. Two genome-wide studies conducted first in yeast and then in human cells have demonstrated that in Mec1/ATR defective cells the replisome stability is not altered[139,140]. An interpretation could be that Mec1/ATR, even without influencing the replisome composition and association to DNA, can regulate fork processing with a protective effect that avoids fork collapse[141,142]. Other roles have been assigned to the S-phase checkpoint, like resumption of stalled DNA replication forks[132,143], transcriptional induction of DNA damage response genes[144] and choice of the repair pathway[145]. What is extremely evident is that S-phase checkpoint has a huge impact on cell survival after replication stress.

3.2 - Replication fork reversal in eukaryotes

Replication fork reversal is defined as the conversion of a typical replication fork (three-way junction) into a four-way junction by the coordinated annealing of the two newly synthesized strands and the re-annealing of the parental strands, to form a fourth 'regressed' arm at the fork elongation point. Different works suggest that fork reversal acts as a mechanism for DNA damage bypass[146,147] and as an evolutionarily conserved response to various types of DNA replication stress, including topological constraints, DNA lesions, DNA secondary structures and template discontinuity[148].

Although replication perturbation by nucleotide pool depletion, or by DNA damage caused by ultraviolet light or methylating agents, fail to induce detectable levels of fork reversal in checkpoint-proficient yeast cells[149,150], anticancer agents that increase topological stress during replication were recently shown to induce frequent fork reversal in wild type *S. cerevisiae* cells[151]. In yeast, two 5′-3′ DNA helicases, Pif1 and Rrm3, are thought to act concertedly to generate regressed replication forks. Another way to generate fork regression is through *S. cerevisiae* Rad5 protein[152].

Replication fork reversal could be considered a “double-edged sword”, having both physiological roles and potentially pathological consequences. Indeed it’s important to take into account that replication fork reversal is a frequent event not only in response to a variety of genotoxic stresses but also during unperturbed DNA replication[153,154]. A transient pausing of the replication fork could prevent continued synthesis across lesions or discontinuities on the template, which may otherwise be converted into more deleterious DSBs[151,155]. Furthermore, by transiently stalling replication fork progression, fork reversal could prevent the excessive accumulation of ssDNA, allow more time for repair of DNA lesions and enable excision repair by re-positioning a lesion[151,153]. In this scenario, fork reversal acts as an 'emergency brake' that transiently protects replication forks. Fork reversal could also have pathological consequences. Under specific circumstances, fork reversal and restoration on repetitive DNA sequences[154,156] or the nucleolytic cleavage of reversed forks[157], could contribute to

genome instability in neurodegenerative syndromes and cancer. Although fork remodelling may generally assist the replication of sequences that adopt secondary structures[158], the strand exchange that occurs during fork reversal was also proposed to present an opportunity for misalignment of parental and newly synthesized strands, and thus contribute to the disease-relevant genetic instability (expansions and contractions) of such repeats[154,156]. The relevance of replication fork reversal in cancer was recently underscored by a study showing that reversed forks are among the most frequent atypical replication intermediates observed following the activation of oncogenes that induce replication stress[157]. One of the most intriguing implications of fork reversal process is the formation of a new DNA end (the regressed arm). Similarly to DSBs and telomeres, such exposition of DNA ends at the regressed arm of reversed forks could contribute to replication stress-induced Mec1/ATR signaling. Moreover, ATM signaling was found to be associated with fork reversal following mild Top1 inhibition and nucleotide depletion, in the absence of detectable DSBs[151,159]. So, Tel1/ATM and Mec1/ATR signal the presence of the regressed arms in a different way from DSBs. It is conceivable that the signaling potential resides in specific structural features of the regressed arms, which may be present at reversed forks only under certain conditions and may escape direct observation by electron microscopy (for example, the presence of nicks and small ssDNA gaps). A second, not mutually exclusive possibility is that the binding of different factors, either specific to regressed arms or belonging to DSB repair pathways, may modulate checkpoint signaling from the DNA end at the regressed arm, similarly to what has been comprehensively documented at telomeres[160].

3.3 - DNA end resection at stalled replication fork

The control of resection is important both at DSB and at replication fork. Nevertheless, while the molecular mechanism underpinning resection control at DSBs has been analysed in depth, how resection is controlled at stalled replication forks and if DSB

proteins share their function even at replication forks remains to be determined. However, in both yeast and mammals, several nucleases have been implicated in the processing of stalled replication fork intermediates[117,118]. While extensive resection is associated with fork collapse and, thus, with poor survival after replication stress, controlled nucleolytic degradation can be beneficial for replication fork stability.

Cotta-Ramusino and colleagues demonstrated that Exo1 nuclease is recruited at HU stalled replication forks and checkpoint mutants accumulate detrimental ssDNA at replication fork in an Exo1 dependent manner[119]. Anyway, the abrogation of Exo1 activity results in an increase of fork reversal. To correctly analyse this data, it must be taken in account that Rad53 inhibits Exo1 action[114]. In this context, in checkpoint mutants where Exo1 could be hyperactive, excessive resection induces degradation of stalled replication forks. On the contrary, deletion of the nuclease increases pathological fork reversal indicating that both over-processing and inefficient processing of replication intermediates are detrimental to cell survival upon replication stress. Thus, controlled resection of replication intermediates is important for replication fork stabilization. In this regard, it has been recently shown that Exo1-, Dna2- and Sae2-dependent processing has a positive effect in avoiding reversed replication fork formation[161]. In particular, Exo1 and Dna2 can resect reversed nascent strands. This counteracts the formation of reversed replication forks that, once formed, can be processed by endonucleases like Mus81, Yen1 and Slx1 that induce DSB creation.

In mammalian cells, unscheduled resection conducted by MRE11 nuclease has been associated to replication fork collapse[162–164]. Resection by MRE11 was firstly observed in BRCA1/2 or RAD51 deficient cells where, together with CtIP and EXO1, MRE11 is responsible for the over-processing that induces fork degradation[163]. In fact, BRCA1 and BRCA2 protect against MRE11 resection by promoting and stabilizing the RAD51 filament formation[164]. As observed in yeast, nucleolytic degradation is a double-edge sword. If uncontrolled it can lead to fork degradation and genome instability, but a

physiological activity of all the nucleases described above is required for replication fork restart and thus for maintaining genome stability. For example, limited MRE11 activity avoids DSBs formation and promotes the removal of stalled polymerases supporting fork repriming mechanisms[102]. Furthermore, a limited resection is required for MUS81 processing that, in turn, promotes fork rescue[163]. In summary, it is evident that the resection process must be tightly controlled at both DSB and stalled replication forks.

4 - Camptothecin, a DNA Topoisomerase I Inhibitor

DNA topoisomerases resolve topological constraints that may arise from DNA strand separation and are therefore important for transcription and replication[165]. A common feature of topoisomerases is their catalytic mechanism, which in all cases consists in a nucleophilic attack of a DNA phosphodiester bond by a catalytic tyrosyl residue from the topoisomerase. The resulting covalent attachment of the tyrosine to the DNA phosphate is either at the 3'-end of the broken DNA in the case of Top1 enzymes (Top1 and Top1mt) or at the 5'-end of the broken DNA for the other topoisomerases[166]. Thus, Top1 enzymes (a large protein of 100 KDa) are the only topoisomerases that form a covalent link with the 3'-end of the broken DNA while generate a 5'-hydroxyl end at the other end of the break.

Another unique feature of Top1 enzymes is their DNA relaxation mechanism by "controlled rotation" (*Figure 6B*) rather than by "strand passage"[167,168]. In other words, Top1 enzymes relax DNA by letting the 5'-hydroxyl end rotate around the intact strand. This processive reaction does not require energy cofactor like ATP or divalent metal binding and the remarkable efficiency of the nicking-closing activity of Top1 enables the enzyme to relax both negatively and positively supercoiled DNA with similar efficiency[225]. In particular, the resolution of positive supercoils is required for replication and transcription progression. Once the DNA is relaxed, Top1 religate the breaks by reversing its covalent binding. Religation requires the DNA end 5'-hydroxyl-group to be aligned with the tyrosine-DNA phosphodiester bond[225] for nucleophilic

attack[169]. Under normal condition the cleavage intermediates, called Top1 cleavage complexes (Top1cc), are transient and religation is favoured over cleavage[169].

Camptothecin (CPT) is a plant alkaloid first identified from the Chinese tree, *Camptotheca acuminata* by Monroe Wall and coworkers[170]. CPT inhibits Top1 by selectively trapping Top1cc[171,172] and no other topoisomerases, indeed yeast strains deleted for *TOP1* gene are not sensitive to CPT[173,174]. CPT traps Top1 cleavage complexes binding the enzyme-DNA interface[175,176]. Two key pharmacological properties of CPT need to be described. First, CPT binds reversibly to Top1 cleavage complexes. Hence, once CPT is diluted out and removed from cell culture, the cleavage complexes reverse rapidly[177]. Second, CPT traps only a subset of the existing Top1 cleavage complexes, including those with a guanine at the 5'-end of the break[178,179]. Two water-soluble camptothecin derivatives are presently approved by the FDA for IV administration: topotecan (used to treat ovarian cancers and small-cell lung cancers, SCLC) and irinotecan.

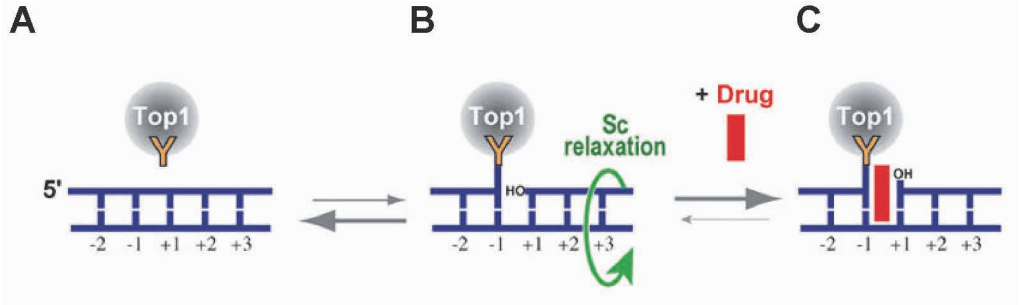

Figure 6 - Schematic architecture of the topoisomerase cleavage complexes. ***A.*** *Under physiological conditions, Top1 is associated with chromatin in non-covalent complexes.* ***B.*** *Top1 relaxes DNA by controlled rotation of the cleaved strand around the intact strand (green curved arrow). For this relaxation process Top1 makes single-strand breaks that are generated by the covalent linkage of Top1 to the 3'-end of DNA (Top1cc).* ***(C)*** *Camptothecin binds reversibly to the Top1cc and slow down DNA religation. (Adapted from Pommier et al., 2006).*

The normally transient Top1cc complexes can be converted into potential DNA lesions. Top1cc complexes can be trapped by DNA lesions including abasic sites, mismatches, oxidized bases, nicks and carcinogenic DNA adducts[180]. By contrast to CPT and other Top1 inhibitory drugs, these DNA modifications can produce irreversible cleavage

complexes when the 5'-end of the DNA is irreversibly misaligned as in the case of abasic sites[181] or DNA breaks[182]. In such cases, Top1cc complexes remains without effective legitimate religation partner. Those Top1-DNA covalent complexes are commonly known as "suicide complexes". Under such conditions, Top1 can nevertheless religate an illegitimate ("foreign") 5'-hydroxyl-DNA end and act as a recombinase[183]. This property is routinely used for molecular cloning (TOPO® Cloning, Invitrogen) using vaccinia Top1[184]. Reversible cleavage complexes can also produce irreversible Top1cc and DNA lesions after processing by DNA and RNA polymerases[185,186]. For example, camptothecin-induced Top1 cleavage complexes can be converted into replication double-strand breaks (Rep-DSB) as demonstrated by rapid phosphorylation of histone H2AX[187], which is a hallmark for DSBs[188,189]. Inhibition of DNA synthesis occurs within minutes following camptothecin treatment and persists for several hours following drug removal[190]. At least two mechanisms lead to DNA synthesis inhibition: i) direct block of replication forks that have collided with the Top1 cleavage complexes, and ii) indirect replication arrest by S-phase checkpoint activation[190,191]. Moreover, camptothecin is a potent inhibitor of nucleolar transcription[192,193]. It has been proposed that the elongating RNA polymerase collides with trapped Top1 cleavage complexes on the transcribed strand, resulting in the conversion of reversible Top1 cleavage complexes into irreversible strand breaks[194,195]. Inhibition of Top1 catalytic activity by CPT might also inhibit transcription by producing an accumulation of positive supercoils upstream RNA polymerase[196,197] and by compacting chromatin domains[197,198]. The transcriptional effects of CPT could also be related to functions of Top1 besides its DNA nicking-closing activity. For example, Top1 regulates transcription initiation by interacting with TATA binding proteins[199,200]. By contrast to replication[190], transcription inhibition recovers rapidly following CPT treatment[201,202].

4.1 - Repair of Topoisomerase I-mediated DNA Damage

Multiple pathways have been uncovered for the repair of Top1-associated DNA damage. There are three main repair pathways: i) reversal of the covalent Top1-DNA

complexes by 5'-end religation, ii) Top1 excision by Tdp1, and iii) Top1 excision by endonucleases (*Figure 7*).

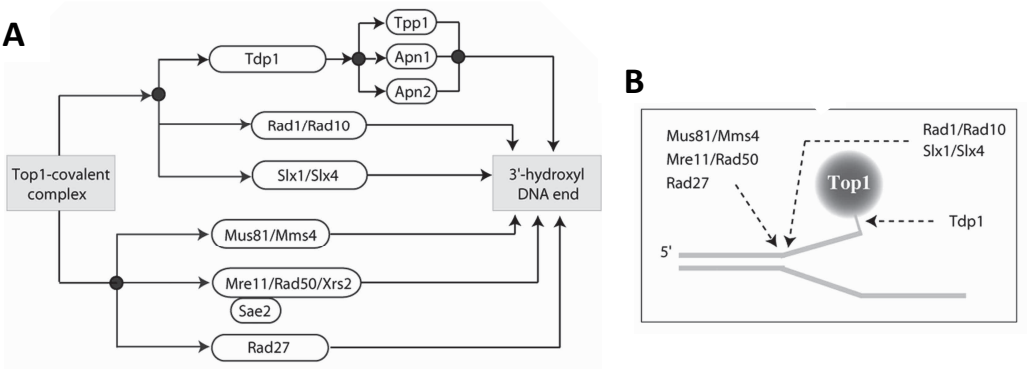

*Figure 7 - **A.** Schematic representation of the genetic pathways implicated in the removal of the Top1-DNA covalent complexes. Tdp1 appear to function in alternative pathways with Rad1/Rad10 and Slx1/Slx4. The other endonucleases (Mus81/Mms4; Mre11/Rad50/Xrs2 and Rad27) appear to function in parallel. Tpp1, Apn1 and Apn2 are 3'-phosphatases that remove the 3'-phosphate left after Tdp1 hydrolyzes the tyrosyl-DNA adduct. **B.** Shematic representation of the sites of attack for Tdp1 and the endonucleases described in panel A. (Pommier et al., 2006)*

As described before, reversal of Top1-DNA covalent complexes by 5' end religation requires that the intact 5'-hydroxyl end is aligned with the 3'-end bonded to Top1 for nucleophilic attack of the tyrosyl-phosphoester bond. Thus, this pathway excludes the Top1 suicide complexes generated by DNA lesions affecting the 5'-end of the broken DNA. Because Top1 is very effective in joining a 5'-hydroxyl end from a non-homologous substrate to the Top1 covalent complex, Top1cc might reverse by religation of a non-homologous end, which leads to DNA recombinations[183]. CPT is indeed a potent inducer of sister chromatid exchanges and chromosomal abnormalities[203,204].

Another repair pathway for Top1 excision require the Tyrosyl-DNA-phoshodiesterase 1 (Tdp1). Tdp1 was discovered by Nash and coworkers[205] as the enzyme capable of hydrolyzing the covalent bond between the Top1 catalytic tyrosine and the 3'-end of the DNA[206]. Tdp1 is ubiquitous and highly conserved in eukaryotes from yeast to humans. Budding yeast *tdp1Δ* cells are hypersensitive to high levels of Top1cc only when the checkpoint gene Rad9 is simultaneously inactivated (so Tdp1 is primarily

required when the checkpoints is deficient)[207] or when some endonuclease pathways (Rad1/Rad10 and Slx1/Slx4) are inactive[208,209]. Because Tdp1 specifically processes 3'- but not 5'-tyrosyl-DNA complexes[205,206], Tdp1 cannot hydrolyze the cleavage complexes produced by other topoisomerases besides Top1. However, Tdp1 function is probably not limited to the repair of Top1 cleavage complexes. Tdp1 can remove 3'-phosphoglycolate generated by oxidative DNA damage, which suggests a broader role for Tdp1 in the maintenance of genomic stability[210]. Optimum Tdp1 activity requires: i) a DNA segment consisting of at least few nucleotides; ii) an exposed phosphotyrosyl bond at the Top1-DNA junction; and iii) a short Top1 polypeptide segment. In fact, Top1 needs to be proteolyzed or denatured for efficient Tdp1 activity[211,212].

Tdp1 generates 3'-phosphate ends that need to be hydrolysed to 3'-hydroxyl for further processing by DNA polymerases and/or ligases. In budding yeast, this 3'-phosphatase activity is carried out by Tpp1 (ortholog of PNKP in human)[213] and by two functionally overlapping apurinic (AP) endonucleases, Apn1 and Apn2[208] (*Figure 7*A). Simultaneous inactivation of Tpp1, Apn1 and Apn2 is required to sensitize yeast cells to CPT[213], indicating the functional redundancy of the 3'-phosphatase pathways. Remarkably, the hypersensitivity of the *tpp1 apn1 apn2* triple mutant is rescued by the inactivation of Tdp1[214], which indicates that in the absence of Tdp1, yeast cells use alternative endonuclease pathways for removal of the Top1 covalent complexes. *Figure 7* summarizes the multiple endonuclease pathways implicated in Top1cc repair[208,209]. Rad1/Rad10 and Slx1/Slx4 appear to function in parallel and redundant pathways with Tdp1[286]. In particular, like Tdp1, Rad1/Rad10 (ortholog of the human endonucleases XPF/ERCC1 involved in nucleotide excision repair[11]) requires a single-stranded gap between the 3'-end to be processed and the 5'-end of the DNA (*Figure 7B*)[215], suggesting that Tdp1 and Rad1/Rad10 share common substrates. Additionally, Mus81/Mms4 preferentially cleaves broken replication forks and requires the presence of duplex DNA near the 3'-end to be processed[215]. The Mre11/Rad50/Xrs2 complex (MRX) preferentially cleaves gapped substrates and hairpin structures; moreover Sae2

is required for the endonuclease activity of MRX[216]. MRX appears to function independently from the Tdp1 pathway, which is also the case for Mus81/Mms4[209]. Surprisingly, the 5'-flap endonuclease Rad27 (ortholog of human FEN-1) also contributes to the repair of Top1 covalent complexes. Indeed, FEN-1 in coordination with the Werner syndrome protein and replication protein A (RPA) possesses gap 5'-endonuclease activity (GEN activity) and can process substrates that mimic stalled replication forks[217].

At the end, after the removal of Top1 all these repair mechanisms require a recombination step mediated by Rad52 in order to repair the nick or the gap leaved by the repair pathways.

5 - Telomeres and genome stability

Eukaryotic chromosomes are linear DNA molecules with physical ends, called telomeres. Telomeres are essential for the stable maintenance of chromosomes indeed they protect the natural ends of linear chromosomes from fusion and degradation events, so they must be retained. Exactly the opposite applies to DSBs: they must be repaired by either HR or NHEJ, and this repair often involves regulated degradation of the DSB. So telomeres provide a distinction between the natural ends of linear chromosomes and the ends of DSBs, a function known as capping. Capping is also used to describe how telomeres prevent their degradation and fusion through recombination[218]. As a consequence of capping, the regions near telomeres are gene-poor. In many organisms, telomere proximal genes are subjected to a special type of transcriptional regulation called telomere position effect (TPE), so genes transcription near telomeres is repressed[219]. Another key feature of telomeres is their replication mechanism. Telomere replication is carried out by telomerase, a specialized ribonucleoprotein complex that is mechanistically related to reverse transcriptases[220]. Furthermore, telomeres are essential to solve the end replication problem, preventing sequence loss at each replication round of linear DNA.

5.1 - Telomere structure and telomeric proteins

In budding yeast, telomeres are made of 275–375 base pairs (bp) of simple $C_{1-3}A/TG_{1-3}$ double-stranded repeats (TTAGGG in human, 15 kb long in the human germline) that end with a 3' single-stranded G-rich overhang (G-tail; *Figure 8A*). The G-tail is 12-15 nucleotides (nt) long during most of the cell cycle but 30-100 nt long in late S/G_2 phases[221,222] due to telomerase-mediated addition of telomeric repeats to the G-tail and to the regulated degradation of the opposite strand, the C-strand[223,224]. Telomeres sequence heterogeneity is due to a combination of effects. In particular, in a given extension-cycle, only a portion of the RNA template for telomeres replication is used and/or the RNA template and telomeric DNA align in different registers in different extension cycles[225]. The heterogeneity of yeast telomeric DNA is experimentally useful as it makes possible to distinguish newly synthesized from pre-existing telomeric DNA[226]. Under most conditions, only the terminal half of the telomere is subject to degradation and/or telomerase lengthening[227]. These repeats in conjunction with the proteins that bind them are necessary and sufficient for telomere function.

S. cerevisiae telomeres are bound by highly specialized proteins, which orchestrate all telomere-related processes (*Figure 8B*). Telomeric double-stranded repeats are bound in a sequence-specific manner by Rap1. In vitro data indicates that one Rap1 molecule binds every 18 bp[228]. Rap1 function is not restricted to telomeres, as it is also involved in transcription activation and repression at multiple loci in the genome[229]. The C-terminus of Rap1 is required for the recruitment of Rif1/Rif2 and Sir3/Sir4 to telomeres, which compete with each other for Rap1 binding[230]. The G-tail is bound by Cdc13, which in turn recruits Stn1 and Ten1, thereby forming the CST complex. The CST complex has been dubbed "telomeric RPA" due to its resemblance to the trimeric ssDNA biding complex RPA[231]. Cdc13 has been proposed to outcompete with RPA for G-tail binding due to its high affinity and sequence specificity for telomeric repeats, although RPA can be detected at telomeres especially in S-phase, when the G-tail is longest[232,233]. Finally, Ku70 and Ku80 (which form the Ku complex) also bind telomeres although in a

sequence-unspecific manner[234]. Ku binds at the border between telomeric repeats and subtelomeres as well as at internal telomeric repeats[235], and is reported to be able to bind directly to the telomeric DNA but also to localize to telomeres via protein-protein interaction with Sir4[236,237].

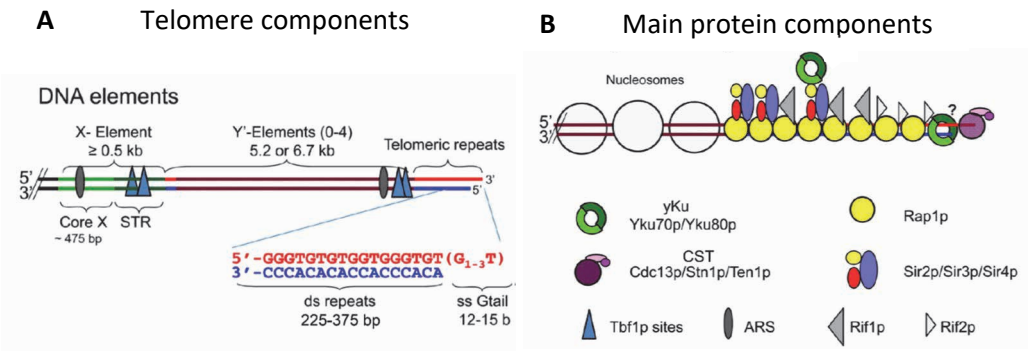

*Figure 8 - **A.** Telomeric DNA composition. S. cerevisiae telomeres are composed of 300 ± 75 ds repetitive sequences which end in a ss 3' G-tail of 12-15 bases. Subtelomeric sequences located on the centromere-oriented side of telomeres always contain an X element and 0-4 copies of Y' elements, often separated by short tracts of telomeric repeats. **B.** Telomere binding proteins. The G-tail is bound by the CST complex and the ds telomeric repeats are bound by Rap1, which in turn recruits either Rif1 and Rif2 or Sir2-4. The Ku complex was proposed to bind at the border between ss and ds telomeric repeats, but also localize to telomeres by interacting with Sir4. The subtelomere is organized in nucleosomes. (Wellinger and Zakian, 2012).*

Centromere-proximal to telomeres are gene-poor regions referred to as subtelomeres. In *S. cerevisiae*, all subtelomeres contain the so called X element, while about half of the subtelomeres additionally contain Y' elements that are always between the X element and the telomeric repeats[238]. these elements are often called TAS elements (Telomere Associated Sequences). While X elements vary in sequence and size and are always present in single copy at each telomere, Y' elements can either be 6.7 kb (Y' long) or 5.2 kb (Y' short) long and can be present in zero to four tandem copies[238]. Subtelomeric regions are dynamic, undergoing frequent recombination[239]. Moreover, subtelomeric repeats diverge rapidly even among related yeast strains[238]. Both X and Y' elements contain potential autonomously replicating sequences (ARS)[238] and often short tracts of telomeric repeats are found between X-Y' and Y'-Y' elements[240]. Whereas complete loss of the telomeric repeats from a chromosome end results in

extremely high loss-rates for the affected chromosome, chromosomes that loss X and Y' elements at one or even both ends have normal mitotic stability[241]. However, Y' amplification by recombination can provide a telomere maintenance function to cells lacking telomerase[242].

While telomeric repeats are presumably nucleosome free, *S. cerevisiae* subtelomeres are organized in nucleosomes[243] and are characterized by heterochromatin formation, causing the silencing of genes near the telomeres (TPE)[219]. Telomeric heterochromatin formation is established by the Sir2-4 complex, which localizes to telomeres by the interaction with Rap1[244], but also by Sir4 interaction with the Ku complex[245]. Telomeres cluster in three to eight foci at the nuclear periphery[246,247] and are anchored to the nuclear envelope by two redundant pathways, established by Sir4 and Ku80[248,249]. These telomeric foci are enriched in Sir proteins and are repressive for transcription and subtelomeric recombination[334].

5.2 - Capping of Chromosome Ends

Eukaryotic chromosomes ends are not subjected to DNA repair events and do not activate DDR, despite being physical DNA ends. Several studies on *S. cerevisiae* and mammals have revealed that protein complexes with specificity for double-stranded and single-stranded telomeric DNA prevent the natural chromosome ends from being recognized as intrachromosomal DSBs[250] (*Figure 9*). As discussed before, DSBs can be repaired by two pathways: non-homologous end joining (NHEJ) and homologous recombination (HR). NHEJ especially would result in catastrophic end-to-end chromosome fusions, while HR would result in recombination between telomeres. For this reason, the capping function of telomeres prevent repair events. Additionally, capping of telomeres also prevents checkpoint activation by Mec1 and Tel1 kinases. Indeed, loss of a single telomere in budding yeast, and thereby loss of capping, leads to the activation of a Rad9-dependent checkpoint[241]. The capping of telomeres is accomplished by multiple players that will be described in the next paragraphs.

First of all, Cdc13 binding to the single-stranded telomeric DNA reduces the association of RPA with these DNA ends and subsequent Mec1 activation[251]. Moreover, CST complex protects telomeric DNA from degradation. Exposure to restrictive conditions of cells harbouring *cdc13*, *stn1*, or *ten1* conditional alleles causes telomere degradation by progressive resection of the 5'-ended strand and a checkpoint-dependent cell cycle arrest. The 5'-3' exonuclease Exo1 appears to be the major nuclease that degrades telomeres in *cdc13* mutants[252].

Double-stranded telomeric DNA in *S. cerevisiae* is bound by the Rap1-Rif1-Rif2 complex[253]. Loss of function of this complex has less catastrophic consequences than CST inactivation. In particular dysfunction of Rap1 or Rif2 leads to increased amounts of telomeric ssDNA and NHEJ-mediated fusion events[254]. Generation of telomeric ssDNA in cells defective for Rif2 or Rap1 requires the MRX complex, suggesting that Rap1 and Rif2 prevent resection at telomeric ends by interfering with the association of MRX. On the other hand, inactivation of Rap1 or Rif2 does not leads to checkpoint activation[255], suggesting that the exposed telomeric ssDNA is still covered by Cdc13, which limits association of Mec1 with telomeres. Unlike Rif2 and Rap1, Rif1 is not involved in the prevention of telomeric fusions by NHEJ and plays a very minor role in protecting telomeres from degradation[256]. Instead, Rif1 prevents checkpoint activation at short telomeric ends by inhibiting the recruitment of checkpoint proteins to these ends[105]. Furthermore, it plays a unique role in supporting cell viability and prevents nucleolytic degradation in mutants with a defective CST complex[257]. Degradation of telomeric DNA is also counteracted by the Ku complex, which acts in a different pathway from Rif2. In fact, while MRX is primarily responsible for nucleolytic degradation of telomeres in *rif2Δ* cells[255], Exo1 is the nuclease that degrades telomeric DNA in *ku70Δ* cells[252].

In vertebrates, telomeres are protected from eliciting the DDR and undergoing degradation or fusion events by a specialized group of proteins collectively called shelterin, which includes TRF1, TRF2, RAP1, TIN2, TPP1, and POT1. Although the

shelterin complex represents a functional unit, the individual components have specific protective functions[250] (*Figure 9*). In mammals, the telomeric single-stranded overhang can fold back on the double-stranded part of the telomere to form a lariat structure, called t-loop, which is predicted to prevent the binding of DNA repair/checkpoint proteins. As TRF2 is required for the formation and/or maintenance of t-loops[258], TRF2-dependent remodeling of telomeres into t-loop structures might explain how TRF2 represses NHEJ and ATM signaling at telomeres[259]. In human, repression of ATR is performed by POT1[260] preventing RPA binding to the telomeric ssDNA[261]. This switch from RPA to POT1 on telomeric ssDNA is promoted by the heterogeneous nuclear ribonucleoprotein A1 (hnRNPA1) through a mechanism that is regulated by telomeric repeat containing TERRA, a non-coding RNA that is transcribed from the telomeric C-rich strand[262]. Inhibition of RPA binding by POT1 may also play an important role in preventing HR, which is repressed at telomeres in a redundant manner by POT1 and RAP1[263]. Thus, multiple pathways act in a highly redundant manner to block telomere degradation.

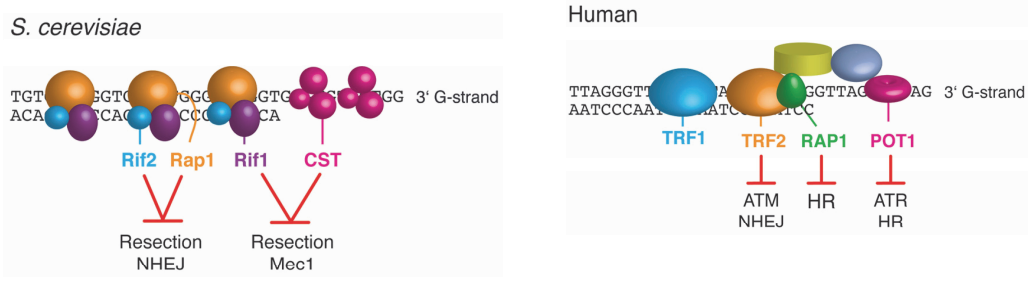

Figure 9 - Capping activities at S. cerevisiae and human telomeres. In S. cerevisiae, Rap1 and Rif2 inhibit 5'-3' resection of the telomeric DNA ends and also repress the NHEJ repair pathway. Rif1 supports the function of the CST complex in preventing excessive resection at telomeric ends and Mec1-dependent checkpoint activation. In humans, TRF2 represses ATM signaling and the NHEJ pathway, whereas POT1 prevents ATR activation by inhibiting the binding of RPA. POT1 and RAP1 block HR. (Gobbini et al., 2014).

5.3 - Telomerase and the "End replication problem"

Most telomeric DNA is replicated by standard semiconservative DNA replication. As a result of the gap left by the replication machinery after removal of the terminal RNA primer on the lagging strand, telomeric DNA sequences become shorter each round of

DNA replication (the so called “end-replication problem”). So, cells need an additional mechanism to avoid loss of genetic information. In most eukaryotes, this loss of telomeric DNA is counteracted by a ribonucleoprotein enzyme called telomerase, which uses its RNA component as a template to add telomere repeats at the telomeric 3’ overhang in a reverse transcriptase reaction[264]. In mammalian cells, the minimal catalytic core of telomerase consists of the telomerase reverse transcriptase (TERT) and the telomerase RNA (TERC). In *S. cerevisiae*, telomerase consists of the reverse transcriptase Est2, the template RNA TLC1, and two accessory proteins Est1 and Est3[265]. Completion of telomere elongation is provided by Cdc13-mediated recruitment of Polα-primase to promote fill-in synthesis of the complementary C-strand via conventional replication[266,267]. The low abundance of each telomerase component (approximately 30 copies of telomerase per haploid cell, for 64 telomeres in late S-phase)[268] suggests the need to act at a limited amount of telomeres per replication round. Telomerase access and action at telomeres is therefore tightly coordinated by multiple telomeric factors. First of all, telomere elongation by telomerase is cell cycle regulated. Although Est2 can bind telomeres throughout the cell cycle thanks to TLC1 interaction with ku80, this localization alone is not productive in terms of elongation capacity[269]. Cdk1-dependent phosphorylation of Cdc13 in late S/G_2 phases promotes Cdc13 interaction with Est1, which leads to Est3 recruitment and formation of a functional complex. Telomerase cannot act on blunt ends, which are generated after the replication of the leading strand, thereby it requires the action of MRX complex to degrade the C-strand[270]. The main regulator of telomere elongation is the checkpoint kinase Tel1. Tel1 is recruited to telomeres by the MRX complex, and its kinase activity is necessary to promote telomere elongation, although how this is accomplished is still elusive. So far, Tel1-dependent phosphorylation of Cdc13 has been proposed to regulate Cdc13-Est1 interaction[271]. Importantly, Tel1 binding to telomeres is inhibited by Rif1 and Rif2, which are thereby two critical negative regulators of telomerase action. Rif1 and Rif2 act via two different pathways, indeed the double mutant *rif1 rif2* has longer telomeres then the two single mutants[272]. Rif2 inhibits Tel1 localization to

telomeres by competing with Tel1 for the binding of Xrn2, while Rif1 inhibition of Tel1 recruitment occurs in a still unknown manner[273].

Telomerase does not act on every telomere of a cell but preferentially elongates the shortest ones[274]. Additionally, telomerase is more processive at critically short telomeres, in a process promoted by Tel1. Indeed, loss of Rap1 binding sites at short telomeres leads to decreased Rap1-Rif1-Rif2 accumulation, which lead to Tel1-mediated telomerase activation allowing telomere elongation[275]. Once the telomere is long again, the increased amount of Rap1-Rif1-Rif2 re-establishes telomerase inhibition. Finally, the Pif1 helicase is also a regulator of telomerase in a telomere-length dependent manner. Pif1, which *in vitro* was shown to dissolve RNA-DNA hybrids, binds preferentially to long telomeres[276], where it acts as a potent telomerase inhibitor, presumably by displacing telomerase from chromosome ends[277]. In addition to telomerase action, the bulk of telomere replication is accomplished by the canonical replication machinery. Telomere replication is initiated at replication origins proximal to telomeres or by the ARS contained in Y' and X elements, although some X elements' ARS are inactive[278]. Importantly, the timing of telomere replication, which directly correlates with origin firing, is dictated by telomere length: while telomeres of wild type length replicate in late S-phase[279], short telomere replication is anticipated to early S-phase[280]. Rif1 is involved in preventing early firing of telomeric origins[281]. Tel1, which binds to short telomeres[282], was shown to act upstream of Rif1 in regulating telomeric origin firing, and to phosphorylate Rif1 at short telomeres, although preventing this event is not sufficient to inhibit early replication of short telomeres. Consistently, *tel1* mutants, which have short telomeres, replicate late[283].

In a recent work, Teixeira's group demonstrated that replication-driven telomere shortening arises from distinct processing of leading and lagging strands at each replication cycle[284]. As previously described, the shortening of the lagging strand telomere is determined by the position of the last Okazaki fragment, which they observed to be always located at the very end of telomeric repeats, thereby leaving

only a 5-10 nt gap after Okazaki primer degradation. On the other hand, replication of the leading strand creates a blunt end, which needs to be further processed to generate a 3' single-stranded G-tail. This nucleolytic processing occurs after telomere replication and is mediated by Tel1 and MRX. End-processing creates a G-tail overhang of about 40 nt, and is followed by fill-in synthesis of the C-strand[284]. The activities responsible for telomere processing in *S. cerevisiae* share common players with the resection machinery of DSBs (*Figure 4*). The MRX complex plays an important role in the generation of telomeric ssDNA[285], indeed MRX localizes preferentially at leading-strand telomeres[286]. As for DSB resection, MRX acts in the same pathway of Sae2 protein to generate G-tails, and Sae2 function at telomeres needs phosphorylation on Ser267 by the cyclin-dependent kinase Cdk1. This requirement can explain why telomere resection can occur only in S and G_2 phases of the cell cycle, when Cdk1 activity is high[287]. MRX and Sae2 are required to initiate resection of modified ends with protein-DNA complexes. Consistent with this indication, MRX and Sae2 are not required for processing telomeres that are deprotected due to the lack of the CST complex, and whose extensive processing depends on Exo1[252]. Although G-tails are short in *mre11Δ* cells, they still increase in length in late S/G_2 phase[221]. Likewise, loss of Sae2 does not abolish ssDNA telomeric generation, indicating that partially overlapping processing activities exist. Indeed, Sgs1 and Exo1 are responsible for the residual resection that occurs in a *sae2Δ* mutant[288], indicating that Exo1 and Sgs1, acting in cooperation with Dna2, provide compensatory activities for processing telomeric ends when Sae2-MRX activity is compromised.

5.4 - Telomere recombination

Although, as stated before, homologous recombination between telomeres is usually repressed to avoid the risk of generating harmful recombination intermediates and genome instability, it can be a means to maintain telomeres in telomerase deficient cells. Indeed, while in telomerase positive cells the exchange of genetic material between telomeres would have virtually no beneficial effect on telomere stability,

when a short telomere is generated in telomerase negative cells recombination between this telomere and another telomere would benefit cell viability by replenishing the pool of telomeric repeats and preventing checkpoint activation[289].

When telomerase deficient cells are propagated for long periods, they lose viability due to checkpoint activation stemming from short uncapped telomeres (replicative senescence, *see section 6*)[290].Strikingly, rare "survivor" cells can overcome senescence and re-gain wild type growth kinetics. These survivors are dependent on the Pol32-mediated break-induced replication (BIR) pathway and on Rad52- dependent recombinational telomere elongation which bears resemblance to alternative lengthening of telomeres (ALT) in mammalian cells[242,291]. Two types of survivors have been described based on their arrangement of telomeric DNA and genetic requirements. Type I survivors maintain telomeres by recombining Y' elements, while telomeric repeats remain short (50-150 bp). This is the leading cause of the poor growth of type I survivors, which experience frequent cell cycle arrests probably due to damage signaling stemming from these short uncapped telomeres[292]. Type I survivors rely on the homologous recombination proteins Rad51, Rad54, Rad57 and Rad55[293]. On the other hand, type II survivors maintain telomeres recombining telomeric repeats with other chromosomes[294]. Telomere length in type II survivors is extremely heterogeneous, ranging from extremely long (up to 12 kb) to quite short[295], but this type of survivor have a wild type growth capacity. This survivor pathway relies on the MRX complex, Rad59, Rad52 and Sgs1[296].

6 - Replicative senescence and cancer

Telomeres can function both as tumour suppressors by limiting the number of cell divisions and as tumour promoters by inducing genome instability. Although telomerase is continuously expressed in unicellular eukaryotes, its expression is downregulated in most human somatic tissues[297]. The inability of the replication

machinery to fully replicate DNA ends, coupled with low/absent telomerase activity, results in progressive telomere shortening that causes cell cycle arrest in a process called replicative senescence[298]. Senescent cells are characterized by a set of common features like permanent proliferative arrest (although senescent cells are still metabolically active), expression of anti-proliferative molecules and persistent DNA damage response activation[299]. In the absence of other genetic changes, these cells can remain in a quiescent state that essentially functions as an anticancer mechanism for long-lived species like humans. However, genetic alterations that cause a defect in checkpoint response may allow additional cell divisions, during which the dysfunctional telomeres continue to erode until they eventually become too short to protect the chromosome termini from unscheduled DNA repair events. Then cells enter a period called “crisis”, during which the chromosomes ends undergo end-to-end fusion events and enter a breakage-bridge fusion cycle that leads to genomic instability (*Figure 10*). Although cells entering this state can be eliminated by apoptosis, most cancer cells acquire the ability to divide indefinitely activating alternative telomere lengthening mechanisms. While around 85% of cancer types gain immortality by reactivating telomerase, the remaining 15% of cancers maintain their telomeres by BIR-based telomere maintenance mechanisms, which defines these cancers as alternative lengthening of telomeres (ALT) cancers[297,300].

Short telomeres due to the absence of telomerase are different from dysfunctional telomeres due to lack of end protection and they trigger a cellular response that is generally different. Accordingly, partially uncapped or unprotected telomeres are more vulnerable to senescence, as illustrated by the accelerated senescence observed in many mutants of telomere protein components[301,302]. So the question is, what causes the DNA damage checkpoint activation at eroded telomeres? The fact that Mec1 is activated in senescence suggests that ssDNA is accumulated at the most eroded telomeres. Single-stranded telomeric DNA already arises during normal telomere replication. Thus, it is possible that in telomerase-negative cells, Tel1 accumulation at

short telomere(s) stimulates resection. In addition, short telomeres are less prone to inhibit the resection process[303]. The combination of both effects would then result in increased resection of one or few telomeres in the cell. This would subsequently expose subtelomeric ssDNA, recruit RPA, and activate Mec1[304,305]. However, deletion of Exo1 has a slight effect in delaying senescence[252,306]. Therefore, accumulation of ssDNA due to exacerbated telomere processing may not be the only signal for senescence, at least not for all cells. However, in addition to ssDNA, some other DNA structures may activate the S-phase checkpoint. Bidimensional gels show that *S. cerevisiae* telomeric repeats impose a replication pause up to 100 bp before the telomeric repeats[307], in accordance with observations in other species[308,309]. This pause seems decreased at shorter telomeres, indicating that the loss of telomeric repeats suppresses the replication stress. In contrast, a similar independent analysis revealed an increase in X-shaped structures, which can activate the checkpoint, in *tlc1Δ* cells[310].

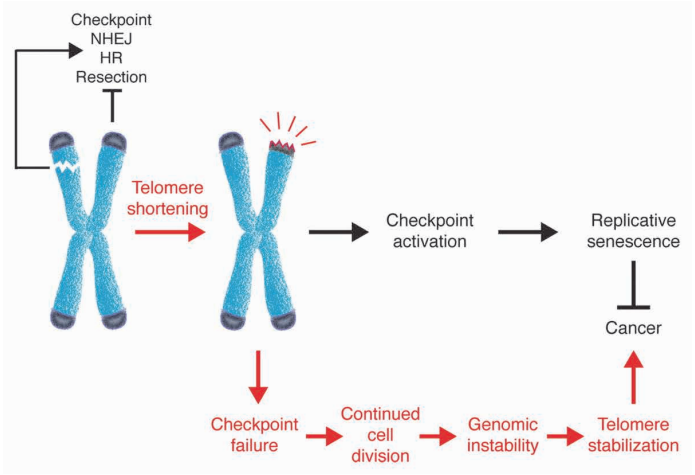

Figure 10 - The natural chromosome ends are protected from fusion and degradation and do not activate the checkpoint (capping). Loss of capping induces a DNA damage checkpoint response that leads to cell cycle arrest and senescence, thus providing a potent anticancer mechanism. However, rare failure to activate the checkpoint may allow cells to undergo cell divisions during which uncapped telomeres can be subjected to DNA repair events. The resulting genomic instability, coupled with activation of telomere restabilising mechanisms, can drive the oncogenic process (Gobbini et al.*, 2014).*

An important issue raised by checkpoint activation during senescence is whether it stems from the telomeres themselves or from a consequence of genome instability

triggered by telomere dysfunction when telomeres erode. For instance, the telomeric cap structure is important for preventing telomere fusions in many species[311,312], and in budding yeast telomeres are more prone to NHEJ in the absence of telomerase[313,314]. Thus, as they erode, telomeres may become more prone to fusions, leading to dicentric chromosomes and random DNA breaks in the subsequent mitosis, causing cell unviability. In order to understand the impact of short telomeres on genome stability, Carol Greider and colleagues devised a system to measure genome stability upon transient exposure to telomerase depletion and progressive telomere shortening[306,315]. In a strain in which *EST1* gene was mutated, they engineered a yeast-dispensable chromosome to contain several genetic markers that could reveal the remaining chromosome structure after telomerase depletion. The authors observed a gradient, with sequence losses being more frequent at the ends of the chromosomes rather than at internal sites. This strongly suggests that genomic instability occurs near telomeres and is not a secondary consequence of a general genomic instability induced by telomerase loss or short telomeres. Therefore, the checkpoint activated during senescence likely emanate from the telomeres themselves. Because telomeres can adopt different states within the cells, it is reasonable to think that not all telomeres will initiate the checkpoint activation at the same time during senescence. In yeast, one critically short telomere is enough to trigger senescence[304]. This suggests that a single very short telomere is sufficient to activate DNA damage checkpoint and it was found that Tel1 and Mec1 are enriched at the critically short telomere[304,305].

So, aging is one of the most important causes of cancer, with cancer incidence drastically raising with increased age. Therefore, preserving genome stability is thought to be the main mean to prevent cancer and delay/overcome aging diseases. Selective clearance of senescent cells is currently being investigated as a mean to benefit the organism fitness, delay aging pathologies and prevent carcinogenesis.

RESULTS

Published online: May 8, 2018

Article

EMBO reports

Tel1/ATM prevents degradation of replication forks that reverse after topoisomerase poisoning

Luca Menin[1], Sebastian Ursich[2], Camilla Trovesi[1,3], Ralph Zellweger[2], Massimo Lopes[2], Maria Pia Longhese* and Michela Clerici*

1. Dipartimento di Biotecnologie e Bioscienze, Università di Milano-Bicocca, Milano, Italy
2. Institute of Molecular Cancer Research, University of Zurich, Zurich, Switzerland
3. Present Address: Istituto Nazionale di Genetica Molecolare "Romeo ed Enrica Invernizzi", Milano, Italy

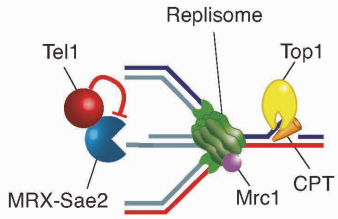

The topoisomerase poison camptothecin (CPT) induces fork reversal, which is thought to stabilize replication forks. Here, yeast Tel1, orthologue of human ATM, protects CPT-induced reversed forks from nucleolytic degradation by the MRX complex.

- The absence of Tel1 or its kinase activity causes a specific hypersensitivity to CPT and decreases fork reversal in CPT.
- The decreased reversed fork levels in the absence of Tel1 are due to unscheduled nucleolytic processing that depends mainly on Mre11 nuclease activity.
- Tel1 function in reversed fork stabilization becomes dispensable when fork reversal is prevented by the lack of the replisome-associated factor Mrc1, whose absence also relieves the hypersensitivity to CPT of *tel1Δ* cells.

Keywords camptothecin; fork reversal; Mrc1; MRX; Tel1
Subject Categories DNA Replication, Repair & Recombination
DOI 10.15252/embr.201745535 | Received 23 November 2017 | Revised 12 April 2018 | Accepted 19 April 2018 | Published online 8 May 2018
EMBO Reports (2018) 19: e45535

1 Dipartimento di Biotecnologie e Bioscienze, Università di Milano-Bicocca, Milano, Italy
2 Institute of Molecular Cancer Research, University of Zurich, Zurich, Switzerland
*Corresponding author. Tel: +39 0264483425; Fax: +39 0264483565; E-mail: mariapia.longhese@unimib.it
**Corresponding author. Tel: +39 0264483547; Fax: +39 0264483565; E-mail: michela.clerici@unimib.it
†Present address: Istituto Nazionale di Genetica Molecolare "Romeo ed Enrica Invernizzi", Milano, Italy

Tel1 kinase is the Saccharomyces cerevisiae ortholog of human ATM, which is mutated in ataxia telangiectasia, an inherited disorder characterized by cerebellar neuropathy, immunodeficiency, premature aging and cancer predisposition. Furthermore, ATM mutations or expression changes have been often found in tumours. Together with the other kinase Mec1/ATR, Tel1/ATM is the master regulator of the DNA damage response (DDR), a multifaceted cellular response that is activated by DNA lesions or replication stress and preserves genome stability by promoting DNA repair and regulating cell cycle progression[20]. Tel1/ATM is known to be activated by DNA double strand breaks (DSBs), where it is recruited through the interaction with the MRX (Mre11-Rad50-Xrs2)/MRN (Mre11-Rad50-Nbs1) complex. Conversely, Mec1/ATR and its interactor Ddc2/ATRIP primarily recognize single stranded DNA (ssDNA) regions coated by the Replication Protein A (RPA) complex[20,129]. Once activated, Tel1/ATM and Mec1/ATR trigger a checkpoint that temporarily arrest cell cycle progression through the phosphorylation of the effector kinases Rad53/Chk2 and Chk1, whose activation requires the adaptors Rad9/53BP1 and Mrc1/Claspin[20,129]. Tel1/ATM also participates in DSB repair. DSBs can be repaired by directly re-joining together the two broken ends (non-homologous end joining or NHEJ), or by homologous recombination (HR), which is triggered by the nucleolytic degradation of the 5' DSB ends in a process called resection[17]. MRX/MRN together with the Sae2/CtIP protein initiates resection by catalyzing an endonucleolytic cleavage of the 5’ strands, and creating a substrate for the nucleases Exo1 and Dna2 that generate long 3’-ended ssDNA tails[316]. Once loaded to DSB ends, Tel1 assists MRX in initial resection[116] and also promotes proper MRX association at DSBs needed for maintaining DNA ends in close proximity, thus favouring both NHEJ and HR[317,318]. Besides regulating DSB response, Tel1/ATM has been implicated in the regulation of oxidative stress, mitotic spindle checkpoint and homeostasis of telomeres, the nucleoprotein structures that characterize the ends of eukaryotic chromosomes. In particular, Tel1 promotes telomere elongation by triggering the recruitment of telomerase enzyme at short telomeres[37]. Despite the multiple functions of Tel1 in DNA

damage and stress response, Tel1-deficient cells do not show obvious hypersensitivity to DNA damaging agents. However, recent studies reported that *tel1Δ* cells are sensitive to camptothecin (CPT)[99,317], which is an inhibitor of topoisomerase I currently used in cancer therapy. Topoisomerase I (Top1 in yeast) relaxes DNA supercoiling by nicking the DNA, enabling the broken strand to rotate around the Top1-bound DNA strand and finally re-ligating the breaks. CPT binding to the Top1-DNA intermediate delays the ligation reaction and blocks Top1 onto DNA, thus creating topological stress and a physical barrier to replication fork progression. Repair of Top1-mediated DNA damage requires the removal of the Top1-DNA intermediates, followed by the repair of DNA break and the restart of the replication fork, and involves multiple pathways, including the phosphodiesterase Tdp1, the endonucleases Rad1/Rad10, Slx1/Slx4, Mus81/Mms4, Rad27, and MRX together with Sae2, base excision repair and HR[38,208,209,319]. Recent works have challenged the classical model of CPT cytotoxicity, showing that in both yeast and mammals Top1 inhibition induces replication fork slowing down and reversal[151]. Reversed forks are four-way junctions generated by the annealing of the two newly synthesized strands and the concomitant re-annealing of the parental strands at a replication forks[117,148]. Although reversed forks have long been considered pathological structures generated in checkpoint-defective mutants[120], their recent observation in checkpoint proficient cells exposed to different stress have led to the model that they pause replication forks in a stable conformation, thus providing time for lesion removal and supporting replication restart[151,153]. Consistently, degradation of reversed forks by nucleases has been found to cause chromosome breakage and cell lethality, and is prevented by human FANC2, BRCA1 and BRCA2 proteins[161].

By investigating the molecular basis for the sensitivity to CPT of tel1 mutants, here we found that Tel1/ATM protects reversed replication forks from nucleolytic degradation by Mre11 in CPT. In fact, the lack of Tel1 reduces the amount of reversed forks in CPT and this reduction is caused by the Mre11 nuclease activity. Conversely, inactivation of

the replisome component Mrc1 prevents fork reversal in wild type, tel1 and mre11-H125N cells, and relieves the hypersensitivity to CPT of tel1 cells, indicating that fork reversal triggered by Mrc1 is detrimental in the absence of Tel1.

Tel1 specifically supports resistance to camptothecin

We further extended the previous observation that *tel1Δ* cells are hypersensitive to CPT[99,317] by showing that the lack of Tel1 decreased cell viability in the presence of CPT, but not in the presence of the alkylating agent methyl-methansulfonate (MMS), the DNA replication inhibitor hydroxyurea (HU) or the radiomimetic drug phleomycin (*Figure 11A*). Cell viability in the presence of CPT requires Tel1 kinase activity. In fact, cells carrying the *tel1-kd* allele causing the G2611D, D2612A, N2616K, and D2631E amino acid substitutions that abolishes Tel1 kinase activity in vitro[320] were as sensitive as *tel1Δ* cells to CPT, while they grew as wild type cells on MMS-, HU- and phleomycin-containing plates (*Figure 11A*). Furthermore, both *tel1Δ* and *tel1-kd* cells lost viability with similar kinetics compared to wild type when they were exposed to increasing CPT concentrations (*Figure 11B*). Altogether, these results indicate that Tel1 plays a specific and non-redundant function in counteracting the toxic effects of Top1 trapped on DNA through phosphorylation events.

As human ATM regulates Top1 turnover after Top1 removal from DNA[321], we asked whether Tel1 might regulate the levels of Top1 protein. Wild type and *tel1Δ* cells, both carrying a fully functional Top1-HA tagged version, were arrested in G_1 with α-factor and released in S phase in the presence of CPT. When similar amounts of protein extracts prepared at different time points from CPT addition were analyzed by Western blot, we detected similar Top1 levels in wild type and *tel1Δ* cells (*Figure 11C*), indicating that Tel1 does not control the amount of Top1. Furthermore, *TOP1* deletion completely relieved CPT hypersensitivity of *tel1Δ* cells (*Figure 11D*), indicating that Top1 poisoning is responsible for the hypersensitivity to CPT of *tel1* mutant cells.

Tel1 plays a role at telomeres, where it promotes the recruitment of telomerase and

telomere elongation independently of the Ku complex[282]. Besides exacerbating telomere shortening, the lack of either Ku70 or Ku80 subunit of the Ku complex also increases the sensitivity to CPT of *tel1Δ* cells[322] (*Figure 11E*). The hypersensitivity to CPT of *tel1Δ ku70Δ* double mutant cells can be partially rescued by the expression of a *CDC13-EST1* gene fusion, which is known to induce telomere elongation in *tel1Δ* or *ku70Δ* mutants[322], suggesting that telomere elongation protects the ends of chromosomes from CPT-induced damage. If the sensitivity to CPT of *tel1Δ* cells is due the short telomeres, restoration of telomere length in *tel1Δ* cells by *CDC13-EST1* expression should attenuate the sensitivity to CPT of these cells. We found that a plasmid carrying the *CDC13-EST1* fusion[323] suppressed the hypersensitivity to CPT of both *tel1Δ ku70Δ*, as expected[322], and *ku70Δ* single mutant cells, while was unable to attenuate the sensitivity to CPT of *tel1Δ* cells (*Figure 11E*), indicating that the hypersensitivity to CPT of *tel1Δ* cells is not due to telomere shortening.

Tel1 is recruited to DSBs by the MRX complex[32], which acts together with Tel1 in promoting DSB resection, with MRX playing the major role[116]. Consistent with a more severe repair defect observed upon MRX than Tel1 inactivation[116,317], cells lacking the Mre11 subunit of MRX were more sensitive to CPT than *tel1Δ* cells (*Figure 11F* and *G*). Furthermore, *TEL1* deletion did not increase the CPT hypersensitivity of *mre11Δ* cells (*Figure 11F* and *G*), strongly suggesting that Tel1 and MRX act in the same pathway also to support CPT resistance.

The collision between replication forks and Top1-DNA intermediates has been proposed to generate DSBs, which require resection to be repaired by HR[316]. As the lack of Tel1 causes a slight resection defect[116] and the integrity of the resection machinery is important to maintain cell viability in CPT[316] Tel1 might promote CPT resistance by initiating resection of CPT-induced DSBs. If this were the case, the hypersensitivity to CPT of *tel1Δ* cells should be suppressed by elevated levels of the exonuclease Exo1, which restore DSB resection in *tel1Δ* cells[116] and partially suppress both the resection defects and the hypersensitivity to genotoxic agents of *sae2Δ* and *mre11Δ* cells[97,324].

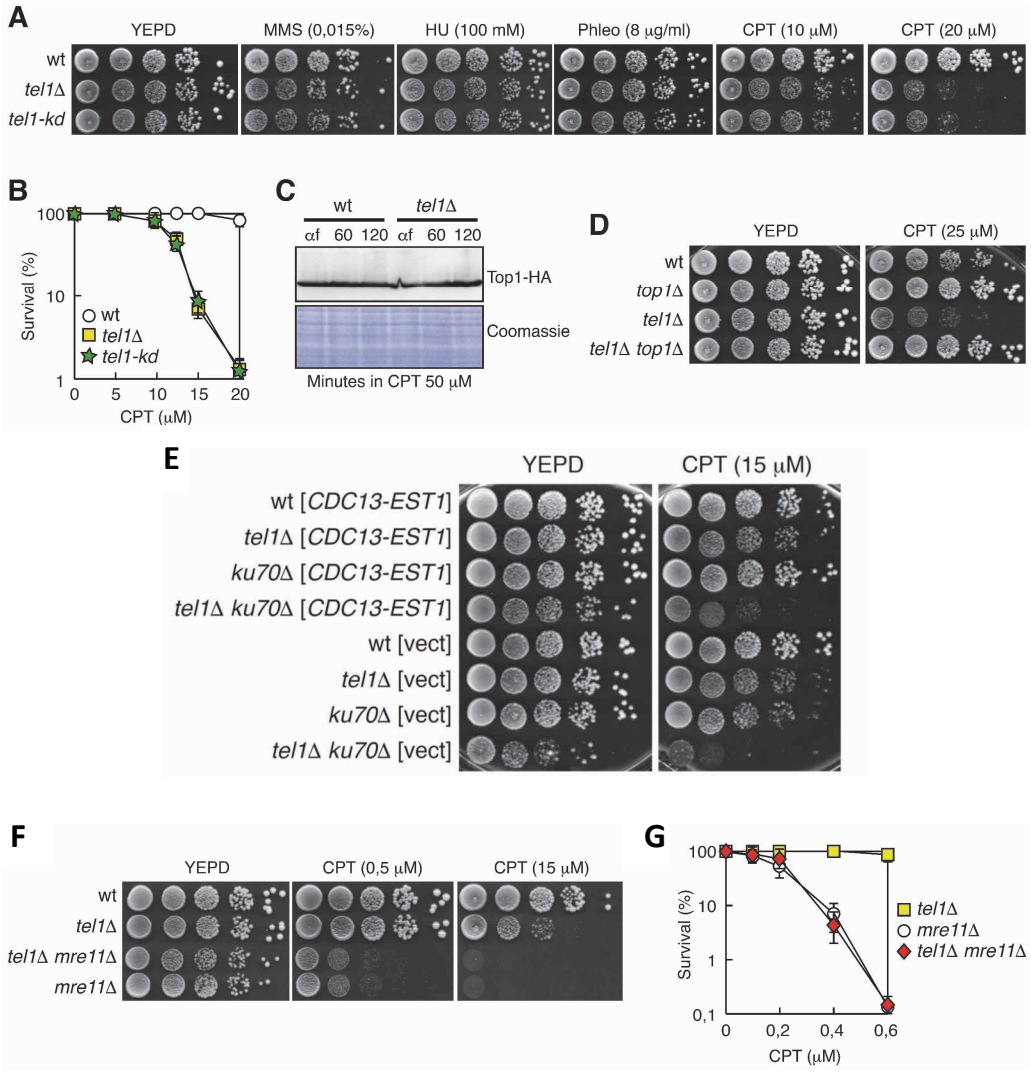

Figure 11 - The lack of Tel1 causes a specific hypersensitivity to CPT. A,D,F*. Exponentially growing cell cultures were serially diluted (1:10) before being spotted out onto YEPD plates with or without methyl methanesulfonalte (MMS), hydroxyurea (HU), phleomycin (Phleo) or camptothecin (CPT) at the indicated concentrations.* ***B,G****. Appropriate dilutions of cell cultures were distributed on YEPD plates with or without different concentrations of CPT. Plates were incubated 3 days at 25°C to determine the colony-forming units. Plotted values are the mean values with error bars denoting SD (n = 3).* ***C****. Wild type and tel1Δ strains expressing a fully functional Top1-HA tagged protein were arrested in G_1 with α-factor (αf) and released into YEPD supplemented with CPT (50 µM). Western blot with anti-HA antibodies (top) and Coomassie staining (bottom) of protein extracts prepared at the indicated time points.* ***E****. Exponentially growing cell cultures of wild type and isogenic tel1Δ, ku70Δ and tel1Δ ku70Δ strains, all transformed with a centromeric plasmid either empty (vect) or carrying the CDC13-EST1 gene fusion, were serially diluted (1:10) before being spotted out onto YEPD plates with or without CPT.*

Therefore, a 2µ plasmid either carrying the EXO1 gene or empty was transformed into wild type, *tel1Δ* or *sae2Δ* cells as a control. As expected, the 2µ EXO1 plasmid partially suppressed the hypersensitivity to CPT of *sae2Δ* cells (*Figure 12A*). Conversely, it did not restore CPT resistance in *tel1Δ* cells (*Figure 12A*), strongly suggesting that a resection defects is unlikely to be the cause of the CPT hypersensitivity of *tel1Δ* cells. This conclusion is supported by the findings that the kinase activity of Tel1 is required to maintain cell viability in CPT (*Figure 11A* and *B*) but not for resection and DSB repair[325].

As *tel1Δ* cells are hypersensitive to CPT, but not to other genotoxic treatments that cause DSBs (*Figure 11A*), Tel1 might prevent conversion of Top1-DNA intermediates into DSBs. These intermediates can be removed by redundant pathways (Tdp1, Rad1/Rad10, Slx1/Slx4, Mus81/Mms4, and Rad27), whose action creates single-strand breaks and/or single-strand gaps that are mainly repaired by recombination[326]. To investigate whether Tel1 belongs to either the Tdp1 or one endonuclease pathway, we performed epistasis analyses by combining *TEL1* deletion with deletions of genes involved in these pathways and analyzing the sensitivity to CPT of the resulting double mutants compared to single mutants. The lack of Tel1 increased the hypersensitivity to CPT of *slx4Δ* (*Figure 12B*), *rad27Δ* (*Figure 12C*), and *mms4Δ* (*Figure 12D*), indicating that Tel1 supports cell viability in CPT by acting in a pathway that is different from those involving the above genes. Recombination is required to complete the repair of Top1-induced DNA damage after Top1 removal[208], and the deletion of the master recombination gene *RAD52* causes a very strong sensitivity to CPT[319] (*Figure 12E*). Strikingly, the absence of Tel1 further increased the hypersensitivity to CPT of *rad52Δ* cells (*Figure 12E*), indicating that Tel1 participates in the cellular response to CPT independently of recombination pathways.

The lack of either Tdp1 or Rad1, which caused very mild sensitivity only to high CPT doses, did not increase the hypersensitivity to CPT of *tel1Δ* cells (*Figure 12F*). As both *tel1Δ* and *rad1Δ tdp1Δ* cells (*Figure 12F*)[208,209,319] were more sensitive to CPT than either

rad1Δ or *tdp1Δ* single mutant cells, Tel1 might control both the Tdp1- and the Rad1-dependent pathways, which are known to induce the removal of Top1-DNA intermediates in a redundant manner[38,208,319]. However, *tel1Δ* cells were less sensitive to CPT than *rad1Δ tdp1Δ* double mutant cells (*Figure 12F*), whose hypersensitivity was not further increased by the lack of Tel1 (*Figure 12F* and *G*).

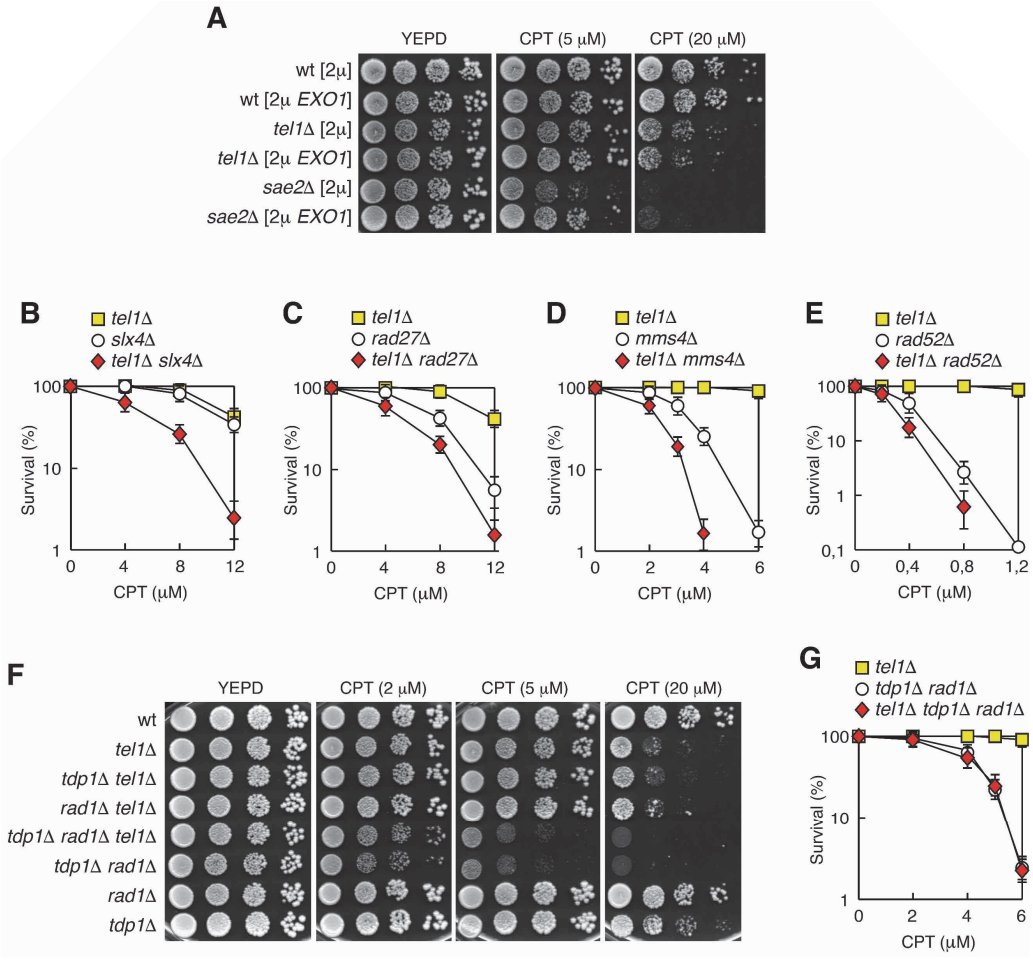

Figure 12 - The lack of Tel1 increases the hypersensitivity to CPT of repair mutants. A*. Exponentially growing cell cultures were serially diluted (1:10) before being spotted out onto YEPD plates with or without CPT at the indicated concentrations. 2μ, multicopy empty vector.* ***B-E,G****. Colony-forming units on YEPD plates with or without different concentrations of CPT. Plates were incubated 3 days at 25°C to determine the colony-forming units. Plotted values are the mean values with error bars denoting SD (n = 3).* ***F****. Exponentially growing cell cultures were serially diluted (1:10) before being spotted out onto YEPD plates with or without CPT at the indicated concentrations.*

These genetic interactions suggest that Tel1 does not simply promote the action of Tdp1 and Rad1/Rad10. Rather, Top1 removal by these two pathways appears important to allow Tel1 action at Top1-induced DNA damage.

Tel1 counteracts the activation of a Mec1-dependent checkpoint in CPT

Tel1 might support cell survival to CPT treatment by activating a checkpoint response that temporarily arrests the cell cycle, and its absence might allow cell cycle progression in the presence of Top1-DNA intermediates that can be converted into more toxic DNA damage. Alternatively, Tel1 may counteract the accumulation of CPT-induced damage through an unknown pathway, and its absence could cause prolonged checkpoint activation due to persistence of CPT-induced checkpoint signals. To distinguish between these possibilities, we analyzed checkpoint activation in wild type, *tel1Δ* and *tel1-kd* cells arrested in G_1 with α-factor and released either in the presence or in the absence of CPT. Cell cycle progression was monitored by evaluating DNA content at different time points by fluorescence-activated cell sorting (FACS) and nuclear division by fluorescence microscopy. Furthermore, Rad53 phosphorylation, which is used as a marker of checkpoint activation and reduces the electrophoretic mobility of the protein[51], was analyzed by Western blot. Consistent with the finding that CPT delays nuclear division without affecting bulk DNA replication[327], CPT-treated and untreated wild type cells completed DNA replication with similar kinetics (*Figure 13A*), whereas nuclear division in CPT-treated wild type cells took place 30 minutes later than in untreated cells (*Figure 13B*). Conversely, CPT-treated *tel1Δ* and *tel1-kd* cells arrested with 2C DNA content (*Figure 13A*) and undivided nuclei (*Figure 13B*). This cell cycle arrest correlated with hyperphosphorylation of the checkpoint kinase Rad53, which accumulated as slowly-migrating phosphorylated forms in CPT-treated *tel1Δ* and *tel1-kd* cells, while only a mild reduction of Rad53 electrophoretic mobility can be detected in wild type cells (*Figure 13C*). Furthermore, Rad53 phosphorylation persisted longer in *tel1Δ* cells than in wild type after a transient CPT treatment (*Figure 13D*).

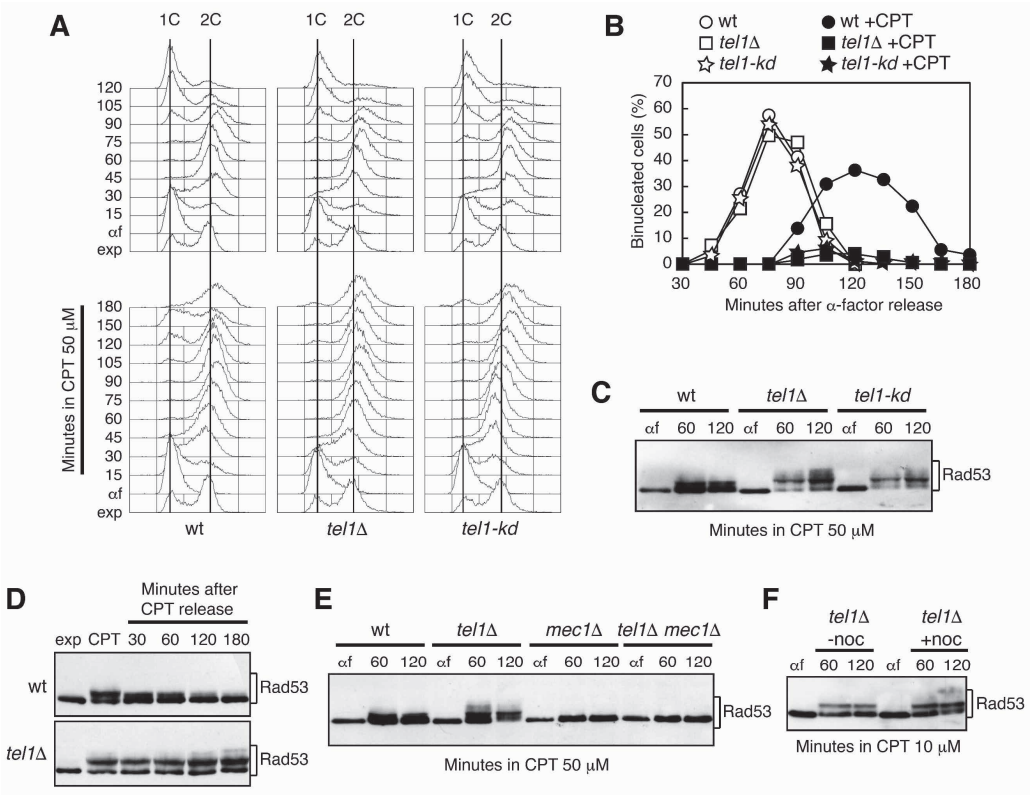

Figure 13 - CPT triggers the hyperactivation of a Mec1-dependent checkpoint in the absence of Tel1. A-C*. Exponentially growing cell cultures (exp) were arrested in G_1 with α-factor (αf) and released into YEPD with or without CPT (50 μM). Cell samples were harvested at the indicated time points to evaluate DNA contents by flow cytometry (**A**), nuclear division by fluorescence microscopy (**B**) and Rad53 phosphorylation by Western blot with anti-Rad53 antibodies (**C**). **D**. Exponentially growing cell cultures (exp) were treated with CPT (50 μM) for 1 hour, before being released in fresh medium without CPT. Western blot analysis with anti-Rad53 antibodies of protein extracts prepared at the indicated time points. **E-F.** G_1-arrested cell cultures (αf) were released in YEPD supplemented with CPT (50 μM) (E) or in YEPD supplemented with CPT (10 μM) with (+noc) or without (-noc) nocodazole (**F**). Western blot analysis with anti-Rad53 antibodies.*

Rad53 phosphorylation in CPT-treated *tel1Δ* cells depends on the checkpoint kinase Mec1. In fact, it was abolished in both CPT-treated *mec1Δ* and *tel1Δ mec1Δ* cells (*Figure 13E*), which were kept viable by the lack of the ribonucleotide reductase inhibitor Sml1[328]. On the contrary, treatment with the microtubule-depolimerizing drug nocodazole did not reduce Rad53 hyperphosphorylation in CPT-treated *tel1Δ* cells (*Figure 13F*). This result indicates that the signals activating Mec1 in these cells are not generated by the attempt to separate sister chromatids with trapped Top1.

Altogether, these findings indicate that Tel1 is not required to activate the checkpoint upon CPT treatment. Rather, a Mec1-dependent checkpoint is hyperactivated in CPT-treated *tel1* cells, suggesting that CPT-induced lesions persist longer in *tel1* mutants than in wild type cells. As ssDNA is proposed to be the signal for Mec1 activation[45], Tel1 might counteract the accumulation of ssDNA after Top1 inhibition.

The lack of Mrc1 suppresses the sensitivity to CPT of *tel1Δ* cells

Mec1 activates both the DNA replication checkpoint and the DNA damage checkpoint, which require respectively the mediators Mrc1 and Rad9 to phosphorylate and activate Rad53[129]. So, we have investigated whether the Mec1-dependent checkpoint hyperactivated in CPT-treated *tel1Δ* cells require Mrc1 or Rad9.

Activation of the CPT-induced checkpoint in the presence of Tel1 is almost completely Rad9-dependent. In fact, wild type and *mrc1Δ* cells showed similar CPT-induced Rad53 phosphorylation, which was instead almost abolished in *rad9Δ* cells (*Figure 14A* and *B*). Conversely, both Rad9 and Mrc1 appear to participate in checkpoint activation in the absence of Tel1, as the lack of either Mrc1 or Rad9 reduced Rad53 phosphorylation (*Figure 14A* and *B*) and allowed nuclear division (*Figure 14C*) in CPT-treated *tel1Δ* cells, with *RAD9* deletion showing the strongest effect. We can conclude that, while the CPT-induced checkpoint in wild type cells is almost completely Rad9-dependent, both Rad9 and Mrc1 appear to participate in checkpoint activation in the absence of Tel1. The lack of Rad9, which strongly reduced checkpoint activation in CPT-treated *tel1Δ* cells (*Figure 14A-C*), slightly increased the CPT hypersensitivity of the same cells (*Figure 14D*), suggesting that a Rad9-dependent DNA damage checkpoint supports cell survival both in the presence and in the absence of Tel1 by delaying progression through mitosis. Strikingly, *tel1Δ mrc1Δ* double mutant cells were less sensitive to CPT than *tel1Δ* cells and lost viability only at high CPT doses, similar to *mrc1Δ* cells (*Figure 14D* and *E*), indicating that *MRC1* deletion is epistatic to *TEL1* deletion for CPT sensitivity.

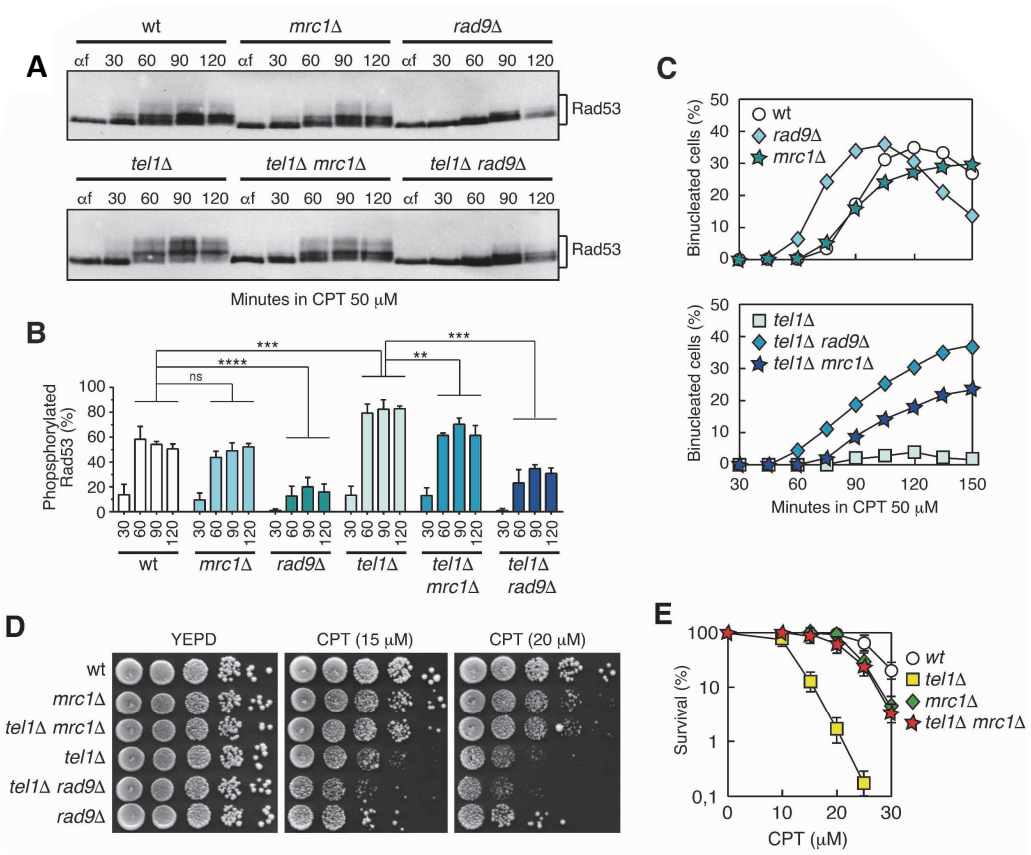

Figure 14 - Mrc1 inactivation restores CPT resistance in the absence of Tel1. A-C*. Exponentially growing cell cultures were arrested in G_1 with α-factor (αf) and released in YEPD supplemented with CPT (50 μM). (**A**) Western blot analysis with anti-Rad53 antibodies. (**B**) Quantitative analysis of Rad53 phosphorylation was performed by calculating the ratio of band intensities for slowly-migrating bands to the total amount of protein. Plotted values are the mean values with error bars denoting SD (n = 3). Statistical analysis: Student's t-test.; ns, not significant; **, P< 0.01; ***, P< 0.001; ****, P< 0.0001. (**C**) Nuclear division determined by florescence microscopy. **D**. Exponentially growing cell cultures were serially diluted (1:10) before being spotted out onto YEPD plates with or without CPT at the indicated concentrations. **E.** Cells were distributed on YEPD plates with or without CPT at different concentrations to determine colony-forming units after 3 days at 25°C. Plotted values are the mean values with error bars denoting SD (n = 3).*

Mrc1 forms a complex with both Tof1 and Csm3 that, together with Mrc1, promote checkpoint activation and support DNA replication in untreated and stressed conditions[64]. These three proteins play also independent functions, as Mrc1 exerts a major role in promoting both checkpoint activation and fast DNA replication in untreated conditions, while only Tof1 and Csm3 are critical for replication fork pausing

at the ribosomal DNA locus[64,68,329]. Tof1 and Csm3 play also a major role compared to Mrc1 in supporting cell viability upon CPT treatment. In fact, the lack of either Tof1 or Csm3 caused a strong sensitivity to CPT.

Moreover, the lack of Tof1 or Csm3, exacerbated the CPT sensitivity of *tel1Δ* cells (*Figure 15A*). Therefore, the absence of Mrc1, but not of Csm3 or Tof1, relieves the CPT hypersensitivity caused by the lack of Tel1. Furthermore, suppression of the CPT hypersensitivity by the lack of Mrc1 is specific for *tel1Δ* cells, as *MRC1* deletion did not suppress, but rather increased, the CPT hypersensitivity of *rad27Δ*, *sae2Δ* and *tdp1Δ rad1Δ* cells (*Figure 15B-D*). Altogether, these results indicate that Mrc1 action is detrimental when Top1 is inhibited in the absence of Tel1.

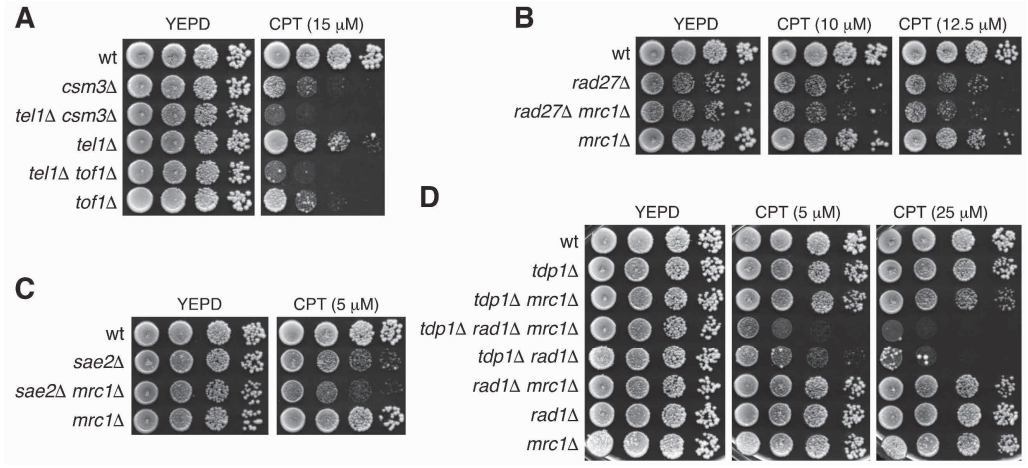

Figure 15 - The hypersensitivity to CPT of tel1Δ cells is specifically relieved by MRC1 deletion. *Exponentially growing cell cultures were serially diluted (1:10) before being spotted out onto YEPD plates with or without CPT at the indicated concentrations.*

The lack of Mrc1 DNA replication function relieves hypersensitivity and checkpoint hyperactivation of CPT-treated *tel1Δ* cells

As Mrc1 promotes checkpoint activation and supports unperturbed DNA replication[65,68], we asked which of these Mrc1 functions are detrimental in *tel1Δ* cells

treated with CPT. These two Mrc1 functions are genetically separable. In fact, the *mrc1-AQ* allele, which abolishes the Mec1-dependent phosphorylation of Mrc1, causes checkpoint defects without affecting unperturbed replication. Conversely, cells expressing the *mrc1-C15* allele, which cause C-terminal truncations of 193 amino acids, are checkpoint proficient but replicate their DNA as slowly as *mrc1Δ* cells[65,68,330]. *tel1Δ mrc1-AQ* cells were as sensitive as *tel1Δ* cells to CPT (*Figure 16A*), and both these strains hyperactivated the CPT-induced checkpoint compared to wild type and *mrc1-AQ* cells (*Figure 16B* and *C*). Therefore, the lack of the Mrc1 checkpoint function does not alleviate the defects of *tel1Δ* cells in CPT, indicating that the lethality of *tel1Δ* cells in CPT is not caused by the hyperactivation of the replication checkpoint.

By contrast, *mrc1-C15* allele completely relieved the sensitivity to CPT of *tel1Δ* cells (*Figure 16A*), and reduced Rad53 hyperphosphorylation (*Figure 16D*) and allowing nuclear division in CPT-treated *tel1Δ* cells (*Figure 16E*). Thus, Mrc1 replication function, but not its checkpoint function, is responsible for the hypersensitivity of *tel1Δ* cells to Top1 inhibition.

MRC1 deletion was proposed to suppress the hypersensitivity to MMS and CPT of cells lacking the ubiquitin ligase component Rtt107 by increasing origin firing[331]. We asked whether increasing origin firing is sufficient to alleviate the hypersensitivity to CPT of *tel1Δ* cells. We combined *TEL1* deletion with the deletion of the histone deacetylase-encoding gene *RPD3*, whose lack causes a precocious late-origin firing[332]. Rpd3 inactivation increased the sensitivity to CPT of *tel1Δ* cells (*Figure 16F*), strongly suggesting that the hypersensitivity of *tel1Δ* cells can not be suppressed simply by increasing origin firing. According to these findings, the lack of Tel1 increased CPT hypersensitivity of *rtt107Δ* cells (*Figure 16G*), indicating that Tel1 and Rtt107 play different functions in CPT resistance.

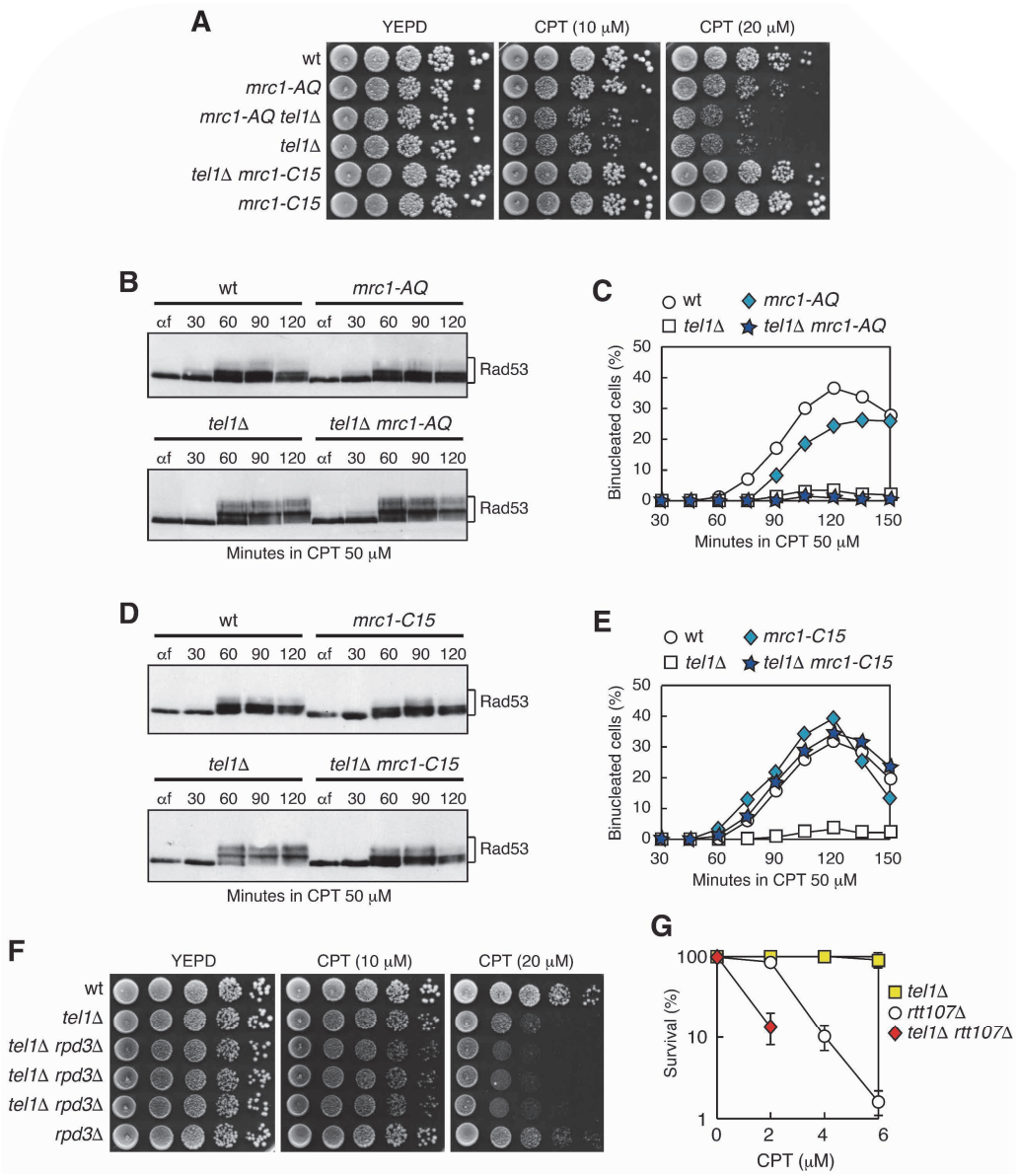

Figure 16 - The lack of Mrc1 function in DNA replication restores CPT resistance in the absence of Tel1. ***A,F****. Exponentially growing cell cultures were serially diluted (1:10) before being spotted out onto YEPD plates with or without CPT at the indicated concentrations.* ***B-E****. G_1-arrested cell cultures (αf) were released in YEPD supplemented with CPT (50 μM). Sample collected at the indicated time points were subjected to Western blot analysis with anti-Rad53 antibodies (**B,D**) or stained with propidium iodide to analyze the kinetics of nuclear division (**C,E**).* ***G****. Colony-forming units on YEPD plates with or without CPT at different concentrations. Plates were incubated 3 days at 25°C. Plotted values are the mean values with error bars denoting SD (n = 3).*

Tel1 counteracts Mre11-mediated degradation of CPT-induced reversed forks

The lack of Tel1 increases the hypersensitivity to CPT of DNA repair mutants (*Figure 12*) suggesting that Tel1 prevents the conversion of Top1-DNA intermediates into DNA lesions. Furthermore, the findings that the hypersensitivity to CPT of *tel1Δ* cells is completely suppressed by the lack of the Mrc1 replication function (*Figure 16*) suggest that the Tel1 function in supporting cell viability in CPT is linked to DNA replication.

Top1 inhibition by CPT slows down replication fork progression and causes reversal of a significant percentage of replication forks in both yeast and mammals[151]. Importantly, Top1 inhibition is the only genotoxic treatment, among those tested (HU, UV, MMS), to be reported to induce frequent fork reversal in checkpoint proficient *S. cerevisiae* cells[120,149,151], providing a hint towards the specific CPT sensitivity observed in *tel1Δ* cells. We directly visualized fork architecture by *in vivo* psoralen crosslinking and electron microscopy (EM) in wild type and *tel1Δ* cells synchronously released from an α-factor arrest into S-phase in the presence of CPT (*Figure 18A and B*). Reversed forks appeared as replication forks with a regressed arm forming a four-way junction (*Figure 17A*). As expected[151], about 20% of replication forks reversed in CPT-treated wild type cells (*Figure 17B* and *C*). Their frequency was 2-fold decreased in the absence of Tel1 (*Figure 17B* and *C*, and *Figure 18C*), suggesting that Tel1 promotes formation or stability of CPT-induced reversed forks.

Nucleolytic degradation of reversed forks was observed in both yeast and mammals[161,333]. Thus, Tel1 might counteract nuclease action at reversed forks, thereby limiting Mec1 activation upon CPT treatment. We then directly visualized fork reversal by EM in CPT-treated wild type and *tel1Δ* cells optionally carrying the *EXO1* deletion or the *mre11-H125N* allele, which abolishes Mre11 nuclease activity without affecting checkpoint activation and MRX recruitment to DNA[21,334] (*Figure 17B* and *C*). Both Exo1 and MRX nuclease activity turned out to be dispensable for fork reversal. In fact, both CPT-treated *exo1Δ* and *mre11-H125N* cells showed wild type levels of reversed forks.

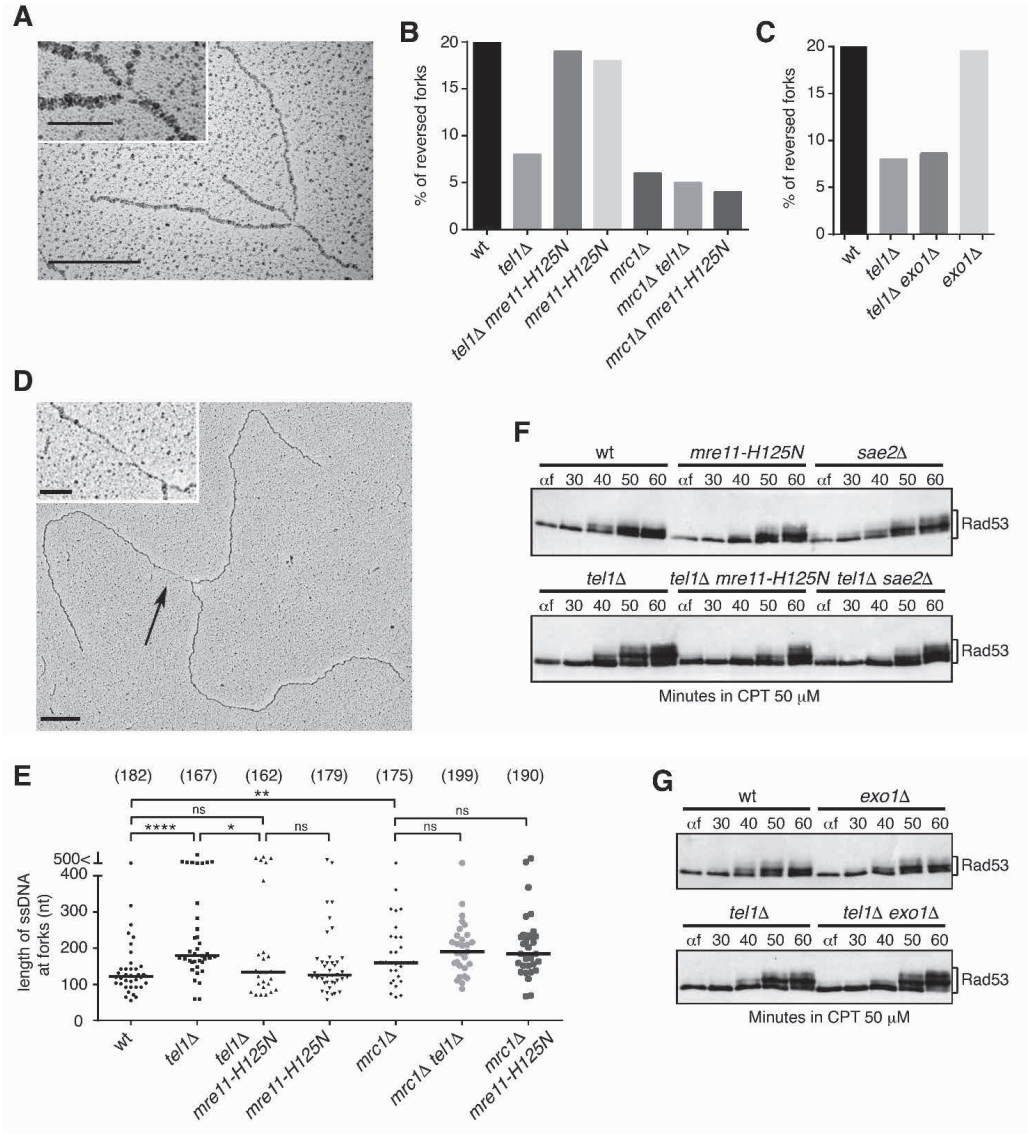

Figure 17 - The lack of Tel1 allows Mre11-dependent degradation of reversed forks in CPT-treated cells. ***A-E****. G_1-arrested cell cultures were released in YEPD supplemented with CPT (50 μM). (**A,D**) Electron micrographs of a representative reversed fork with the four-way junction magnified in the inset (**A**) and a three-way replication fork exposing ssDNA at the junction (**D**). In (**D**) the black arrow indicates the ssDNA region, which is magnified in the inset. Scale bars: 200nm, 50nm in the insets. (**B,C**) Frequency of reversed replication forks in CPT (40 minutes, 50 μM CPT). Two independent experiments were performed with very similar results. The results of the individual biological replicates and the number of analyzed molecules are shown in Fig EV4C. (**E**) Graphical distribution of ssDNA length at the junction (black arrow in (**D**)) in forks isolated after CPT treatment (40 minutes, 50 μM CPT). Only molecules with detectable ssDNA stretches are included in the analysis. The lines show the median length of ssDNA regions at the fork in the specific set of analyzed molecules. Statistical analysis: Mann-Whitney test; ns, not significant; **, P< 0.01; ***, P< 0.001; ****, P< 0.0001. The number of analyzed molecules is in brackets.* ***F-G.*** *G_1-arrested cell cultures (αf) were released into YEPD supplemented with CPT (50 μM). Western blot analysis with anti-Rad53 antibodies.*

Remarkably, the *mre11-H125N* mutation restored wild type amount of fork reversal even in *tel1Δ* cells (*Figure 17B*), while we observed very similar frequencies of reversed forks in *exo1Δ* and *exo1Δ tel1Δ* cells (*Figure 17C*). These results strongly suggest that decreased reversed fork levels in the absence of Tel1 are due to unscheduled nucleolytic processing that depends mainly on Mre11. In line with unscheduled Mre11-dependent fork processing, *tel1Δ* cells showed extended ssDNA stretches at replication forks (*Figure 17D* and *E*) compared to wild type cells. This phenotype was fully suppressed by the lack of Mre11 nuclease activity (*mre11-H125N*; *Figure 17E*). As ssDNA was proposed to trigger Mec1 activation[45], this unscheduled nucleolytic processing could also account for checkpoint hyperactivation in CPT-treated *tel1Δ* cells. Indeed, *TEL1* deletion in *mre11-H125N* cells did not lead to the same extent of CPT-induced Rad53 hyperphosphorylation observed when Mre11 is functional (*Figure 17F*). A similar decrease of Rad53 phosphorylation was observed upon inactivation of Sae2 (*Figure 17F*), which stimulates Mre11 nuclease activity but not its recruitment to DNA ends[21,96,98]. Conversely, the lack of Exo1, which did not restore fork reversal in the absence of Tel1 (*Figure 17C*), did not affect Rad53 phosphorylation in CPT-treated wild type or *tel1Δ* cells (*Figure 17G*). Thus, MRX likely generates long ssDNA stretches at replication intermediates in the absence of Tel1. This fork degradation seems to primarily target reversed replication forks and to be responsible for checkpoint hyperactivation in CPT-treated *tel1Δ* cells.

Mrc1-dependent fork reversal triggers fork degradation in CPT-treated *tel1Δ* cells

Recent reports in metazoan show that preventing fork reversal by inactivating fork remodeling enzymes suppresses unscheduled MRE11-dependent fork degradation in BRCA1- or BRCA2-defective cells[163,333,335]. We asked whether a similar mechanism could underlie the suppression of CPT hypersensitivity by Mrc1 inactivation in *tel1Δ* cells

(*Figure 14*). EM analysis upon CPT treatment revealed that reversed fork levels were markedly reduced by *MRC1* deletion, both in the presence and in the absence of Tel1, and regardless of Mre11 nuclease activity (*Figure 17B*). Thus, Mrc1 likely works upstream of Tel1 and Mre11, promoting CPT-induced fork reversal and thereby generating the structures that are then targeted by Tel1 and/or Mre11, in agreement with the epistatic relationship observed for CPT sensitivity (*Figure 14D* and *E*).

As for other genetic perturbations that impair fork reversal[153], in *mrc1Δ* cells we observed long replication fork-associated ssDNA stretches (*Figure 17E*), which were not reduced by the lack of Mre11 nuclease activity (*Figure 17E*). Therefore, this ssDNA likely foregoes Mrc1-mediated fork reversal and could be generated by uncoupled activities at the replication fork in the absence of Mrc1. Whether the lack of Mrc1 causes uncoupling between helicase and polymerase activity is still unclear[64,140]. However, recent work showed that the checkpoint kinase Rad53, which requires Mrc1 to be fully activated upon replication stress[129], couples leading- and lagging-strand synthesis in these conditions[336]. This finding, together with the observation that Mrc1 directly increases the rate of leading-strand synthesis[329], suggest that *mrc1Δ* cells accumulate ssDNA on the under-replicated leading-strand template.

While Mrc1 inactivation relieved the hypersensitivity to CPT of *tel1Δ* cells (*Figure 14D* and *E*), it was unable to suppress CPT sensitivity of *mre11-H125N* cells (*Figure 18D*). Furthermore, both *tel1Δ mre11-H125N* and *tel1Δ sae2Δ* double mutants were more sensitive to CPT than *tel1Δ* cells (*Figure 18E and F*). This is expected, as Mre11 cleaves DNA ends that are covalently linked by Top1[38,337], and Sae2 participates in DSB processing and repair together with MRX[316]. Thus, the CPT hypersensitivity caused by either the *mre11-H125N* or *sae2Δ* alleles is likely due to repair defects rather than to abnormal fork metabolism. Our results indicate that, besides being involved in later steps of CPT-induced damage repair, the MRX nuclease activity processes reversed forks and generates ssDNA in CPT-treated *tel1Δ* cells.

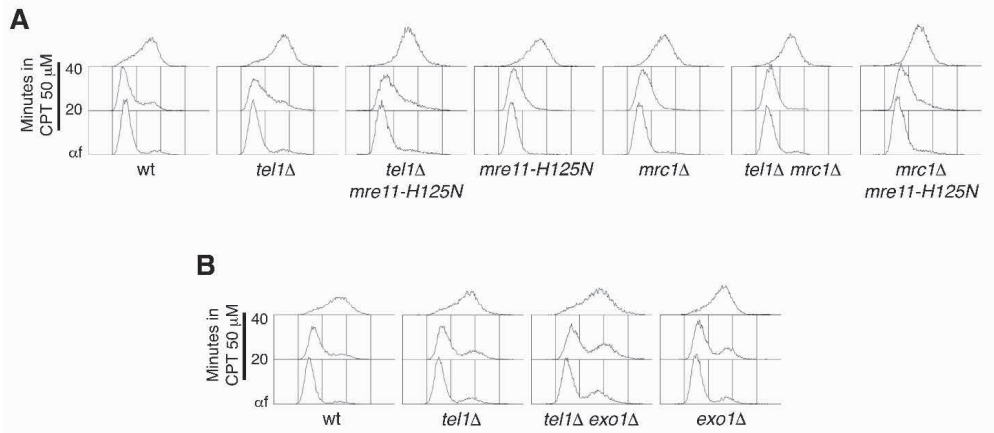

C

	wt	*tel1Δ*	*tel1Δ mre11-H125N*	*mre11-H125N*	*mrc1Δ*	*tel1Δ mrc1Δ*	*mrc1Δ mre11-H125N*
CPT	+	+	+	+	+	+	+
Exp1	21 (75)	8 (93)	19 (72)	18 (70)	6 (81)	5 (86)	4 (81)
Exp2	18 (107)	10 (74)	21 (90)	17 (109)	4 (94)	4 (113)	4 (109)

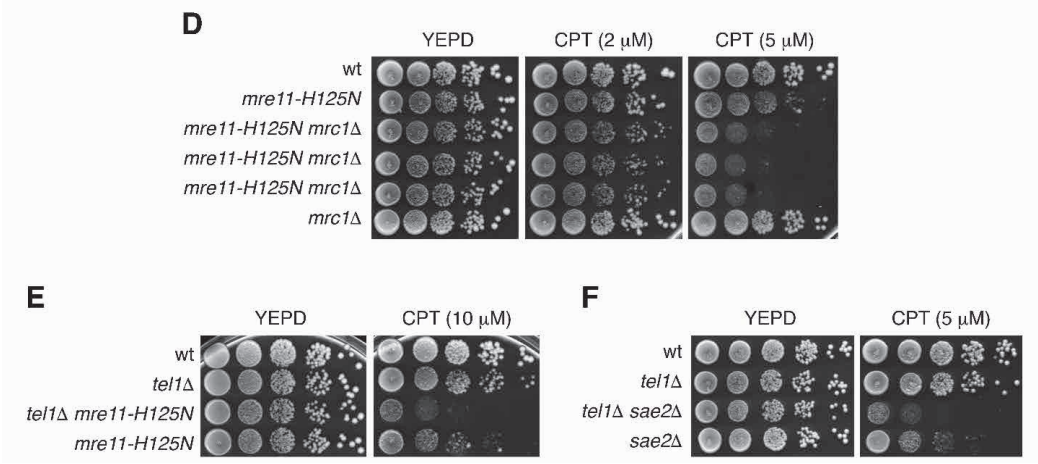

Figure 18 - The lack of Mre11 nuclease activity increases fork reversal but not CPT resistance in tel1Δ cells. ***A-C.*** *G_1-arrested cultures of the indicated strains (αf) were released into YEPD with or without CPT (50 μM).* (***A,B***) *FACS analysis of DNA content.* (***C***) *Cells collected 40 minutes after α-factor release were subjected to psoralen crosslinking before genomic DNA extraction and enrichment in replication intermediates. Replication intermediates were visualized by electron microscopy. Reversed forks frequencies (%) evaluated in two different experiments are reported. The number of analyzed replication intermediates is in brackets.* ***D-F****. Exponentially growing cell cultures were serially diluted (1:10) before being spotted out onto YEPD plates with or without CPT at the indicated concentrations.*

[IN PREPARATION]

Tel1/ATM contributes to replicative senescence in the absence of telomerase by signaling to the checkpoint

Luca Menin, Giorgia Maestrini, Maria Pia Longhese* and Michela Clerici*

Dipartimento di Biotecnologie e Bioscienze, Università di Milano-Bicocca, 20126 Milano, Italy

* Corresponding Authors:
michela.clerici@unimib.it; Tel: +39 0264483547; Fax: +39 0264483565.
mariapia.longhese@unimib.it; Tel: +39 0264483425; Fax: +39 0264483565.

tel1Δ and *TEL1-hy184* alleles exert opposite effect on the onset of replicative senescence in telomerase-negative cells

Tel1 is recruited at short telomeres in telomerase-deficient cells[282,304] and promotes replicative senescence[50,302,304]. However, the molecular mechanism by which Tel1 promotes senescence is still unknown. To investigate the function of Tel1 in promoting replicative senescence we took advantage on hyperactive *TEL1-hy* mutant alleles that partially relieve both the hypersensitivity to genotoxic agents and the checkpoint defects of cells lacking the checkpoint kinase Mec1[338]. Most of these alleles also cause telomere over-elongation compared to wild type cells and generates Tel1 protein variants with an increased intrinsic kinase activity compared to wild type Tel1[338]. For this study we focused on the *TEL1-hy184* allele, which causes the F1752I, D1985N, E2133K, R2735G, E2737V amino acid substitutions. This allele restores Rad53 phosphorylation in *mec1Δ* cells more efficiently than other *TEL1-hy* alleles, while it increases only slightly telomere length and produces a Tel1 protein variant with an intrinsic kinase activity a bit higher to that of wild type Tel1[338]. We assayed the effect of *TEL1-hy184* and *tel1Δ* alleles on the onset of the proliferative decline in the absence of telomerase by performing standard senescence assay in liquid medium in cells lacking the Est2 telomerase subunit. To this purpose we derived from the meiotic products of heterozygous *EST2*/*est2Δ TEL1*/*TEL1-hy184* and *EST2*/*est2Δ TEL1*/*tel1Δ* diploids multiple *est2Δ*, *est2Δ TEL1-hy184* and *est2Δ tel1Δ* spore clones, as well as wild type, *TEL1-hy184* and *tel1Δ* cells, which were inoculated in liquid rich medium at 30°C. Every 24 hours we determined cell concentration and corresponding population doublings (PDs) to record cell growth as a function of PDs, and we collected samples to determine cell viability before diluting cell cultures to the starting concentration of 5 x 10^4 cell/mL (*Figure 19A*). *est2Δ* cells showed the expected senescence phenotype with a gradual reduction of cell density starting from around 50 PDs until they reach the minimum cell density at around 67 PDs, followed by the accumulation of survivors and the restoration of near wild type growth capacity[293] (*Figure 19B*).

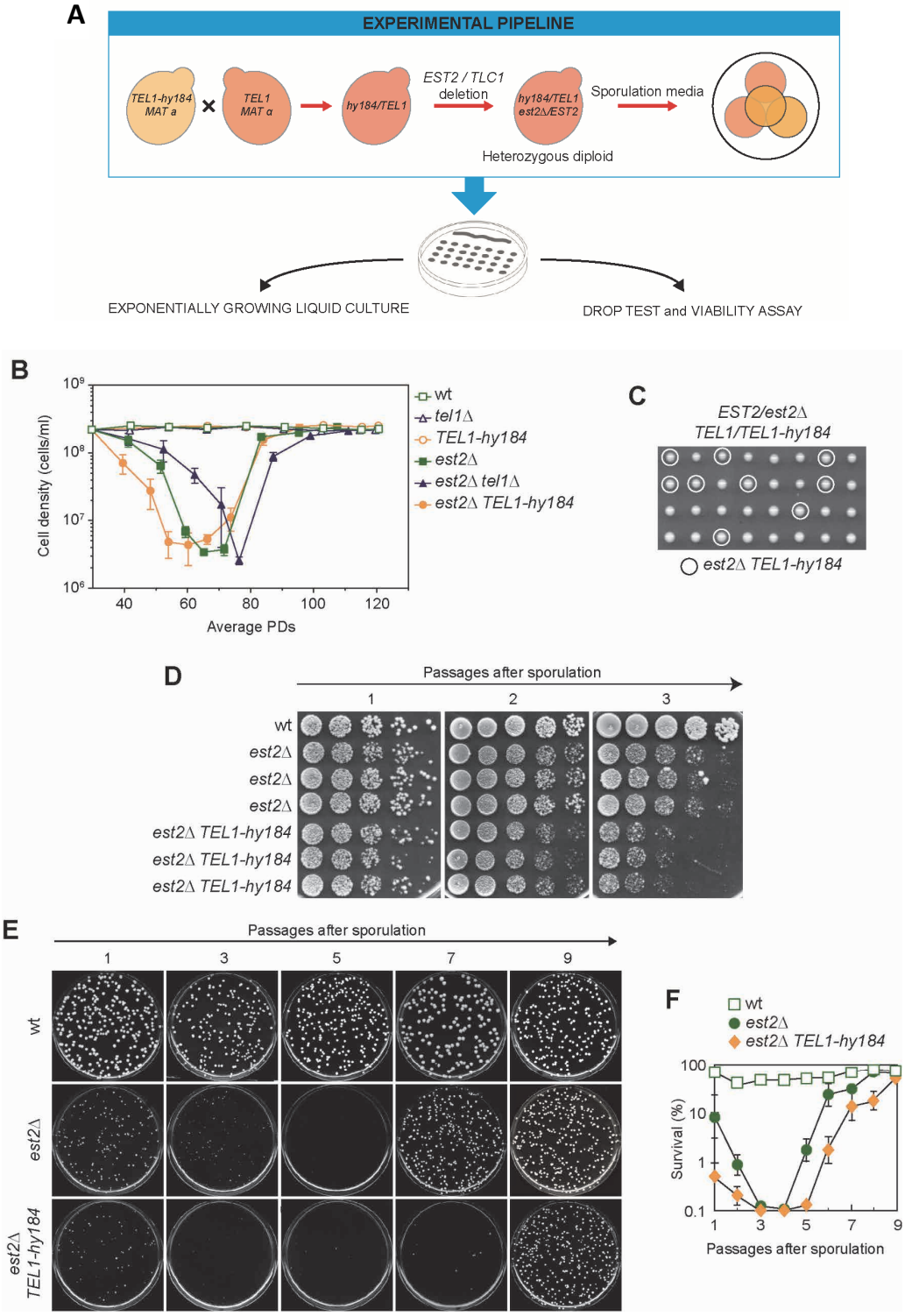
A
EXPERIMENTAL PIPELINE
TEL1-hy184 MAT a
TEL1 MAT α
hy184/TEL1
EST2 / TLC1 deletion
hy184/TEL1 est2Δ/EST2
Heterozygous diploid
Sporulation media
EXPONENTIALLY GROWING LIQUID CULTURE
DROP TEST and VIABILITY ASSAY
B
Cell density (cells/ml)
Average PDs
wt
tel1Δ
TEL1-hy184
est2Δ
est2Δ tel1Δ
est2Δ TEL1-hy184
C
EST2/est2Δ
TEL1/TEL1-hy184
est2Δ TEL1-hy184
D
Passages after sporulation
wt
est2Δ
est2Δ TEL1-hy184
E
Passages after sporulation
wt
est2Δ
est2Δ TEL1-hy184
F
wt
est2Δ
est2Δ TEL1-hy184
Survival (%)
Passages after sporulation

Figure 19 - TEL1-hy184 alleles accelerates the onset of replicative senescence in telomerase-negative cells. A. *Schematic representation of a senescence experiment. After the generation of the heterozygous diploids of interest where one copy of the gene encoding the telomerase subunit Est2 (or the gene encoding the telomerase RNA subunit, TLC1) was deleted, the obtained spore colonies were inoculated in YEPD medium at the concentration of 5x10^4 cells/mL. Every 24 hours, cell cultures were diluted back to 5x10^4 cells/mL in YEPD. Determination of cell density, as well as drop test and viability assay were performed during serial passages in liquid YEPD medium* ***B.*** *Senescence experiment was performed as described in (**A**). The mean cell concentration of at least four independent spores with the same genotype against the number of generations (Population Doublings, PDs) is plotted in the graph. We assumed that the spore colonies have undergone 30 generations when they were inoculated.* ***C.*** *Meiotic tetrads of a EST2/est2Δ TEL1/TEL1-hy184 diploid were dissected on YEPD plates and incubated at 25°C.* ***D.*** *Exponentially growing cell cultures with the indicated genotypes were serially diluted (1:10) before being spotted out onto YEPD plates during the first three day after sporulation (Day 0). Plates were incubated 3 days at 25°C.* ***E-F.*** *300 cells with the indicated genotypes were plated onto YEPD plates every day after sporulation (Day 0) of a EST2/est2Δ TEL1/TEL1-hy184 diploid. Plates were incubated 3 days at 25°C to determine the colony-forming units. Plotted values in (**F**) are the mean values with error bars denoting SD (n = 3).*

As expected, the absence of Tel1 delayed the onset of senescence of approximatively 10 PDs, with *est2Δ tel1Δ* cells reaching the minimum cell density at around 75 PDs[339] (*Figure 19B*). Conversely, *est2Δ TEL1-hy184* cells lost proliferative capacity approximately 15 PDs earlier than *est2Δ* cells and reached the minimum cell density at around 52 PDs (*Figure 19B* and *Figure 20B*). This early decrease in proliferative capacity is not due to a growth defect caused by the *TEL1-hy184* allele *per se*. In fact, *TEL1-hy184* cells showed constant growth rates after each dilution, similarly to both wild type and *tel1Δ* cells (*Figure 19B*). Furthermore, meiotic tetrads of *EST2*/*est2Δ TEL1*/*TEL1-hy184* diploids generated spore colonies of similar size independently of the presence of the *TEL1-hy184* allele (Figure *19C*). The same anticipated decrease in proliferative capacity caused by *TEL1-hy184* allele was observed when cell cultures were spotted on YEPD plates after each day of growth. In fact, *est2Δ TEL1-hy184* strains showed a decrease in colony size and density (*Figure 19D*), as well as a strong decrease in cell viability (*Figure 19E* and *F*) starting from the first passage in liquid medium, while *est2Δ* cells generated smaller colonies compared to wild type cells and showed a similar viability loss starting from the second passage in liquid medium (*Figure* 19*D-F*). In both *est2Δ* and *est2Δ TEL1-hy184* strains the decrease in cell growth and viability correlated with the accumulation of cells with 2C DNA content, as indicated by FACS analysis (*Figure 20A*). Finally, after

90-100 PDs *est2Δ TEL1-hy184* cells restored near wild type growth as expected with the appearance of survivors (*Figure 19B*). The accumulation of survivors is indicated by the appearance of colonies of wild type dimension, by the increase of cell viability (*Figure 19D-F*) and by the recovery of cell cycle progression (*Figure 20A*). The effect of the *TEL1-hy184* allele is not specific for *EST2* deletion. In fact, *TEL1-hy184* allele anticipated the onset of senescence of approximately 15 PDs also in *tlc1Δ* cells, which lack the telomerase RNA subunit (*Figure 20B*).

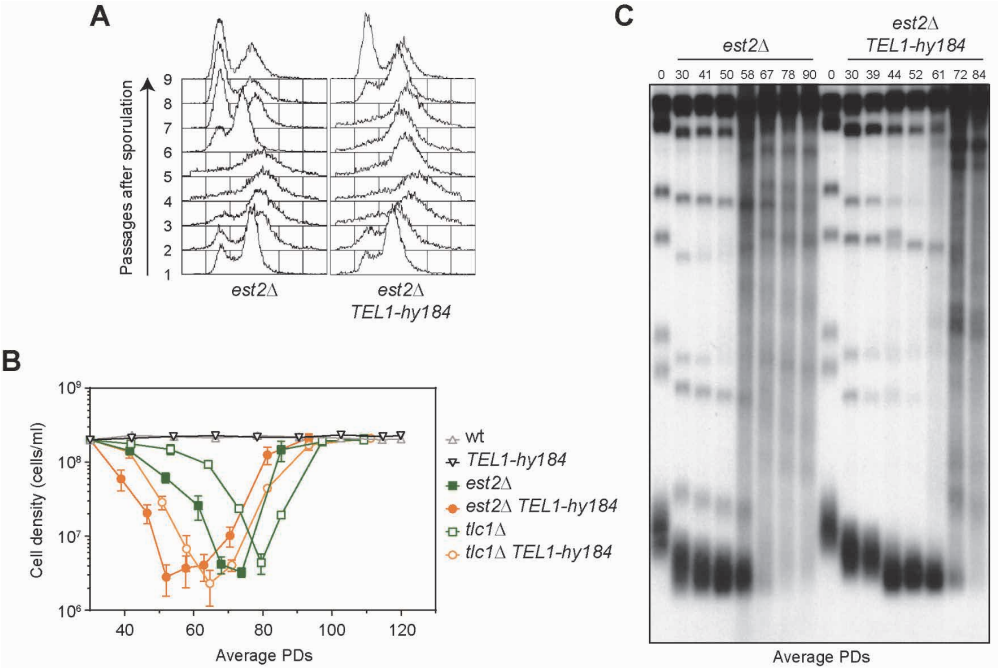

Figure 20 - Tel1-hy184 variant accelerates senescence without affecting telomere shortening kinetic. *Senescence analysis was performed as described in Figure 19A.* ***A.*** *Cells samples were harvested every day for subsequent Fluorescence activated cell sorting (FACS) analysis of DNA content.* ***B.*** *The mean cell concentration of at least four independent spores with the same genotype against the number of generations (PDs) is plotted in the graph.* ***C.*** *During the senescence assay showed in (**B**), cells samples were harvested daily for subsequent DNA extraction. Genomic DNA digested with XhoI restriction enzyme was subjected to Southern blot analysis with a poly(GT) telomere-specific probe to detect telomeres length.*

Altogether, these results indicate that, while the lack of Tel1 delays the onset of senescence, the Tel1-hy184 variant promotes anticipated senescence in the absence of telomerase. The early senescence induced by *TEL1-hy184* in telomerase-negative cells could be caused by a fast shortening of telomeres and/or an increased telomere loss.

We therefore performed a liquid senescence assay where we daily collected samples for DNA extraction and Southern blot analysis with a telomeric TG-rich DNA probe concomitantly determining cell concentration and PDs to evaluate telomere shortening as a function of PDs. Telomere shortening occurred with similar kinetics in *est2Δ* and *est2Δ TEL1-hy184* cells, both showing telomeric signals until approximatively 60 PDs (*Figure 20C*), when *est2Δ TEL1-hy184* cells were senescing (*Figure* 19*B*). We can conclude that the Tel1-hy184 variant induces a faster senescence without increasing the kinetics of bulk telomere shortening or telomere loss. Furthermore, in both *est2Δ* and *est2Δ TEL1-hy184* cells the probe detected at similar PDs smeared signals concomitantly with the disappearance of the telomeric signals (*Figure 20C*) and the reacquisition of growth capacity (*Figure* 19*B* and *E*), indicating that Tel1-hy184 variant does not affect the formation of survivors.

Early senescence in *TEL1-hy184* cells is triggered by the activation of a DNA damage checkpoint that depends on Rad9 and only partially on Mec1

The DNA damage checkpoint promotes replicative senescence in the absence of telomerase. In fact, the decrease in cell density after telomerase inactivation correlates with checkpoint activation and is delayed in the absence of checkpoint factors such as Rad9 and Mec1[340,341]. To test whether the fast senescence promoted by *TEL1-hy184* depends on checkpoint activation we performed a senescence assay in telomerase-negative cells where DNA damage checkpoint is abrogated by the lack of the adaptor protein Rad9. During the experiment we daily collected samples to monitor by Western blot Rad53 phosphorylation, which is considered a marker of checkpoint activation and is induced in senescing telomerase-negative cells[341]. Mobility shifts corresponding to Rad53 phosphorylated forms were detectable in both *est2Δ* and *est2Δ TEL1-hy184* cells after 2-3 passages from the inoculum of spore clones, while they were under the detection level in *est2Δ rad9Δ* and *est2Δ TEL1-hy184 rad9Δ* cells (*Figure 21A*).

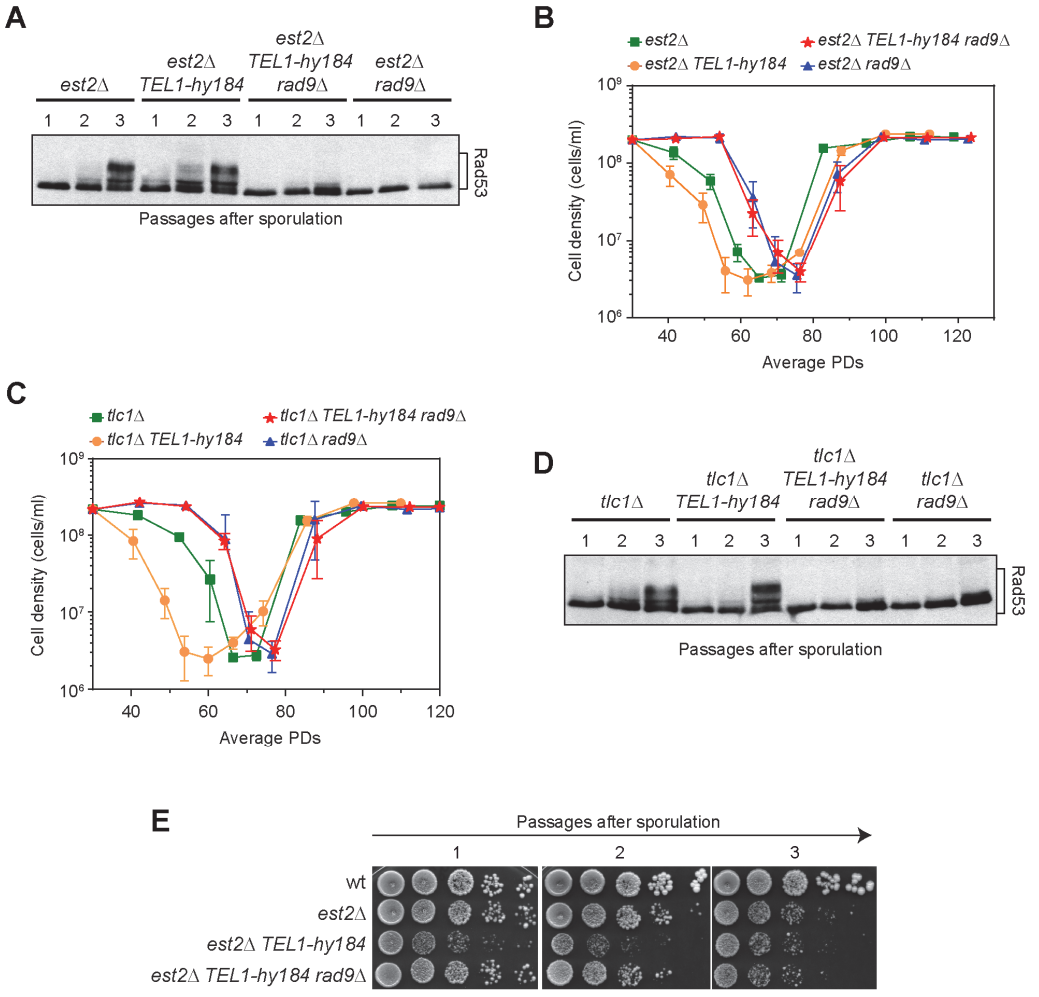

Figure 21 - Tel1-hy184 variant accelerates senescence activating a Rad9-dependent checkpoint. *Senescence analysis was performed as described in Figure 19A.* ***A,D.*** *During the senescence assay cells samples were harvested at the indicated time points after sporulation and the protein extracts were analysed by Western blot with anti-Rad53 antibodies.* ***B,C.*** *The mean cell concentration of at least four independent spores with the same genotype against the number of generations (PDs) is plotted in the graph.* ***E.*** *Exponentially growing cell cultures with the indicated genotypes were serially diluted (1:10) before being spotted out onto YEPD plates during the first three day after sporulation (Day 0).*

This indicates that a Rad9-dependent checkpoint is activated in senescing *est2Δ* and *est2Δ TEL1-hy184* cells. Moreover, *RAD9* deletion delayed the onset of senescence in *est2Δ* cells and completely relieved the early-senescent phenotype of *est2Δ TEL1-hy184* cells. In fact, both *est2Δ rad9Δ* and *est2Δ TEL1-hy184 rad9Δ* cells lost proliferative

capacity starting from around 60 PDs and reached the minimum cell density at around 75 PDs, approximatively 10 PDs later than *est2Δ* cells and 20 PDs later than *est2Δ TEL1-hy184* cells (*Figure 21B*). The lack of Rad9 completely relieved also the anticipated senescence caused by *TEL1-hy184* allele in cells lacking *TLC1* (*Figure 21C*) and abolished Rad53 phosphorylation in both *tlc1Δ* and *tlc1Δ TEL1-hy184* cells (*Figure 21D*). Furthermore, Rad9 contributes to reduce the growth capacity of *est2Δ TEL1-hy184* cells spotted on YEPD plates, as *est2Δ TEL1-hy184* cells showed small colonies starting from the first passage after sporulation, while in *est2Δ TEL1-hy184 rad9Δ* strain a decrease in the colony number and size was detectable starting from the second passage after sporulation (*Figure 21E*). Altogether, these results indicate that the anticipated senescence induced by the Tel1-hy184 variant in telomerase-negative cells depends on the activation of a Rad9-dependent checkpoint.

Tel1 contributes to checkpoint activation both by generating ssDNA that activates Mec1 and by acting in a parallel pathway respect to Mec1[19]. So, we tested whether Mec1 is required for the anticipated senescence induced by Tel1-hy184 by repeating the senescence assays in telomerase-negative cells lacking Mec1 as well as the ribonucleotide inhibitor Sml1, which causes cell lethality in *mec1Δ* background[328]. As expected, the onset of senescence was delayed of almost 10 PDs in *est2Δ mec1Δ* cells compared to *est2Δ* cells (*Figure 22A*). Interestingly, *est2Δ TEL1-hy184 mec1Δ* cells lost proliferative capacity approximately 15 PDs earlier than *est2Δmec1Δ* cells (*Figure 22A*), indicating that *TEL1-hy184* anticipates the onset of senescence also in the absence of Mec1. The same effect was observed in a *tlc1Δ* background, where *tlc1Δ TEL1-hy184 mec1Δ* cells decreased cell proliferation approximately 7 PDs earlier than *tlc1Δ mec1Δ* cells (*Figure 22C*). Furthermore, Rad53 was partially phosphorylated in senescing *est2Δ TEL1-hy184 mec1Δ* (*Figure 22B*) and *tlc1Δ TEL1-hy184 mec1Δ* cells (*Figure 22D*), while phosphorylated Rad53 bands were undetectable in both *est2Δmec1Δ* and *tlc1Δ mec1Δ* cells (*Figure 22B* and *D*), indicating that a partial Rad53 phosphorylation is promoted by Tel1-hy184 independently of Mec1. However, senescence was faster in *est2Δ TEL1-*

hy184 and *tlc1Δ TEL1-hy184* cells than in *est2Δ TEL1-hy184 mec1Δ* and *tlc1Δ TEL1-hy184 mec1Δ* cells, respectively (*Figure 22A* and *C*), indicating that Mec1 contributes only partially to the reduction of cell proliferation in the presence of Tel1-184 variant. Altogether, these results indicate that Tel1-hy184 variant directly cooperate with Mec1 to activate a Rad9-dependent checkpoint in the absence of telomerase.

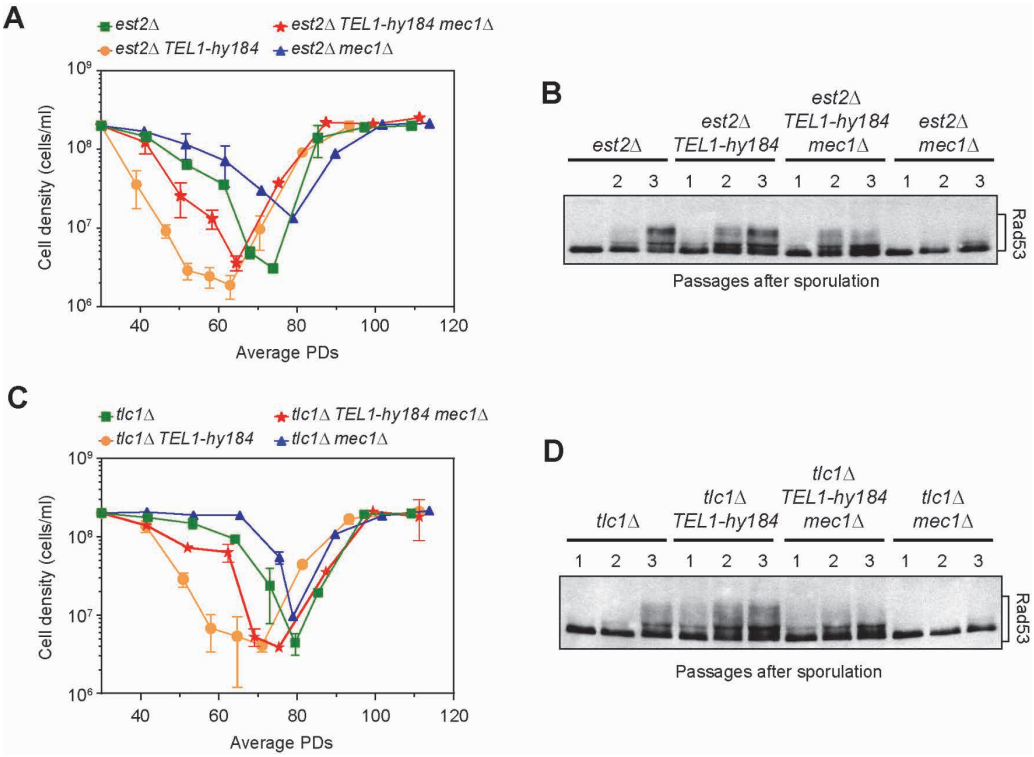

Figure 22 - Tel1-hy184 variant induces senescence acting in a parallel pathway respect to Mec1. A,C. *Senescence analysis was performed as described in Figure 19A.* ***A,C.*** *The mean cell concentration of at least four independent spores with the same genotype against the number of generations (PDs) is plotted in the graph.* ***B,D.*** *During the senescence assay cells samples were harvested at the indicated time points after sporulation and the protein extracts were analysed by Western blot with anti-Rad53 antibodies*

TEL1-hy184 does not increase ssDNA generation at telomeres

Tel1 promotes DNA end resection at both DSBs and telomeres[116,160]. As ssDNA was proposed to trigger senescence[342], the delayed senescence of telomerase-deficient

tel1Δ cells could be ascribed to the resection defects of these cells[344]. If this were the case, we would expect that Tel1-hy184 variant increases ssDNA generation at telomeres. On the other hand, the finding that Tel1-hy184 promotes the activation of a Rad9-dependent checkpoint independently of Mec1 suggests that Tel1 may act in parallel with Mec1 in checkpoint signaling rather than promoting the accumulation of ssDNA that activates Mec1. We therefore asked whether Tel1-hy184 increases telomeric ssDNA after telomerase inactivation.

As ssDNA at telomeres is generated mainly by the Exo1 exonuclease, we evaluated whether the faster senescence of *est2Δ TEL1-hy184* compared to *est2Δ* cells depends on Exo1, which is known to promote senescence[252,306]. *EXO1* deletion delayed the onset of senescence of approximatively 10 PDs in *est2Δ* but delayed only partially the senescence of *est2Δ TEL1-hy184* cells (*Figure 23A*), indeed *est2Δ TEL1-hy184 exo1Δ* cells reached the minimum cell density only 2-3 PDs after *est2Δ TEL1-hy184* cells. This result suggests that ssDNA generated by Exo1 does not account for the anticipated senescence induced by the Tel1-hy184 variant. Telomeric DNA is also resected by the MRX complex, whose activity at telomeres is limited by Rif2 and promoted by Tel1, which counteracts the inhibitory effect of Rif2 on MRX[160,273]. We asked whether Tel1-hy184 accelerates senescence by overcoming the Rif2-mediated MRX inhibition. However, *est2Δ rif2Δ TEL1-hy184* cells senesced faster than either *est2Δ TEL1-hy184* and *est2Δ rif2Δ* strains, both anticipating the onset of senescence of approximatively 15 PDs compared to *est2Δ* cells (*Figure 23B*). This result suggests that the lack of Rif2 and the presence of the Tel1-hy184 variant promote fast senescence by affecting different pathways. We then monitored directly the amount of ssDNA at native telomeres after telomerase inactivation. Genomic DNA prepared from cells collected daily after the inoculum of *est2Δ* and *est2Δ TEL1-hy184* spore clones was analyzed by nondenaturing in-gel hybridization with a C-rich radiolabeled oligonucleotide that detect the telomeric G-rich ssDNA overhangs[287]. The ssDNA signals were then normalized for each time point to the total amount of TG repeats detected by the C-rich probe after denaturation of the gel.

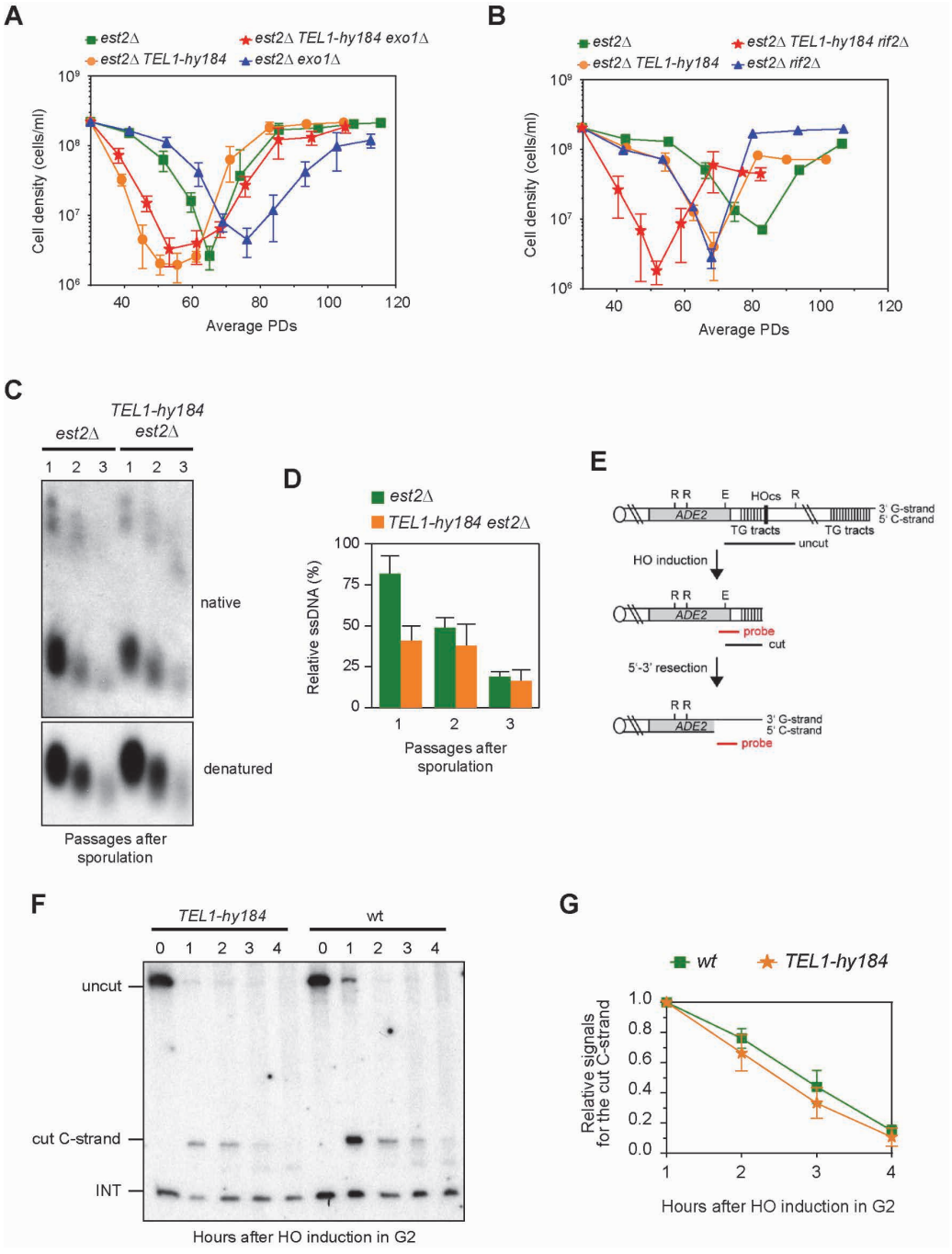
A
est2Δ
est2Δ TEL1-hy184
est2Δ TEL1-hy184 exo1Δ
est2Δ exo1Δ
Cell density (cells/ml)
Average PDs
B
est2Δ
est2Δ TEL1-hy184
est2Δ TEL1-hy184 rif2Δ
est2Δ rif2Δ
Cell density (cells/ml)
Average PDs
C
TEL1-hy184
est2Δ
est2Δ
native
denatured
Passages after sporulation
D
est2Δ
TEL1-hy184 est2Δ
Relative ssDNA (%)
Passages after sporulation
E
R R E HOcs R
ADE2
3' G-strand
5' C-strand
TG tracts
TG tracts
uncut
HO induction
probe
cut
5'-3' resection
3' G-strand
5' C-strand
probe
F
TEL1-hy184
wt
uncut
cut C-strand
INT
Hours after HO induction in G2
G
wt
TEL1-hy184
Relative signals for the cut C-strand
Hours after HO induction in G2

Figure 23 - TEL1-hy184 allele did not increase the levels of telomeric ssDNA. A,B. *Senescence analysis was performed as described in Figure 19A. The mean cell concentration of at least four independent spores with the same genotype against the number of generations (Population Doublings, PDs) is plotted in the graph. We assumed that the spore colonies have undergone 30 generations when they were inoculated.* ***C.*** *Analysis of telomeric ssDNA in est2Δ and est2Δ TEL1-hy184 cells. Every 24 hours after sporulation, cells samples were harvested for subsequent DNA extraction. Genomic DNA was digested with XhoI restriction enzyme and single-stranded G-tails were visualized by non-denaturing in-gel hybridization using an end-labeled C-rich oligonucleotide as a probe (native). The gel was then denatured and hybridized again with the same probe for loading control (denatured).* ***D.*** *Quantification of telomeric ss-DNA in (**C**). The amount of native TG-ssDNA was normalized to the total amount of TG sequences detected in each denatured sample.* ***E.*** *Schematic representation of the HO-induced telomere system. Galactose-induced HO endonuclease generates a single DSB at an HO cleavage site (HOcs) adjacent to 81-bp TG repeat sequence (TG tracts) that is inserted at the ADH4 locus on chromosome VII-L. RsaI- and EcoRV-digested genomic DNA was hybridized with a single-stranded riboprobe (in red), which anneal to the 5' C-strand to a site located 212 bp from the HO cutting site. The probe reveals an uncut 390 nt DNA fragment (uncut), which is converted by HO cleavage into a 166 nt fragment (cut) that can be detected by the probe. Degradation of the 5' C-strand leads to disappearance of the signal. The probe also detects a 138 nt fragment from the ade2-101 locus on chromosome XV (INT), which serves as internal loading control.* ***F.*** *HO expression was induced at time zero by galactose addition to nocodazole-arrested wild type and TEL1-hy184 cell cultures that were then kept arrested in G_2. RsaI- and EcoRV-digested genomic DNA was hybridized with the 5' C-strand probe as showed in (**E**).* ***G.*** *Densitometric analysis. Plotted values are the mean value ±SD from three independent experiments as in (**F**).*

Both the ssDNA signals (native) and the TG repeats signals (denatured) decreased during the experiment, as expected by the progressive reduction of telomeric sequences in the absence of telomerase (*Figure 23C* and *D*). *TEL1-hy184* allele did not increase the levels of G-rich ssDNA overhangs in an *est2Δ* background (*Figure 23C* and *D*). Rather, the amount of telomeric ssDNA appeared to be slightly reduced in *est2Δ TEL1-hy184* cells compared to *est2Δ* cells, supporting the idea that the anticipated senescence triggered by the Tel1-hy184 variant is not caused by an increased telomere processing. We also test whether Tel1-hy184 affects the generation of ssDNA at a HO-inducible short telomere, whose processing is known to be promoted by Tel1[160]. We inserted the *TEL1-hy184* allele in a yeast strain carrying 81-bp TG repeat sequence placed immediately adjacent to a HO endonuclease recognition sequence at the *ADH4* locus on chromosome VII, and expressing the *HO* gene from a galactose-inducible *GAL1* promoter[285]. The HO cleavage creates a centromere-proximal TG-rich DNA end, which

is considered a bona fide short telomere[285]. Processing of this TG-rich DNA end was evaluated by Southern blot under denaturing conditions using a single-stranded RNA probe that anneals to the 5' C-rich strand. The HO cleavage converts the uncut 390-nt DNA fragment (uncut) revealed by this probe into a 166-nt fragment (cut C-strand), whose subsequent disappearance indicates that resection has proceeded beyond the hybridization region of the probe (*Figure 23E*). The cut C-strand signals were then normalized to an internal control band (int) for each time point. Resection of the TG-rich end produced by the HO cleavage was evaluated in wild type and *TEL1-hy184* cells kept arrested with nocodazole in G_2 phase, because generation of ssDNA at telomeres is known to occur during S and G_2/M cell cycle phases[224]. The band corresponding to the cut C-rich strand disappeared with similar kinetics in both wild type and *TEL1-hy184* cells (*Figure 23F* and *G*), indicating that the Tel1-hy184 variant does not affect the processing of a HO-induced short telomere.

Furthermore, Tel1-hy184 did not increase resection at a HO-induced chromosomal DSB, which were induced at the *MAT* locus in both wild type and *TEL1-hy184* strains expressing the *HO* gene from the *GAL1* promoter[343]. As ssDNA is resistant to cleavage by restriction enzymes, ssDNA formation at the HO-induced DSB results in the accumulation of resection intermediates that can be revealed by a single-strand RNA probe that recognizes the 3' end at one side of the break (*Figure 24A*). These resection intermediates appeared with very similar kinetics in both wild type and *TEL1-hy184* cells (*Figure 24B* and *C*).

Altogether, these results indicate that the Tel1-hy184 variant does not increase ssDNA generation at DNA ends. As the Rad9-dependent anticipated senescence in *TEL1-hy184* correlates with the induction of a Mec1-independent Rad53 phosphorylation but not with an increased telomere processing, these results suggest that Tel1 triggers replicative senescence by generating directly a checkpoint signal rather that by producing telomeric ssDNA.

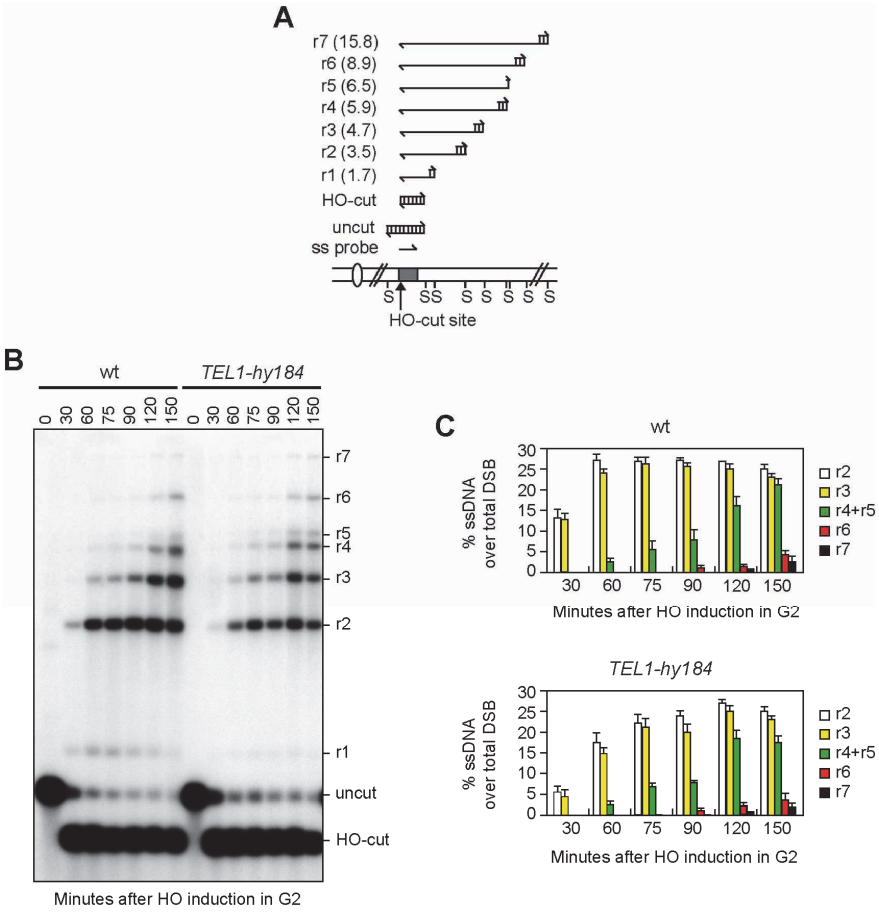

Figure 24 - TEL1-hy184 allele did not increase the levels of ssDNA at DSB ends. A. *Schematic representation of the system to detect DSB resection. Gel blots of SspI-digested genomic DNA separated on alkaline agarose gel were hybridized with a single-stranded RNA probe (ss probe) that anneals to the unresected strand at the MAT locus. 5´-3´ resection progressively eliminates SspI sites (S), producing larger SspI fragments (r1 through r7) detected by the probe.* ***B,C.*** *Exponentially growing YEPR cell cultures were arrested in G2 with nocodazole and transferred to YEPRG (time zero) in the presence of nocodazole. (**B**) DSB resection as described in (**A**). (**C**) Resection products in (**B**) were analyzed by densitometry. The mean values are represented with error bars denoting SD (n = 5).*

Tel1-hy184 binds telomeric DNA ends more robustly than wild type Tel1

We asked how the Tel1-hy184 variant may increase checkpoint signaling at critically short telomeres in telomerase-negative cells. One possibility is that the Tel1-hy184 variant is more robustly associated to short telomeres compared to wild type Tel1. To test this possibility, we evaluated the recruitment of Tel1 and Tel1-hy184 to a HO-

induced short telomere. We therefore introduced either the *TEL1-HA* or *TEL1-hy184-HA* allele in the strain carrying both the 81-bp TG repeats adjacent to the HO cutting site at the *ADH4* locus and the *GAL1-HO* inducible gene[285]. Upon HO induction in G_2-arrested cells that were kept in G_2 phase by nocodazole, we performed chromatin immunoprecipitation (ChIP) with anti-HA antibodies followed by quantitative qPCR with primer pairs located at both telomeric (TG-HO) and non-telomeric (HO) side of the HO cutting site (*Figure 25A*).

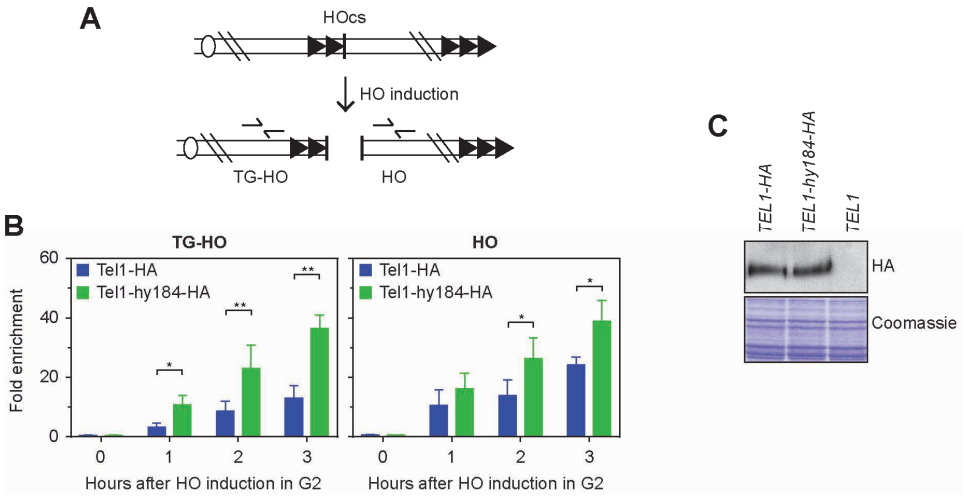

Figure 25 - TEL1-hy184 allele increase Tel1 binding/persistence at DNA ends. A. *Schematic representation of The HO-induced telomere system as in Figure 23E; TG repeat sequences (81 bp; black triangles). This system was used to generate TG-HO and HO DNA ends after HO expression regulated by GAL promoter.* ***B.*** *Chromatin samples, prepared at the indicated time points after HO induction by galactose addition to G_2-arrested TEL1-HA (wild-type) and TEL1-hy184-HA cells, were immunoprecipitated with anti-HA antibodies. Coimmunoprecipitated DNA was analysed by qPCR using primer (black arrows) pairs located 640 bp centromere proximal to the HO cleavage site (TG) or located 550 bp centromere distal to the HO cleavage site (HO) and at the non-telomeric ARO1 fragment of chromosome IV (CON). In the graphs, data are expressed as relative fold enrichment of the TG-HO or HO signal over the CON signal after normalization to the input signals for each primer set. The data presented are means ± SDs from three different experiments. (t-test: * P<0.05; ** P<0.01).* ***C.*** *Exponentially growing cell cultures of strains expressing the HA tagged Tel1 variants were harvested and the same amounts of protein extracts were separated on SDS-PAGE and either subjected to Western blot with anti-HA antibodies or stained with Coomassie as a loading control.*

As expected, DSB formation caused the accumulation of wild-type Tel1-HA at both sides of the break, with a reduced amount of Tel1-HA bound to the TG-HO side compared to that associated to the non-telomeric HO side[160,273] (*Figure 25B*). Conversely, similar

levels of the Tel1-hy184-HA variant were recruited at both sides of the HO-induced DSB and these levels were higher compared to the levels of wild type Tel1-HA at both DNA ends (*Figure 25B*). This increased association of Tel1-hy184 to DNA ends cannot be ascribed to increased levels of the protein as we observed similar amount of Tel1-HA and Tel1-hy184-HA in the cells (*Figure 25C*). Therefore, Tel1-hy184 was associated to DNA ends and in particular to the TG-rich end more efficiently than wild type Tel1-HA.

TEL1-hy184 N-terminal mutations are responsible for early senescence

The Tel1-hy184 variant carries five amino acid substitutions grouped in two different clusters. Two substitutions (R2735G, E2737V) are located in the C-terminal kinase domain while the other three substitutions (F1752I, D1985N, E2133K) are grouped in the FAT domain of the protein (*Figure 26A*). We asked which group of substitutions was responsible for the anticipated senescence triggered by Tel1-hy184. We therefore constructed strains expressing the *TEL1-hy184-3N* or the *TEL1-hy184-2C* allele, which causes the F1752I, D1985N, E2133K or the R2735G, E2737V amino acid substitutions, respectively (*Figure 26A*). Interestingly, both *TEL1-hy184-3N* and *TEL1-hy184-2C* alleles suppressed the hypersensitivity of *mec1Δ* cells to HU similar to the *TEL1-hy184* allele (*Figure 26B*), indicating that each group of mutations in the *TEL1* gene is sufficient to compensate for the lack of Mec1 functions in response to HU treatment.

Tel1-hy184 was found to possesses an intrinsic kinase activity higher than wild type Tel1 and to cause a mild telomere over-elongation[338]. We therefore measured the *in vitro* kinase activities of immunoprecipitates with anti-HA antibodies from cells expressing *TEL1*, *TEL1-HA*, *TEL1-hy184-HA*, *TEL1-hy184-3N-HA* or *TEL1-hy184-2C-HA* alleles on PHAS-I, the artificial substrate of the ATM kinase family[320,338]. As expected, the Tel1-hy184 variant has an intrinsic kinase activity higher than the wild type Tel1 and mutations in the kinase domain are responsible for this increased kinase activity. In fact, the amount of phosphorylated PHAS-I was higher in both the assays containing Tel1-hy184-HA and Tel1-hy184-2C-HA than in the assays containing wild type Tel1-HA

or Tel1-hy184-3N-HA (*Figure 26C*). PHAS-I phosphorylation depends on Tel1, as it was not detectable when the immunoprecipitate was prepared from cells expressing untagged *TEL1* (*Figure 26C*). Consistent with the observed correlation between Tel1 kinase activity and telomere elongation[33,160,320,338], Southern blot analysis with a TG-rich probe on genomic DNA prepared from exponentially growing cells revealed that both *TEL1-hy184* and *TEL1-hy184-2C* alleles, which increased Tel1 kinase activity (*Figure 26C*), caused a mild telomere over-elongation in *mec1Δ* background compared to both wild type and *mec1Δ* cells (*Figure 26D*). Conversely, telomeres were of wild type length in the presence of the *TEL1-hy184-3N* allele (*Figure 26D*), which did not increase Tel1 kinase activity (*Figure 26C*). We then assayed the senescence kinetics of *est2Δ TEL1-hy184-3N* and *est2Δ TEL1-hy184-2C* cells compared to *est2Δ* cells after sporulation of *EST2/est2Δ TEL1/TEL1-hy184-3N* or *EST2/est2Δ TEL1/TEL1-hy184-2C* diploids cells, respectively. *est2Δ* strains derived from the *EST2/est2Δ TEL1/TEL1-hy184-2C* diploid decreased cell proliferation approximately 10 PDs later than *est2Δ* strains derived from the *EST2/est2Δ TEL1/TEL1-hy184-3N* diploid (*Figure 26E* and *F*), likely because the *TEL1-hy184-2C* allele increased telomere length in *EST2/est2Δ TEL1/TEL1-hy184-2C* diploid and in its derivative spore clones. *est2Δ* and *est2Δ TEL1-hy184-2C* strains decreased cell proliferation with similar kinetics starting approximately from 60 PDs (*Figure 26E*). Conversely, *est2Δ TEL1-hy184-3N* cells decreased proliferative capacity starting approximately from 45 PDs, 10 PDs earlier than *est2Δ* cells derived from the same diploid (*Figure 26F*). Therefore, anticipated senescence appears to be exclusively caused by the F1752I, D1985N, E2133K substitutions, which did not increase both Tel1 kinase activity (*Figure 26C*) and telomere length (*Figure 26D*). However, like the Tel1-hy184-HA variant (*Figure 25B*), also the Tel1-hy184-3N-HA variant was most efficiently bound than wild type Tel1 to both the TG-rich and the non-telomeric side of the HO-induced DSB located adjacent to 81-TG repeats at the *ADH4* locus (*Figure 26G*). Altogether, these results indicate that the Tel1 aminoacidic substitutions F1752I, D1985N, E2133K located in the FAT domain of the protein increased Tel1 signaling at short telomeres likely by increasing Tel1 binding/persistence at DNA ends.

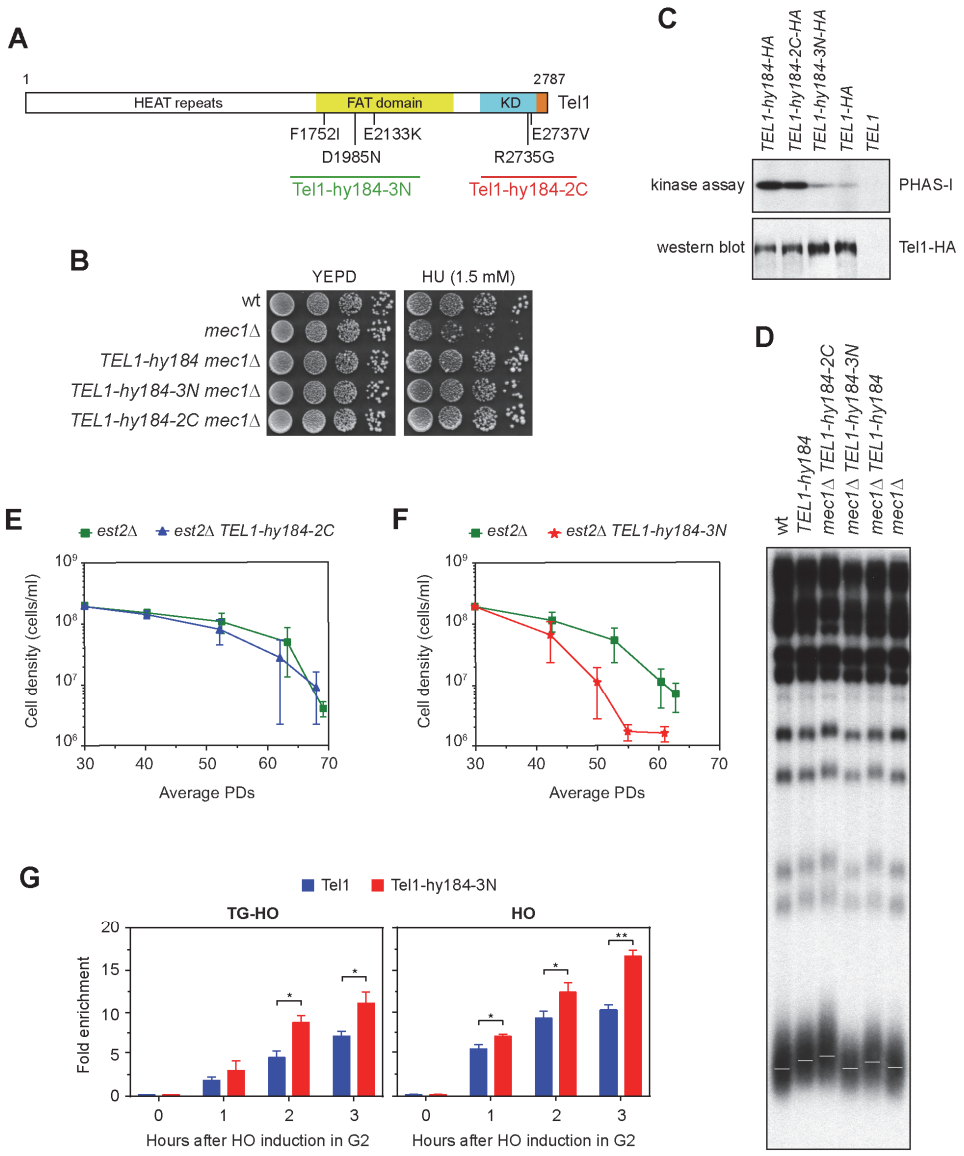

Figure 26 - TEL1-hy184 N-terminal mutations increased Tel1 signaling at short telomeres. A. *Schematic representation of the Tel1 protein with the position of the TEL1-hy184 point mutations.* ***B.*** *Exponentially growing cultures of strains with the indicated genotypes were serially diluted (1:10) and each dilution was spotted out onto YEPD plates with or without hydroxyurea (HU) at the indicated concentration.* ***C.*** *Western blot and in vitro kinase assays of the indicated Tel1 variants. Products of a kinase reaction using γ-32P-labeled ATP were analyzed by SDS-polyacrylamide gel electrophoresis (kinase assay). All of the immunoprecipitates also were subjected to Western blot analysis using anti-HA antibodies (Western blot).* ***D.*** *Genomic DNA extracted from exponentially growing cell cultures of strains with the indicated genotypes were digested with XhoI restriction enzyme and subjected to Southern blot analysis with a poly(GT) telomere-specific probe to detect telomeres length.* ***E,F.*** *Senescence analysis was performed as described in Figure 19A.* ***G.*** *Chromatin immunoprecipitation assay to analyse the level of Tel1-HA and Tel1-hy184-3N at TG-HO and HO DNA ends as described in Figure 25B.*

Tel1 kinase activity is required to induce senescence while it is dispensable for telomere processing

The above results obtained with the *TEL1-hy184* and *TEL1-hy184-3N* hyperactive mutant alleles suggest that Tel1 recruitment at short telomeres in telomerase-negative cells trigger senescence by increasing Tel1-mediated checkpoint signaling rather than by increasing telomeric ssDNA generation as previously hypothesized[344].We would like to generalize these conclusions by analyzing other *tel1* mutant alleles. We focused on the *tel1-kd* allele, which causes the G2611D, D2612A, N2616K, and D2631E amino acid substitutions that abolish Tel1 kinase activity *in* vitro[320]. Tel1 kinase activity is required for both telomere elongation and checkpoint signaling, as it promotes H2A phosphorylation and Rad9 accumulation at DSBs[33,320,325], while it is dispensable for Tel1 and MRX recruitment to telomeres as well as for Tel1-mediated regulation of resection at DSB ends[273,317,325,345]. As the presence of Tel1, but not its kinase activity, promotes resection of DSB ends[317,325], we first asked whether Tel1 kinase activity influences telomere processing. We therefore inserted the *tel1-kd* allele in the strain where a short telomere can be generated by the HO-inducible cleavage at the *ADH4* locus. When we analyzed the resection kinetic of this HO-induced telomere, the cut C-strand signals disappeared with similar (or slightly faster) kinetics in both wild type and *tel1-kd* cells, while they persisted longer in *tel1Δ* cells, as expected[160] (*Figure 27A* and *B*). Similar results were obtained at native telomeres. In fact, the amount of the G-rich ssDNA overhangs in senescing telomerase-negative cells was similar in *est2Δ* and *est2Δ tel1-kd* cells, while it was reduced by the lack of Tel1 (*Figure 27C* and *D*). Therefore, also telomeric processing is stimulated by the presence of Tel1 and not by its kinase activity. Importantly, during senescence analysis, *est2Δ tel1-kd* cells decreased proliferation capacity starting from 50 PDs and reached the minimum cell density at 70 PDs, approximately 10 PDs later than *est2Δ* cells (*Figure 27E*). Thus, the expression of *tel1-kd* allele in *est2Δ* cells delay the senescence onset without reducing telomeric ssDNA as the deletion of *TEL1* gene.

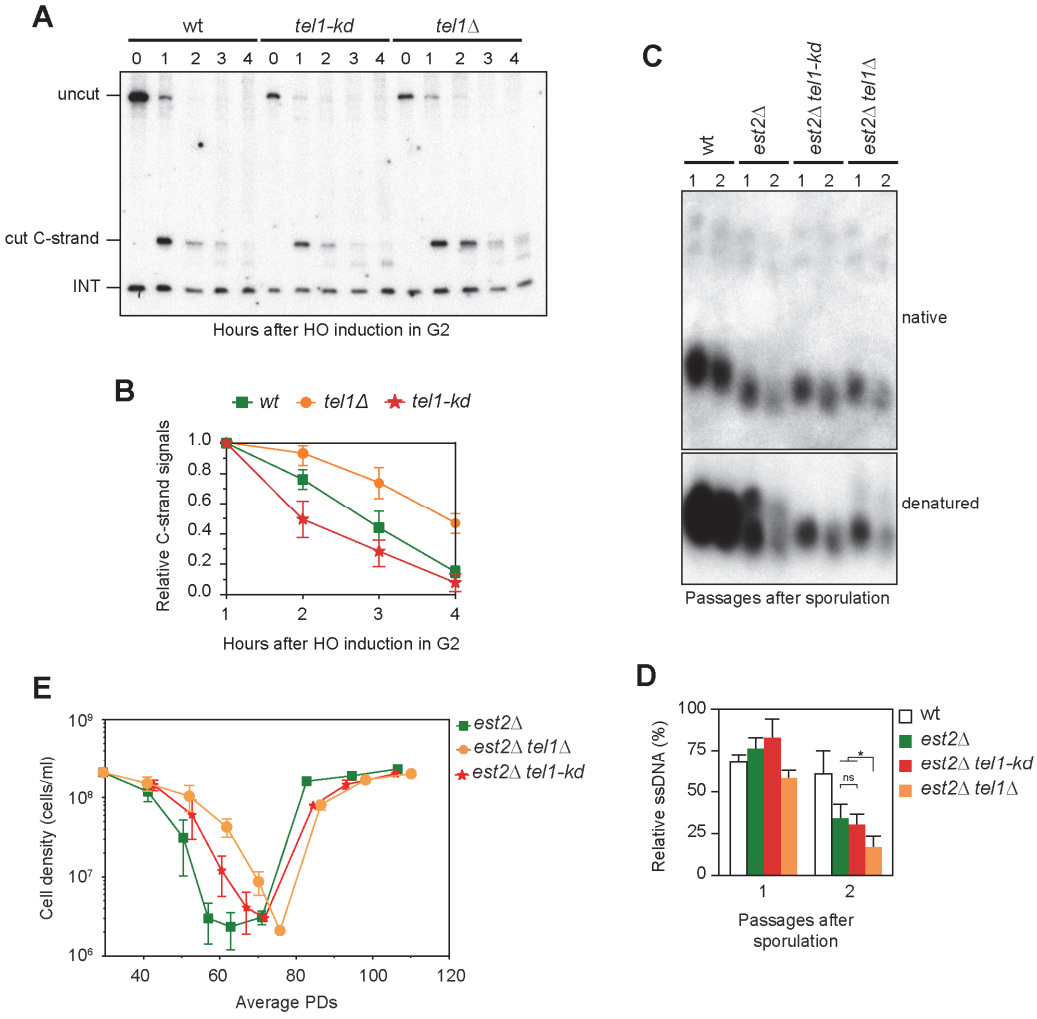

Figure 27 - Tel1 kinase activity is required to induce senescence but not for telomere processing. A. *HO expression was induced at time zero by galactose addition to nocodazole-arrested wild type, tel1-kd and tel1Δ cell cultures that were then kept arrested in G_2. RsaI- and EcoRV-digested genomic DNA was hybridized with the 5' C-strand probe to visualize the processing of the HO-induced short telomere (as previously showed in Figure 23E).* ***B.*** *Densitometric analysis. Plotted values are the mean value ±SD from three independent experiments as in (**A**).* ***C.*** *Analysis of telomeric ssDNA in est2Δ, est2Δ tel1-kd and est2Δ tel1Δ cells. Every 24 hours after sporulation, cells samples were harvested for subsequent DNA extraction. Genomic DNA was digested with XhoI restriction enzyme and single-stranded G-tails were visualized by non-denaturing in-gel hybridization using an end-labeled C-rich oligonucleotide as a probe (native). The gel was then denatured and hybridized again with the same probe for loading control (denatured).* ***D.*** *Quantification of telomeric ss-DNA as in Figure23D. Plotted values are the mean value ±SD from three independent experiments as in (**C**). The amount of native TG-ssDNA was normalized to the total amount of TG sequences detected in each denatured sample.* ***E.*** *Senescence analysis was performed as described in Figure 19A.*

As the lack of Tel1 kinase activity did not affect the generation of ssDNA at telomeres (*Figure 27C* and *D*), these results indicate that Tel1 kinase activity promotes replicative senescence in the presence of wild type levels of ssDNA at telomeres. However, the onset of senescence was anticipated of approximately 5 PDs in *est2Δ tel1-kd* cells compared to *est2Δ tel1Δ* cells (*Figure 27E*). Therefore, while Tel1 kinase activity strongly contributes to senescence induction, also kinase-independent functions of Tel1 are involved in the same process. Altogether, these results support a model in which the main function of Tel1 in promoting replicative senescence is the activation of the Rad9-dependent checkpoint, which requires Tel1 kinase activity, that is unrelated to the telomeric ssDNA level (*Figure 29*).

DISCUSSION

Tel1 kinase is the *Saccharomyces cerevisiae* ortholog of human ATM protein. Patients with ATM deficiency are affected by the human autosomal recessive disorder ataxia telangiectasia (AT), a rare neurodegenerative disease that causes multiple stress symptoms, including cerebellar degeneration, increased incidence of cancer, growth retardation, immune deficiencies, and premature aging[346]. Ataxia telangiectasia was first described in 1957, as a distinct disease that can occur early in childhood, with incidence varying from 1 out of 40.000 to 1 out of 100.000 new births and a carrier frequency that approximates 1% (only in the United States)[347]. Several hundred ATM mutations have been identified in AT patients[348]. About 85% are null mutations that result in the production of truncated forms of the protein and complete inactivation of the gene function, while less than 15% are classified as missense mutations[348]. In the presence of DNA lesions or replication stress, Tel1/ATM and Mec1/ATR activate the DNA damage checkpoint starting the signal transduction pathways that block the cell cycle and promote the repair of DNA damage or eventually activate cell death programs. Thus, as a consequence of dysfunctional ATM signaling, different effects have been reported, such as reduced phosphorylation levels of DNA damage response (DDR) targets[349], failure to arrest the cell cycle, and reduced efficiency of DNA damage repair[350,351]. Additionally, telomere abnormalities are frequently observed in cells derived from AT patients[352,353], and cells expressing dominant negative ATM variants show accelerated telomere shortening[354]. Furthermore, ATM mutations or expression changes have been often found in different kinds of tumours.

Despite the differences between humans and budding yeast, what is clear is that Tel1 and ATM are key elements in the DDR. In this thesis, I have analysed the role of Tel1/ATM in response to camptothecin (CPT), an inhibitor of type I DNA topoisomerases, and in telomere regulation and senescence induction, in order to highlight the overall importance of its dual nature in genome stability and long-term cell survival.

In the first part of this experimental work, we found out a novel function of Tel1/ATM in stabilizing CPT-induced reversed forks by counteracting the nucleolytic activity of MRX. This Tel1 function becomes dispensable when fork reversal is prevented by the lack of Mrc1, suggesting that Tel1 and MRX target replication forks after their reversal (*Figure 28*). Alternatively, Tel1 and Mre11 might function before fork reversal, with Tel1 promoting this transition at stalled forks and MRX triggering fork degradation that prevents fork reversal in the absence of Tel1. We favor the first hypothesis because purified MRE11-RAD50 complex was found to degrade reversed forks *in vitro*[355]. Furthermore, four independent groups recently demonstrated that in metazoan fork reversal is required for MRE11-dependent degradation of stalled forks in the absence of the protective function exerted by BRCA1 or BRCA2[163,335,355]. Tel1 may counteract MRX activity either directly or through a still unknown factor that prevents MRX action at reversed forks (*Figure 28*). Reversed forks stabilization by Tel1 can support the completion of DNA replication after the repair of CPT-induced damage by either reversed fork reactivation or fusion with an incoming fork (*Figure 28*). Consistently, we found that Tel1 inactivation causes a Mre11-dependent increase in the length of ssDNA gaps at three-way fork junctions. A similar phenotype was observed in BRCA-depleted cells, which also displayed MRE11-dependent extensive degradation of nascent DNA that proceeds behind the stalled forks and can be suppressed by preventing fork reversal[335,355]. Similarly, extended ssDNA at three-way fork junctions in *tel1Δ* cells might result from nucleolytic degradation starting from the regressed arm of the reversed forks and proceeding behind the fork.

Mrc1 inactivation prevents fork reversal and relieves the hypersensitivity to CPT of *tel1Δ* cells, suggesting that unscheduled MRX-dependent processing of reversed forks in the absence of Tel1 may account for the CPT hypersensitivity of these cells. Interestingly, the lack of Tel1 does not increase the CPT hypersensitivity of *rad1Δ tdp1Δ* double mutant cells, indicating that Tel1 somehow participates in the CPT response together with Tdp1 and Rad1. As a strong retention of Top1 on DNA was observed in

CPT-treated *rad1Δ tdp1Δ* cells compared to wild type[38], our results suggest that Top1 removal is required to repair the CPT-induced damage even when the integrity of stalled forks is preserved by Tel1.

We show that Mrc1 plays an unexpected function in promoting fork reversal in CPT, which is the only condition that was found to trigger fork reversal in checkpoint-proficient yeast cells[120,149,151]. As CPT prevents the release of DNA supercoilings by Top1[356], torsional stress is expected to participate in CPT-induced fork reversal[151]. Therefore, Mrc1 may indirectly promote fork reversal in CPT by supporting fork progression despite the accumulation of torsional stress and/or by avoiding the redistribution of supercoilings behind the moving fork. Alternatively, Mrc1 may directly promote fork reversal by assisting specialized enzymes in fork remodeling. Interestingly, although several fork remodeling activities were identified in both yeast and mammals[117,148], a potential role in fork reversal for the Mrc1 human orthologue Claspin has not been assessed to date.

Our finding that MRX degrades reversed forks in CPT-treated *tel1Δ* cells, while Exo1 is dispensable, is somehow surprising. In fact, Exo1 was found to nucleolytically process reversed forks generated in *mec1* and *rad53* checkpoint mutants treated with HU[119,161]. Furthermore, human EXO1 contributes to MRE11-dependent degradation of stalled forks in BRCA-defective cells[163]. As a Rad53-dependent phosphorylation was proposed to inhibit Exo1 activity[114] and a Mec1-dependent checkpoint is activated in CPT-treated *tel1Δ* cells, checkpoint activation may limit Exo1 action in these cells. Alternatively, different structures generated at replication forks that stall because of nucleotide depletion or of torsional constrains may be targeted by different nucleases. Indeed, nucleotide depletion in checkpoint mutants causes both uncoupling of leading- and lagging-strand synthesis and re-annealing of the daughter strands in a four-way junction with extensive fork-associated ssDNA regions, which can be the entry point for Exo1[120,161]. By contrast, torsional stress ahead of a replication fork was proposed to trigger parental strand re-winding and extrusion of the newly synthesized filaments[357].

MRX and Tel1 participate in the metabolism of replication forks arrested by a DSB or by transcription[358,359], or involved in replication of telomeric regions[283,360]. The same factors can also recognize abnormal forks generated in CPT. One possibility is that the regressed arms of CPT-induced reversed forks terminate with blunt or minimally processed DNA ends, which are known to recruit MRX and Tel1[32]. However, as Mre11 triggers Top1 release from DNA[38,337], we cannot exclude the possibility that MRX is recruited to the Top1-DNA intermediates and might be able to attack replication forks that reach the Top1-binding sites and revers in close proximity to these intermediates. In mammals, reversed forks accumulate in response to different stress[153] and are protected against degradation by mechanisms that involve tumor suppressors and HR proteins[162,164,333]. Unscheduled degradation of reversed forks in the absence of these protective mechanisms is mainly MRN-dependent and causes genomic instability and cell death[163,335,355,361]. It will be interesting to test whether ATM also contributes to reversed fork protection by preventing MRN action. However, a detailed understanding of ATM functions in CPT is important to develop novel therapies based on Top1 poisoning against cancers with defective ATM function.

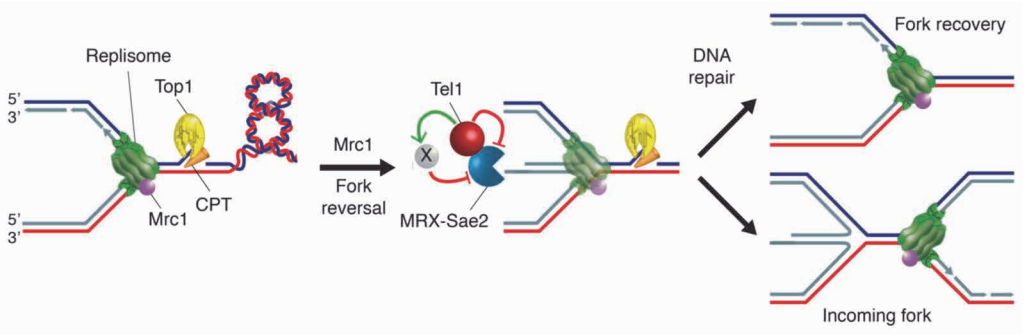

Figure 28 - Working model for Tel1 function at replication forks in CPT. *CPT-induced Top1 trapping on DNA results in the accumulation of DNA supercoiling ahead of an incoming replication fork. In the presence of this torsional stress Mrc1 promotes fork reversal. Reversed forks can be targeted by nucleases, mainly MRX-Sae2, which nucleolitically process the regressed arm. Tel1 counteracts the action of MRX-Sae2 either directly or through a still unknown factor (X), thus preventing unscheduled fork degradation. Reversed forks stabilization by Tel1 can support the completion of DNA replication after the repair of CPT-induced damage by either reversed fork reactivation or fusion with an incoming fork.*

In the second part of this work, I focused my attention on the study of the role of Tel1/ATM in the induction of replicative senescence. In the current senescence model, telomere shortening in the absence of telomerase activity leads to a progressive loss of telomere protective capping function. In this way, telomeres may be progressively recognized as accidental DSBs[342]. Eroded telomeres activate a DNA damage checkpoint, which depends on Mec1, Rad24, Mec3, Ddc2, Rad9, Chk1 and Rad53 proteins and leads to a prolonged cell cycle arrest and senescence[340–342]. Senescence is also triggered by the accumulation of telomeric ssDNA and its kinetics is affected by the inactivation/alteration of factors involved in telomere processing[342]. Although senescence is known to be delayed by the lack of Tel1[50,304,339,344], how this protein kinase induces replicative senescence is still unclear. In particular, the lack of Tel1 causes both a defect in checkpoint signaling[116,325,362] and a delay in the processing and the production of ssDNA at both telomeres and non-telomeric DNA ends[116,160]. This double Tel1 function makes it difficult to define whether Tel1 role in promoting replicative senescence can be ascribed to a direct function of Tel1 in signaling critically short telomeres to the checkpoint or to the generation of telomeric ssDNA that induces cell cycle arrest through the activation of the Mec1-dependent checkpoint. Here we dissected the function of Tel1 in inducing senescence by taking advantage of two different *TEL1* alleles: the *TEL1-hy184* hypermorphic allele, which was identified because it partially compensates for the lack of Mec1 functions in response to DNA damage[338], and the hypomorphic kinase-dead *tel1-kd* allele[320]. Both these alleles separate the Tel1 control of ssDNA generation from the Tel1 role in checkpoint signaling. In fact, neither *TEL1-hy184* nor *tel1-kd* affects the generation of ssDNA at telomeres. Conversely, both alleles affect checkpoint signaling, with *TEL1-hy184* allele being able to increase Rad53 phosphorylation in the absence of Mec1 both in the presence of damaged DNA and of eroded telomeres[338], while *tel1-kd* allele impaired histone H2A phosphorylation and Rad9 binding at a chromosomal DSB[325], thus decreasing checkpoint signaling compared to wild type cells.

Here, we show that in the absence of telomerase Tel1-hy184 accelerates the decline of cell proliferation without affecting the kinetics of telomere shortening. While this anticipated senescence induced by Tel1-hy184 completely depends on a Rad9-mediated checkpoint, Tel1-hy184 is able to anticipate senescence and to promote Rad53 phosphorylation in cells lacking Mec1 protein. Altogether, these results indicate that Tel1-hy184 not only can partially compensate for the lack of Mec1 function in inducing senescence, but it also enhances checkpoint signalling that triggers senescence in the presence of Mec1. This means that respect to Mec1, Tel1 has a direct and not completely redundant role in the induction of senescence.

This role can depend on telomere processing (resection), which induces Mec1-dependent checkpoint activation, or on a Tel1-mediated checkpoint activation. We found that the Tel1-hy184 and Tel1-kd variants exert opposite effects on senescence kinetics without affecting the generation of ssDNA at telomeres. This indicates that Tel1 function in regulating senescence is not linked to Tel1 function in promoting telomere processing, as previously hypothesized[344]. So, we propose a model in which, upon telomerase inactivation, Tel1 could induce replicative senescence by directly contributing to checkpoint signaling at dysfunctional telomeres (*Figure 29*).

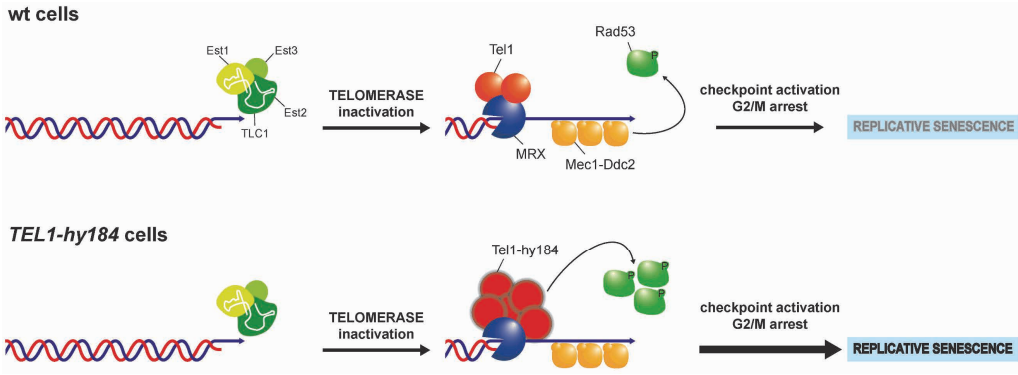

Figure 29 - Working model for Tel1-dependent induction of replicative senescence. *Upon telomerase inactivation, replicative senescence is triggered by the activation of DNA damage checkpoint. Tel1-hy184 accelerates senescence compared to wild type Tel1, while it does not appear to increase telomeric ssDNA. Since Tel1-hy184 variant shows an increased binding of Tel1 at telomeric DNA ends, our results suggest that Tel1 could induce replicative senescence by directly contributing to checkpoint signaling at dysfunctional telomeres.*

When we separated the two groups of mutations characterizing the *TEL1-hy184* allele, we found that the R2735G, E2737V amino acid substitutions, located in the kinase domain, increase both the kinase activity and the telomere length, indicating a tight correlation between Tel1 kinase activity and telomere length/telomerase activity. However, these mutations do not affect the onset of senescence, indicating that increased kinase activity alone is not sufficient to anticipate senescence. Interestingly, the F1752I, D1985N, E2133K substitutions, grouped in the FAT domain of the protein, cause anticipated senescence without affecting telomere length or Tel1 kinase activity. Furthermore, we show that *TEL1-hy184* allele and *TEL1-hy184-3N* allele enhance Tel1 binding at DNA ends. So, while increased kinase activity does not cause anticipated senescence, a more robust Tel1 binding at short telomeres seems to cause early senescence (*Figure 29*).

A recent work has revealed that the C-pincer of the N-terminal helical solenoid domain (residues: 1-1.762) of the ATM/Tel1 kinase is covalently connected to the FAT domain[40]. Therefore, the entire catalytic core of ATM/Tel1 appears tightly coupled to the N-terminal helical solenoid, which is consistent with the previous finding that the N-terminal helical solenoid may serve as a scaffold domain for the PIKKs proteins[363]. Furthermore, the N-terminal helical solenoid has also been reported to bind proteins that are associated with the PIKKs and to regulate their activities and cellular localizations[363]. In general, as FAT domain was proposed to be involved in protein-protein interactions[40], the F1752I, D1985N, E2133K substitutions might cause alterations in the interaction with substrates involved in checkpoint activation, but not in resection control. Alternatively, the increased binding/persistence of Tel1 could be sufficient to generate a local Tel1-dependent checkpoint signal that is then propagated through Rad9 and Rad53, both in the presence and in the absence of Mec1.

Consistent with previous findings that Tel1 mutant variants with both increased and reduced kinase activity compared to wild type Tel1 enhance DNA damage response and suppress *mec1Δ* cells hypersensitivity to genotoxic agents[338], here we show that both

TEL1-hy184-3N allele and *TEL1-hy184-2C* alleles, which have wild type and enhanced kinase activity respectively, suppress *mec1Δ* cells hypersensitivity to hydroxyurea. Thus, the ability of Tel1-hy184 to suppress the hypersensitivity to genotoxic agents and the checkpoint defects of *mec1Δ* cells, might be due to changes in its ability to interact with specific proteins and/or with damaged DNA. Conversely, Tel1 kinase activity is important both to promote telomere elongation and to induce senescence, while it is dispensable to enhance ssDNA at telomeres. This supports the idea that Tel1 has both kinase-dependent and -independent functions.

However, as cellular response to short telomeres is now considered one of the most potent barriers to cancer emergence[364], it is important to understand how short telomeres trigger a crucial signal for the fate of cells and the organism. The finding that Tel1/ATM participates, together with Mec1/ATR, to the activation of the checkpoint that promotes senescence in the absence of telomerase, contributes to this field and elucidates the multiple functions of Tel1/ATM at telomeres.

MATERIALS AND METHODS

Yeast and bacterial strains

Yeast strains and plasmids

All *Saccharomyces cerevisiae* strains used in this work are listed in Table 2 and are isogenic to W303 (MATa/α ade2-1 can1-100 his3-11,15 leu2-3,112 trp1-1 ura3-1 rad5-535), JKM139 (*MATa ho hmlΔ::ADE1 hmrΔ::ADE1 ade1-100 leu2-3,112 lys5 trp1::hisG ura3-52 ade3::GAL-HO*, from J. Haber, Brandeis University, Waltham, USA) , UCC5913 (*MATa-inc ade2-101 lys2-801 his3-Δ200 trp1-Δ63 ura3-52 leu2-Δ1::GAL1-HO-LEU2 VII-L::ADE2-TG(1-3)-HO site-LYS2,* kindly provided by D. Gottschling, Fred Hutchinson Cancer Research Center, Seattle, USA). All genetic manipulations were verified by polymerase chain reaction (PCR) and/or Southern blot analyses. Gene deletions were carried out by one-step PCR methods. A PCR one-step tagging method was used to obtain strains carrying the TOP1-3HA allele and the Tel1-3HA allele, which express a fully functional HA-tagged Top1 or Tel1 protein. The centromeric pVL1091 plasmid, carrying a *CDC13-EST1* gene fusion, was kindly provided by V. Lundblad (Salk Institute for Biological Sciences, La Jolla, CA, USA). A 2μ EXO1 plasmid was kindly provided by E. Alani (Cornell University, New York, NY, USA). Centromeric plasmids carrying either the wild-type MRC1 allele (pMRC1) or the mrc1-AQ mutant allele (pAO138), as well as yeast strains carrying mrc1-C14 and mrc1-C15 alleles at the endogenous chromosomal locus, were kindly provided by S. Elledge (Harvard Medical School, Boston, MA, USA). Strains carrying either the *tel1-kd* or the *mre11-H125N* alleles were kindly provided by T.D. Petes (Duke University School of Medicine, Durham, NC, USA) and L. Symington (Columbia University, New York, NY, USA), respectively. Cells were grown in YEP medium (1% yeast extract, 2% peptone, 50 mg/l adenine) supplemented with 2% glucose (YEPD) or 2% raffinose (YEPR) or 2% raffinose and 2% galactose (YEPRG). (S)-(+)-Camptothecin was dissolved in 1.2% DMSO before addition to the medium.

Table 2 - *Saccharomyces cerevisiae* strains used in this study

STRAIN	RELEVANT GENOTYPE	SOURCE
K699	W303 *MATa ade2-1 can1-100 his3-11,15 leu2-3,112 trp1-1 ura3-1 rad5-535*	[317]
UCC5913	*MATa-inc ade2-101 lys2-801 his3-Δ200 trp1-Δ63 ura3-52 leu2-Δ1::GAL1-HO-LEU2 VII-L::ADE2-TG(1-3)-HO site-LYS2*	[285]
JKM139	*MATa ho hmlΔ::ADE1 hmrΔ::ADE1 ade1-100 leu2-3,112 lys5 trp1::hisG ura3-52 ade3::GAL-HO*	[343]
K699 *tel1Δ*	W303 *MATa tel1Δ::HIS3*	[317]
YLL3575	W303 *MATa tel1-kd::LEU2*	[317]
K699 *top1*	W303 *MATa top1Δ::KANMX4*	This study
DMP6235/2A	W303 *MATa tel1Δ::HIS3 top1Δ::KANMX4*	This study

YLL3512	W303 *MATa TOP1-3HA::URA3*	This study
DMP6144/10A	W303 *MATa tel1Δ::HIS3 TOP1-3HA::URA3*	This study
YLL936	W303 *MATa mre11Δ::HIS3*	This study
DMP5878/2C	W303 *MATa mre11Δ::KANMX4 tel1Δ::HIS3*	This study
YLL941	W303 *MATa ku70Δ::HIS3*	This study
DMP2165/15B	W303 *MATα tel1Δ::HIS3*	This study
YLL1070	W303 *MATa sae2Δ::HIS3*	This study
YLL3326	W303 *MATa slx4Δ::HPHMX*	This study
DMP6174/9A	W303 *MATa tel1Δ::HIS3 slx4Δ::HPHMX*	This study
YLL254	W303 *MATa rad27Δ::KANMX4*	This study
DMP6173/5B	W303 *MATa tel1Δ::HIS3 rad27Δ::KANMX4*	This study
YLL3079	W303 *MATa mms4Δ::NATMX*	This study
DMP6175/1C	W303 *MATa tel1Δ::HIS3 mms4Δ::NATMX*	This study
K699 *rad52Δ*	W303 *MATa rad52Δ::TRP1*	This study
DMP6172/3B	W303 *MATa tel1Δ::HIS3 rad52Δ::TRP1*	This study
DMP6152/1C	W303 *MATa rad1Δ::URA3*	This study
YLL3588	W303 *MATa tdp1Δ::KANMX4*	This study
DMP6162/5A	W303 *MATa tdp1Δ::KANMX4 rad1Δ::URA3*	This study
DMP6162/1C	W303 *MATa tel1Δ::HIS3 rad1Δ::URA3*	This study
DMP6151/8C	W303 *MATa tel1Δ::HIS3 tdp1Δ::KANMX4*	This study
DMP6162/5A	W303 *MATa tel1Δ::HIS3 tdp1Δ::KANMX4 rad1Δ::URA3*	This study
YLL490	W303 *MATa mec1Δ::HIS3 sml1Δ::KANMX4*	This study
DMP5652/12B	W303 *MATa mrc1Δ::KANMX4*	This study
DMP5653/15C	W303 *MATa rad9Δ::URA3*	This study
DMP6220/3A	W303 *MATa tel1Δ::HIS3 mrc1Δ::KANMX4*	This study
DMP6221/2D	W303 *MATa tel1Δ::HIS3 rad9Δ::URA3*	This study
Y2545	W303 *MATa mrc1-C15-MYC5::KANMX4*	[65]
DMP6279/3A	W303 *MATa tel1Δ::HIS3 mrc1-C15-MYC5::KANMX4*	This study
DMP4527/17B	W303 *MATa rpd3Δ::HIS3*	This study
DMP6259	W303 *MATa tel1Δ::HIS3 rpd3Δ::HIS3*	This study
YLL3712	W303 *MATa rtt107Δ::HPHMX*	This study
YLL3713	W303 *MATa tel1Δ::HIS3 rtt107Δ::HPHMX*	This study
YLL2402	W303 *MATa exo1Δ::LEU2*	This study
DMP6425/1D	W303 *MATa tel1Δ::HIS3 exo1Δ::LEU2*	This study
LSY1397	W303 *MATa mre11-H125N*	[334]
DMP5958/13A	W303 *MATa tel1Δ::HIS3 mre11-H125N*	This study
DMP4242/2B	W303 *MATa sae2Δ::KANMX tel1Δ::HIS3*	This study
DMP6500/6C	W303 *MATa mrc1Δ::KANMX4 mre11-H125N*	This study
YLL3645	W303 *MATa csm3Δ::HPHMX*	This study
YLL3651	W303 *MATa tel1Δ::HIS3 csm3Δ::HPHMX*	This study
DMP5885/1C	W303 *MATa tof1Δ::HPHMX*	This study

DMP6229/4D	W303 *MATa tel1Δ::HIS3 tof1Δ::HPHMX*	This study
DMP5232/2C	W303 *MATa rad27Δ::KANMX4 mrc1Δ::HIS3*	This study
DMP6228/4D	W303 *MATa sae2Δ::HIS3 mrc1Δ::KANMX4*	This study
DMP6232/14B	W303 *MATa mrc1Δ::HIS3 tdp1Δ::KANMX4*	This study
DMP6232/12A	W303 *MATa mrc1Δ::HIS3 tdp1Δ::KANMX4 rad1Δ::URA3*	This study
DMP6232/10B	W303 *MATa mrc1Δ::HIS3 rad1Δ::URA3*	This study
Y2544	W303 *MATa mrc1-C14-MYC5::KANMX4*	[65]
DMP6278	W303 *MATa tel1Δ::HIS3 mrc1-C14-MYC5::KANMX4*	This study
YLL3854.2	W303 *MATa/α tel1Δ::HIS3/TEL1 est2Δ::KANMX4/EST2*	This study
YLL3854.3	W303 *MATa/α tel1Δ::HIS3/TEL1 est2Δ::KANMX4/EST2*	This study
YLL3855.3	W303 *MATa/α TEL1-hy184::LEU2/TEL1 est2Δ::KANMX4/EST2*	This study
YLL3855.6	W303 *MATa/α TEL1-hy184::LEU2/TEL1 est2Δ::KANMX4/EST2*	This study
YLL3905.4	W303 *MATa/α TEL1-hy184::LEU2/TEL1 est2Δ::HPHMX/EST2 rad9Δ::URA3/RAD9*	This study
YLL3881.3	W303 *MATa/α TEL1-hy184::LEU2/TEL1 est2Δ::HPHMX/EST2 mec1Δ::HIS3/MEC1 sml1Δ::KANMX4/SML1*	This study
YLL3881.26	W303 *MATa/α TEL1-hy184::LEU2/TEL1 est2Δ::HPHMX/EST2 mec1Δ::HIS3/MEC1 sml1Δ::KANMX4/SML1*	This study
YLL4016.1	W303 *MATa/α TEL1-hy184::LEU2/TEL1 tlc1Δ::KANMX4/TLC1 rad9Δ::URA3/RAD9*	This study
YLL4016.3	W303 *MATa/α TEL1-hy184::LEU2/TEL1 tlc1Δ::KANMX4/TLC1 rad9Δ::URA3/RAD9*	This study
YLL3920.1	W303 *MATa/α TEL1-hy184::LEU2/TEL1 tlc1Δ::HPHMX/TLC1 mec1Δ::HIS3/MEC1 sml1Δ::KANMX4/SML1*	This study
YLL3920.12	W303 *MATa/α TEL1-hy184::LEU2/TEL1 tlc1Δ::HPHMX/TLC1 mec1Δ::HIS3/MEC1 sml1Δ::KANMX4/SML1*	This study
YLL4039.3	W303 *MATa/α TEL1-hy184::LEU2/TEL1 est2Δ::HPHMX/EST2 exo1Δ::HIS3/EXO1*	This study
YLL4039.4	W303 *MATa/α TEL1-hy184::LEU2/TEL1 est2Δ::HPHMX/EST2 exo1Δ::HIS3/EXO1*	This study
YLL3918.5	W303 *MATa/α TEL1-hy184::LEU2/TEL1 est2Δ::KANMX4/EST2 rif2Δ::HIS3/RIF2*	This study

YLL3988.1	W303 *MATa/α tel1-kd::LEU2/TEL1 est2Δ::KANMX4/EST2*	This study
TEL1-hy184/6C	W303 *MATa TEL1-hy184::LEU2*	This study
DMP6736/1D	W303 *MATa TEL1-hy184::LEU2 mec1Δ::HIS3 sml1Δ::KANMX4*	This study
YLL3930.7	W303 *MATa TEL1-hy2C::LEU2 mec1Δ::HIS3 sml1Δ::KANMX4*	This study
YLL3936.10	W303 *MATa TEL1-hy3N::LEU2 mec1Δ::HIS3 sml1Δ::KANMX4*	This study
YLL3985.6	W303 *MATa/α TEL1-hy3N::LEU2/TEL1 est2Δ::HPHMX/EST2 mec1Δ::HIS3/MEC1 sml1Δ::KANMX4/sml1Δ::KANMX4*	This study
YLL3978.5	W303 *MATa/α TEL1-hy2C::LEU2/TEL1 est2Δ::HPHMX/EST2 mec1Δ::HIS3/MEC1 sml1Δ::KANMX4/sml1Δ::KANMX4*	This study
YLL2599/4A	*UCC5913 MATa bar1Δ::HPHMX*	This study
YLL3969.9	*UCC5913 MATa bar1Δ::HPHMX TEL1-hy184::KANMX4*	This study
YLL2820.1	*UCC5913 MATa bar1Δ::HPHMX tel1Δ::HIS3*	This study
YLL4060.2	*UCC5913 MATa bar1Δ::HPHMX tel1-kd::KANMX4*	This study
YLL3068.6	*UCC5913 MATa bar1Δ::HPHMX TEL1-3HA::NATMX*	This study
YLL3970.14	*UCC5913 MATa bar1Δ::HPHMX TEL1-3HA::NATMX-hy184::KANMX4*	This study
YLL4128.7	*UCC5913 MATa bar1Δ::HPHMX TEL1-3HA::NATMX-hy184-3N:KANMX4*	This study
DMP6260/1D	*JKM139 MATa TEL1-hy184::LEU2*	This study

E. coli strain

E. coli DH5αTM strain (*F-, φ80 dlacZM15, D(lacZTA-argF) U169, deoR, recA1, endA1, hsdR17, (rK-,mK+) phoA supE44, λ−, thi-1, gyrA96, relA1*) was used as bacterial host for plasmid manipulation and amplification. *E. coli* DH5αTM competent cells to transformation were purchased from Invitrogen.

Growth media

S. cerevisiae media

YEP (Yeast-Extract Peptone) is the standard rich media for *S. cerevisiae* and contains 10 g/L yeast extract, 20 g/L peptone and 50 mg/L adenine. YEP must be supplemented with 2% glucose (YEPD), 2% raffinose (YEP+raf) or 2% raffinose and 2% galactose

(YEP+raf+gal) as carbon source. YEP-based selective media are obtained including 400 µg/mL G418, 300 µg/mL hygromicin-B or 100 µg/mL nourseotricin. Solid media are obtained including 2% agar. Stock solutions are 50% glucose, 30% raffinose, 30% galactose, 80 mg/mL G418, 50 mg/mL hygromicin-B and 50 mg/mL nourseotricin. YEP and glucose stock solution are autoclave-sterilized and stored at RT. Sugars and antibiotics stock solutions are sterilized by microfiltration and stored at RT and 4°C respectively. S.C. (Synthetic Complete) is the minimal growth media for *S. cerevisiae* and contains 1.7 g/L YNB (Yeast Nitrogen Base) without amino acids, 5 g/L ammonium sulphate, 200µM inositol, 25 mg/L uracil, 25 mg/L adenine, 25 mg/L hystidine, 25 mg/L leucine, 25 mg/L tryptophan. S.C. can be supplemented with drop-out solution (20 mg/L arginine, 60 mg/L isoleucine, 40 mg/L lysine, 10 mg/L methionine, 60 mg/L phenylalanine, 50 mg/L tyrosine) based on yeast strains requirements. Different carbon sources can be used in rich media (2% glucose, 2% raffinose or 2% raffinose and 3% galactose). One or more amino acid/base can be omitted to have S.C.-based selective media (e.g. S.C.-ura is S.C. lacking uracil). To obtain G418 or NAT S.C. selective medium the 5 g/L ammonium sulphate are replaced with 1 g/L monosodic glutamic acid. Solid media are obtained by including 2% agar. Stock solutions are 17 g/L YNB + 50 g/L ammonium sulphate (or 10g/L monosodic glutamic acid), 5 g/L uracil, 5 g/L adenine, 5 g/L hystidine, 5 g/L leucine, 5 g/L tryptophan, 100X drop out solution (2 g/L arginine, 6 g/L isoleucine, 4 g/L lysine, 1 g/L methionine, 6 g/L phenylalanine, 5 g/L tyrosine), 20mM inositol. All these solutions are sterilized by micro-filtration and stored at 4°C. VB sporulation medium contains 13.6 g/L sodium acetate, 1.9 g/L KCl, 0.35 g/L MgSO4, 1.2 g/L NaCl. pH is adjusted to 7.0. To obtain solid medium include 2% agar. pH is adjusted to 7.0. Sterilization by autoclavation.

E. coli media

LD is the standard growth medium for *E. coli.* LD medium contains 10 g/L tryptone, 5 g/L yeast extract and 5 g/L NaCl. Solid medium is obtained by including 1% agar. LD+Amp selective medium is obtained including 50 µg/mL Ampicillin. LD is autoclave-sterilized and stored at RT. Ampicillin stock solution (2.5 g/L) is sterilized by micro-filtration and stored at 4°C.

Conservation and storage of *S. cerevisiae* and *E. coli* strains

Yeast cells are grown 2-3 days at 30°C on YEPD plates, resuspended in 15% glycerol and stored at -80°C. Bacteria are grown o/n at 37°C on LD+Amp plates, resuspended in 50% glycerol and stored at -80°C. Yeast and bacteria cells can be stored for years in these conditions.

Synchronization of yeast cells

Synchronization of yeast cells with α-factor

α-factor allows to synchronize a population of yeast cells in G_1 phase. This pheromone activates a signal transduction cascade which arrests yeast cells in G_1 phase. Only *MATa* cells are responsive to α-factor. To synchronize in G_1 a population of exponentially growing yeast cells in YEPD, 2 µg/mL α-factor is added to $6x10^6$ cells/mL culture. As the percentage of budded cells will fall below 5% cells are considered to be G_1-arrested. Cells are then washed and resuspended in fresh medium with or without 3 µg/mL α-factor to keep cells G1-arrested or release them into the cell cycle respectively. At this time cell cultures can be either treated with genotoxic agents or left untreated. If cells carry the deletion of *BAR1* gene, that encodes a protease that degrades the α-factor, 0.5 µg/mL α-factor is sufficient to induce a G_1-arrest that lasts several hours.

Synchronization of yeast cells with nocodazole

Nocodazole allows to synchronize a population of yeast cells in G_2 phase. This drug causes the depolimerization of microtubules, thus activating the mitotic checkpoint which arrests cells at the metaphase to anaphase transition (G_2 phase). To synchronize in G_2 a population of exponentially growing yeast cells in YEPD, 0.5 µg/mL nocodazole is added to $6x10^6$ cells/mL culture together with DMSO at a final concentration of 1% (use a stock solution of 100X nocodazole in 100% DMSO). As the percentage of dumbbell cells will reach 95% cells are considered to be G_2-arrested. Cells are then washed and resuspended in fresh medium with or without 1.5 µg/mL nocodazole to keep cells G_2-arrested or release them into the cell cycle respectively. At this time cell cultures can be either treated with genotoxic agents or left untreated.

Molecular biology techniques

Transformation of *E. coli* DH5α cells

DH5α competent cells are thawed on ice. Then, 50-100 µL cells are incubated 30 minutes in ice with 1 µL plasmid DNA. Cells are then subjected to heat shock at 37°C for 30 seconds and then incubated on ice for 2 minutes. Finally, 900 µL LD are added to the tube and cells are incubated 30 minutes at 37°C to allow expression of ampicillin resistance. Cells are then plated on LD+Amp and overnight incubated at 37°C.

Transformation of *S. cerevisiae* cells

YEPD exponentially growing yeast cells are harvested by centrifugation and washed with 1 mL 1M lithium acetate (LiAc) pH 7.5. Cells are then resuspended in 1M LiAc pH

7.5 to obtain a cells/LiAc 1:1 solution. 12 µL cells/LiAc are incubated 30-45 minutes at RT with 45 µL 50% PEG (PolyEthyleneGlycol) 3350, 4 µL carrier DNA (salmon sperm DNA) and 1-4 µL DNA of interest (double each quantity when transform with PCR products). After addition of 6 µL 60% glycerol cells are incubated at RT for 30-45 minutes, heat-shocked at 42°C for 5-10 minutes and plated on appropriate selective medium.

Plasmid DNA extraction from *E. coli*: minipreps with QIAGEN columns

This protocol allows the purification of up to 20 µg high copy plasmid DNA from 1-5 mL overnight *E. coli* culture in LD medium. Cells are pelleted by centrifugation and resuspended in 250 µL buffer P1 (100 µg/mL RNase, 50mM Tris HCl pH 8, 10mM EDTA pH 8). After addition of 250 µL buffer P2 (200mM NaOH, 1% SDS) the solution is mixed thoroughly by inverting the tube 4-6 times, and the lysis reaction occur in 5 minutes at RT. 350 µL N3 buffer (QIAGEN) are added to the solution, which is then centrifuged for 10 minutes. The supernatant is applied to a QIAprep spin column which is washed once with PB buffer (QIAGEN) and once with PE buffer (QIAGEN). The DNA is eluted with EB buffer (10mM Tris HCl pH 8.5).

Extraction of yeast genomic DNA (Teeny yeast DNA preps)

Yeast cells are harvested from overnight cultures by centrifugation, washed with 1 mL of 0.9M sorbytol 0.1M EDTA pH 7.5 and resuspended in 0.4 mL of the same solution supplemented with 14mM β-mercaptoethanol. Yeast cell wall is digested by 45 minutes incubation at 37°C with 0.4 mg/mL 20T zimoliase. Spheroplasts are harvested by 30 seconds centrifugation and resuspended in 400 µL TE. After addition of 90 µL of a solution containing EDTA pH 8.5, Tris base and SDS, spheroplasts are incubated 30 minutes at 65°C. Samples are kept on ice for 1 hour following addition of 80 µL 5M potassium acetate. Cell residues are eliminated by 15 minutes' centrifugation at 4°C. DNA is precipitated with chilled 100% ethanol, resuspended in 500 µL TE and incubated 30 minutes with 25 µL 1 mg/mL RNase to eliminate RNA. DNA is then precipitated with isopropanol and resuspended in the appropriate volume (typically 50 µL) of TE.

Polymerase Chain Reaction (PCR)

PCR allows to obtain high copy number of a specific DNA fragment of interest starting from very low quantity of DNA fragment. The reaction is directed to a specific DNA fragment by using a couple of oligonucleotides flanking the DNA sequence of interest. These oligonucleotides work as primers for the DNA polymerase. The reaction consists of a number of polymerization cycles which are based on 3 main temperature-dependent steps: denaturation of DNA (which occur over 90°C), primer annealing to DNA (typically take place at 45- 55°C depending on primer characteristic), synthesis of the DNA sequence of interest by a thermophilic DNA polymerase (which usually works

at 68 or 72°C). Different polymerases with different properties (processivity, fidelity, working temperature, etc) are commercially available and suitable for different purpose. Taq polymerase works at 72°C and is generally used for analytical PCR. Polymerases with higher fidelity like Pfx and VENT polymerases, which work respectively at 68 and 72°C, are generally employed when 100% polymerization accuracy is required. The typical 50 µL PCR mixture contains 1µL of template DNA, 0.5 µM each primer, 200µM dNTPs, 5 µL of 10X Reaction Buffer, 1mM $MgCl_2$, 1-2 U DNA polymerase and water to 50 µL. The typical cycle-program for a reaction is: 1. 2 minutes' denaturation at 94-95°C; 2. 30 seconds denaturation at 94-95°C; 3. 30 seconds annealing at primers Tm (melting temperature); 4. 1 minute polymerization per kb at 68 or 72°C (depending on polymerase); 5. repeat 30 times from step 2; 6. 51-minutes polymerization at 68-72°C. The choice of primer sequences determines the working Tm, which depends on the length (L) and GC% content of the oligonucleotides and can be calculated as follows: $Tm = 59.9 + 0.41(GC\%) - 675/L$.

Agarose gel electrophoresis

Agarose gel electrophoresis is the easiest and common way of separating and analyzing DNA molecules. This technique allows the separation of DNA fragments based on their different molecular weight (or length in kb). The purpose of this technique might be to visualize the DNA, to quantify it or to isolate a particular DNA fragment. The DNA is visualized by the addition in the gel of ethidium bromide, which is a fluorescent dye that intercalates between bases of nucleic acids. Ethidium bromide absorbs UV light and transmits the energy as visible orange light, revealing the DNA molecules to which is bound. To pour a gel, agarose powder is mixed with TAE (0.04M TrisAcetate 0.001M EDTA) to the desired concentration, and the solution is microwaved until completely melted. Most gels are made between 0.8% and 2% agarose. A 0.8% gel will show good resolution of large DNA fragments (5-10 Kb) and a 2% gel will show good resolution for small fragments (0.2-1 Kb). Ethidium bromide is added to the gel at a final concentration of 1 µg/mL to facilitate visualization of DNA after electrophoresis. After cooling the solution to about 60°C, it is poured into a casting tray containing a sample comb and allowed to solidify at RT or at 4°C. The comb is then removed, and the gel is placed into an electrophoresis chamber and just covered with the buffer (TAE). Sample containing DNA mixed with loading buffer are then pipetted into the sample wells. The loading buffer contains 0.05% bromophenol blue and 5% glycerol, which give colour and density to the sample. A marker containing DNA fragments of known length and concentration is loaded in parallel to determine size and quantity of DNA fragments in the samples. Then current is applied and DNA will migrate toward the positive electrode. When adequate migration has occurred, DNA fragments are visualized by placing the gel on a UV trans illuminator.

DNA extraction from agarose gel (paper strip method)

This method allows to isolate a DNA fragment of interest. Using a scalpel blade cut a slit immediately in front of the band to be extracted. Cut a piece of GF-C filter to size to fit inside the slit. Place the paper strip in the slit and switch on the current for 1-2 minutes at 150 V. The DNA runs onward into the paper and is delayed in the smaller mesh size of the paper. Remove the strip of paper and place it into a 0.5 mL micro centrifuge tube. Make a tiny hole in the bottom of the tube using a syringe needle, place the 0.5 mL tube inside a 1.5 mL tube and spin for 30 seconds. Buffer and DNA are retained in the 1.5 mL tube. Extract the DNA with 1 volume of phenol/chloroform and precipitate the DNA with 100mM sodium acetate and 3 volumes of 100% ethanol. After micro centrifugation re-dissolve DNA in an appropriate volume of water, TRIS (10mM Tris HCl pH 8.5) or TE (10mM Tris HCl, 1mM EDTA pH7.4) buffer.

Southern blot analysis of telomere length

Yeast genomic DNA prepared with standard methods is digested with *Xho*I restriction enzyme. The resulting DNA fragments are separated by agarose gel electrophoresis (in TBE 1X buffers) in a 0.8% agarose gel. When adequate migration has occurred, gel is washed 40 minutes with a denaturation buffer (0.2N NaOH, 0.6M NaCl), and 40 minutes with a neutralization buffer (1.5M NaCl, 1M Tris HCl, pH 7.4). DNA is blotted onto a GeneScreen nylon membrane (New England Nuclear, Boston) by overnight capillary transfer with 10X SSC buffer (20X SSC: 3M sodium chloride, 0.3M sodium citrate, pH 7.5). Membrane is then washed with 4X SSC and UV-crosslinked. Hybridization is carried out by incubating membrane for 5 hours at 50°C with pre-hybridization buffer following by o/n incubation at 50°C with pre-hybridization buffer complemented probe. The probe (^{32}P-labelled poly(GT) probe) is obtained by random priming method (DECAprimeTM kit by Ambion) on a suitable DNA template and with ^{32}P d-ATP. Filter is then washed (45 minutes + 15 minutes) at 55°C with a washing solution (0.2M sodium phosphate buffer pH 7.2, SDS 1%, water), air dried and then exposed to an autoradiography film.

In-Gel Hybridization for the visualization of G-tail

Visualization of the single-stranded overhangs at native telomeres was done by in-gel hybridization as previously described[287]. The same gel was denatured and hybridized with the end-labeled C-rich oligonucleotide for loading control.

Southern blot analysis of DSB end resection

DSB end resection at the *MAT* locus in JKM139 derivative strains was analyzed on alkaline agarose gels as described in[365], by using a single-stranded RNA (ssRNA) probe complementary to the unresected DSB strand. The ssRNA probe was obtained by *in vitro* transcription using Promega Riboprobe System-T7 and a pGEM-7Zf based plasmid

as a template. Quantitative analysis of DSB resection was performed by calculating the ratio of band intensities for ssDNA and total amount of DSB products.
Instead, to monitor DNA end resection at the HO-derived telomere, RsaI- and EcoRV-digested genomic DNA was subjected to denaturing polyacrylamide gel electrophoresis and transferred to a positively charged nylon membrane. The filter is then hybridized with a single-stranded riboprobe complementary to the 5′ C-strand to a site located 212 nt from the HO cutting site. For quantitative analysis of C-strand signals, the ratios between the intensities of C-strand and loading control bands were calculated by using the NIH image program.

Chromatin ImmunoPrecipitation (ChIP) analysis

growing cells (50 mL of culture at the concentration of $8x10^6$ cells/mL) were treated with 1.4 mL of 37% formaldehyde for 10 minutes while shaking, in order to create DNA-protein and protein-protein covalent bounds (crosslink). Then 2.5 mL of 2.5M glycine were added for other 5 minutes while shaking. Treated cells were kept on ice until centrifugation at 1800 rpm for 5 minutes at 4°C. Cell pellet was then washed first with HBS buffer (50mM HEPES pH 7.5, 140mM NaCl) and then with ChIP buffer (50mM HEPES pH 7.5, 140mM NaCl, 1mM EDTA pH 8, 1% IGEPAL CA-630, 0.1% Sodium deoxycholate, 1mM PMSF). Before each wash cells were pelleted by centrifugation at 1800 rpm for 5 minutes at 4°C. After the wash with ChIP buffer and subsequent centrifugation, the supernatant was carefully and completely removed. Then 0.4 mL of ChIP buffer + complete anti-proteolitic tablets (Roche) was added and samples were stored at -80°C until the following day. After breaking cells for 30 minutes at 4°C with glass beads, the latter were eliminated. This passage was followed by centrifugation at 4°C for 30 minutes. Pellet was resuspended in 0.5 mL ChIP buffer + antiproteolitics and then sonicated, in order to share DNA in 500-1000 bp fragments (4 cycles of 25 seconds). At this point 5 µL as “input DNA” for PCR reactions and 20 µL as “input” for Western blot analysis were taken. Then 400 µL of the remaining solution was immunoprecipitated with specific Dynabeads-coated antibodies. After proper incubation with desired antibodies, Dynabeads could be washed RT as follow: 2X with SDS buffer (50mM HEPES pH 7.5, 1mM EDTA pH 8, 140mM NaCl, 0.025% SDS), 1X with High-salt buffer (50mM HEPES pH 7.5, 1mM EDTA pH 8, 1M NaCl), 1X with T/L buffer (20mM Tris-Cl, pH 7.5, 250mM LiCl, 1mM EDTA pH 8, 0.05% sodium deoxycholate, 0.5%IGEPALCA630), and then 2X with T/E buffer (20mM Tris-Cl pH 7.5, 0.1mM EDTA pH 8). All washes were done by pulling down Dynabeads 1 minute and then nutating for 4 minutes with the specific buffer. After the last wash Dynabeads were resuspended in 145 µL TE + 1% SDS buffer, shaked on a vortex, put at 65°C for 2 minutes, shaked on vortex again and then pulled down. Then 120 µL of the supernatant were put at 65°C over-night for reverse cross-linking, while 20 µL were stored as sample for Western blot analysis of the immunoprecipitated protein amount. Previously taken input DNA samples must be put at 65°C over-night with 115 µL of TE + 1% SDS buffer. The next

day DNA must be purified for PCR analysis with QIAGEN columns. Quantification of immunoprecipitated DNA was achieved by quantitative real-time (qPCR) on a Bio-Rad MiniOpticon apparatus. qPCR at the HO-induced DSB in UCC5913 derived strains was carried out by using primer pairs located at the ADH locus and at the *ARO1* fragment of chromosome IV. Data were expressed as fold enrichment at the HO-induced DSB over that at the non-cleaved *ARO1* locus, after normalization of each ChIP signals to the corresponding input for each time point. Fold enrichment was then normalized to the efficiency of DSB induction. qPCR at the HO-induced telomere was carried out by using primer pairs located at 640 bp centromere-proximal to the HO cutting site at chromosome VII and at the nontelomeric *ARO1* fragment of chromosome IV (CON). qPCR at native telomeres was carried out by using primer pairs located at 70 bp and 139 bp from the TG sequences on telomeres VI-R (right) and XV-L (left), respectively HA-tagged proteins were immunoprecipitated with anti-HA (ab9110) from Abcam.

EM analysis of reversed forks

This procedure was performed as recently described[366], with the modifications below. Cell cultures were arrested in G_1 phase with α-factor and then released into fresh medium supplemented with 50 µM CPT (CPT was dissolved in 2% DMSO). After 40 min of CPT treatment, 5×10^9 cells were harvested, rinsed with ice-cold water, and suspended in 20 ml of ice-cold water. Each sample was transferred into two petri dishes (diameter 4.5 cm) and cross-linked with three cycles of treatment with 3,5,8-trimethylpsoralen (TMP, dissolved in 100% EtOH, 10 µg/ml final concentration). After TMP addition, samples were incubated for 5 min at 4°C in a dark room and then irradiated with 365 nm UV monochromatic light (UV Lamps CAMAG 2 × 366 8W) in a customized chamber for 3 min. Cells suspension was then transferred into a 50-ml tube and rinsed with ice-cold water to remove ethanol. DNA extraction was carried out with Qiagen Genomic-tip 100/G. Briefly, cells were lysed with 3.12 mg/ml zymolyase 20T in Y1 Qiagen Buffer with β-mercaptoethanol at 30°C for 40 min and then incubated in G^2 Qiagen Buffer with 0.2 mg/ml RNaseA and 0.4 mg/ml proteinaseK at 37°C for 2 h. After column purification with Qiagen Genomic-tip 100/G, DNA was eluted with QF Qiagen Buffer and precipitated with 0.7 volumes of isopropanol. Finally, DNA was dissolved in 200 µl TE 1× (10 mM Tris-HCl, 1 mM EDTA, pH 8). 100 U of PvuI restriction enzyme (New England Biolabs) was used to digest 12 µg of yeast genomic DNA for 4-5 h. Replication intermediates enrichment was performed by Qiagen Plasmid Mini Kit columns. The Qiagen-tip 20 surface tension was reduced by applying 1 ml QBT buffer. The columns were rinsed with 10 mM Tris-HCl (pH 8.0), 1 M NaCl, followed by equilibration with 10 mM Tris-HCl (pH 8.0), 300 mM NaCl. DNA was then loaded onto the columns. The columns were rinsed with high NaCl solution (10 mM Tris–HCl pH 8.0 and 900 mM NaCl) and eluted with caffeine solution (10 mM Tris-HCl pH 8.0, 1 M NaCl, and 1.8% w/v caffeine). To purify and concentrate the DNA, an Amicon size-exclusion column was used. DNA was then resuspended in TE 1× buffer. The benzyldimethylalkylammonium

chloride (BAC) method was used to spread the DNA on the water surface and then load it on carbon-coated 400-mesh copper grids. Subsequently, DNA was coated with platinum using a High Vacuum Evaporator MED 020 (BalTec). Microscopy analysis was performed with a transmission electron microscope (Tecnai G2 Spirit; FEI; LaB6 filament; high tension ≤ 120 kV) and picture acquisition with a side mount charge-coupled device camera (2,600 × 4,000 pixels; Orius 1000; Gatan, Inc.). For each experimental condition, at least 70 replication fork molecules were analyzed. DigitalMicrograph version 1.83.842 (Gatan, Inc.) and ImageJ (National Institutes of Health) were used to process and analyse the images. Every EM experiment was repeated twice, and at least 70 molecules per sample were analysed. The results were analyzed using GraphPad Prism 6 for Mac OS X, using Mann–Whitney test. Whiskers: 10–90th percentile (****P < 0.0001; ***P < 0.001; **P < 0.01; *P < 0.05; ns, not significant).

Total protein extracts

Total protein extracts were prepared from 10^8 cells collected from exponentially growing yeast cultures. Cells are harvested by centrifugation and washed with 20% trichloracetic acid (TCA) in order to prevent proteolysis and resuspended in 50 µL 20% TCA. After addition of 200 µL of glass beads, cells are disrupted by vortexing for 8 minutes. Glass beads are washed with 400 µL 5% TCA, and the resulting extract are centrifuged at 3000 rpm for 10 minutes. The pellet is resuspended in 70 µL Laemmli buffer (0.62M Tris, 2% SDS, 10% glycine, 0.001% Bfb, 100mM DTT), neutralized with 30 µL 1M Tris base, boiled for 2 minutes, and finally clarified by centrifugation.

SDS-PAGE and Western blot analysis

Protein extracts for Western blot analysis were prepared by TCA precipitation. Protein extracts are loaded in 10% polyacrylamide gels (composition). Proteins are separated based on their molecular weight by polyacrylamide gel electrophoresis in the presence of sodium dodecyl sulphate (SDS-PAGE). When adequate migration has occurred proteins are blotted onto nitrocellulose membrane. Membrane is saturated by 1-hour incubation with 4% milk in TBS containing 0.2% TRITON X-100 and incubated for 2 hours with primary antibodies. Membrane is washed three times with TBS for 10 minutes, incubated for 1 hour with secondary antibodies and again washed with TBS. Detection is performed with ECL (Enhanced ChemiLuminescence -Genespin) and X-ray films according to the manufacturer. Primary monoclonal 12CA5 anti-HA and 9E10 anti-MYC antibodies are purchased at GE Healthcare, as well as peroxidase conjucated IgG antirabbit and anti-mouse secondary antibodies. Rad53 was detected by using anti-Rad53 (ab104232) polyclonal antibodies from Abcam.

Immunoprecipitation and kinase assay

Protein extracts for the immunoprecipitations were prepared in a lysis buffer containing 50mM HEPES (pH 7.4), 100mM KCl, 0.1mM EDTA (pH 7.5), 0.2% Tween-20, 1mM dithiothreitol (DTT), 25mM NaFl, 100µM sodium orthovanadate, 0.5 mM phenylmethylsulfonyl fluoride, 25mM β-glycerophosphate, and a protease inhibitor cocktail (Roche Diagnostics). After the addition of a 1:1 volume of acid-washed glass beads and breakage, equal amounts of protein of the different clarified extracts were incubated for 2 hours at 4°C with 75 µL of a 50% (vol/vol) protein A-Sepharose resin covalently linked to 12CA5 monoclonal antibody. For the Kinase Assay, resin was washed three times in the lysis buffer and were resuspended in 450 µL of a kinase buffer containing 10mM HEPES (pH 7.4), 50mM NaCl, 10mM MgCl2, 10mM MnCl2, 1mM DTT. Resuspended resins (150 µL) were dried, followed by the addition of 11.5 µL of kinase buffer, 1.5 µL of 20µM unlabeled ATP, 10 µCi of 32P-labeled ATP, and 1 µL of Phosphorylated Heat- and Acid-Stable protein I (PHAS-I; 1 µg/µL; Stratagene). Kinase reactions were incubated at 30°C for 30 minutes. Sodium dodecyl sulfate (SDS) gel-loading buffer (15 µL) was added to the resins, boiled and bound proteins were resolved by SDS-18% polyacrylamide gel electrophoresis and visualized after exposure of the gels to autoradiography films. The residual 300 µL of each resuspended resin was dried, resuspended in 10 µL of loading buffer, boiled and subjected to Western blot analysis with anti-HA antibody.

Other techniques

Senescence assay

Senescence analysis was performed by serial passages in liquid YEPD medium of spore clones obtained from heterozygous diploid (without *EST2* or *TLC1* gene and the mutation of interest), thus ensuring that all the strains inherit telomeres of similar length and from the same epigenetic environment. Meiotic tetrads were dissected on YEPD plates that were incubated at 25°C, followed by spore genotyping. Spore colonies were inoculated in YEPD medium at the concentration of $5x10^4$ cells/mL. Every 24 hours, cell cultures were diluted back to $5x10^4$ cells/mL in YEPD. The mean cell concentration of at least four independent spores with the same genotype against the number of generations (Population Doublings, PDs) is plotted in a graph to visualize the senescence kinetic. We assume that the spore colonies have undergone 30 generations when they were inoculated.

FACS analysis of DNA content

FACS (Fluorescence-Activated Cell Sorting) analysis allows to determine the DNA content of every single cell of a given population of yeast cells. $6x10^6$ cells are harvested by centrifugation, resuspended in 70% ethanol and incubated at RT for 1 hour. Cells are

then washed with 1 mL 50mM Tris pH 7.5 and incubated overnight at 37°C in the same solution with 1 mg/mL RNase. Samples are centrifuged and cells are incubated at 37°C for 30 minutes with 5 mg/mL pepsin in 55mM HCl, washed with 1 mL FACS Buffer and stained in 0.5 mL FACS buffer with 50 µg/mL propidium iodide. 100 µL of each sample are diluted in 1 mL 50mM Tris pH 7.5 and analysed with a BectonDickinson FACS Scan. The same samples can also be analysed by fluorescence microscopy to score nuclear division.

Drop test

For spot assays, exponentially growing overnight cultures were counted, and 10-fold serial dilutions of equivalent cell numbers were spotted onto plates containing the indicated media. Images were scanned 2-3 days after plating and growth at 28°C.

REFERENCES

1. Hartwell, L. H. & Kastan, M. B. Cell cycle control and cancer. *Science* **266,** 1821–1828 (1994).
2. BW, S. & CP, W. *World Cancer Report 2014*.
3. Hanahan, D. & Weinberg, R. A. Hallmarks of cancer: the next generation. *Cell* **144,** 646–674 (2011).
4. Deng, Y. & Chang, S. Role of telomeres and telomerase in genomic instability, senescence and cancer. *Lab. Investig. J. Tech. Methods Pathol.* **87,** 1071–1076 (2007).
5. Negrini, S., Gorgoulis, V. G. & Halazonetis, T. D. Genomic instability--an evolving hallmark of cancer. *Nat. Rev. Mol. Cell Biol.* **11,** 220–228 (2010).
6. Brosh, R. M. DNA helicases involved in DNA repair and their roles in cancer. *Nat. Rev. Cancer* **13,** 542–558 (2013).
7. O'Neil, N. J., Bailey, M. L. & Hieter, P. Synthetic lethality and cancer. *Nat. Rev. Genet.* **18,** 613–623 (2017).
8. Beijersbergen, R. L., Wessels, L. F. A. & Bernards, R. Synthetic Lethality in Cancer Therapeutics. *Annu. Rev. Cancer Biol.* **1,** 141–161 (2017).
9. Aylon, Y. & Kupiec, M. DSB repair: the yeast paradigm. *DNA Repair* **3,** 797–815 (2004).
10. Hoeijmakers, J. H. J. DNA damage, aging, and cancer. *N. Engl. J. Med.* **361,** 1475–1485 (2009).
11. Hoeijmakers, J. H. Genome maintenance mechanisms for preventing cancer. *Nature* **411,** 366–374 (2001).
12. Weber, S. Light-driven enzymatic catalysis of DNA repair: a review of recent biophysical studies on photolyase. *Biochim. Biophys. Acta* **1707,** 1–23 (2005).
13. Hoeijmakers, J. H. Nucleotide excision repair. II: From yeast to mammals. *Trends Genet. TIG* **9,** 211–217 (1993).
14. Almeida, K. H. & Sobol, R. W. A unified view of base excision repair: lesion-dependent protein complexes regulated by post-translational modification. *DNA Repair* **6,** 695–711 (2007).
15. Aguilera, A. & García-Muse, T. Causes of genome instability. *Annu. Rev. Genet.* **47,** 1–32 (2013).
16. So, A., Le Guen, T., Lopez, B. S. & Guirouilh-Barbat, J. Genomic rearrangements induced by unscheduled DNA double strand breaks in somatic mammalian cells. *FEBS J.* **284,** 2324–2344 (2017).
17. Mehta, A. & Haber, J. E. Sources of DNA double-strand breaks and models of recombinational DNA repair. *Cold Spring Harb. Perspect. Biol.* **6,** a016428 (2014).
18. Finn, K., Lowndes, N. F. & Grenon, M. Eukaryotic DNA damage checkpoint activation in response to double-strand breaks. *Cell. Mol. Life Sci. CMLS* **69,** 1447–1473 (2012).
19. Gobbini, E., Cesena, D., Galbiati, A., Lockhart, A. & Longhese, M. P. Interplays between ATM/Tel1 and ATR/Mec1 in sensing and signaling DNA double-strand breaks. *DNA Repair* **12,** 791–799 (2013).
20. Ciccia, A. & Elledge, S. J. The DNA damage response: making it safe to play with knives. *Mol. Cell* **40,** 179–204 (2010).
21. Lisby, M., Barlow, J. H., Burgess, R. C. & Rothstein, R. Choreography of the DNA damage response: spatiotemporal relationships among checkpoint and repair proteins. *Cell* **118,** 699–713 (2004).
22. Rupnik, A., Lowndes, N. F. & Grenon, M. MRN and the race to the break. *Chromosoma* **119,** 115–135 (2010).

23. Slijepcevic, P. The role of DNA damage response proteins at telomeres--an 'integrative' model. *DNA Repair* **5,** 1299–1306 (2006).
24. Borde, V. The multiple roles of the Mre11 complex for meiotic recombination. *Chromosome Res. Int. J. Mol. Supramol. Evol. Asp. Chromosome Biol.* **15,** 551–563 (2007).
25. Williams, R. S., Williams, J. S. & Tainer, J. A. Mre11-Rad50-Nbs1 is a keystone complex connecting DNA repair machinery, double-strand break signaling, and the chromatin template. *Biochem. Cell Biol. Biochim. Biol. Cell.* **85,** 509–520 (2007).
26. Hopfner, K. P. *et al.* Structural biology of Rad50 ATPase: ATP-driven conformational control in DNA double-strand break repair and the ABC-ATPase superfamily. *Cell* **101,** 789–800 (2000).
27. Hopfner, K.-P. *et al.* The Rad50 zinc-hook is a structure joining Mre11 complexes in DNA recombination and repair. *Nature* **418,** 562–566 (2002).
28. Tsukamoto, Y., Mitsuoka, C., Terasawa, M., Ogawa, H. & Ogawa, T. Xrs2p regulates Mre11p translocation to the nucleus and plays a role in telomere elongation and meiotic recombination. *Mol. Biol. Cell* **16,** 597–608 (2005).
29. Tauchi, H. *et al.* The forkhead-associated domain of NBS1 is essential for nuclear foci formation after irradiation but not essential for hRAD50[middle dot]hMRE11[middle dot]NBS1 complex DNA repair activity. *J. Biol. Chem.* **276,** 12–15 (2001).
30. Lee, J.-H. *et al.* Regulation of Mre11/Rad50 by Nbs1: effects on nucleotide-dependent DNA binding and association with ataxia-telangiectasia-like disorder mutant complexes. *J. Biol. Chem.* **278,** 45171–45181 (2003).
31. Trujillo, K. M. *et al.* Yeast xrs2 binds DNA and helps target rad50 and mre11 to DNA ends. *J. Biol. Chem.* **278,** 48957–48964 (2003).
32. Nakada, D., Matsumoto, K. & Sugimoto, K. ATM-related Tel1 associates with double-strand breaks through an Xrs2-dependent mechanism. *Genes Dev.* **17,** 1957–1962 (2003).
33. Greenwell, P. W. *et al.* TEL1, a gene involved in controlling telomere length in S. cerevisiae, is homologous to the human ataxia telangiectasia gene. *Cell* **82,** 823–829 (1995).
34. Clouaire, T., Marnef, A. & Legube, G. Taming Tricky DSBs: ATM on duty. *DNA Repair* **56,** 84–91 (2017).
35. McKinnon, P. J. ATM and ataxia telangiectasia. *EMBO Rep.* **5,** 772–776 (2004).
36. Lempiäinen, H. & Halazonetis, T. D. Emerging common themes in regulation of PIKKs and PI3Ks. *EMBO J.* **28,** 3067–3073 (2009).
37. Di Domenico, E. G., Romano, E., Del Porto, P. & Ascenzioni, F. Multifunctional role of ATM/Tel1 kinase in genome stability: from the DNA damage response to telomere maintenance. *BioMed Res. Int.* **2014,** 787404 (2014).
38. Fukunaga, K., Kwon, Y., Sung, P. & Sugimoto, K. Activation of Protein Kinase Tel1 through Recognition of Protein-Bound DNA Ends ▿. *Mol. Cell. Biol.* **31,** 1959–1971 (2011).
39. Guleria, A. & Chandna, S. ATM kinase: Much more than a DNA damage responsive protein. *DNA Repair* **39,** 1–20 (2016).
40. Wang, X. *et al.* Structure of the intact ATM/Tel1 kinase. *Nat. Commun.* **7,** 11655 (2016).
41. Paull, T. T. Mechanisms of ATM Activation. *Annu. Rev. Biochem.* **84,** 711–738 (2015).
42. You, Z., Chahwan, C., Bailis, J., Hunter, T. & Russell, P. ATM activation and its recruitment to damaged DNA require binding to the C terminus of Nbs1. *Mol. Cell. Biol.* **25,** 5363–5379 (2005).

43. Clerici, M., Trovesi, C., Galbiati, A., Lucchini, G. & Longhese, M. P. Mec1/ATR regulates the generation of single-stranded DNA that attenuates Tel1/ATM signaling at DNA ends. *EMBO J.* **33,** 198–216 (2014).
44. Jazayeri, A. *et al.* ATM- and cell cycle-dependent regulation of ATR in response to DNA double-strand breaks. *Nat. Cell Biol.* **8,** 37–45 (2006).
45. Zou, L. & Elledge, S. J. Sensing DNA damage through ATRIP recognition of RPA-ssDNA complexes. *Science* **300,** 1542–1548 (2003).
46. Navadgi-Patil, V. M. & Burgers, P. M. A tale of two tails: activation of DNA damage checkpoint kinase Mec1/ATR by the 9-1-1 clamp and by Dpb11/TopBP1. *DNA Repair* **8,** 996–1003 (2009).
47. Majka, J., Niedziela-Majka, A. & Burgers, P. M. J. The checkpoint clamp activates Mec1 kinase during initiation of the DNA damage checkpoint. *Mol. Cell* **24,** 891–901 (2006).
48. Kumagai, A., Lee, J., Yoo, H. Y. & Dunphy, W. G. TopBP1 activates the ATR-ATRIP complex. *Cell* **124,** 943–955 (2006).
49. Mordes, D. A., Nam, E. A. & Cortez, D. Dpb11 activates the Mec1-Ddc2 complex. *Proc. Natl. Acad. Sci. U. S. A.* **105,** 18730–18734 (2008).
50. Ritchie, K. B., Mallory, J. C. & Petes, T. D. Interactions of TLC1 (which encodes the RNA subunit of telomerase), TEL1, and MEC1 in regulating telomere length in the yeast Saccharomyces cerevisiae. *Mol. Cell. Biol.* **19,** 6065–6075 (1999).
51. Sanchez, Y. *et al.* Regulation of RAD53 by the ATM-like kinases MEC1 and TEL1 in yeast cell cycle checkpoint pathways. *Science* **271,** 357–360 (1996).
52. Usui, T., Ogawa, H. & Petrini, J. H. A DNA damage response pathway controlled by Tel1 and the Mre11 complex. *Mol. Cell* **7,** 1255–1266 (2001).
53. Pellicioli, A. & Foiani, M. Signal transduction: how rad53 kinase is activated. *Curr. Biol. CB* **15,** R769–771 (2005).
54. Gardner, K. A., Rine, J. & Fox, C. A. A region of the Sir1 protein dedicated to recognition of a silencer and required for interaction with the Orc1 protein in saccharomyces cerevisiae. *Genetics* **151,** 31–44 (1999).
55. Sanchez, Y. *et al.* Control of the DNA damage checkpoint by chk1 and rad53 protein kinases through distinct mechanisms. *Science* **286,** 1166–1171 (1999).
56. Nyberg, K. A., Michelson, R. J., Putnam, C. W. & Weinert, T. A. Toward maintaining the genome: DNA damage and replication checkpoints. *Annu. Rev. Genet.* **36,** 617–656 (2002).
57. Guo, B., Styles, C. A., Feng, Q. & Fink, G. R. A Saccharomyces gene family involved in invasive growth, cell-cell adhesion, and mating. *Proc. Natl. Acad. Sci. U. S. A.* **97,** 12158–12163 (2000).
58. Alcasabas, A. A. *et al.* Mrc1 transduces signals of DNA replication stress to activate Rad53. *Nat. Cell Biol.* **3,** 958–965 (2001).
59. Schwartz, M. F. *et al.* Rad9 phosphorylation sites couple Rad53 to the Saccharomyces cerevisiae DNA damage checkpoint. *Mol. Cell* **9,** 1055–1065 (2002).
60. Sweeney, F. D. *et al.* Saccharomyces cerevisiae Rad9 acts as a Mec1 adaptor to allow Rad53 activation. *Curr. Biol. CB* **15,** 1364–1375 (2005).
61. Gilbert, C. S., Green, C. M. & Lowndes, N. F. Budding yeast Rad9 is an ATP-dependent Rad53 activating machine. *Mol. Cell* **8,** 129–136 (2001).
62. Blankley, R. T. & Lydall, D. A domain of Rad9 specifically required for activation of Chk1 in budding yeast. *J. Cell Sci.* **117,** 601–608 (2004).

63. Tanaka, K. & Russell, P. Mrc1 channels the DNA replication arrest signal to checkpoint kinase Cds1. *Nat. Cell Biol.* **3,** 966–972 (2001).
64. Katou, Y. *et al.* S-phase checkpoint proteins Tof1 and Mrc1 form a stable replication-pausing complex. *Nature* **424,** 1078–1083 (2003).
65. Osborn, A. J. & Elledge, S. J. Mrc1 is a replication fork component whose phosphorylation in response to DNA replication stress activates Rad53. *Genes Dev.* **17,** 1755–1767 (2003).
66. Nedelcheva, M. N. *et al.* Uncoupling of unwinding from DNA synthesis implies regulation of MCM helicase by Tof1/Mrc1/Csm3 checkpoint complex. *J. Mol. Biol.* **347,** 509–521 (2005).
67. Szyjka, S. J., Viggiani, C. J. & Aparicio, O. M. Mrc1 is required for normal progression of replication forks throughout chromatin in S. cerevisiae. *Mol. Cell* **19,** 691–697 (2005).
68. Tourrière, H., Versini, G., Cordón-Preciado, V., Alabert, C. & Pasero, P. Mrc1 and Tof1 promote replication fork progression and recovery independently of Rad53. *Mol. Cell* **19,** 699–706 (2005).
69. Takayama, Y. *et al.* GINS, a novel multiprotein complex required for chromosomal DNA replication in budding yeast. *Genes Dev.* **17,** 1153–1165 (2003).
70. Gambus, A. *et al.* GINS maintains association of Cdc45 with MCM in replisome progression complexes at eukaryotic DNA replication forks. *Nat. Cell Biol.* **8,** 358–366 (2006).
71. Lou, H. *et al.* Mrc1 and DNA polymerase epsilon function together in linking DNA replication and the S phase checkpoint. *Mol. Cell* **32,** 106–117 (2008).
72. Navas, T. A., Sanchez, Y. & Elledge, S. J. RAD9 and DNA polymerase epsilon form parallel sensory branches for transducing the DNA damage checkpoint signal in Saccharomyces cerevisiae. *Genes Dev.* **10,** 2632–2643 (1996).
73. Zannini, L., Delia, D. & Buscemi, G. CHK2 kinase in the DNA damage response and beyond. *J. Mol. Cell Biol.* **6,** 442–457 (2014).
74. Patil, M., Pabla, N. & Dong, Z. Checkpoint kinase 1 in DNA damage response and cell cycle regulation. *Cell. Mol. Life Sci. CMLS* **70,** 4009–4021 (2013).
75. Zhang, Y. & Hunter, T. Roles of Chk1 in cell biology and cancer therapy. *Int. J. Cancer* **134,** 1013–1023 (2014).
76. Ceccaldi, R., Rondinelli, B. & D'Andrea, A. D. Repair Pathway Choices and Consequences at the Double-Strand Break. *Trends Cell Biol.* **26,** 52–64 (2016).
77. Li, J. & Xu, X. DNA double-strand break repair: a tale of pathway choices. *Acta Biochim. Biophys. Sin.* **48,** 641–646 (2016).
78. Hefferin, M. L. & Tomkinson, A. E. Mechanism of DNA double-strand break repair by non-homologous end joining. *DNA Repair* **4,** 639–648 (2005).
79. Dudásová, Z., Dudás, A. & Chovanec, M. Non-homologous end-joining factors of Saccharomyces cerevisiae. *FEMS Microbiol. Rev.* **28,** 581–601 (2004).
80. Chang, H. H. Y., Pannunzio, N. R., Adachi, N. & Lieber, M. R. Non-homologous DNA end joining and alternative pathways to double-strand break repair. *Nat. Rev. Mol. Cell Biol.* **18,** 495–506 (2017).
81. San Filippo, J., Sung, P. & Klein, H. Mechanism of eukaryotic homologous recombination. *Annu. Rev. Biochem.* **77,** 229–257 (2008).
82. Symington, L. S. & Gautier, J. Double-strand break end resection and repair pathway choice. *Annu. Rev. Genet.* **45,** 247–271 (2011).
83. Symington, L. S., Rothstein, R. & Lisby, M. Mechanisms and regulation of mitotic recombination in Saccharomyces cerevisiae. *Genetics* **198,** 795–835 (2014).

84. Krejci, L., Altmannova, V., Spirek, M. & Zhao, X. Homologous recombination and its regulation. *Nucleic Acids Res.* **40,** 5795–5818 (2012).
85. Holloman, W. K. Unraveling the mechanism of BRCA2 in homologous recombination. *Nat. Struct. Mol. Biol.* **18,** 748–754 (2011).
86. Bizard, A. H. & Hickson, I. D. The dissolution of double Holliday junctions. *Cold Spring Harb. Perspect. Biol.* **6,** a016477 (2014).
87. Lilley, D. M. J. Holliday junction-resolving enzymes-structures and mechanisms. *FEBS Lett.* **591,** 1073–1082 (2017).
88. Cejka, P. DNA End Resection: Nucleases Team Up with the Right Partners to Initiate Homologous Recombination. *J. Biol. Chem.* **290,** 22931–22938 (2015).
89. Daley, J. M., Niu, H., Miller, A. S. & Sung, P. Biochemical mechanism of DSB end resection and its regulation. *DNA Repair* **32,** 66–74 (2015).
90. Paull, T. T. & Deshpande, R. A. The Mre11/Rad50/Nbs1 complex: recent insights into catalytic activities and ATP-driven conformational changes. *Exp. Cell Res.* **329,** 139–147 (2014).
91. Mimitou, E. P. & Symington, L. S. Sae2, Exo1 and Sgs1 collaborate in DNA double-strand break processing. *Nature* **455,** 770–774 (2008).
92. Deshpande, R. A. *et al.* ATP-driven Rad50 conformations regulate DNA tethering, end resection, and ATM checkpoint signaling. *EMBO J.* **33,** 482–500 (2014).
93. Nicolette, M. L. *et al.* Mre11-Rad50-Xrs2 and Sae2 promote 5' strand resection of DNA double-strand breaks. *Nat. Struct. Mol. Biol.* **17,** 1478–1485 (2010).
94. Andres, S. N. & Williams, R. S. CtIP/Ctp1/Sae2, molecular form fit for function. *DNA Repair* **56,** 109–117 (2017).
95. Huertas, P., Cortés-Ledesma, F., Sartori, A. A., Aguilera, A. & Jackson, S. P. CDK targets Sae2 to control DNA-end resection and homologous recombination. *Nature* **455,** 689–692 (2008).
96. Cannavo, E. & Cejka, P. Sae2 promotes dsDNA endonuclease activity within Mre11-Rad50-Xrs2 to resect DNA breaks. *Nature* **514,** 122–125 (2014).
97. Clerici, M., Mantiero, D., Lucchini, G. & Longhese, M. P. The Saccharomyces cerevisiae Sae2 protein promotes resection and bridging of double strand break ends. *J. Biol. Chem.* **280,** 38631–38638 (2005).
98. Clerici, M., Mantiero, D., Lucchini, G. & Longhese, M. P. The Saccharomyces cerevisiae Sae2 protein negatively regulates DNA damage checkpoint signalling. *EMBO Rep.* **7,** 212–218 (2006).
99. Puddu, F. *et al.* Synthetic viability genomic screening defines Sae2 function in DNA repair. *EMBO J.* **34,** 1509–1522 (2015).
100. Chen, H. *et al.* Sae2 promotes DNA damage resistance by removing the Mre11-Rad50-Xrs2 complex from DNA and attenuating Rad53 signaling. *Proc. Natl. Acad. Sci. U. S. A.* **112,** E1880–1887 (2015).
101. Symington, L. S. End resection at double-strand breaks: mechanism and regulation. *Cold Spring Harb. Perspect. Biol.* **6,** (2014).
102. Kolinjivadi, A. M. *et al.* Moonlighting at replication forks - a new life for homologous recombination proteins BRCA1, BRCA2 and RAD51. *FEBS Lett.* **591,** 1083–1100 (2017).
103. Ira, G. *et al.* DNA end resection, homologous recombination and DNA damage checkpoint activation require CDK1. *Nature* **431,** 1011–1017 (2004).

104. Zierhut, C. & Diffley, J. F. X. Break dosage, cell cycle stage and DNA replication influence DNA double strand break response. *EMBO J.* **27,** 1875–1885 (2008).
105. Chen, X. *et al.* Cell cycle regulation of DNA double-strand break end resection by Cdk1-dependent Dna2 phosphorylation. *Nat. Struct. Mol. Biol.* **18,** 1015–1019 (2011).
106. Balestrini, A. *et al.* The Ku heterodimer and the metabolism of single-ended DNA double-strand breaks. *Cell Rep.* **3,** 2033–2045 (2013).
107. Sun, J., Lee, K.-J., Davis, A. J. & Chen, D. J. Human Ku70/80 protein blocks exonuclease 1-mediated DNA resection in the presence of human Mre11 or Mre11/Rad50 protein complex. *J. Biol. Chem.* **287,** 4936–4945 (2012).
108. Lazzaro, F. *et al.* Histone methyltransferase Dot1 and Rad9 inhibit single-stranded DNA accumulation at DSBs and uncapped telomeres. *EMBO J.* **27,** 1502–1512 (2008).
109. Ferrari, M. *et al.* Functional Interplay between the 53BP1-Ortholog Rad9 and the Mre11 Complex Regulates Resection, End-Tethering and Repair of a Double-Strand Break. *PLoS Genet.* **11,** (2015).
110. Escribano-Díaz, C. *et al.* A cell cycle-dependent regulatory circuit composed of 53BP1-RIF1 and BRCA1-CtIP controls DNA repair pathway choice. *Mol. Cell* **49,** 872–883 (2013).
111. Di Virgilio, M. *et al.* Rif1 prevents resection of DNA breaks and promotes immunoglobulin class switching. *Science* **339,** 711–715 (2013).
112. Zimmermann, M., Lottersberger, F., Buonomo, S. B., Sfeir, A. & de Lange, T. 53BP1 regulates DSB repair using Rif1 to control 5' end resection. *Science* **339,** 700–704 (2013).
113. Baroni, E., Viscardi, V., Cartagena-Lirola, H., Lucchini, G. & Longhese, M. P. The Functions of Budding Yeast Sae2 in the DNA Damage Response Require Mec1- and Tel1-Dependent Phosphorylation. *Mol. Cell. Biol.* **24,** 4151–4165 (2004).
114. Morin, I. *et al.* Checkpoint-dependent phosphorylation of Exo1 modulates the DNA damage response. *EMBO J.* **27,** 2400–2410 (2008).
115. Mimitou, E. P. & Symington, L. S. Ku prevents Exo1 and Sgs1-dependent resection of DNA ends in the absence of a functional MRX complex or Sae2. *EMBO J.* **29,** 3358–3369 (2010).
116. Mantiero, D., Clerici, M., Lucchini, G. & Longhese, M. P. Dual role for Saccharomyces cerevisiae Tel1 in the checkpoint response to double-strand breaks. *EMBO Rep.* **8,** 380–387 (2007).
117. Berti, M. & Vindigni, A. Replication stress: getting back on track. *Nat. Struct. Mol. Biol.* **23,** 103–109 (2016).
118. Giannattasio, M. & Branzei, D. S-phase checkpoint regulations that preserve replication and chromosome integrity upon dNTP depletion. *Cell. Mol. Life Sci. CMLS* **74,** 2361–2380 (2017).
119. Cotta-Ramusino, C. *et al.* Exo1 processes stalled replication forks and counteracts fork reversal in checkpoint-defective cells. *Mol. Cell* **17,** 153–159 (2005).
120. Sogo, J. M., Lopes, M. & Foiani, M. Fork reversal and ssDNA accumulation at stalled replication forks owing to checkpoint defects. *Science* **297,** 599–602 (2002).
121. Lopes, M. *et al.* The DNA replication checkpoint response stabilizes stalled replication forks. *Nature* **412,** 557–561 (2001).
122. Paulsen, R. D. & Cimprich, K. A. The ATR pathway: fine-tuning the fork. *DNA Repair* **6,** 953–966 (2007).
123. Friedel, A. M., Pike, B. L. & Gasser, S. M. ATR/Mec1: coordinating fork stability and repair. *Curr. Opin. Cell Biol.* **21,** 237–244 (2009).
124. Zhou, B. B. & Elledge, S. J. The DNA damage response: putting checkpoints in perspective. *Nature* **408,** 433–439 (2000).

125. Harrison, J. C. & Haber, J. E. Surviving the breakup: the DNA damage checkpoint. *Annu. Rev. Genet.* **40,** 209–235 (2006).
126. Byun, T. S., Pacek, M., Yee, M., Walter, J. C. & Cimprich, K. A. Functional uncoupling of MCM helicase and DNA polymerase activities activates the ATR-dependent checkpoint. *Genes Dev.* **19,** 1040–1052 (2005).
127. Van, C., Yan, S., Michael, W. M., Waga, S. & Cimprich, K. A. Continued primer synthesis at stalled replication forks contributes to checkpoint activation. *J. Cell Biol.* **189,** 233–246 (2010).
128. Tsai, F.-L. *et al.* Mcm2-7 Is an Active Player in the DNA Replication Checkpoint Signaling Cascade via Proposed Modulation of Its DNA Gate. *Mol. Cell. Biol.* **35,** 2131–2143 (2015).
129. Pardo, B., Crabbé, L. & Pasero, P. Signaling pathways of replication stress in yeast. *FEMS Yeast Res.* **17,** (2017).
130. Chabes, A. *et al.* Survival of DNA damage in yeast directly depends on increased dNTP levels allowed by relaxed feedback inhibition of ribonucleotide reductase. *Cell* **112,** 391–401 (2003).
131. Elledge, S. J., Zhou, Z., Allen, J. B. & Navas, T. A. DNA damage and cell cycle regulation of ribonucleotide reductase. *BioEssays News Rev. Mol. Cell. Dev. Biol.* **15,** 333–339 (1993).
132. Desany, B. A., Alcasabas, A. A., Bachant, J. B. & Elledge, S. J. Recovery from DNA replicational stress is the essential function of the S-phase checkpoint pathway. *Genes Dev.* **12,** 2956–2970 (1998).
133. Zhao, H. & Piwnica-Worms, H. ATR-mediated checkpoint pathways regulate phosphorylation and activation of human Chk1. *Mol. Cell. Biol.* **21,** 4129–4139 (2001).
134. Lopez-Mosqueda, J. *et al.* Damage-induced phosphorylation of Sld3 is important to block late origin firing. *Nature* **467,** 479–483 (2010).
135. Zegerman, P. & Diffley, J. F. X. Checkpoint-dependent inhibition of DNA replication initiation by Sld3 and Dbf4 phosphorylation. *Nature* **467,** 474–478 (2010).
136. Duch, A. *et al.* A Dbf4 mutant contributes to bypassing the Rad53-mediated block of origins of replication in response to genotoxic stress. *J. Biol. Chem.* **286,** 2486–2491 (2011).
137. Pellicioli, A. *et al.* Activation of Rad53 kinase in response to DNA damage and its effect in modulating phosphorylation of the lagging strand DNA polymerase. *EMBO J.* **18,** 6561–6572 (1999).
138. Lemoine, F. J., Degtyareva, N. P., Lobachev, K. & Petes, T. D. Chromosomal translocations in yeast induced by low levels of DNA polymerase a model for chromosome fragile sites. *Cell* **120,** 587–598 (2005).
139. Dungrawala, H. *et al.* The Replication Checkpoint Prevents Two Types of Fork Collapse without Regulating Replisome Stability. *Mol. Cell* **59,** 998–1010 (2015).
140. De Piccoli, G. *et al.* Replisome stability at defective DNA replication forks is independent of S phase checkpoint kinases. *Mol. Cell* **45,** 696–704 (2012).
141. Liberi, G. *et al.* Rad51-dependent DNA structures accumulate at damaged replication forks in sgs1 mutants defective in the yeast ortholog of BLM RecQ helicase. *Genes Dev.* **19,** 339–350 (2005).
142. Cobb, J. A., Bjergbaek, L., Shimada, K., Frei, C. & Gasser, S. M. DNA polymerase stabilization at stalled replication forks requires Mec1 and the RecQ helicase Sgs1. *EMBO J.* **22,** 4325–4336 (2003).
143. Szyjka, S. J. *et al.* Rad53 regulates replication fork restart after DNA damage in Saccharomyces cerevisiae. *Genes Dev.* **22,** 1906–1920 (2008).

144. Allen, J. B., Zhou, Z., Siede, W., Friedberg, E. C. & Elledge, S. J. The SAD1/RAD53 protein kinase controls multiple checkpoints and DNA damage-induced transcription in yeast. *Genes Dev.* **8,** 2401–2415 (1994).
145. Kai, M., Furuya, K., Paderi, F., Carr, A. M. & Wang, T. S. F. Rad3-dependent phosphorylation of the checkpoint clamp regulates repair-pathway choice. *Nat. Cell Biol.* **9,** 691–697 (2007).
146. Branzei, D. & Foiani, M. Maintaining genome stability at the replication fork. *Nat. Rev. Mol. Cell Biol.* **11,** 208–219 (2010).
147. Saugar, I., Ortiz-Bazán, M. Á. & Tercero, J. A. Tolerating DNA damage during eukaryotic chromosome replication. *Exp. Cell Res.* **329,** 170–177 (2014).
148. Neelsen, K. J. & Lopes, M. Replication fork reversal in eukaryotes: from dead end to dynamic response. *Nat. Rev. Mol. Cell Biol.* **16,** 207–220 (2015).
149. Lopes, M., Foiani, M. & Sogo, J. M. Multiple mechanisms control chromosome integrity after replication fork uncoupling and restart at irreparable UV lesions. *Mol. Cell* **21,** 15–27 (2006).
150. Mojas, N., Lopes, M. & Jiricny, J. Mismatch repair-dependent processing of methylation damage gives rise to persistent single-stranded gaps in newly replicated DNA. *Genes Dev.* **21,** 3342–3355 (2007).
151. Chaudhuri, A. R. *et al.* Topoisomerase I poisoning results in PARP-mediated replication fork reversal. *Nat. Struct. Mol. Biol.* **19,** 417–423 (2012).
152. Meng, X. & Zhao, X. Replication fork regression and its regulation. *FEMS Yeast Res.* **17,** (2016).
153. Zellweger, R. *et al.* Rad51-mediated replication fork reversal is a global response to genotoxic treatments in human cells. *J Cell Biol* **208,** 563–579 (2015).
154. Follonier, C., Oehler, J., Herrador, R. & Lopes, M. Friedreich's ataxia–associated GAA repeats induce replication-fork reversal and unusual molecular junctions. *Nat. Struct. Mol. Biol.* **20,** 486–494 (2013).
155. Neelsen, K. J. *et al.* Deregulated origin licensing leads to chromosomal breaks by rereplication of a gapped DNA template. *Genes Dev.* **27,** 2537–2542 (2013).
156. McMurray, C. T. Mechanisms of trinucleotide repeat instability during human development. *Nat. Rev. Genet.* **11,** 786–799 (2010).
157. Neelsen, K. J., Zanini, I. M. Y., Herrador, R. & Lopes, M. Oncogenes induce genotoxic stress by mitotic processing of unusual replication intermediates. *J. Cell Biol.* **200,** 699–708 (2013).
158. León-Ortiz, A. M., Svendsen, J. & Boulton, S. J. Metabolism of DNA secondary structures at the eukaryotic replication fork. *DNA Repair* **19,** 152–162 (2014).
159. Fugger, K. *et al.* FBH1 Catalyzes Regression of Stalled Replication Forks. *Cell Rep.* **10,** 1749–1757 (2015).
160. Longhese, M. P., Anbalagan, S., Martina, M. & Bonetti, D. The role of shelterin in maintaining telomere integrity. *Front. Biosci. Landmark Ed.* **17,** 1715–1728 (2012).
161. Colosio, A., Frattini, C., Pellicanò, G., Villa-Hernández, S. & Bermejo, R. Nucleolytic processing of aberrant replication intermediates by an Exo1-Dna2-Sae2 axis counteracts fork collapse-driven chromosome instability. *Nucleic Acids Res.* **44,** 10676–10690 (2016).
162. Schlacher, K. *et al.* Double-strand break repair-independent role for BRCA2 in blocking stalled replication fork degradation by MRE11. *Cell* **145,** 529–542 (2011).
163. Lemaçon, D. *et al.* MRE11 and EXO1 nucleases degrade reversed forks and elicit MUS81-dependent fork rescue in BRCA2-deficient cells. *Nat. Commun.* **8,** 860 (2017).

164. Schlacher, K., Wu, H. & Jasin, M. A distinct replication fork protection pathway connects Fanconi anemia tumor suppressors to RAD51-BRCA1/2. *Cancer Cell* **22,** 106–116 (2012).
165. Pommier, Y., Leo, E., Zhang, H. & Marchand, C. DNA topoisomerases and their poisoning by anticancer and antibacterial drugs. *Chem. Biol.* **17,** 421–433 (2010).
166. Champoux, J. J. DNA topoisomerases: structure, function, and mechanism. *Annu. Rev. Biochem.* **70,** 369–413 (2001).
167. Stewart, L., Redinbo, M. R., Qiu, X., Hol, W. G. & Champoux, J. J. A model for the mechanism of human topoisomerase I. *Science* **279,** 1534–1541 (1998).
168. Koster, D. A., Croquette, V., Dekker, C., Shuman, S. & Dekker, N. H. Friction and torque govern the relaxation of DNA supercoils by eukaryotic topoisomerase IB. *Nature* **434,** 671–674 (2005).
169. Wang, J. C. Cellular roles of DNA topoisomerases: a molecular perspective. *Nat. Rev. Mol. Cell Biol.* **3,** 430–440 (2002).
170. Wall, M. E. & Wani, M. C. Camptothecin and taxol: discovery to clinic--thirteenth Bruce F. Cain Memorial Award Lecture. *Cancer Res.* **55,** 753–760 (1995).
171. Hsiang, Y. H., Hertzberg, R., Hecht, S. & Liu, L. F. Camptothecin induces protein-linked DNA breaks via mammalian DNA topoisomerase I. *J. Biol. Chem.* **260,** 14873–14878 (1985).
172. Dexheimer, T. S. & Pommier, Y. DNA cleavage assay for the identification of topoisomerase I inhibitors. *Nat. Protoc.* **3,** 1736–1750 (2008).
173. Eng, W. K., Faucette, L., Johnson, R. K. & Sternglanz, R. Evidence that DNA topoisomerase I is necessary for the cytotoxic effects of camptothecin. *Mol. Pharmacol.* **34,** 755–760 (1988).
174. Bjornsti, M. A., Benedetti, P., Viglianti, G. A. & Wang, J. C. Expression of human DNA topoisomerase I in yeast cells lacking yeast DNA topoisomerase I: restoration of sensitivity of the cells to the antitumor drug camptothecin. *Cancer Res.* **49,** 6318–6323 (1989).
175. Staker, B. L. *et al.* The mechanism of topoisomerase I poisoning by a camptothecin analog. *Proc. Natl. Acad. Sci. U. S. A.* **99,** 15387–15392 (2002).
176. Chrencik, J. E. *et al.* Mechanisms of camptothecin resistance by human topoisomerase I mutations. *J. Mol. Biol.* **339,** 773–784 (2004).
177. Covey, J. M., Jaxel, C., Kohn, K. W. & Pommier, Y. Protein-linked DNA strand breaks induced in mammalian cells by camptothecin, an inhibitor of topoisomerase I. *Cancer Res.* **49,** 5016–5022 (1989).
178. Jaxel, C., Capranico, G., Kerrigan, D., Kohn, K. W. & Pommier, Y. Effect of local DNA sequence on topoisomerase I cleavage in the presence or absence of camptothecin. *J. Biol. Chem.* **266,** 20418–20423 (1991).
179. Tanizawa, A., Kohn, K. W., Kohlhagen, G., Leteurtre, F. & Pommier, Y. Differential stabilization of eukaryotic DNA topoisomerase I cleavable complexes by camptothecin derivatives. *Biochemistry (Mosc.)* **34,** 7200–7206 (1995).
180. Pourquier, P. & Pommier, Y. Topoisomerase I-mediated DNA damage. *Adv. Cancer Res.* **80,** 189–216 (2001).
181. Pourquier, P. *et al.* Effects of uracil incorporation, DNA mismatches, and abasic sites on cleavage and religation activities of mammalian topoisomerase I. *J. Biol. Chem.* **272,** 7792–7796 (1997).
182. Pourquier, P. *et al.* Trapping of mammalian topoisomerase I and recombinations induced by damaged DNA containing nicks or gaps. Importance of DNA end phosphorylation and camptothecin effects. *J. Biol. Chem.* **272,** 26441–26447 (1997).

183. Pommier, Y., Jenkins, J., Kohlhagen, G. & Leteurtre, F. DNA recombinase activity of eukaryotic DNA topoisomerase I; effects of camptothecin and other inhibitors. *Mutat. Res.* **337,** 135–145 (1995).
184. Shuman, S. DNA strand transfer reactions catalyzed by vaccinia topoisomerase I. *J. Biol. Chem.* **267,** 8620–8627 (1992).
185. Holm, C., Covey, J. M., Kerrigan, D. & Pommier, Y. Differential requirement of DNA replication for the cytotoxicity of DNA topoisomerase I and II inhibitors in Chinese hamster DC3F cells. *Cancer Res.* **49,** 6365–6368 (1989).
186. Hsiang, Y. H., Lihou, M. G. & Liu, L. F. Arrest of replication forks by drug-stabilized topoisomerase I-DNA cleavable complexes as a mechanism of cell killing by camptothecin. *Cancer Res.* **49,** 5077–5082 (1989).
187. Furuta, T. *et al.* Phosphorylation of histone H2AX and activation of Mre11, Rad50, and Nbs1 in response to replication-dependent DNA double-strand breaks induced by mammalian DNA topoisomerase I cleavage complexes. *J. Biol. Chem.* **278,** 20303–20312 (2003).
188. Rogakou, E. P., Pilch, D. R., Orr, A. H., Ivanova, V. S. & Bonner, W. M. DNA double-stranded breaks induce histone H2AX phosphorylation on serine 139. *J. Biol. Chem.* **273,** 5858–5868 (1998).
189. Redon, C. *et al.* Histone H2A variants H2AX and H2AZ. *Curr. Opin. Genet. Dev.* **12,** 162–169 (2002).
190. Shao, R. G. *et al.* Replication-mediated DNA damage by camptothecin induces phosphorylation of RPA by DNA-dependent protein kinase and dissociates RPA:DNA-PK complexes. *EMBO J.* **18,** 1397–1406 (1999).
191. Kohn, E. A., Ruth, N. D., Brown, M. K., Livingstone, M. & Eastman, A. Abrogation of the S phase DNA damage checkpoint results in S phase progression or premature mitosis depending on the concentration of 7-hydroxystaurosporine and the kinetics of Cdc25C activation. *J. Biol. Chem.* **277,** 26553–26564 (2002).
192. Horwitz, S. B., Chang, C. K. & Grollman, A. P. Studies on camptothecin. I. Effects of nucleic acid and protein synthesis. *Mol. Pharmacol.* **7,** 632–644 (1971).
193. Kann, H. E. & Kohn, K. W. Effects of deoxyribonucleic acid-reactive drugs on ribonucleic acid synthesis in leukemia L1210 cells. *Mol. Pharmacol.* **8,** 551–560 (1972).
194. Bendixen, C., Thomsen, B., Alsner, J. & Westergaard, O. Camptothecin-stabilized topoisomerase I-DNA adducts cause premature termination of transcription. *Biochemistry (Mosc.)* **29,** 5613–5619 (1990).
195. Wu, J. & Liu, L. F. Processing of topoisomerase I cleavable complexes into DNA damage by transcription. *Nucleic Acids Res.* **25,** 4181–4186 (1997).
196. Collins, I., Weber, A. & Levens, D. Transcriptional consequences of topoisomerase inhibition. *Mol. Cell. Biol.* **21,** 8437–8451 (2001).
197. Mondal, N. & Parvin, J. D. DNA topoisomerase IIalpha is required for RNA polymerase II transcription on chromatin templates. *Nature* **413,** 435–438 (2001).
198. Sun, M., Duann, P., Lin, C. T., Zhang, H. & Liu, L. F. Rapid chromatin reorganization induced by topoisomerase I-mediated DNA damage. *Ann. N. Y. Acad. Sci.* **922,** 340–342 (2000).
199. Merino, A., Madden, K. R., Lane, W. S., Champoux, J. J. & Reinberg, D. DNA topoisomerase I is involved in both repression and activation of transcription. *Nature* **365,** 227–232 (1993).
200. Shykind, B. M., Kim, J., Stewart, L., Champoux, J. J. & Sharp, P. A. Topoisomerase I enhances TFIID-TFIIA complex assembly during activation of transcription. *Genes Dev.* **11,** 397–407 (1997).

201. Ljungman, M. & Hanawalt, P. C. The anti-cancer drug camptothecin inhibits elongation but stimulates initiation of RNA polymerase II transcription. *Carcinogenesis* **17,** 31–35 (1996).
202. Desai, S. D. *et al.* Transcription-dependent degradation of topoisomerase I-DNA covalent complexes. *Mol. Cell. Biol.* **23,** 2341–2350 (2003).
203. Huang, C. C. *et al.* Cytotoxicity and sister chromatid exchanges induced in vitro by six anticancer drugs developed in the People's Republic of China. *J. Natl. Cancer Inst.* **71,** 841–847 (1983).
204. Fasullo, M., Zeng, L. & Giallanza, P. Enhanced stimulation of chromosomal translocations by radiomimetic DNA damaging agents and camptothecin in Saccharomyces cerevisiae rad9 checkpoint mutants. *Mutat. Res.* **547,** 123–132 (2004).
205. Pouliot, J. J., Yao, K. C., Robertson, C. A. & Nash, H. A. Yeast gene for a Tyr-DNA phosphodiesterase that repairs topoisomerase I complexes. *Science* **286,** 552–555 (1999).
206. Yang, S. W. *et al.* A eukaryotic enzyme that can disjoin dead-end covalent complexes between DNA and type I topoisomerases. *Proc. Natl. Acad. Sci. U. S. A.* **93,** 11534–11539 (1996).
207. Pouliot, J. J., Robertson, C. A. & Nash, H. A. Pathways for repair of topoisomerase I covalent complexes in Saccharomyces cerevisiae. *Genes Cells Devoted Mol. Cell. Mech.* **6,** 677–687 (2001).
208. Liu, C., Pouliot, J. J. & Nash, H. A. Repair of topoisomerase I covalent complexes in the absence of the tyrosyl-DNA phosphodiesterase Tdp1. *Proc. Natl. Acad. Sci. U. S. A.* **99,** 14970–14975 (2002).
209. Deng, C., Brown, J. A., You, D. & Brown, J. M. Multiple endonucleases function to repair covalent topoisomerase I complexes in Saccharomyces cerevisiae. *Genetics* **170,** 591–600 (2005).
210. Inamdar, K. V. *et al.* Conversion of phosphoglycolate to phosphate termini on 3' overhangs of DNA double strand breaks by the human tyrosyl-DNA phosphodiesterase hTdp1. *J. Biol. Chem.* **277,** 27162–27168 (2002).
211. Debéthune, L., Kohlhagen, G., Grandas, A. & Pommier, Y. Processing of nucleopeptides mimicking the topoisomerase I-DNA covalent complex by tyrosyl-DNA phosphodiesterase. *Nucleic Acids Res.* **30,** 1198–1204 (2002).
212. Interthal, H., Chen, H. J. & Champoux, J. J. Human Tdp1 cleaves a broad spectrum of substrates, including phosphoamide linkages. *J. Biol. Chem.* **280,** 36518–36528 (2005).
213. Vance, J. R. & Wilson, T. E. Uncoupling of 3'-phosphatase and 5'-kinase functions in budding yeast. Characterization of Saccharomyces cerevisiae DNA 3'-phosphatase (TPP1). *J. Biol. Chem.* **276,** 15073–15081 (2001).
214. Vance, J. R. & Wilson, T. E. Repair of DNA strand breaks by the overlapping functions of lesion-specific and non-lesion-specific DNA 3' phosphatases. *Mol. Cell. Biol.* **21,** 7191–7198 (2001).
215. Bastin-Shanower, S. A., Fricke, W. M., Mullen, J. R. & Brill, S. J. The mechanism of Mus81-Mms4 cleavage site selection distinguishes it from the homologous endonuclease Rad1-Rad10. *Mol. Cell. Biol.* **23,** 3487–3496 (2003).
216. D'Amours, D. & Jackson, S. P. The Mre11 complex: at the crossroads of dna repair and checkpoint signalling. *Nat. Rev. Mol. Cell Biol.* **3,** 317–327 (2002).
217. Zheng, L. *et al.* Novel function of the flap endonuclease 1 complex in processing stalled DNA replication forks. *EMBO Rep.* **6,** 83–89 (2005).

218. McClintock, B. The Behavior in Successive Nuclear Divisions of a Chromosome Broken at Meiosis. *Proc. Natl. Acad. Sci. U. S. A.* **25,** 405–416 (1939).
219. Gottschling, D. E., Aparicio, O. M., Billington, B. L. & Zakian, V. A. Position effect at S. cerevisiae telomeres: reversible repression of Pol II transcription. *Cell* **63,** 751–762 (1990).
220. Greider, C. W. & Blackburn, E. H. The telomere terminal transferase of Tetrahymena is a ribonucleoprotein enzyme with two kinds of primer specificity. *Cell* **51,** 887–898 (1987).
221. Larrivée, M., LeBel, C. & Wellinger, R. J. The generation of proper constitutive G-tails on yeast telomeres is dependent on the MRX complex. *Genes Dev.* **18,** 1391–1396 (2004).
222. Wellinger, R. J., Wolf, A. J. & Zakian, V. A. Saccharomyces telomeres acquire single-strand TG1-3 tails late in S phase. *Cell* **72,** 51–60 (1993).
223. Dionne, I. & Wellinger, R. J. Processing of telomeric DNA ends requires the passage of a replication fork. *Nucleic Acids Res.* **26,** 5365–5371 (1998).
224. Frank, C. J., Hyde, M. & Greider, C. W. Regulation of telomere elongation by the cyclin-dependent kinase CDK1. *Mol. Cell* **24,** 423–432 (2006).
225. Förstemann, K. & Lingner, J. Molecular basis for telomere repeat divergence in budding yeast. *Mol. Cell. Biol.* **21,** 7277–7286 (2001).
226. Teixeira, M. T., Arneric, M., Sperisen, P. & Lingner, J. Telomere length homeostasis is achieved via a switch between telomerase- extendible and -nonextendible states. *Cell* **117,** 323–335 (2004).
227. Wang, S. S. & Zakian, V. A. Telomere-telomere recombination provides an express pathway for telomere acquisition. *Nature* **345,** 456–458 (1990).
228. Gilson, E., Roberge, M., Giraldo, R., Rhodes, D. & Gasser, S. M. Distortion of the DNA double helix by RAP1 at silencers and multiple telomeric binding sites. *J. Mol. Biol.* **231,** 293–310 (1993).
229. Shore, D. & Nasmyth, K. Purification and cloning of a DNA binding protein from yeast that binds to both silencer and activator elements. *Cell* **51,** 721–732 (1987).
230. Moretti, P., Freeman, K., Coodly, L. & Shore, D. Evidence that a complex of SIR proteins interacts with the silencer and telomere-binding protein RAP1. *Genes Dev.* **8,** 2257–2269 (1994).
231. Gao, H., Cervantes, R. B., Mandell, E. K., Otero, J. H. & Lundblad, V. RPA-like proteins mediate yeast telomere function. *Nat. Struct. Mol. Biol.* **14,** 208–214 (2007).
232. Anderson, E. M., Halsey, W. A. & Wuttke, D. S. Delineation of the high-affinity single-stranded telomeric DNA-binding domain of Saccharomyces cerevisiae Cdc13. *Nucleic Acids Res.* **30,** 4305–4313 (2002).
233. Schramke, V. *et al.* RPA regulates telomerase action by providing Est1p access to chromosome ends. *Nat. Genet.* **36,** 46–54 (2004).
234. Gravel, S., Larrivée, M., Labrecque, P. & Wellinger, R. J. Yeast Ku as a regulator of chromosomal DNA end structure. *Science* **280,** 741–744 (1998).
235. Larcher, M. V., Pasquier, E., MacDonald, R. S. & Wellinger, R. J. Ku Binding on Telomeres Occurs at Sites Distal from the Physical Chromosome Ends. *PLoS Genet.* **12,** e1006479 (2016).
236. Martin, S. G., Laroche, T., Suka, N., Grunstein, M. & Gasser, S. M. Relocalization of telomeric Ku and SIR proteins in response to DNA strand breaks in yeast. *Cell* **97,** 621–633 (1999).
237. Roy, R., Meier, B., McAinsh, A. D., Feldmann, H. M. & Jackson, S. P. Separation-of-function mutants of yeast Ku80 reveal a Yku80p-Sir4p interaction involved in telomeric silencing. *J. Biol. Chem.* **279,** 86–94 (2004).

238. Chan, C. S. & Tye, B. K. Organization of DNA sequences and replication origins at yeast telomeres. *Cell* **33,** 563–573 (1983).
239. Louis, E. J. & Haber, J. E. Mitotic recombination among subtelomeric Y' repeats in Saccharomyces cerevisiae. *Genetics* **124,** 547–559 (1990).
240. Walmsley, R. W., Chan, C. S., Tye, B. K. & Petes, T. D. Unusual DNA sequences associated with the ends of yeast chromosomes. *Nature* **310,** 157–160 (1984).
241. Sandell, L. L. & Zakian, V. A. Loss of a yeast telomere: arrest, recovery, and chromosome loss. *Cell* **75,** 729–739 (1993).
242. Lundblad, V. & Blackburn, E. H. An alternative pathway for yeast telomere maintenance rescues est1- senescence. *Cell* **73,** 347–360 (1993).
243. Wright, J. H., Gottschling, D. E. & Zakian, V. A. Saccharomyces telomeres assume a non-nucleosomal chromatin structure. *Genes Dev.* **6,** 197–210 (1992).
244. Aparicio, O. M., Billington, B. L. & Gottschling, D. E. Modifiers of position effect are shared between telomeric and silent mating-type loci in S. cerevisiae. *Cell* **66,** 1279–1287 (1991).
245. Boulton, S. J. & Jackson, S. P. Components of the Ku-dependent non-homologous end-joining pathway are involved in telomeric length maintenance and telomeric silencing. *EMBO J.* **17,** 1819–1828 (1998).
246. Gotta, M. *et al.* The clustering of telomeres and colocalization with Rap1, Sir3, and Sir4 proteins in wild-type Saccharomyces cerevisiae. *J. Cell Biol.* **134,** 1349–1363 (1996).
247. Palladino, F. *et al.* SIR3 and SIR4 proteins are required for the positioning and integrity of yeast telomeres. *Cell* **75,** 543–555 (1993).
248. Schober, H., Ferreira, H., Kalck, V., Gehlen, L. R. & Gasser, S. M. Yeast telomerase and the SUN domain protein Mps3 anchor telomeres and repress subtelomeric recombination. *Genes Dev.* **23,** 928–938 (2009).
249. Taddei, A., Hediger, F., Neumann, F. R., Bauer, C. & Gasser, S. M. Separation of silencing from perinuclear anchoring functions in yeast Ku80, Sir4 and Esc1 proteins. *EMBO J.* **23,** 1301–1312 (2004).
250. de Lange, T. How Telomeres Solve the End-Protection Problem. *Science* **326,** 948 (2009).
251. Hirano, Y. & Sugimoto, K. Cdc13 Telomere Capping Decreases Mec1 Association but Does Not Affect Tel1 Association with DNA Ends. *Mol. Biol. Cell* **18,** 2026–2036 (2007).
252. Maringele, L. & Lydall, D. EXO1-dependent single-stranded DNA at telomeres activates subsets of DNA damage and spindle checkpoint pathways in budding yeast yku70Δ mutants. *Genes Dev.* **16,** 1919–1933 (2002).
253. Shi, T. *et al.* Rif1 and Rif2 shape telomere function and architecture through multivalent Rap1 interactions. *Cell* **153,** 1340–1353 (2013).
254. Pobiega, S. & Marcand, S. Dicentric breakage at telomere fusions. *Genes Dev.* **24,** 720–733 (2010).
255. Bonetti, D. *et al.* Shelterin-like proteins and Yku inhibit nucleolytic processing of Saccharomyces cerevisiae telomeres. *PLoS Genet.* **6,** e1000966 (2010).
256. Ribeyre, C. & Shore, D. Anticheckpoint pathways at telomeres in yeast. *Nat. Struct. Mol. Biol.* **19,** 307–313 (2012).
257. Anbalagan, S., Bonetti, D., Lucchini, G. & Longhese, M. P. Rif1 supports the function of the CST complex in yeast telomere capping. *PLoS Genet.* **7,** e1002024 (2011).
258. Doksani, Y., Wu, J. Y., de Lange, T. & Zhuang, X. Super-resolution fluorescence imaging of telomeres reveals TRF2-dependent T-loop formation. *Cell* **155,** 345–356 (2013).

259. Celli, G. B. & de Lange, T. DNA processing is not required for ATM-mediated telomere damage response after TRF2 deletion. *Nat. Cell Biol.* **7,** 712–718 (2005).
260. Hockemeyer, D., Sfeir, A. J., Shay, J. W., Wright, W. E. & de Lange, T. POT1 protects telomeres from a transient DNA damage response and determines how human chromosomes end. *EMBO J.* **24,** 2667–2678 (2005).
261. Gong, Y. & de Lange, T. A Shld1-controlled POT1a provides support for repression of ATR signaling at telomeres through RPA exclusion. *Mol. Cell* **40,** 377–387 (2010).
262. Flynn, R. L. *et al.* TERRA and hnRNPA1 orchestrate an RPA-to-POT1 switch on telomeric single-stranded DNA. *Nature* **471,** 532–536 (2011).
263. Sfeir, A., Kabir, S., van Overbeek, M., Celli, G. B. & de Lange, T. Loss of Rap1 induces telomere recombination in the absence of NHEJ or a DNA damage signal. *Science* **327,** 1657–1661 (2010).
264. Greider, C. W. & Blackburn, E. H. Identification of a specific telomere terminal transferase activity in Tetrahymena extracts. *Cell* **43,** 405–413 (1985).
265. Wellinger, R. J. & Zakian, V. A. Everything you ever wanted to know about Saccharomyces cerevisiae telomeres: beginning to end. *Genetics* **191,** 1073–1105 (2012).
266. Grossi, S., Puglisi, A., Dmitriev, P. V., Lopes, M. & Shore, D. Pol12, the B subunit of DNA polymerase alpha, functions in both telomere capping and length regulation. *Genes Dev.* **18,** 992–1006 (2004).
267. Qi, H. & Zakian, V. A. The Saccharomyces telomere-binding protein Cdc13p interacts with both the catalytic subunit of DNA polymerase alpha and the telomerase-associated est1 protein. *Genes Dev.* **14,** 1777–1788 (2000).
268. Mozdy, A. D. & Cech, T. R. Low abundance of telomerase in yeast: implications for telomerase haploinsufficiency. *RNA N. Y. N* **12,** 1721–1737 (2006).
269. Taggart, A. K. P., Teng, S.-C. & Zakian, V. A. Est1p as a cell cycle-regulated activator of telomere-bound telomerase. *Science* **297,** 1023–1026 (2002).
270. Liu, C.-C., Gopalakrishnan, V., Poon, L.-F., Yan, T. & Li, S. Cdk1 regulates the temporal recruitment of telomerase and Cdc13-Stn1-Ten1 complex for telomere replication. *Mol. Cell. Biol.* **34,** 57–70 (2014).
271. Tseng, S.-F., Lin, J.-J. & Teng, S.-C. The telomerase-recruitment domain of the telomere binding protein Cdc13 is regulated by Mec1p/Tel1p-dependent phosphorylation. *Nucleic Acids Res.* **34,** 6327–6336 (2006).
272. Wotton, D. & Shore, D. A novel Rap1p-interacting factor, Rif2p, cooperates with Rif1p to regulate telomere length in Saccharomyces cerevisiae. *Genes Dev.* **11,** 748–760 (1997).
273. Hirano, Y., Fukunaga, K. & Sugimoto, K. Rif1 and Rif2 inhibit localization of Tel1 to DNA ends. *Mol. Cell* **33,** 312–322 (2009).
274. Marcand, S., Brevet, V. & Gilson, E. Progressive cis-inhibition of telomerase upon telomere elongation. *EMBO J.* **18,** 3509–3519 (1999).
275. Marcand, S., Gilson, E. & Shore, D. A protein-counting mechanism for telomere length regulation in yeast. *Science* **275,** 986–990 (1997).
276. Phillips, J. A., Chan, A., Paeschke, K. & Zakian, V. A. The pif1 helicase, a negative regulator of telomerase, acts preferentially at long telomeres. *PLoS Genet.* **11,** e1005186 (2015).
277. Boulé, J.-B., Vega, L. R. & Zakian, V. A. The yeast Pif1p helicase removes telomerase from telomeric DNA. *Nature* **438,** 57–61 (2005).
278. Louis, E. J. & Vershinin, A. V. Chromosome ends: different sequences may provide conserved functions. *BioEssays News Rev. Mol. Cell. Dev. Biol.* **27,** 685–697 (2005).

279. McCarroll, R. M. & Fangman, W. L. Time of replication of yeast centromeres and telomeres. *Cell* **54,** 505–513 (1988).
280. Bianchi, A. & Shore, D. Early replication of short telomeres in budding yeast. *Cell* **128,** 1051–1062 (2007).
281. Lian, H.-Y. *et al.* The effect of Ku on telomere replication time is mediated by telomere length but is independent of histone tail acetylation. *Mol. Biol. Cell* **22,** 1753–1765 (2011).
282. Sabourin, M., Tuzon, C. T. & Zakian, V. A. Telomerase and Tel1p preferentially associate with short telomeres in S. cerevisiae. *Mol. Cell* **27,** 550–561 (2007).
283. Sridhar, A., Kedziora, S. & Donaldson, A. D. At Short Telomeres Tel1 Directs Early Replication and Phosphorylates Rif1. *PLoS Genet.* **10,** (2014).
284. Soudet, J., Jolivet, P. & Teixeira, M. T. Elucidation of the DNA end-replication problem in Saccharomyces cerevisiae. *Mol. Cell* **53,** 954–964 (2014).
285. Diede, S. J. & Gottschling, D. E. Exonuclease activity is required for sequence addition and Cdc13p loading at a de novo telomere. *Curr. Biol. CB* **11,** 1336–1340 (2001).
286. Faure, V., Coulon, S., Hardy, J. & Géli, V. Cdc13 and telomerase bind through different mechanisms at the lagging- and leading-strand telomeres. *Mol. Cell* **38,** 842–852 (2010).
287. Dionne, I. & Wellinger, R. J. Cell cycle-regulated generation of single-stranded G-rich DNA in the absence of telomerase. *Proc. Natl. Acad. Sci. U. S. A.* **93,** 13902–13907 (1996).
288. Bonetti, D., Martina, M., Clerici, M., Lucchini, G. & Longhese, M. P. Multiple pathways regulate 3' overhang generation at S. cerevisiae telomeres. *Mol. Cell* **35,** 70–81 (2009).
289. Fallet, E. *et al.* Length-dependent processing of telomeres in the absence of telomerase. *Nucleic Acids Res.* **42,** 3648–3665 (2014).
290. Lundblad, V. & Szostak, J. W. A mutant with a defect in telomere elongation leads to senescence in yeast. *Cell* **57,** 633–643 (1989).
291. Lydeard, J. R., Jain, S., Yamaguchi, M. & Haber, J. E. Break-induced replication and telomerase-independent telomere maintenance require Pol32. *Nature* **448,** 820–823 (2007).
292. Cohen, H. & Sinclair, D. A. Recombination-mediated lengthening of terminal telomeric repeats requires the Sgs1 DNA helicase. *Proc. Natl. Acad. Sci. U. S. A.* **98,** 3174–3179 (2001).
293. Chen, Q., Ijpma, A. & Greider, C. W. Two survivor pathways that allow growth in the absence of telomerase are generated by distinct telomere recombination events. *Mol. Cell. Biol.* **21,** 1819–1827 (2001).
294. Larrivée, M. & Wellinger, R. J. Telomerase- and capping-independent yeast survivors with alternate telomere states. *Nat. Cell Biol.* **8,** 741–747 (2006).
295. Teng, S. C. & Zakian, V. A. Telomere-telomere recombination is an efficient bypass pathway for telomere maintenance in Saccharomyces cerevisiae. *Mol. Cell. Biol.* **19,** 8083–8093 (1999).
296. Johnson, F. B. *et al.* The Saccharomyces cerevisiae WRN homolog Sgs1p participates in telomere maintenance in cells lacking telomerase. *EMBO J.* **20,** 905–913 (2001).
297. Kim, N. W. *et al.* Specific association of human telomerase activity with immortal cells and cancer. *Science* **266,** 2011–2015 (1994).
298. Harley, C. B., Futcher, A. B. & Greider, C. W. Telomeres shorten during ageing of human fibroblasts. *Nature* **345,** 458–460 (1990).
299. Childs, B. G., Durik, M., Baker, D. J. & van Deursen, J. M. Cellular senescence in aging and age-related disease: from mechanisms to therapy. *Nat. Med.* **21,** 1424–1435 (2015).

300. Henson, J. D. & Reddel, R. R. Assaying and investigating Alternative Lengthening of Telomeres activity in human cells and cancers. *FEBS Lett.* **584,** 3800–3811 (2010).
301. Nugent, C. I., Hughes, T. R., Lue, N. F. & Lundblad, V. Cdc13p: a single-strand telomeric DNA-binding protein with a dual role in yeast telomere maintenance. *Science* **274,** 249–252 (1996).
302. Chang, M., Dittmar, J. C. & Rothstein, R. Long Telomeres are Preferentially Extended During Recombination-Mediated Telomere Maintenance. *Nat. Struct. Mol. Biol.* **18,** 451–456 (2011).
303. Negrini, S., Ribaud, V., Bianchi, A. & Shore, D. DNA breaks are masked by multiple Rap1 binding in yeast: implications for telomere capping and telomerase regulation. *Genes Dev.* **21,** 292–302 (2007).
304. Abdallah, P. *et al.* A two-step model for senescence triggered by a single critically short telomere. *Nat. Cell Biol.* **11,** 988–993 (2009).
305. Khadaroo, B. *et al.* The DNA damage response at eroded telomeres and tethering to the nuclear pore complex. *Nat. Cell Biol.* **11,** 980–987 (2009).
306. Hackett, J. A. & Greider, C. W. End resection initiates genomic instability in the absence of telomerase. *Mol. Cell. Biol.* **23,** 8450–8461 (2003).
307. Makovets, S., Herskowitz, I. & Blackburn, E. H. Anatomy and dynamics of DNA replication fork movement in yeast telomeric regions. *Mol. Cell. Biol.* **24,** 4019–4031 (2004).
308. Miller, K. M., Rog, O. & Cooper, J. P. Semi-conservative DNA replication through telomeres requires Taz1. *Nature* **440,** 824–828 (2006).
309. Sfeir, A. *et al.* Mammalian telomeres resemble fragile sites and require TRF1 for efficient replication. *Cell* **138,** 90–103 (2009).
310. Lee, J. Y., Kozak, M., Martin, J. D., Pennock, E. & Johnson, F. B. Evidence That a RecQ Helicase Slows Senescence by Resolving Recombining Telomeres. *PLOS Biol.* **5,** e160 (2007).
311. Marcand, S., Pardo, B., Gratias, A., Cahun, S. & Callebaut, I. Multiple pathways inhibit NHEJ at telomeres. *Genes Dev.* **22,** 1153–1158 (2008).
312. Jain, D. & Cooper, J. P. Telomeric strategies: means to an end. *Annu. Rev. Genet.* **44,** 243–269 (2010).
313. Chan, S. W.-L. & Blackburn, E. H. Telomerase and ATM/Tel1p protect telomeres from nonhomologous end joining. *Mol. Cell* **11,** 1379–1387 (2003).
314. Mieczkowski, P. A., Mieczkowska, J. O., Dominska, M. & Petes, T. D. Genetic regulation of telomere-telomere fusions in the yeast Saccharomyces cerevisae. *Proc. Natl. Acad. Sci. U. S. A.* **100,** 10854–10859 (2003).
315. Hackett, J. A., Feldser, D. M. & Greider, C. W. Telomere dysfunction increases mutation rate and genomic instability. *Cell* **106,** 275–286 (2001).
316. Villa, M., Cassani, C., Gobbini, E., Bonetti, D. & Longhese, M. P. Coupling end resection with the checkpoint response at DNA double-strand breaks. *Cell. Mol. Life Sci. CMLS* **73,** 3655–3663 (2016).
317. Cassani, C. *et al.* Tel1 and Rif2 Regulate MRX Functions in End-Tethering and Repair of DNA Double-Strand Breaks. *PLoS Biol.* **14,** (2016).
318. Iwasaki, D. *et al.* The MRX Complex Ensures NHEJ Fidelity through Multiple Pathways Including Xrs2-FHA-Dependent Tel1 Activation. *PLoS Genet.* **12,** e1005942 (2016).
319. Vance, J. R. & Wilson, T. E. Yeast Tdp1 and Rad1-Rad10 function as redundant pathways for repairing Top1 replicative damage. *Proc. Natl. Acad. Sci. U. S. A.* **99,** 13669–13674 (2002).

320. Mallory, J. C. & Petes, T. D. Protein kinase activity of Tel1p and Mec1p, two Saccharomyces cerevisiae proteins related to the human ATM protein kinase. *Proc. Natl. Acad. Sci. U. S. A.* **97,** 13749–13754 (2000).
321. Katyal, S. *et al.* Aberrant topoisomerase-1 DNA lesions are pathogenic in neurodegenerative genome instability syndromes. *Nat. Neurosci.* **17,** 813–821 (2014).
322. Li, X., O'Neil, N. J., Moshgabadi, N. & Hieter, P. Synthetic Cytotoxicity: Digenic Interactions with TEL1/ATM Mutations Reveal Sensitivity to Low Doses of Camptothecin. *Genetics* **197,** 611–623 (2014).
323. Evans, S. K. & Lundblad, V. Est1 and Cdc13 as comediators of telomerase access. *Science* **286,** 117–120 (1999).
324. Lewis, L. K., Karthikeyan, G., Westmoreland, J. W. & Resnick, M. A. Differential suppression of DNA repair deficiencies of Yeast rad50, mre11 and xrs2 mutants by EXO1 and TLC1 (the RNA component of telomerase). *Genetics* **160,** 49–62 (2002).
325. Gobbini, E. *et al.* Sae2 Function at DNA Double-Strand Breaks Is Bypassed by Dampening Tel1 or Rad53 Activity. *PLoS Genet.* **11,** e1005685 (2015).
326. Pommier, Y., Sun, Y., Huang, S.-Y. N. & Nitiss, J. L. Roles of eukaryotic topoisomerases in transcription, replication and genomic stability. *Nat. Rev. Mol. Cell Biol.* **17,** 703–721 (2016).
327. Redon, C. *et al.* Yeast histone 2A serine 129 is essential for the efficient repair of checkpoint-blind DNA damage. *EMBO Rep.* **4,** 678–684 (2003).
328. Zhao, X., Muller, E. G. & Rothstein, R. A suppressor of two essential checkpoint genes identifies a novel protein that negatively affects dNTP pools. *Mol. Cell* **2,** 329–340 (1998).
329. Yeeles, J. T. P., Janska, A., Early, A. & Diffley, J. F. X. How the Eukaryotic Replisome Achieves Rapid and Efficient DNA Replication. *Mol. Cell* **65,** 105–116 (2017).
330. Naylor, M. L., Li, J., Osborn, A. J. & Elledge, S. J. Mrc1 phosphorylation in response to DNA replication stress is required for Mec1 accumulation at the stalled fork. *Proc. Natl. Acad. Sci. U. S. A.* **106,** 12765–12770 (2009).
331. Hang, L. E. *et al.* Rtt107 Is a Multi-functional Scaffold Supporting Replication Progression with Partner SUMO and Ubiquitin Ligases. *Mol. Cell* **60,** 268–279 (2015).
332. Vogelauer, M., Rubbi, L., Lucas, I., Brewer, B. J. & Grunstein, M. Histone acetylation regulates the time of replication origin firing. *Mol. Cell* **10,** 1223–1233 (2002).
333. Kolinjivadi, A. M. *et al.* Smarcal1-Mediated Fork Reversal Triggers Mre11-Dependent Degradation of Nascent DNA in the Absence of Brca2 and Stable Rad51 Nucleofilaments. *Mol. Cell* **67,** 867–881.e7 (2017).
334. Moreau, S., Ferguson, J. R. & Symington, L. S. The nuclease activity of Mre11 is required for meiosis but not for mating type switching, end joining, or telomere maintenance. *Mol. Cell. Biol.* **19,** 556–566 (1999).
335. Mijic, S. *et al.* Replication fork reversal triggers fork degradation in BRCA2-defective cells. *Nat. Commun.* **8,** 859 (2017).
336. Gan, H. *et al.* Checkpoint Kinase Rad53 Couples Leading- and Lagging-Strand DNA Synthesis under Replication Stress. *Mol. Cell* **68,** 446–455.e3 (2017).
337. Hartsuiker, E., Neale, M. J. & Carr, A. M. Distinct requirements for the Rad32(Mre11) nuclease and Ctp1(CtIP) in the removal of covalently bound topoisomerase I and II from DNA. *Mol. Cell* **33,** 117–123 (2009).
338. Baldo, V., Testoni, V., Lucchini, G. & Longhese, M. P. Dominant TEL1-hy mutations compensate for Mec1 lack of functions in the DNA damage response. *Mol. Cell. Biol.* **28,** 358–375 (2008).

339. Chang, M. & Rothstein, R. Rif1/2 and Tel1 function in separate pathways during replicative senescence. *Cell Cycle* **10,** 3798–3799 (2011).
340. Enomoto, S., Glowczewski, L. & Berman, J. MEC3, MEC1, and DDC2 Are Essential Components of a Telomere Checkpoint Pathway Required for Cell Cycle Arrest during Senescence in Saccharomyces cerevisiae. *Mol. Biol. Cell* **13,** 2626–2638 (2002).
341. IJpma, A. S. & Greider, C. W. Short telomeres induce a DNA damage response in Saccharomyces cerevisiae. *Mol. Biol. Cell* **14,** 987–1001 (2003).
342. Teixeira, M. T. Saccharomyces cerevisiae as a Model to Study Replicative Senescence Triggered by Telomere Shortening. *Front. Oncol.* **3,** (2013).
343. Lee, S. E. *et al.* Saccharomyces Ku70, mre11/rad50 and RPA proteins regulate adaptation to G2/M arrest after DNA damage. *Cell* **94,** 399–409 (1998).
344. Ballew, B. J. & Lundblad, V. Multiple genetic pathways regulate replicative senescence in telomerase-deficient yeast. *Aging Cell* **12,** 719–727 (2013).
345. Takata, H., Kanoh, Y., Gunge, N., Shirahige, K. & Matsuura, A. Reciprocal association of the budding yeast ATM-related proteins Tel1 and Mec1 with telomeres in vivo. *Mol. Cell* **14,** 515–522 (2004).
346. Rotman, G. & Shiloh, Y. ATM: from gene to function. *Hum. Mol. Genet.* **7,** 1555–1563 (1998).
347. Swift, M. *et al.* The incidence and gene frequency of ataxia-telangiectasia in the United States. *Am. J. Hum. Genet.* **39,** 573–583 (1986).
348. Concannon, P. & Gatti, R. A. Diversity of ATM gene mutations detected in patients with ataxia-telangiectasia. *Hum. Mutat.* **10,** 100–107 (1997).
349. Kastan, M. B. Our cells get stressed too! Implications for human disease. *Blood Cells. Mol. Dis.* **39,** 148–150 (2007).
350. Painter, R. B. & Young, B. R. Radiosensitivity in ataxia-telangiectasia: a new explanation. *Proc. Natl. Acad. Sci. U. S. A.* **77,** 7315–7317 (1980).
351. Kühne, M. *et al.* A double-strand break repair defect in ATM-deficient cells contributes to radiosensitivity. *Cancer Res.* **64,** 500–508 (2004).
352. Pandita, T. K. *et al.* Chromosome end-to-end associations and telomerase activity during cancer progression in human cells after treatment with alpha-particles simulating radon progeny. *Oncogene* **13,** 1423–1430 (1996).
353. Pandita, T. K., Pathak, S. & Geard, C. R. Chromosome end associations, telomeres and telomerase activity in ataxia telangiectasia cells. *Cytogenet. Cell Genet.* **71,** 86–93 (1995).
354. Metcalfe, J. A. *et al.* Accelerated telomere shortening in ataxia telangiectasia. *Nat. Genet.* **13,** 350–353 (1996).
355. Taglialatela, A. *et al.* Restoration of Replication Fork Stability in BRCA1- and BRCA2-Deficient Cells by Inactivation of SNF2-Family Fork Remodelers. *Mol. Cell* **68,** 414–430.e8 (2017).
356. Koster, D. A., Palle, K., Bot, E. S. M., Bjornsti, M.-A. & Dekker, N. H. Antitumour drugs impede DNA uncoiling by topoisomerase I. *Nature* **448,** 213–217 (2007).
357. Postow, L. *et al.* Positive torsional strain causes the formation of a four-way junction at replication forks. *J. Biol. Chem.* **276,** 2790–2796 (2001).
358. Doksani, Y., Bermejo, R., Fiorani, S., Haber, J. E. & Foiani, M. Replicon dynamics, dormant origin firing, and terminal fork integrity after double-strand break formation. *Cell* **137,** 247–258 (2009).

359. Brambati, A. *et al.* Dormant origins and fork protection mechanisms rescue sister forks arrested by transcription. *Nucleic Acids Res.* **46,** 1227–1239 (2018).
360. Cooley, C., Davé, A., Garg, M. & Bianchi, A. Tel1ATM dictates the replication timing of short yeast telomeres. *EMBO Rep.* **15,** 1093–1101 (2014).
361. Ray Chaudhuri, A. *et al.* Replication fork stability confers chemoresistance in BRCA-deficient cells. *Nature* **535,** 382–387 (2016).
362. D'Amours, D. & Jackson, S. P. The yeast Xrs2 complex functions in S phase checkpoint regulation. *Genes Dev.* **15,** 2238–2249 (2001).
363. Baretić, D. & Williams, R. L. PIKKs--the solenoid nest where partners and kinases meet. *Curr. Opin. Struct. Biol.* **29,** 134–142 (2014).
364. Maciejowski, J. & de Lange, T. Telomeres in cancer: tumour suppression and genome instability. *Nat. Rev. Mol. Cell Biol.* **18,** 175–186 (2017).
365. Colombo, C. V., Menin, L. & Clerici, M. Alkaline Denaturing Southern Blot Analysis to Monitor Double-Strand Break Processing. *Methods Mol. Biol. Clifton NJ* **1672,** 131–145 (2018).
366. Zellweger, R. & Lopes, M. Dynamic Architecture of Eukaryotic DNA Replication Forks In Vivo, Visualized by Electron Microscopy. *Methods Mol. Biol. Clifton NJ* **1672,** 261–294 (2018).

APPENDIX

Chapter 11

Alkaline Denaturing Southern Blot Analysis to Monitor Double-Strand Break Processing

Chiara Vittoria Colombo, Luca Menin, and Michela Clerici

Abstract

Generation of 3′ single-stranded DNA (ssDNA) tails at the ends of a double-strand break (DSB) is essential to repair the break through accurate homology-mediated repair pathways. Several methods have been developed to measure ssDNA accumulation at a DSB in the budding yeast *Saccharomyces cerevisiae*. Here, we describe one of these assays, which is based on the inability of restriction enzymes to cleave ssDNA. Digestion of genomic DNA prepared at different time points after DSB generation leads to the formation of ssDNA fragments whose length increases as the 5′ strand degradation proceeds beyond restriction sites. After the separation by electrophoresis on alkaline denaturing agarose gel, these ssDNA fragments can be visualized by hybridization with an RNA probe that anneals with the 3′-undegraded DSB strand. This assay allows a direct and comprehensive visualization of DSB end processing.

Key words DNA double-strand breaks, Resection, Single-stranded DNA, HO endonuclease, *MAT* locus, Southern blot, Electrophoresis, Alkaline denaturing conditions, RNA probe

1 Introduction

DNA double-strand breaks (DSBs) can be repaired either by non-homologous end-joining (NHEJ), which directly rejoins the two broken ends together, or by homologous recombination (HR) that uses intact homologous duplex DNA sequences as a template for accurate repair. HR initiates with the nucleolytic degradation of the 5′ DNA strand on both the DSB sides (a process referred to as resection) to yield 3′ single-stranded DNA (ssDNA) tails. One of these tails invades the homologous duplex and primes reparative DNA synthesis [1, 2]. The initiation of resection is thought to channel DSB repair to HR and is tightly regulated [3, 4].

Much of our knowledge of the DNA end resection mechanism and regulation comes from genetic and biochemical studies in *Saccharomyces cerevisiae*, where DNA end processing of a DSB located at a specific genomic locus can be followed by both PCR-based and electrophoretic methods. Among these methods, a

Marco Muzi-Falconi and Grant W. Brown (eds.), *Genome Instability: Methods and Protocols*, Methods in Molecular Biology, vol. 1672, DOI 10.1007/978-1-4939-7306-4_11,

Southern blot analysis of genomic DNA that has been run on an alkaline denaturing agarose gel [5] allows a direct and comprehensive visualization of resection. When genomic DNA from a time-course experiment is used, the kinetics of both resection initiation and elongation can be determined in a single gel blot. This assay is based on the inability of many restriction enzymes to cleave ssDNA. As resection proceeds beyond restriction sites, additional, slower migrating bands are revealed by an RNA or ssDNA probe that anneals to the 3′-unresected strand on one side of the break (Fig. 1).

Here, we describe the protocol to monitor DNA end processing in haploid yeast cells where a DSB is generated at the *MAT* locus by the homothallic switching endonuclease HO, whose expression is regulated by a galactose inducible promoter [6]. The same method can be used to study ssDNA generation at DSBs located at different genomic loci and/or generated by different nucleases. This method was successfully employed to monitor end resection of both an HO-induced DSB at *LEU2* locus [7] and a Spo11-induced DSB at the *YCR048W* meiotic recombination hotspot [8]. Furthermore, a modified version of this assay that used denaturing polyacrilamide gels allowed us to measure ssDNA accumulation at telomeres [9]. Resection analysis at DSBs located in different genomic loci requires a detailed analysis of each locus to

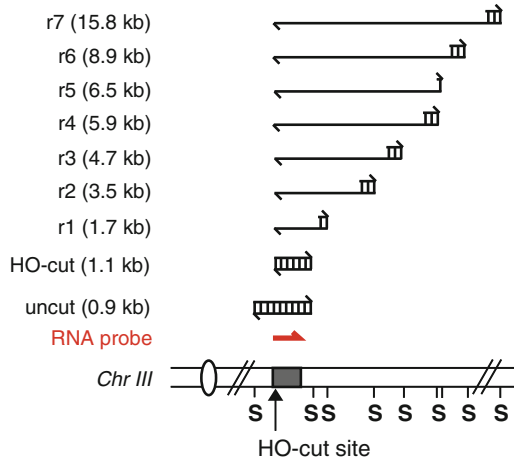

Fig. 1 System to detect DSB end resection at the *MAT* locus. Schematic representation of the region immediately centromere-distal to the *MAT* HO site (*bottom*), and of the DSB and 5′-to-3′ resection products (*top*) detectable with the indicated RNA probe after alkaline gel electrophoresis of SspI (S)-digested DNA. The probe reveals a 1.1 kb fragment representing the uncut *MAT* locus. When HO cuts this locus, a smaller HO-cut fragment is produced. 5′-to-3′ nucleolytic degradation progressively eliminates SspI sites, generating larger ssDNA SspI fragments (r1–r7) detected by the probe

determine both the most appropriate restriction enzyme and the probe sequence for Southern blot.

Extensive resection of a DSB induced at *MAT* locus can be monitored in JKM139 derivative strains [6]. In these strains the *GAL-HO* fusion is stably integrated in the genome and allows the expression of the HO endonuclease when galactose is added to the media. As transcription from the *GAL* promoter is repressed by glucose, cells are grown in raffinose-containing media before galactose addition. The HO endonuclease recognizes a 24-bp cleavage sequence, which is unique in the yeast genome and is located adjacent to the Y region at the *MAT* locus. HO cleavage yields 4-bp, 3′-overhanging ends [10]. JKM139 derivative strains also carry the deletion of both the *HML* and *HMR* cassettes, which are homologous to the *MAT* locus and are normally used to repair the HO-induced DSB by a gene conversion event that triggers mating type switching [10]. Therefore, HO expression in these cells generates an irreparable DSB, whose 5′ end degradation proceeds for several kilobases.

With the aim of highlighting some critical steps, here we divide the protocol into three main parts: (1) DSB induction in yeast cells; (2) genomic DNA extraction; (3) alkaline denaturing electrophoresis and Southern blot analysis. Indeed, we experienced that, beside the alkaline Southern blot, the efficient and simultaneous DSB induction in the yeast population, as well as the preparation of a high quality genomic DNA, is crucial to obtain a clear result with good resection kinetics.

2 Materials

Prepare all the solutions using filtered and deionized ultrapure water (ddH_2O; resistivity 18.2 MΩ·cm at 25 °C) and analytical grade reagents. Prepare and store all solutions at room temperature (unless indicated otherwise).

2.1 Double-Strand Break Induction in Yeast Cells

1. YEPD: 2% Bacto peptone, 1% yeast extract, 2% D−(+)−glucose monohydrate, 0.005% adenine hemisulfate salt. Dissolve in ddH_2O. Autoclave.
2. YEP + raffinose: dissolve 2% Bacto peptone, 1% yeast extract, 0.005% adenine hemisulfate salt in ddH_2O. Autoclave. Add sterilized raffinose from 30% solution to 2%.
3. 30% raffinose: dissolve D−(+)−raffinose pentahydrate in ddH_2O. Autoclave or sterilize by filtration.
4. 30% galactose: dissolve D−(+)−galactose ≥99.0% in ddH_2O. Sterilize by filtration. Do not autoclave (*see* **Note 1**).

2.2 Genomic DNA Extraction

1. Spheroplasting solution: 0.9 M sorbitol, 0.1 M ethylenediaminetetraacetic acid (EDTA), pH 7.5.
2. Zymolyase solution: dissolve 2 mg/mL Zymolyase 20T® (*see* **Note 2**) from *Arthrobacter luteus* (Nacalai Tesque) in spheroplasting solution + 14 mM β–mercaptoethanol.
3. 1× TE: 10 mM Tris–HCl, pH 7.5, 1 mM EDTA, pH 7.4. Autoclave.
4. Lysis solution: 2.2% sodium dodecyl sulfate (SDS), 278 mM EDTA, pH 8.5, 445 mM Tris-base. Prepare the lysis solution just before adding it to the samples by mixing the appropriate amounts of 10% SDS, 0.5 M EDTA, pH 8.5, 2 M Tris-base stock solutions in a 15 mL tube.
5. 5 M potassium acetate: dissolve 5 M potassium acetate in ddH_2O. Autoclave.
6. Ice-cold ethanol: 96% and 70%. Prepare a 70% ethanol solution by diluting 96% ethanol in ddH_2O. Store at −20 °C aliquots of both 70% and 96% ethanol in glass bottles.
7. RNase solution: dissolve 10 mg/mL RNase A, DNase-free, in 10 mL 10 mM Tris–HCl, pH 7.5, 15 mM NaCl. Heat to 100 °C for 5 min and cool down at room temperature. Prepare small aliquots and store them at −20 °C.
8. 2–propanol anhydrous 99.5%.
9. 6× DNA loading buffer: 30% glycerol, 0.25% bromophenol blue.
10. Regular agarose gel: melt 0.8% agarose in 1× TAE buffer. Cool at approximately 60 °C and add 10 mg/mL ethidium bromide solution to a final concentration of 1 μg/mL. Pour the gel into a gel tank and insert a comb.
11. 1× TAE (Tris-acetate-EDTA) buffer: 40 mM Tris, 20 mM acetic acid, 1 mM EDTA. Prepare a 50× TAE buffer: for 1 L dissolve 242 g of Tris-base in approximately 600 mL ddH_2O. Add 57.1 mL glacial acetic acid and 100 mL 0.5 M EDTA, pH 8.0, and bring final volume to 1 L with ddH_2O. Autoclave. Before use, dilute in ddH_2O to a final concentration of 1×.
12. Ethidium bromide solution: prepare a stock of 10 mg/mL ethidium bromide in ddH_2O and store in light-tight containers (*see* **Note 3**).
13. UV lamp with camera.

2.3 Alkaline Denaturing Electrophoresis and Southern Blot

2.3.1 DNA Digestion and Denaturation

1. SspI restriction enzyme (20,000 U/mL; New England Biolabs) and buffer supplied from distributor.
2. 3 M sodium acetate, pH 5.2: dissolve 3 M sodium acetate in ddH_2O. Adjust the pH to 5.2 with glacial acetic acid. Autoclave.

3. 0.5 M EDTA, pH 8.0: dissolve 0.5 M EDTA in ddH_2O. Adjust the pH to 8.0 with sodium hydroxide (NaOH). Autoclave.
4. 1× alkaline loading buffer: 50 mM NaOH, 1 mM EDTA, pH 8.0, 2.5% ficoll (type 400) in ddH_2O, 0.025% bromophenol blue.

2.3.2 Alkaline Denaturing Gel Electrophoresis and Transfer

1. Horizontal electrophoresis system with a large gel running chamber (gel size 25 × 20 cm) and 32-tooth comb (thickness 1.0 mm and width of teeth 4.0 mm).
2. 1× alkaline electrophoresis buffer: 50 mM NaOH, 1 mM EDTA, pH 8.5.
3. Glass plate that fits the gel.
4. 0.25 N hydrochloric acid (HCl): dilute HCl in ddH_2O just before use.
5. 0.5 N NaOH, 1.5 M NaCl: dissolve in ddH_2O just before use.
6. Nylon hybridization transfer membrane (GeneScreen® from Perkinelmer or equivalent).
7. 20× SSC buffer: 3 M NaCl, 300 mM sodium citrate. Adjust the pH to 7.0 with HCl. Autoclave.
8. Whatman 3 MM paper.
9. Parafilm from Bemis NA or equivalent.
10. Paper towels.
11. Neutralization solution: 0.5 M Tris–HCl pH 7.5, 1 M NaCl.
12. UV crosslinker.

2.3.3 Probe Labeling

1. Plasmid pML514 (available upon request), carrying part of the *MAT* locus downstream to the T7 bacteriophage promoter. Plasmid pML514 was constructed by inserting in the pGEM®–7Zf(+/−) (purchased from Promega) EcoRI site a 900–bp fragment of the *MAT* locus, obtained by PCR using yeast genomic DNA as a template and PRP643 (5′–CGG AAT TCC CTG GTT TTG GTT TTG TAG AGT GG–3′) and PRP644 (5′–CGG AAT TCG AAA CAC CAA GGG AGA GAA GAC–3′) as primers.
2. BamHI restriction enzyme (20,000 U/mL; New England Biolabs) and buffer supplied from distributor or equivalent (*see* **Note 4**).
3. In vitro transcription system Riboprobe System–T7 (Purchased from Promega and containing recombinant RNasin® RNase inhibitor, 10 mM rATP, 10 mM rCTP, 10 mM rGTP, 10 mM rUTP, 100 mM dithiothreitol (DTT), 5× transcription optimized buffer, T7 RNA polymerase, RQ1 RNase-free DNase, nuclease-free water, pGEM® Express positive control template), or equivalent.

4. rUTP–α^{32}P. Specific activity: 800 Ci/mmol.
5. Sephadex G–50 grade chromatography-columns (GE–Healthcare) or equivalent.

2.3.4 Filter Hybridization

1. Hybridization oven and hybridization tubes.
2. Formamide hybridization buffer: 5× SSPE, 50% formamide, 6% dextran sulfate sodium salt, 4× Denhardt's solution (dilute 50× Denhardt's solution from Sigma-Aldrich or equivalent), 100 μg/mL deoxyribonucleic acid sodium salt from salmon testes, 200 μg/mL yeast tRNA.
3. 20× SSPE buffer: 3 M NaCl, 0.2 M NaH_2PO_4, 20 mM EDTA. Adjust the pH to 7.4 with NaOH. Autoclave.
4. 1× SSPE, 0.1% SDS.
5. 0.1× SSPE, 0.1% SDS.
6. 0.2× SSPE, 0.1% SDS.
7. Autoradiography cassette with intensifying screens.
8. Autoradiography films.

3 Methods

3.1 Double-Strand Break Induction in Yeast Cells

1. Inoculate cells in 50–100 mL YEPD medium.
2. Grow the cell culture 6–8 h at 26 °C until the exponentially growing cells reach a density of 10^4–10^6 cells/mL.
3. Spin down the cells and wash with YEP + raffinose medium to remove glucose. Resuspend the cells in an equal or larger volume (depending on the number of samples to collect after HO induction) of YEP + raffinose medium (*see* **Notes 5** and **6**).
4. Grow the cell culture overnight at 26 °C.
5. When the cell culture has grown to a density between 6×10^6 and 10^7 cells/mL draw a 50 mL sample for the uninduced control. Then add galactose from 30% solution to 3% final concentration to the remaining cell culture (*see* **Note 7**).
6. Grow the cell culture at 26 °C and take 50 mL samples at the desired time points after galactose addition. During the experiment the efficiency of DSB formation can be determined (*see* **Note 8**).

3.2 Genomic DNA Extraction

1. Pellet the cells by spinning 3 min at 1600 × *g* in 50 mL tubes.
2. Wash the cells in 1 mL spheroplasting solution and transfer the samples to 1.5 mL microcentrifuge tubes.
3. Spin 3 min at 1600 × *g* and completely remove the supernatant with a tip.

4. Freeze and store the cell pellets at −20 °C.
5. Thaw the samples at room temperature and resuspend the cell pellets in 400 µL spheroplasting solution + 14 mM β–mercaptoethanol.
6. Add 100 µL Zymolyase solution to each sample and invert the tube four to six times. Incubate the samples at 37 °C. After 30 min check the formation of spheroplasts under a light microscope (*see* **Note 9**).
7. When >95% cells have become spheroplasts, spin 30 s at 15,000 × *g* and carefully remove the supernatant with a tip.
8. Gently resuspend spheroplasts in 400 µL 1× TE (do not vortex).
9. Add 90 µL lysis solution (prepared just before use). Immediately shake vigorously the tube (a foam should form) and incubate the samples 30 min in a water-bath at 65 °C.
10. Add 80 µL 5 M potassium acetate and mix by inverting the tube several times. Place the tubes on ice for approximately 1 h.
11. Spin for 20 min at 15,000 × *g* at 4 °C. Transfer the supernatant with nucleic acids to new 1.5 mL tubes. Discard the pellets.
12. Add 1 mL ice-cold 96% ethanol and mix by inverting the tube several times. A white cloudy precipitate should form. Place 30 min at −80 °C to facilitate precipitation.
13. Spin 10 min at 15,000 × *g* at 4 °C and remove the supernatant.
14. Wash the pellet with 1 mL ice-cold 70% ethanol and immediately discard the ethanol.
15. Air-dry the pellet until it appears glassy.
16. Add 500 µL 1× TE. Let tubes sit for 30 min at room temperature, then gently dissolve the pellet (do not vortex).
17. When all the pellets are completely dissolved and the solutions appear clear and transparent add 2.5 µL RNase solution to each sample and incubate for 1 h at 37 °C.
18. Add 500 µL 2–propanol and invert the tube several times. A white DNA "clew" should form. Place 30 min–overnight at −80 °C to facilitate precipitation.
19. Spin for 15–30 min at 15,000 × *g* at 4 °C and remove the supernatant.
20. Wash the pellet with 1 mL ice-cold 70% ethanol and immediately discard the ethanol.
21. Air-dry until the pellet appears glassy.
22. Add 30 µL 1× TE. Let tubes sit for 30 min at room temperature, then gently dissolve the DNA pellet (do not vortex).

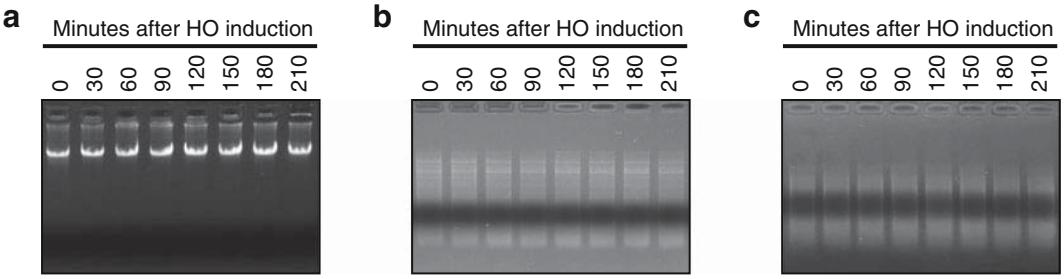

Fig. 2 Evaluation of the DNA quality during sample DNA preparation. (**a**–**c**) JKM139 cells exponentially growing in YEP + raffinose were transferred in YEP + raffinose + galactose to induce HO expression and DSB formation (*time zero*). Genomic DNA was prepared from samples taken at the indicated time points after galactose addition. (**a**) DNA extraction. 1 μL from 30 μL genomic DNA was visualized on regular agarose gel with ethidium bromide. (**b**) DNA digestion. Genomic DNA was digested with SspI. After 5 h at 37 °C, 2 μL of each digestion reaction were analyzed on agarose gel with ethidium bromide. (**c**) DNA denaturation. SspI-digested genomic DNAs were dissolved in 18 μL alkaline loading buffer. 1 μL of each sample was visualized on agarose gel with ethidium bromide

23. Apply 1 μL of each genomic DNA sample (added to 10 μL of 1× DNA loading buffer) on a 0.8% regular agarose gel with ethidium bromide and run in 1× TAE buffer. Check the quality of the extracted DNA under an UV lamp (*see* **Note 10** and Fig. 2a).

3.3 Alkaline Denaturing Electrophoresis and Southern Blot

3.3.1 DNA Digestion and Denaturation

1. Digest each DNA sample (10–15 μg DNA) with 10 U of SspI (New England Biolabs) or other restriction enzymes that cut double-stranded DNA (dsDNA) but not ssDNA (*see* **Notes 11** and **12**). Digest with 1× enzyme buffer in a total volume of 70 μL for 5–6 h at 37 °C.
2. Test 2 μL of each digestion reaction on a 0.8% agarose gel with ethidium bromide and run in 1× TAE buffer to check that all samples are digested (Fig. 2b).
3. Precipitate the digested DNA with 2 volumes 96% ethanol, 5 mM EDTA, pH 8.5, 0.3 M sodium acetate pH 5.2. Place overnight at −80 °C to facilitate precipitation.
4. Spin for 30 min at 15,000 × *g* at 4 °C and remove the supernatant.
5. Wash the pellet with 1 mL ice-cold 70% ethanol and immediately discard the ethanol.
6. Air-dry until the pellet appears glassy.
7. Add 18 μL 1× alkaline loading buffer. Let tubes sit for 30 min at room temperature, then gently dissolve the pellet (do not vortex). Let tubes sit for additional 1.5–2 h at room temperature by gently mixing every 15–30 min. The DNA should denature in single-stranded filaments. A 1 kb DNA ladder can

also be treated with 1× alkaline loading buffer and then used as marker for the size estimation of the DNA resection fragments.

8. Apply 1 μL denatured DNA to 10 μL alkaline loading buffer and load on a 0.8% agarose gel with ethidium bromide. Run in 1× TAE buffer to check whether the DNA is completely denatured (*see* **Note 13** and Fig. 2c) and to evaluate the amount of DNA in each digestion. Equilibrate the DNA concentration in the different tubes by adding an appropriate amount of 1× alkaline loading buffer.

3.3.2 Alkaline Denaturing Gel Electrophoresis and Transfer

1. Melt 0.8% agarose in 450 mL ddH_2O, and pour into a gel tray.
2. When the gel is completely solidified, mount it in a large gel box and submerge the gel in 1× alkaline electrophoresis buffer. Allow the gel to equilibrate for 30 min or longer (*see* **Note 14**).
3. Load on the gel 15 μL of each sample dissolved and equilibrated in alkaline loading buffer.
4. Carry out electrophoresis by running the gel overnight at voltages <3 V/cm. As bromophenol blue diffuses rapidly out of the gel into the alkaline electrophoresis buffer, place a glass plate directly on the top of the gel after the dye has migrated out of the loading slots.
5. After the DNA has migrated far enough (the dye has to migrate approximately 13–14 cm from the loading slots), remove the gel from the tank.
6. Stain the DNA with ethidium bromide by soaking the gel for 30 min–1 h in 1× TAE buffer with 0.5 μg/mL ethidium bromide (*see* **Note 15**).
7. Wash the gel 10 min in ddH_2O.
8. Check the gel under an UV lamp (Fig. 3a).
9. Soak the gel 7 min with gentle agitation in 0.25 N HCl.
10. Rinse the gel with ddH_2O.
11. Soak the gel 30 min with gentle agitation in 0.5 N NaOH, 1.5 M NaCl.
12. Rinse the gel with ddH_2O.
13. Blot overnight the DNA from the gel to a nylon hybridization membrane by capillary transfer with 10× SSC buffer (*see* **Notes 16** and **17**). Fill a tray with 10× SSC buffer (approximately 1.5 L). Place a platform on the tray and create a bridge with a Whatman 3 MM paper onto the platform. Pour 10× SSC buffer over the bridge and remove air bubbles. Place the gel on the Whatman 3 MM paper bridge. Wet a membrane that fits with the size of the gel in 10× SSC and lay on the gel. Remove air bubbles. Wet three sheets of Whatman 3 MM paper in 10× SSC and lay on the membrane. To maintain capillary flow

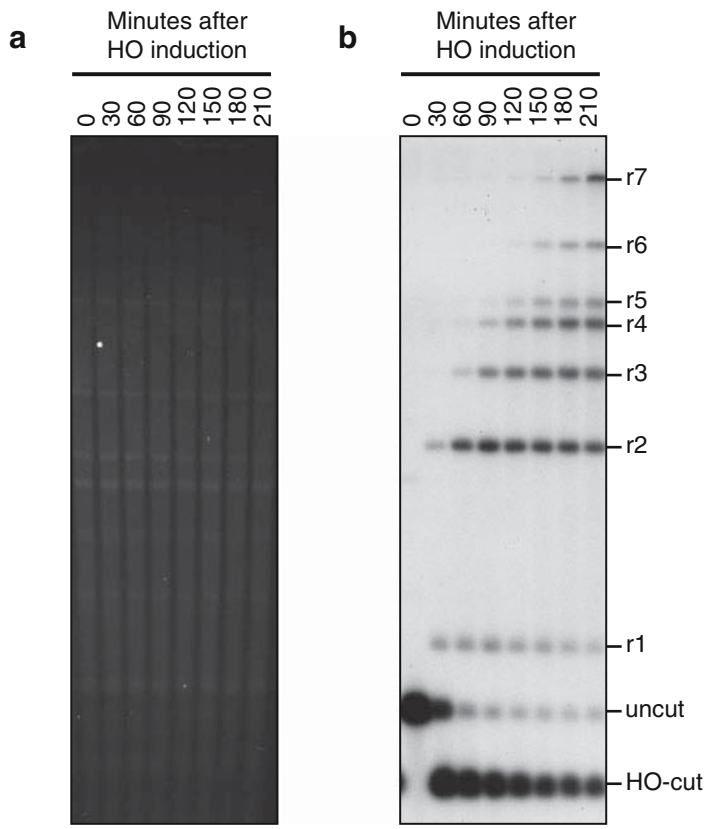

Fig. 3 DSB end resection at *MAT* locus. (**a**) Alkaline denaturing gel electrophoresis. SspI-cut genomic DNA was run overnight at 1.4 V/cm on an alkaline denaturing agarose gel and stained 30 min in 1× TAE buffer with 0.5 μg/mL ethidium bromide. (**b**) Southern blot analysis. ssDNA fragments were transferred on a nylon membrane and hybridized with a *MAT* RNA probe. Before galactose addition the probe reveals the uncut band, which is converted in the smaller HO-cut band after DSB formation. The resection bands r1–r7 appear when resection proceeds and eliminates SspI sites, as depicted in Fig. 1

through the gel instead of around it, place strips of Parafilm on all the sides of the gel and create a barrier between the bridge and the paper towels. Build up a big stack of paper towels and add some weight on the top.

14. After transfer, soak the membrane 15 min in neutralization solution with gentle agitation.
15. Air-dry the filter.
16. Crosslink the DNA on the membrane with an UV crosslinker by following the instructions of the manufacturer.

3.3.3 *Probe Labeling*

1. Digest 5–10 μg pML514 DNA with BamHI at 37 °C to linearize the plasmid downstream the *MAT* insert.

2. Check whether the plasmid is completely linearized by loading 2 μL of the digestion reaction and 1 μL of the uncut plasmid on a 0.8% agarose gel with ethidium bromide (*see* **Note 18**).
3. Precipitate the linearized plasmid and suspend it in a small volume of nuclease-free water (*see* **Note 19**).
4. Prepare the labeled RNA probe with the Promega Riboprobe System-T7 kit or equivalent, according to the instructions of the manufacturer. If the Promega Riboprobe System-T7 is chosen, add the following components in the order listed. 4 μL 5× transcription optimized buffer; 2 μL 100 mM DTT, 20 U recombinant RNasin® RNase inhibitor, 1 μL 10 mM rATP, 1 μL 10 mM rGTP, 1 μL 10 mM rCTP, 1–4 μL linearized template DNA (0.2–1.0 μg/μL in nuclease-free water), nuclease-free water to a 20 μL final volume, 5 μL rUTP–α^{32}P (100 μCi), 15–20 U T7 RNA Polymerase.
5. Incubate for 45 min at 40 °C.
6. Add 1 U RQ1 RNase-free DNase.
7. Incubate for 15 min at 37 °C.
8. Add 180 μL nuclease-free water.
9. Equilibrate a Sephadex G–50 grade chromatography-column with nuclease-free water.
10. Load the in vitro transcription solution on the chromatography-column.
11. Spin for 1 min at 850 × *g* and recover the eluate.

3.3.4 Filter Hybridization

1. Insert the filter in a hybridization tube and soak the filter with ddH_2O.
2. Block the filter by incubating for 5 h in a hybridization oven at 42 °C in 25 mL formamide hybridization buffer (pre-hybridization).
3. Prepare the hybridization solution by adding the RNA probe obtained by in vitro transcription (almost 200 μL; *see* Subheading 3.3.3) to 25 mL of fresh formamide hybridization buffer. Replace the pre-hybridization solution with this hybridization solution.
4. Incubate overnight at 42 °C by gently rotating in the hybridization oven.
5. Remove the hybridization solution.
6. Wash the filter for 30 min at 42 °C in 5× SSPE.
7. Wash for 30 min at 42 °C in 1× SSPE, 0.1% SDS.
8. Wash for 30 min at 42 °C in 0.1× SSPE, 0.1% SDS.
9. Wash for 15 min at 68 °C in 0.2× SSPE, 0.1% SDS.

10. Wash for 5 min at room temperature in 0.2× SSPE.
11. Air-dry the filter.
12. Expose the filter to an autoradiography film in an autoradiography cassette with intensifying screens (*see* **Notes 20** and **21** and Fig. 3b).

4 Notes

1. Galactose should not be autoclaved because it isomerizes at elevated temperatures.
2. There are two preparations of Zymolyase from Nacai Tesque, Zymolyase®–20T, and Zymolyase®–100T, having lytic activity of 20 U/g and 100 U/g, respectively. Zymolyase–100T can be used in place of Zymolyase–20T but the Zymolyase concentration in the spheroplasting solution and/or the time of incubation should be adjusted according to the different activity of the enzyme.
3. Alternatives to ethidium bromide are less-toxic dyes such as GelRed™ or GelGreen™.
4. Templates used for in vitro transcription should either be blunt-ended or carry protruding 5′ termini. As extraneous transcripts can appear in addition to the expected transcript when templates contain 3′ overhangs [11], plasmids should not be linearized with any enzyme that leaves a 3′ overhang.
5. Be sure to transfer in YEP + raffinose medium enough cells to reach a density of at least 6×10^6 cells/mL the next day.
6. HO expression and DSB formation can also be induced in a strain carrying a plasmid. In this case, an appropriate selective medium should be used in place of YEPD to maintain the plasmid selection. However, cells grow poorly in selective media with raffinose as a carbon source. Thus, cells can be grown in glucose selective medium for approximately 8 h and then transferred in YEP + raffinose medium for the overnight growth to minimize the number of cell divisions in a rich medium.
7. As resection is stimulated by the activity of the cyclin-dependent kinases (Cdk1 in *S. cerevisiae*) and the kinetics of resection change in the different cell cycle phases [12, 13], sometimes it might be important to analyze the generation of ssDNA at DSB ends in cells arrested at a particular stage of the cell cycle. To monitor resection in G2/M phase, when Cdk1 activity is high, cells can be arrested in early metaphase before galactose addition by treatment with nocodazole, a drug that interferes with microtubule polymerization. Prepare a 100×

nocodazole stock by dissolving 1.5 mg/mL nocodazole in 100% dimethyl sulfoxide (DMSO). Add the nocodazole stock to the exponentially growing cells in YEP + raffinose medium to a final concentration of 1× (final concentration of nocodazole 15 μg/mL). After 2.5–3 h at 26 °C, visualize cells under a light microscope. Add galactose to induce HO in G2/M-arrested cells when 90–100% cells accumulate as large-budded cells. Nocodazole-mediated arrest can be maintained for 8–10 h [7]. To monitor resection in G1 phase, when Cdk1 activity is low, *MATa* haploid cells can be treated with the α-factor pheromone. As these cells recover from the α-factor block after 1.5–2 h due to α-factor degradation by the Bar1 protease, a persistent G1 arrest with α-factor can be induced in strains carrying the deletion of the *BAR1* gene [14]. Dissolve 1 mg/mL α–factor in ddH_2O and add this solution to the exponentially growing cells in YEP + raffinose to a final α-factor concentration of 0.5 μg/mL. After 2 h at 26 °C, visualize cells under a light microscope. Add galactose to induce HO in G1-arrested cells when 90–100% cells are unbudded. α-factor-mediated arrest in *bar1*Δ cells can be maintained for at least 8 h [15].

8. As a single DSB formation triggers the activation of the DNA damage checkpoint and a G2/M arrest [16], the effectiveness of DSB induction in checkpoint-proficient strains can be determined under a light microscope by evaluating the percentage of large-budded cells after 4–6 h of galactose induction. Alternatively, samples taken before HO induction and at the desired time points after galactose addition (2 and/or 4 h) can be diluted and 300–3000 cells can be plated on YEPD plates to test if galactose addition has efficiently induced the DSB formation. As in this strain the HO-induced DSB is irreparable and its generation leads to cell death [6], strain viability after HO induction can be used to determine the efficiency of DSB formation.
9. Spheroplasts display a rounded morphology in contrast to the ovoid shape of intact yeast cells. Furthermore, as spheroplasts lyse in SDS solution, cells should disappear after the addition of one drop of 10% SDS to 3 μL of cells on a glass slide. We usually obtain >95% spheroplasts in 40–50 min.
10. If high molecular weight DNA molecules were extracted and completely dissolved, a single band should be detectable in the gel without smears or signals retained in the well.
11. Restriction endonucleases digest dsDNA by cleaving two phosphodiester bonds, one within each strand of the duplex DNA. ssDNA generally cannot be cut by restriction enzymes. A few restriction enzymes cleave ssDNA, although usually at low efficiency.

12. The conditions described here were set up for digestion with SspI restriction enzyme purchased from New England Biolabs. If a different enzyme and/or producer were chosen, consult the manufacturer's instructions for optimal digestion conditions.
13. When DNA is completely denatured, a smear is detectable on the agarose gel.
14. The agarose gel is equilibrated in alkaline electrophoresis buffer after solidification because the addition of NaOH to a warm agarose solution causes polysaccharide hydrolysis. Alternatively, the agarose can be melted in ddH_2O and then cooled down to 60 °C, so that NaOH to 50 mM and EDTA pH 8.5 to 1 mM can be added just before pouring the gel.
15. Ethidium bromide is omitted from alkaline agarose gels because it does not bind to DNA at high pH. DNA can be stained with ethidium bromide after the electrophoresis. However, DNA will be faint because the ethidium bromide does not bind very well to ssDNA.
16. Alternatively, a vacuum blotter can be used.
17. DNA can be blotted onto either neutral or positively charged nylon membranes.
18. Plasmid DNA must be cleaved to completion, as trace amounts of uncut supercoiled plasmid DNA can give rise to long transcripts that include vector sequences. These transcripts may incorporate a fraction of the radiolabeled rNTP.
19. The linearized plasmid DNA should be highly concentrated because a small volume of template is required for the in vitro transcription reaction.
20. The film can be also developed in a Typhoon instrument or equivalent.
21. With freshly labeled rUTP-α^{32}P, we usually obtain a good signal after 4 h-overnight exposure at −80 °C.

Acknowledgments

We thank J. Haber (Brandeis University) for the JKM139 yeast strain, and M. P. Longhese and G. Lucchini for critical reading of the manuscript.

References

1. Symington LS, Rothstein R, Lisby M (2014) Mechanisms and regulation of mitotic recombination in *Saccharomyces cerevisiae*. Genetics 198:795–835. doi:10.1534/genetics.114.166140
2. Mehta A, Haber JE (2014) Sources of DNA double-strand breaks and models of recombinational DNA repair. Cold Spring Harb Perspect Biol 6(9):a016428. doi:10.1101/cshperspect.a016428

3. Symington LS (2014) End resection at double-strand breaks: mechanism and regulation. Cold Spring Harb Perspect Biol 6(8):a016436. doi:10.1101/cshperspect.a016436
4. Villa M, Cassani C, Gobbini E, Bonetti D, Longhese MP (2016) Coupling end resection with the checkpoint response at DNA double-strand breaks. Cell Mol Life Sci 73 (19):3655–3663. (in press)
5. White CI, Haber JE (1990) Intermediates of recombination during mating type switching in *Saccharomyces cerevisiae*. EMBO J 9:663–673
6. Lee SE, Moore JK, Holmes A, Umezu K, Kolodner RD, Haber JE (1998) *Saccharomyces* Ku70, mre11/rad50 and RPA proteins regulate adaptation to G2/M arrest after DNA damage. Cell 94:399–409. doi:10.1016/s0092-8674(00)81482-8
7. Clerici M, Mantiero D, Lucchini G, Longhese MP (2005) The *Saccharomyces cerevisiae* Sae2 protein promotes resection and bridging of double strand break ends. J Biol Chem 280:38631–38638
8. Manfrini N, Guerini I, Citterio A, Lucchini G, Longhese MP (2010) Processing of meiotic DNA double strand breaks requires cyclin-dependent kinase and multiple nucleases. J Biol Chem 285:11628–11637. doi:10.1074/jbc.M110.104083
9. Bonetti D, Martina M, Clerici M, Lucchini G, Longhese MP (2009) Multiple pathways regulate 3′ overhang generation at *S. cerevisiae* telomeres. Mol Cell 35:70–81. doi:10.1016/j.molcel.2009.05.015
10. Lee CS, Haber JE (2015) Mating-type gene switching in *Saccharomyces cerevisiae*. Microbiol Spectr 3(2):MDNA3-0013-2014. doi:10.1128/microbiolspec.MDNA3-0013-2014
11. Schenborn ET, Mierendorf RC (1985) A novel transcription property of SP6 and T7 RNA polymerases: dependence on template structure. Nucleic Acids Res 13:6223–6236
12. Aylon Y, Liefshitz B, Kupiec M (2004) The CDK regulates repair of double-strand breaks by homologous recombination during the cell cycle. EMBO J 23:4868–4875
13. Ira G, Pellicioli A, Balijja A, Wang X, Fiorani S, Carotenuto W, Liberi G, Bressan D, Wan L, Hollingsworth NM, Haber JE, Foiani M (2004) DNA end resection, homologous recombination and DNA damage checkpoint activation require CDK1. Nature 431:1011–1017
14. Chan RK, Otte CA (1982) Physiological characterization of *Saccharomyces cerevisiae* mutants supersensitive to G1 arrest by a factor and alpha factor pheromones. Mol Cell Biol 2:21–29
15. Trovesi C, Falcettoni M, Lucchini G, Clerici M, Longhese MP (2011) Distinct Cdk1 requirements during single-strand annealing, noncrossover, and crossover recombination. PLoS Genet 7(8):e1002263. doi:10.1371/journal.pgen.1002263
16. Pellicioli A, Lee SE, Lucca C, Foiani M, Haber JE (2001) Regulation of *Saccharomyces* Rad53 checkpoint kinase during adaptation from DNA damage-induced G2/M arrest. Mol Cell 7:293–300

6530–6545 *Nucleic Acids Research, 2017, Vol. 45, No. 11* *Published online 2 May 2017*
doi: 10.1093/nar/gkx347

The RNA binding protein Npl3 promotes resection of DNA double-strand breaks by regulating the levels of Exo1

Chiara Vittoria Colombo†, Camilla Trovesi†, Luca Menin, Maria Pia Longhese* and Michela Clerici*

Dipartimento di Biotecnologie e Bioscienze, Università di Milano-Bicocca, 20126 Milano, Italy

Received January 11, 2017; Revised April 10, 2017; Editorial Decision April 18, 2017; Accepted April 21, 2017

ABSTRACT

Eukaryotic cells preserve genome integrity upon DNA damage by activating a signaling network that promotes DNA repair and controls cell cycle progression. One of the most severe DNA damage is the DNA double-strand break (DSB), whose 5′ ends can be nucleolitically resected by multiple nucleases to create 3′-ended single-stranded DNA tails that trigger DSB repair by homologous recombination. Here, we identify the *Saccharomyces cerevisiae* RNA binding protein Npl3 as a new player in DSB resection. Npl3 is related to both the metazoan serine-arginine-rich and the heterogeneous nuclear ribonucleo-proteins. *NPL3* deletion impairs the generation of long ssDNA tails at the DSB ends, whereas it does not exacerbate the resection defect of *exo1Δ* cells. Furthermore, either the lack of Npl3 or the inactivation of its RNA-binding domains causes decrease of the exonuclease Exo1 protein levels as well as generation of unusual and extended *EXO1* RNA species. These findings, together with the observation that *EXO1* overexpression partially suppresses the resection defect of *npl3Δ* cells, indicate that Npl3 participates in DSB resection by promoting the proper biogenesis of *EXO1* mRNA.

INTRODUCTION

Eukaryotic cells deal with DNA damage through a multifaceted cellular response, known as DNA damage response (DDR), which promotes DNA repair and couples it with cell cycle progression (1). DNA double-strand breaks (DSBs) are among the most severe lesions. DSBs can be repaired by either non-homologous end-joining (NHEJ), which directly rejoins together the two broken ends, or homologous recombination (HR) that uses intact homologous duplex DNA sequences as a template for accurate repair (2).

HR is promoted by the nucleolytic degradation of the 5′ DSB ends (a process referred to as resection) to yield 3′ single-stranded DNA (ssDNA) tails that invade the homologous duplex and prime reparative DNA synthesis (2). DSB resection is a two-step process that involves multiple nucleases and helicases. A protein complex, which is called MRX (Mre11–Rad50–Xrs2) in the budding yeast *Saccharomyces cerevisiae* and MRN (Mre11–Rad50–Nbs1) in mammals, initiates resection together with the Sae2/CtIP protein by catalyzing an endonucleolytic cleavage of the 5′-terminated DNA strands. This cleavage creates a substrate for two partially overlapping pathways, which depend on the nucleases Exo1 and Dna2, respectively, and promote the generation of long ssDNA tails (reviewed in 3,4). While Exo1 is a 5′-3′ exonuclease capable of efficiently degrading the 5′ end on duplex DNA, the endonuclease Dna2 requires the helicase activity of Sgs1 (orthologue of mammalian BLM) to efficiently remove small fragments from DNA ends (3,4).

DSB end degradation is tightly controlled by both positive and negative regulators, which tune the action of specific resection factors. While the cyclin-dependent kinase (Cdk1 in yeast)-Clb complexes stimulate the activities of both Sae2 and Dna2, the Ku complex and Rad9 inhibit the action of Exo1 and Sgs1-Dna2, respectively (3–5). Exo1 action is also inhibited through phosphorylation by the checkpoint kinase Rad53 (6) and regulated by the ssDNA-binding complex Replication Protein A (RPA), which promotes Exo1 action *in vivo*, and limits Exo1-dependent degradation by increasing Exo1 turnover at DNA ends *in vitro* (7,8). Given the efficiency of Exo1 exonuclease (8), these multiple controls on its action can be important to prevent excessive DNA degradation that could lead to genome instability.

DSB repair is coupled with cell cycle progression by a checkpoint pathway, whose key players are the protein ki-

*To whom correspondence should be addressed. Tel: +39 0264483547; Fax: +39 0264483565; Email: michela.clerici@unimib.it
Correspondence may also be addressed to Maria Pia Longhese. Tel: +39 0264483425; Fax: +39 0264483565; Email: mariapia.longhese@unimib.it
†These authors contributed equally to this work as first authors.
Present address: Camilla Trovesi, Istituto Nazionale di Genetica Molecolare 'Romeo ed Enrica Invernizzi', 20122 Milano, Italy.

nases Mec1 and Tel1, orthologs of mammalian ATR and ATM, respectively (1). While Tel1 is recruited to blunt or minimally processed DNA ends through interaction with MRX (9), Mec1 and its interactor Ddc2 (ATRIP in mammals) are activated by extended RPA-coated ssDNA that is produced by resection (10). Once activated, Mec1 and Tel1 propagate the checkpoint signal to the effector kinases Rad53 and Chk1 (Chk2 and Chk1 in mammals, respectively), whose activation requires the adaptor Rad9 (53BP1 in mammals) and leads to temporarily arrest cell cycle progression (1).

Increasing evidence suggests the existence of intimate connections between RNA metabolism, DDR and genome integrity (11). Pre-mRNA molecules are co-transcriptionally processed by the addition of both a 5′-methylguanosine cap and a 3′ poly(A) tail, and eventually spliced before they are exported to the cytoplasm and translated. These events are mediated by RNA-binding proteins (RBPs), most of which belong to the conserved protein families of heterogeneous nuclear ribonucleo-proteins (hnRNPs) and mammalian serine-arginine-rich (SR) proteins (11). RBPs also protect mRNAs from degradation and contribute to quality control systems that recognize and target to degradation improperly processed mRNAs (12,13). In eukaryotes, mRNAs are mainly degraded either by the exosome multi-subunit complex, which includes both endo- and 3′-5′ exoribonuclease activities, or by the Xrn family of 5′-3′ exoribonucleases (13,14).

In both yeast and mammals, several RBPs participate to the DDR and the stress response. Many of these RBPs bind to nascent transcripts and prevent transcription-associated genome instability by packaging pre-mRNAs into ribonucleoprotein particles. This packaging limits the generation of DNA:RNA hybrids, which could induce replication stress and DNA damage by interfering with the progression of DNA replication forks (reviewed in 11,15). Factors involved in RNA metabolism play also more direct roles in the DDR by either recruiting DDR proteins to the site of damage or regulating the expression of repair and checkpoint genes at different levels (11). Finally, the conserved nonsense-mediated decay (NMD) pathway was recently found to limit HR in *S. cerevisiae* undamaged cells by controlling the transcript and protein levels of HR factors (16).

One of the most abundant *S. cerevisiae* RBPs is Npl3, which shares structural homologies with both SR and hnRNPs protein families, as it possesses two conserved RNA-recognition motifs (RRMs) and a serine- and arginine-rich C-terminal domain (17). Npl3 is recruited to transcribed regions through the interaction with RNA polymerase II (18,19), and participates in pre-mRNA processing and packaging as well as in mRNA export and translation (12). Npl3 accumulates at the 3′ end of transcribed genes (20) and seems to play a role in transcription termination, although this role is somehow controversial. In fact, studies with reporter constructs indicated that Npl3 prevents both early transcription termination and recognition of polyadenylation cryptic sites by competing with polyadenylation/termination factors (18,21,22). However, recent genome-wide analyses showed significant termination defects in the absence of Npl3, suggesting that Npl3 promotes transcription termination (23).

Similar to other RBPs, Npl3 prevents transcription-associated genome instability by limiting the accumulation of DNA:RNA hybrids (20). Interestingly, several findings suggest additional Npl3 functions in the DDR. In particular, cells lacking Npl3 are highly sensitive to DSB-inducing agents (20) and to the expression of the EcoRI endonuclease (24). Furthermore, Npl3 shows negative genetic interactions with the MRX complex (25), and Npl3 inactivation increases the sensitivity of *rad52* or *ku* mutants to genotoxic agents (20). Finally, checkpoint-dependent Npl3 phosphorylation after methyl methanesulfonate (MMS) treatment suggests that Npl3 activity may be regulated in response to DNA damage (26).

Here, we show that Npl3 promotes both checkpoint activation and the generation of long ssDNA tails at the DSB ends. These functions are at least partially linked to the regulation of Exo1 abundance through the control of *EXO1* mRNA biogenesis. Altogether, our results identify a new function of Npl3 in the response to DSBs and contribute to define the role of this multifunctional RBP in preserving genome stability.

MATERIALS AND METHODS

Yeast strains and media

Strain genotypes are listed in Supplementary Table S1. All the strains are derivatives of JKM139 strain, which was kindly provided by J. Haber (Brandeis University, Waltham, MA, USA). The centromeric plasmid carrying the *tetO-RNH1* allele (27) and the control vector were kindly provided by A. Aguilera (University of Seville, Sevilla, Spain); the *EXO1* 2μ plasmid (28) and the control vector by E. Alani (Cornell University, New York, NY, USA); the control vector and the centromeric plasmids carrying the wild type *NPL3* or the mutant alleles *npl3-F160L*, *npl3-SNK* (*L225S, G241N, E244K*), and *npl3-LSNK* (*F160L, L225S, G241N, E244K*) (29) by J. Lee-Soety (Saint Joseph's University, Philadelphia, PA, USA). Gene deletions and gene tagging were obtained by one-step PCR methods. Cells were grown in YEP medium (1% yeast extract, 2% peptone) supplemented with 2% glucose (YEPD) or 2% raffinose (YEPR). 3% galactose was added to YEPR-growing cells to induce HO expression (YEPRG). The HO-cut efficiency was evaluated after quantitative PCR (qPCR) with a primer pair that overlaps the HO cut site and gives rise a product only when the locus is uncut, and primers at the *TRP3* locus as a control. The cleavage efficiency was calculated by dividing the difference between the values of the HO-specific product calculated with the ΔCt method before and two hours after galactose addition to the value of the HO-specific product before induction.

DSB resection

DSB end resection was analyzed on alkaline agarose gels by using a single-stranded RNA probe complementary to the unresected DSB strand as described in (30). This probe was obtained by *in vitro* transcription using Promega Riboprobe System-T7 and plasmid pML514 containing a 900-

bp fragment of the *MAT* locus (coordinates 200 870 to 201 587 on chromosome III) as a template. Quantitative analysis of DSB resection was performed by calculating the ratio of band intensities for ssDNA to total amount of DSB products. The resection efficiency was normalized with respect to the HO cleavage efficiency by subtracting the value of the uncut band from the total amount of DSB products for each time point.

Quantitative reverse transcriptase PCR (qRT-PCR)

Total RNA was prepared with the Bio-Rad Aurum total RNA mini kit. First strand cDNA was synthetized with the Bio-Rad iScript™ cDNA Synthesis Kit. After qRT-PCR on a MiniOpticon Real-time PCR system (Bio-Rad), *EXO1* RNA levels were quantified using the ΔΔCt method and normalized to *ALG9* RNA levels. Primer sequences are listed in Supplementary Table S2.

Northern blot

Total RNA was resolved on a 1% agarose gel in formaldehyde gel running buffer (2.2 M formaldehyde, 20 mM MOPS pH 7.0, 8 mM sodium acetate, 1 mM EDTA pH 8.0). The gel was stained with ethidium bromide to detect 18S and 25S ribosomal RNA and then transferred on a nitrocellulose filter. A BamHI–BglII DNA fragment (1437 bp) internal to the *EXO1* coding sequence (+628 to + 2065 from the ATG initiation codon) was extracted from pML546 plasmid, labeled with [α-32P]-dATP by random priming, and used as a probe. pML546 was constructed by inserting a 3109 bp XhoI–NotI blunt fragment containing the *EXO1* gene from pEAm67 2μ plasmid (28) into the SalI-SmaI YEpLac195 vector (31).

5′ rapid amplification of cDNA ends (RACE)

5 μg of total RNA was subjected to reverse transcription using SuperScript™ II (Invitrogen) and an *EXO1* specific primer to obtain the *EXO1* 5′ partial cDNA ends. After RNA degradation with RNaseH1 and poly(A) tailing of the ss-cDNA, a second DNA strand was synthetized starting from a Q_T (Q_{TOTAL}) primer containing both an oligo-dT sequence capable of annealing with the appended poly(A) tail and a unique sequence. The resulting cDNA was used as a template for two subsequent rounds of amplification using primers that anneal to the Q_T sequence and *EXO1* specific primers. The PCR products were run on 1.5% agarose gels and visualized with ethidium bromide. Primer sequences are listed in Supplementary Table S2.

ChIP analysis

ChIP analysis was performed as previously described (32). Chromatin extracts from both *NPL3-HA* and *NPL3* strains were immunoprecipitated with anti-HA antibodies. Input and immunoprecipitated DNA were purified and analyzed by qPCR. Data are expressed as fold enrichment at the HO-induced DSB over that at the non-cleaved *ARO1* locus, after normalization of ChIP signals to the corresponding input for each time point. Fold enrichment was then normalized to the efficiency of DSB induction.

Other techniques

Flow cytometric DNA analysis was determined on a Becton-Dickinson FACScan. Rad53 was detected by using anti-Rad53 polyclonal antibodies (AB104232) from Abcam. Anti-Rfa2 and anti-Rad9 polyclonal antibodies were kindly provided by B. Stillman (Cold Spring Harbor Laboratory, Cold Spring Harbor, NY, USA) and N. Lowndes (University of Ireland, Galway, Ireland), respectively. Quantitative analysis of phosphorylation normalized to the cut efficiency was performed by calculating the ratio of band intensities for slowly-migrating bands to the total amount of protein, and dividing the obtained values by the cleavage efficiency evaluated by qPCR.

RESULTS

Npl3 promotes the activation of a Mec1-dependent checkpoint

The hypersensitivity of *npl3* mutant cells to DSB-inducing agents (20,24) suggests that Npl3 is involved in the response to DSBs. To explore further this hypothesis, we asked whether the lack of Npl3 affects the checkpoint response to a single DSB that is generated by the HO endonuclease, whose gene is expressed from a galactose-inducible promoter in JKM139 haploid cells (33). Galactose addition to these cells induces the generation at the *MAT* locus of a single DSB that cannot be repaired by HR because the homologous donor loci *HML* and *HMR* are deleted (33). This HO-induced DSB triggers a Mec1-dependent checkpoint that causes a G2/M cell cycle arrest, as well as the phosphorylation of both the checkpoint effector kinase Rad53 and the Mec1 interactor Ddc2 (34–36). We analyzed cell cycle progression and phosphorylation of Rad53 and Ddc2 after the induction of a single irreparable DSB in wild type and *npl3Δ* cells carrying a fully functional Ddc2-HA tagged variant. The cleavage efficiency was evaluated by quantitative PCR (qPCR) at the HO cut site 2 h after galactose addition. Cells carrying the deletion of *MEC1* and kept viable by the lack of the ribonucleotide reductase inhibitor Sml1 were used as a control (37).

When G1-arrested cell cultures were spotted on galactose-containing plates, wild type cells arrested as large-budded cells for at least 8 hours after HO induction, while *mec1Δ sml1Δ* cells, which are unable to activate the checkpoint, formed microcolonies with more than two cells within 4–6 hours (Figure 1A). Although the cleavage efficiency was reduced to 82% in *npl3Δ* cells compared to wild type (95%), 60% of *npl3Δ* cells formed microcolonies 8 hours after HO induction, when >80% wild type cells were still arrested (Figure 1A), indicating that Npl3 contributes to arrest the cell cycle in response to an irreparable DSB.

Rad53 and Ddc2 phosphorylation, which causes decreased electrophoretic mobility of the proteins, was analyzed by western blot of comparable amounts of protein extracts (Supplementary Figure S1) after galactose addition to cell cultures exponentially growing in raffinose. As the HO cleavage efficiency was reduced in *npl3Δ* cells compared to wild type (85% versus 97%), we also performed quantitative analyses of Rad53 and Ddc2 phosphorylation by calculating the ratio of slowly-migrating phospho-

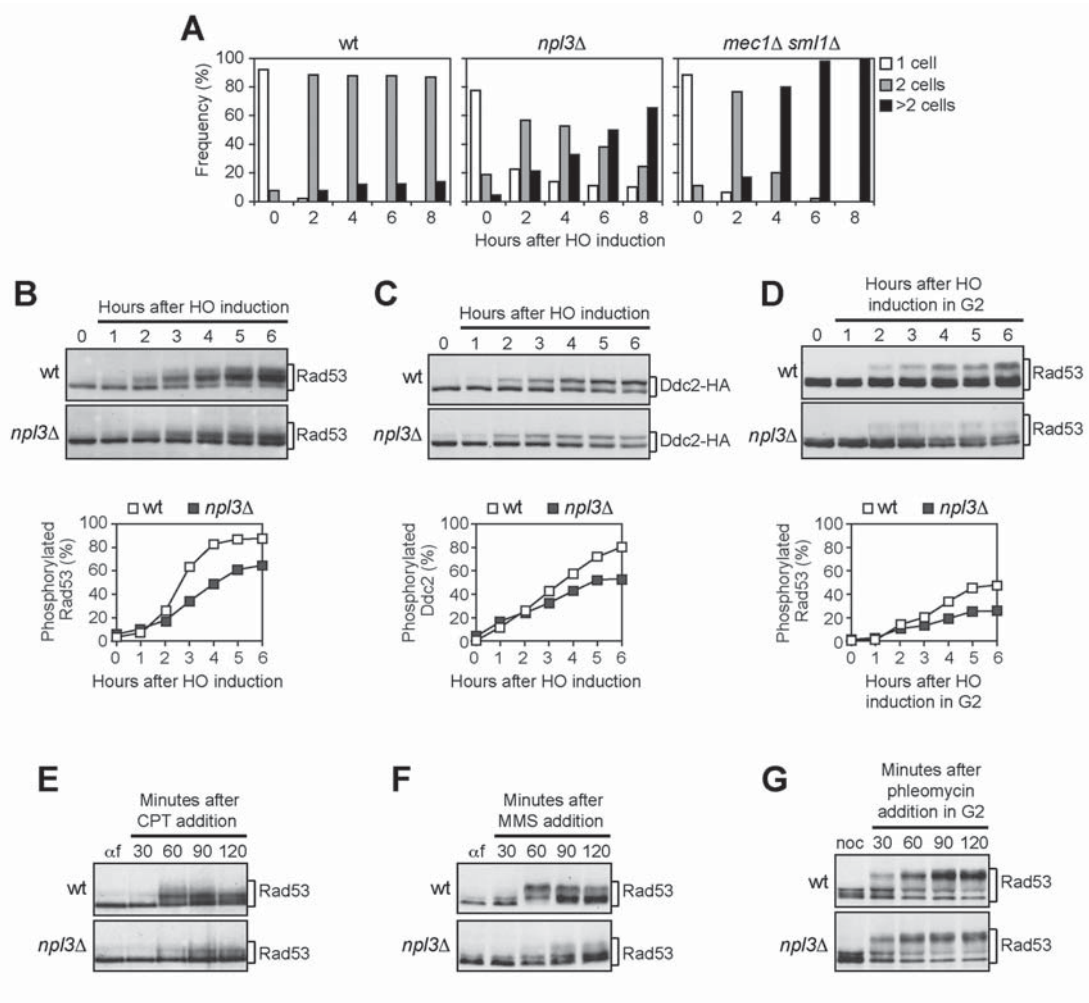

Figure 1. The lack of *NPL3* impairs Mec1 signaling activity. (**A**) YEPR G1-arrested cell cultures of JKM139 derivative strains were plated on galactose-containing plates to induce HO expression (time zero). At the indicated time points, 200 cells for each strain were analyzed to determine the frequency of unbudded cells, large budded cells and microcolonies with more than two cells. (**B** and **C**) Exponentially growing YEPR cell cultures expressing a fully functional Ddc2-HA protein were transferred to YEPRG (time zero). Protein extracts prepared at the indicated time points were subjected to western blot with anti-Rad53 (B) or anti-HA (C) antibodies. Quantitative analysis of Rad53 and Ddc2 phosphorylation was performed by calculating the ratio of band intensities for slowly-migrating bands to total amount of protein, and dividing the obtained values by the HO cleavage efficiency. Cut efficiency was evaluated as the difference in the normalized amount of qPCR products obtained with a primer pair that amplifies only the uncut *MAT* locus before and 2 h after galactose addition. (**D**) YEPR G2-arrested cell cultures were transferred in YEPRG (time zero) in the presence of nocodazole. Protein extracts were analyzed by western blot with anti-Rad53 antibodies. Quantitative analysis of Rad53 phosphorylation was performed as in (B). (**E** and **F**) YEPD G1-arrested cell cultures were released in fresh medium containing camptothecin (CPT) (50 μM) (E) or methyl methanesulfonate (MMS) (0,02%) (F). Rad53 phosphorylation was monitored by western blot with anti-Rad53 antibodies. (**G**) Phleomycin (15 μg/ml) was added to YEPD G2-arrested cell cultures kept arrested in G2. Protein extracts were subjected to western blot with anti-Rad53 antibodies.

rylated forms to total protein amount, and normalizing this value with respect to the efficiency of DSB formation evaluated by qPCR. Slowly-migrating Rad53 bands appeared 2–3 hours after HO induction and then became prevalent in wild type extracts (Figure 1B). Conversely, the unphosphorylated Rad53 species remained abundant until the end of the experiment in *npl3Δ* extracts although some slowly-migrating bands appeared 3–4 hours after HO induction (Figure 1B), indicating that Npl3 promotes the HO-induced Rad53 phosphorylation. Npl3 enhances also the phosphorylation of the Mec1-specific target Ddc2, as the amount of phosphorylated Ddc2 was lower in *npl3Δ* extracts than in wild type after HO induction (Figure 1C). Altogether, these results indicate that Npl3 promotes the activation of the Mec1-dependent checkpoint in response to a single irreparable DSB.

As cells lacking Npl3 showed growth defects (20), we asked whether their checkpoint defect could be ascribed to alterations in cell cycle progression. This was not the case, because Rad53 phosphorylation was defective in *npl3Δ* cells even when the HO cut was induced in cells arrested in G2 with nocodazole and kept in G2 throughout the experiment (Figure 1D).

To test whether Npl3 participates to checkpoint activation specifically after a single HO-induced DSB, we analyzed Rad53 phosphorylation in wild type and *npl3Δ* cells treated with different genotoxic agents. Cell cultures were arrested in G1 with α-factor and released in the presence of the topoisomerase poison camptothecin (CPT) or the alkylating agent MMS. As expected (38), Rad53 phosphorylation was slightly induced by CPT in wild type cells (Figure 1E). However, this phosphorylation was further reduced in *npl3Δ* cells (Figure 1E). Similarly, Rad53 was less phosphorylated in MMS-treated *npl3Δ* cells than in wild type (Figure 1F). Conversely, Rad53 was efficiently phosphorylated in both wild type and *npl3Δ* cells arrested in G2 and treated with the DSB-inducing drug phleomycin (Figure 1G). As checkpoint activation in all these conditions depends specifically on Mec1 (38,39), these results suggest that Npl3 is not directly required to activate Mec1 but rather to generate specific signals that activate Mec1.

Npl3 promotes the generation of ssDNA at DSBs

Mec1 activation requires the formation of RPA-coated ssDNA, which is generated by the 5′-3′ nucleolytic degradation of the DSB ends (10). In both *Schizosaccharomyces pombe* and human cells, RPA loading at DSB ends was found to be inhibited by the presence of DNA:RNA hybrids (40,41). As Npl3 counteracts the accumulation of DNA:RNA hybrids during transcription (20), the reduced Mec1 activation in *npl3Δ* cells could be due to the inability of these cells to remove DNA:RNA hybrids from the DSB ends. If this were the case, the checkpoint defect of *npl3Δ* cells should be alleviated by high levels of ribonuclease H1 (RNase H1), which is known to remove DNA:RNA hybrids *in vivo* (27). We therefore transformed wild type and *npl3Δ* cells carrying the HO system with a centromeric plasmid carrying the RNase H1-encoding gene (*RNH1*) under the control of *tetO* promoter, which acts as a strong promoter in the absence of tetracyclin (27). As expected (20), the *tetO-RNH1* plasmid suppressed the hypersensitivity of *npl3Δ* cells spotted on plates with MMS (Figure 2A). However, the hypersensitivity to CPT of the same cells was only very slightly suppressed by RNase H1 overproduction (Figure 2A), which was also unable to restore the HO-induced checkpoint in cells lacking Npl3. In fact, *npl3Δ* cells carrying either the *tetO-RNH1* plasmid or the empty vector showed similar defects in both Rad53 phosphorylation (Figure 2B) and cell cycle arrest after HO induction compared to wild type cells (Supplementary Figure S2). This finding indicates that the checkpoint defect of *npl3Δ* cells is not likely due to DNA:RNA hybrid accumulation.

We then asked whether Npl3 promotes DSB processing by directly monitoring ssDNA generation at the DSB ends. Galactose was added to cell cultures arrested in G2 with nocodazole to produce the HO-induced DSB in cells that were then maintained in G2. Because ssDNA is resistant to cleavage by restriction enzymes, we measured the 5′ strand degradation of one DSB end by following the loss of SspI restriction fragments at different time points after galactose addition by Southern blot of genomic DNA under alkaline conditions, using a single-stranded RNA probe that anneals to the unresected 3′ strand on one side of the break (Figure 2C and D). We then evaluated the resection efficiency by calculating the ratio of band intensities for ssDNA to total amount of DNA, normalized with respect to the efficiency of DSB formation for each time point (Figure 2E). The 1.7 and 3.5 kb resection fragments (r1-r2 in Figure 2C–E) appeared with similar kinetics in both wild type and *npl3Δ* cells, suggesting that the lack of Npl3 does not affect initiation of DSB resection. However, the generation of resection fragments longer than 3.5 kb (r3–r7 in Figure 2C–E) was severely affected by the absence of Npl3 (Figure 2D and E), indicating that *npl3Δ* cells are specifically impaired in extensive resection. Thus, Npl3 is dispensable to initiate DSB resection, whereas it is required to produce long ssDNA tails.

The Npl3 RNA-binding domains are required for Npl3 functions in the DDR

Npl3 binds RNA through the RNA recognition motifs RRM1 and RRM2 (17). We therefore investigated whether the integrity of Npl3 RRMs is required for cell survival in the presence of DNA damage and/or HO-induced checkpoint activation. We transformed *npl3Δ* cells with either an empty centromeric plasmid or with similar plasmids carrying wild type *NPL3*, the *npl3-F160L* allele, which inactivates RRM1, the *npl3-SNK* (*L225S, G241N, E244K*) allele, which inactivates RRM2, and the *npl3-LSNK* (*F160L, L225S, G241N, E244K*) allele, which disrupts both RRM domains (17,29). Cells expressing the *npl3-F160L* allele were as sensitive as wild type to CPT (Figure 3A) and phosphorylated Rad53 similarly to wild type cells after HO-induction (Figure 3B and Supplementary Figure S3). By contrast, *npl3-SNK* and *npl3-LSNK* cells were more sensitive than wild type to CPT, although their hypersensitivity was less pronounced compared to *npl3Δ* cells (Figure 3A). Furthermore, the HO-induced Rad53 phosphorylation was reduced in *npl3-SNK* and *npl3-LSNK* mutants, similar to *npl3Δ* cells (Figure 3B).

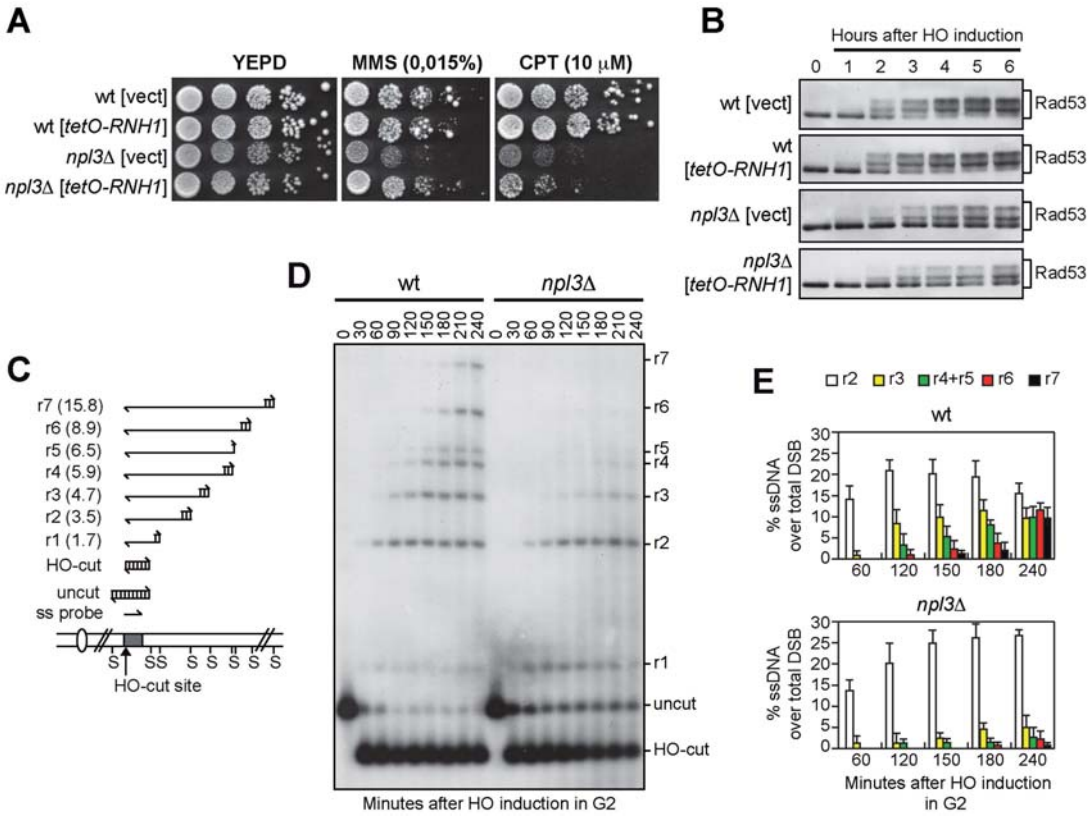

Figure 2. The lack of *NPL3* impairs extensive resection of DSB ends. (**A** and **B**) Exponentially growing cell cultures of wild type and *npl3Δ* strains, both carrying a centromeric plasmid either expressing the *RNH1* gene from the *tetO* promoter or empty (vect), were either serially diluted (1:10) before being spotted out onto YEPD plates with or without MMS or CPT (A), or transferred to YEPRG to monitor Rad53 phosphorylation by western blot (B). (**C**) System to detect DSB resection. Gel blots of SspI-digested genomic DNA separated on alkaline agarose gel were hybridized with a single-stranded RNA *MAT* probe (ss probe) that anneals to the unresected strand. 5′-3′ resection progressively eliminates SspI sites (S), producing larger SspI fragments (r1 through r7) detected by the probe. (**D** and **E**) Exponentially growing YEPR cell cultures were arrested in G2 with nocodazole and transferred to YEPRG (time zero) in the presence of nocodazole. (D) DSB resection as described in (C). (E) Resection products in (D) were analyzed by densitometry. The mean values are represented with error bars denoting SD ($n = 5$).

We also analyzed whether the integrity of Npl3 RRM domains is required for resection by measuring ssDNA generation at the HO-induced DSB in *npl3-LSNK* mutant cells. Similar to the absence of Npl3, the *npl3-LSNK* allele impairs long-range resection. In fact, the r3–r7 resection fragments accumulated less efficiently in both *npl3Δ* and *npl3-LSNK* cells than in wild type (Figure 3C and D). These results indicate that the RRM domains are required to support Npl3 functions in the DDR, with RRM2 playing a major role, suggesting that Npl3 regulates specific RNA molecules involved in the DDR.

The lack of Npl3 reduces Exo1 levels

Npl3 might either directly participate in resection or support DSB processing by promoting the expression of resection proteins. To discriminate between these two possibilities, we first evaluated whether Npl3 is recruited to DNA ends. Chromatin immunoprecipitation (ChIP) and real-time qPCR were performed after generation of an HO-induced DSB in G2-arrested cells expressing a fully functional Npl3-HA variant. Similar amounts of DNA at 0.6 or 5.4 kb from the HO-cut site were recovered in immunoprecipitates from cells expressing either the Npl3-HA variant or untagged Npl3 both before and after DSB formation (Supplementary Figure S4). This suggests that Npl3 is not bound/recruited to DSB ends and thus does not directly participate in resection.

Generation of ssDNA at DSBs is promoted by several proteins, which control either initiation (Mre11, Rad50, Xrs2 and Sae2) or extension (Dna2, Sgs1 and Exo1) of resection (3,4). To assess whether Npl3 supports DSB processing by promoting the expression of resection factors, we measured the amount of the above proteins by western blot of protein extracts from wild type and *npl3Δ* cells ex-

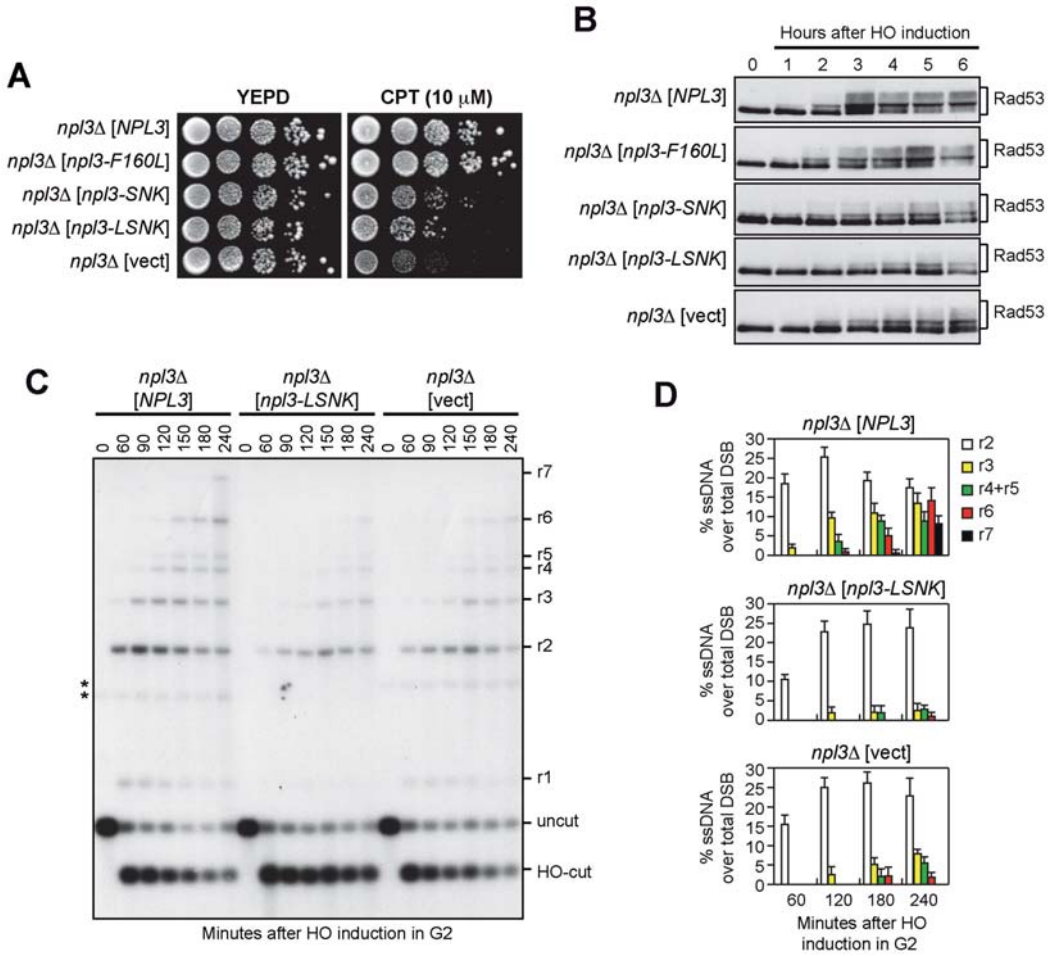

Figure 3. The Npl3 RNA binding domains are required for checkpoint and resection. (**A**–**D**) Exponentially growing cell cultures of a *npl3Δ* strain transformed with an empty centromeric vector (vect) or with the same vector carrying either the wild type *NPL3* gene or the indicated *npl3* mutant alleles were either spotted out onto YEPD plates with or without CPT (A), or transferred to YEPRG to follow Rad53 phosphorylation by western blot (B), or arrested in G2 and transferred to YEPRG (time zero) in the presence of nocodazole to monitor DSB resection as described in Figure 2C (C). *indicates cross hybridization signals likely due to the presence of the plasmids. (D) Resection products in (C) were analyzed by densitometry. The mean values are represented with error bars denoting SD ($n = 3$).

pressing fully functional tagged versions of these proteins and treated with galactose to induce the HO cut. Similar amounts of Sgs1 (Figure 4A), Mre11 and Xrs2 (Supplementary Figure S5A and B) were detected in wild type and *npl3Δ* cells, indicating that Npl3 does not control the levels of these proteins. Consistent with the checkpoint defect of *npl3Δ* cells, Xrs2 and Sgs1, which are known to undergo DNA damage-induced phosphorylation (39,42), were less phosphorylated in *npl3Δ* cells compared to wild type (Figure 4A and Supplementary Figure S5B). The amount of Dna2 (Figure 4B), Rad50 and Sae2 (Supplementary Figure S5C and D) was higher in *npl3Δ* cells than in wild type. However, it is unlikely that these effects can account for the resection defect of *npl3Δ* cells. In fact, overexpression of neither *SAE2* nor *DNA2* affects ssDNA generation at DSB ends in wild type cells (43,44). Furthermore, Rad50 forms the MRX complex together with Mre11 and Xrs2, and Mre11 was found to be limiting for the recruitment of the MRX complex to DSBs (45), suggesting that high Rad50 levels should not affect DSB resection because they do not increase MRX recruitment to DSBs.

Interestingly, the amount of Exo1 was strongly reduced in *npl3Δ* cells compared to wild type both in raffinose and after galactose addition (Figure 4C). As Exo1 levels were not affected by treatment with the proteasome inhibitor MG132 of either wild type or *npl3Δ* cells exponentially

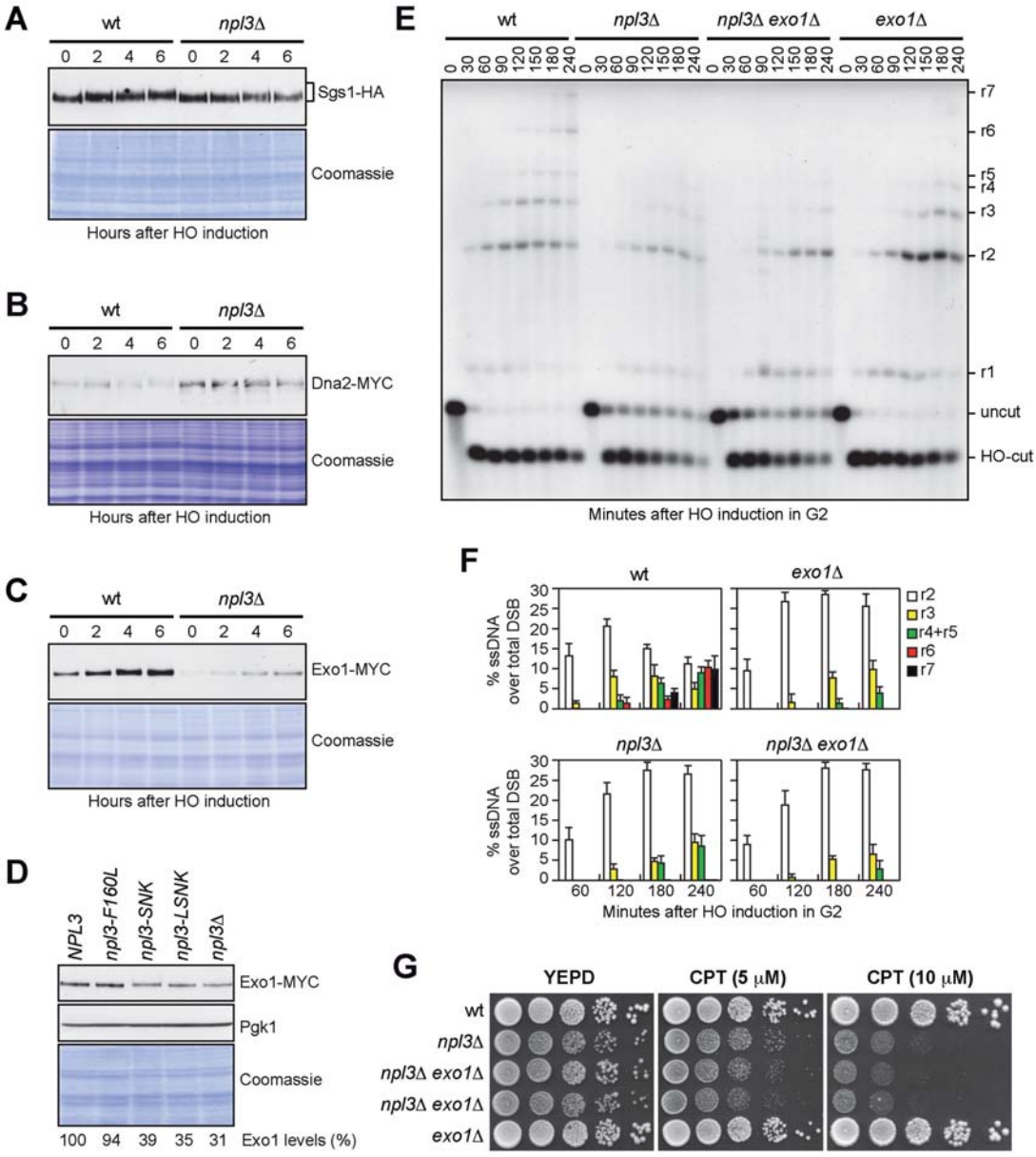

Figure 4. *NPL3* and *EXO1* belong to the same resection pathway. (**A**–**C**) Exponentially growing YEPR cell cultures of strains expressing the indicated tagged proteins were transferred to YEPRG (time zero). The same amounts of protein extracts were separated on SDS-PAGE and either subjected to western blot with antibodies specific for the indicated tags or stained with Coomassie as a loading control. (**D**) The same amounts of protein extracts prepared from exponentially growing YEPD cultures of strains as in Figure 3, all expressing the Exo1-MYC tagged protein, were either stained with Coomassie or subjected to western blot with anti-MYC and anti-Pgk1 (loading control) antibodies. The relative intensity of the Exo1-MYC signal compared to wild type (set to 100%) was estimated after normalization to the Pgk1 band. (**E** and **F**) G2-arrested cell cultures of the indicated strains were transferred to YEPRG (time zero) in the presence of nocodazole. (E) DSB resection as described in Figure 2C. (F) Resection products in (E) were analyzed by densitometry. The mean values are represented with error bars denoting SD ($n = 3$). (**G**) Exponentially growing cell cultures of the indicated strains were spotted out onto YEPD plates with or without CPT.

growing in glucose (Supplementary Figure S6), altogether these data indicate that Npl3 promotes Exo1 production independently of both the DNA damage and the carbon source.

We investigated whether the integrity of the Npl3 RRM motifs is important to regulate Exo1 levels by evaluating the amount of MYC-tagged Exo1 in cells expressing RRM1 and/or RRM2 defective Npl3 variants. The amount of Exo1, quantified using Pgk1 as a normalization control, was reduced of ∼70% in YEPD exponentially growing *npl3Δ* cells compared to wild type (Figure 4D). Npl3 interaction with RNA is important to regulate Exo1 levels, as we detected a similar reduction in *npl3-LSNK* and *npl3-SNK* mutant cells, although inactivation of only RRM1 did not affect Exo1 amount (Figure 4D).

NPL3 and *EXO1* belong to the same epistasis group for resection

As Exo1 is required for extensive resection of DNA ends (46,47), the low Exo1 levels in *npl3Δ* cells could be the cause of the resection defect of these cells. If this were the case, *npl3Δ* and *exo1Δ* cells should show a similar resection defect, and the lack of Exo1 should not increase the resection defect of *npl3Δ* cells. When we monitored ssDNA generation at the HO-induced DSB, both *exo1Δ* and *npl3Δ* single mutant cells efficiently initiated resection, but were impaired in the generation of the r3-r7 ssDNA products, and a similar defect in long-range resection was detectable in *npl3Δ exo1Δ* double mutant cells (Figure 4E). Although the HO-cut is induced more efficiently in *exo1Δ* cells (98%) than in both *npl3Δ* and *npl3Δ exo1Δ* cells (83% and 79%, respectively), a quantitative analysis of the resection products normalized to the cleavage efficiency confirmed that the resection kinetics were similar in these three mutant strains (Figure 4F).

The lack of Exo1 exacerbates the hypersensitivity to DNA damaging agents of mutants affecting other resection pathways, such as *sae2Δ* or *sgs1Δ* (47,48). Similarly, *NPL3* deletion increased the hypersensitivity to CPT of *sae2Δ* cells (Supplementary Figure S7A). Furthermore, the *npl3Δ sgs1Δ* spores obtained by tetrad dissection of a sporulated *NPL3/npl3Δ SGS1/sgs1Δ* diploid strain generated very small colonies (Supplementary Figure S7B), suggesting that Npl3 and Sgs1 participate in different pathways to support cell viability. Conversely, *EXO1* deletion neither increased the growth defect nor the hypersensitivity to CPT of *npl3Δ* cells (Figure 4G), indicating that Exo1 and Npl3 belong to the same resection pathway.

Exo1 high levels partially restore resection in *npl3Δ* cells

If the low Exo1 amount causes the resection defect in *npl3Δ* cells, increased Exo1 levels are expected to restore resection in these cells. We therefore monitored the resection kinetics in wild type and *npl3Δ* cells carrying a high copy number 2μ plasmid with the *EXO1* gene (28). The *EXO1* 2μ plasmid markedly increased the amount of long resection products in *npl3Δ* cells compared to the empty vector (Figure 5A and B). In particular, *npl3Δ* cells with the empty vector were specifically impaired in the generation of resection fragments longer then 3.5 kb, while these longer ssDNA fragments appeared in *npl3Δ* cells carrying the *EXO1* 2μ plasmid. This indicates that Npl3 promotes the generation of long ssDNA tails by positively regulating Exo1 levels.

To verify that the *EXO1* 2μ plasmid increased Exo1 amount in the absence of Npl3, a 2μ plasmid either empty or carrying the *EXO1-MYC* allele was transformed into wild type and *npl3Δ* cells expressing the Exo1-Myc variant from the *EXO1* genomic locus. Although the Exo1 levels were increased by the *EXO1-MYC* 2μ plasmid in both wild type and *npl3Δ* cells, some fast-migrating Exo1 forms appeared specifically in *npl3Δ* cells (Figure 5C), suggesting that overproduced Exo1 may be unstable in the absence of Npl3. This might explain why the *EXO1-MYC* 2μ plasmid only partially restores resection in *npl3Δ* cells (Figure 5A and B).

Interestingly, the *EXO1* 2μ plasmid partially suppressed the hypersensitivity to CPT of *npl3Δ* cells (Figure 5D), indicating that the hypersensitivity of cells lacking Npl3 is at least partially due to the resection defect. Conversely, this plasmid did not suppress the hypersensitivity to MMS of *npl3Δ* cells (Figure 5D), nor the elevated levels of spontaneous recombination caused by the Npl3 lack (Supplementary Figure S8). To measure mitotic recombination frequency, we used strains carrying the *his3-513::TRP1::his3-537* heteroallelic duplication on chromosome XV (49) and transformed with either the *EXO1* 2μ plasmid or the empty vector. As expected (20), *NPL3* deletion increased 12.8-fold the recombination frequency at the *HIS3* locus compared to wild type cells (Supplementary Figure S8). The *EXO1* 2μ plasmid did not reduce, but rather slightly increased the recombination frequency in both wild type and *npl3Δ* cells (Supplementary Figure S8), indicating that the high recombination frequency in *npl3Δ* cells is not due to the low amount of Exo1.

The *EXO1* 2μ plasmid was also unable to restore the DSB-induced checkpoint in *npl3Δ* cells. In fact, HO-induced *npl3Δ* cells carrying either the empty vector or the *EXO1* 2μ plasmid showed similar defective Rad53 phosphorylation compared to wild type cells (Figure 5E and Supplementary Figure S9), indicating that the checkpoint defect of *npl3Δ* cells cannot be ascribed only to the resection defect. This result, together with the finding that the lack of Exo1 only very slightly affects the HO-induced Rad53 phosphorylation despite the resection defect (35,50), suggests that Npl3 might control the levels of other checkpoint proteins. However, we detected similar amounts of the three RPA subunits Rfa1, Rfa2 and Rfa3 in wild type and *npl3Δ* cells (Supplementary Figure S10A–C). Furthermore, the abundance of the checkpoint proteins Tel1, Ddc2, Rad53, and Rad9 was unaffected by the absence of Npl3 (Supplementary Figure S10D-F). Conversely, the amount of Mec1 was slightly lower in *npl3Δ* cells than in wild type (Supplementary Figure S10E). However, a Mec1-dependent checkpoint is strongly activated in *npl3Δ* cells treated with phleomycin (Figure 1G), suggesting that the slightly reduced amount of Mec1 detected in *npl3Δ* cells does not likely account for the checkpoint defect of the same cells. Altogether these results indicate that Npl3 plays two functions in the DDR: it promotes DSB resection by regu-

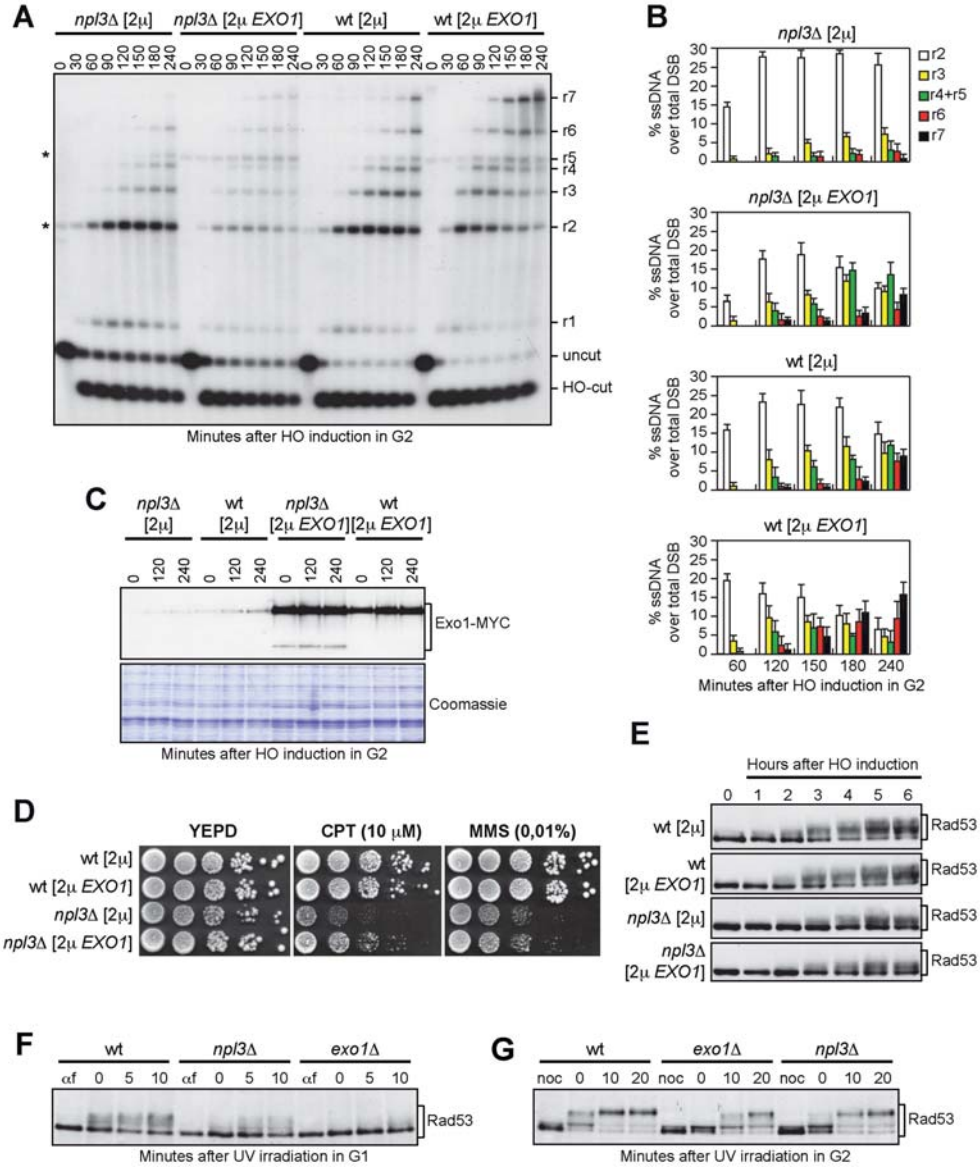

Figure 5. *EXO1* overexpression partially suppresses both the resection defect and the hypersensitivity to CPT of *npl3Δ* cells. (**A** and **B**) G2-arrested YEPR cell cultures of wild type and *npl3Δ* strains, both transformed with a 2μ plasmid either carrying the *EXO1* gene or empty (2μ), were transferred to YEPRG (time zero) in the presence of nocodazole. (A) DSB resection as described in Figure 2C. *indicates cross hybridization signals that partially overlap the r2 or r5 bands, and are due to the presence of the 2μ plasmid. (B) Resection products in (A) were analyzed by densitometry. The mean values are represented with error bars denoting SD ($n = 3$). (**C**) G2-arrested cell cultures of wild type and *npl3Δ* strains, both expressing the Exo1-MYC tagged protein from the *EXO1* locus and transformed with a 2μ plasmid either carrying the *EXO1-MYC* gene or empty (2μ), were transferred to YEPRG (time zero) in the presence of nocodazole. The same amounts of protein extracts were either subjected to western blot with anti-MYC antibodies or stained with Coomassie as a loading control. (**D** and **E**) Exponentially growing cell cultures of the strains described in (A and B) were either spotted out onto YEPD plates with or without CPT or MMS (D), or transferred to YEPRG (time zero) to analyze Rad53 phosphorylation by western blot with anti-Rad53 antibodies (E). (**F**) YEPD G1-arrested cell cultures (αf) of the indicated strains were UV irradiated (75 J/m^2) (time zero) and held in G1 in the presence of α-factor. Protein extracts were subjected to western blot with anti-Rad53 antibodies. (**G**) YEPD G2-arrested cell cultures (noc) of the strains in (F) were UV irradiated (75 J/m^2) (time zero) and held in G2 in the presence of nocodazole. Protein extracts were analyzed by western blot with anti-Rad53 antibodies.

lating Exo1 levels and it contributes to checkpoint activation by regulating some still unknown targets.

Npl3 and Exo1 are required for checkpoint activation after UV irradiation

If the Npl3-mediated control of Exo1 protein levels is biologically relevant, we expect *exo1Δ* and *npl3Δ* cells to show some common phenotypes. Exo1 is required to activate the checkpoint after UV treatment in non-cycling cells by promoting the generation of large ssDNA gaps during nucleotide excision repair (NER) processing (51). We then asked whether *npl3Δ* cells fail to activate the UV-induced checkpoint in G1- and G2-arrested cells, similarly to *exo1Δ* cells. Wild type, *npl3Δ* and *exo1Δ* cells were arrested either in G1 with α-factor or in G2 with nocodazole, UV irradiated, and transferred in fresh medium containing α-factor or nocodazole, respectively, to maintain the cell cycle arrests, as confirmed by FACS analyses (Supplementary Figure S11). As expected (51), Rad53 hyperphosphorylated forms appeared immediately after UV irradiation in wild type cells arrested either in G1 (Figure 5F) or in G2 (Figure 5G), while they were strongly reduced in similarly treated *exo1Δ* cells (Figure 5F and G). Also the lack of Npl3 impaired Rad53 phosphorylation in both G1 (Figure 5F) and G2 (Figure 5G), although to a lesser extent than the absence of Exo1 (Figure 5F and G), possibly because Exo1 is not totally absent in *npl3Δ* cells (Figure 4C and D). Thus, similarly to Exo1, Npl3 is required for checkpoint activation after UV irradiation in G1 and in G2. As Npl3 is not required *per se* to activate the checkpoint, at least in G2-arrested cells (Figure 1G), these results suggest that the low Exo1 levels in *npl3Δ* cells are not sufficient to efficiently process the UV lesions and generate enough ssDNA to activate the checkpoint in non-cycling cells.

Abnormal *EXO1* RNA species are produced in the absence of Npl3

Genome-wide analyses have shown that the absence of Npl3 results in either down- or up-regulation of many protein-coding genes (20,23,52). These analyses did not show significant differences in *EXO1* expression in *npl3Δ* versus wild type cells, suggesting that Npl3 controls the abundance of the Exo1 protein by acting at post-transcriptional level. To verify this possibility, we first employed quantitative reverse transcriptase PCR (qRT-PCR) to measure the amount of *EXO1* RNA either in the presence or in the absence of Npl3. Total RNA was extracted from wild type, *npl3Δ* and *exo1Δ* cells exponentially growing in YEPD and subjected to reverse transcription followed by quantitative real-time PCR with primer pairs located either inside the *EXO1* coding region (PP1 in Figure 6A) or the *ALG9* control gene. The amount of *EXO1* RNA was not diminished in the absence of Npl3 (Figure 6B). Rather, we found a modest increase of *EXO1* RNA levels in *npl3Δ* cells compared to wild type (Figure 6B). The levels of the Exo1 protein (Figure 4C and D) were monitored by using a tagged version of the protein generated by inserting a 18 MYC epitopes coding sequence just before the *EXO1* stop codon. Similarly to *EXO1* RNA, the *EXO1-MYC* RNA was slightly more abundant in *npl3Δ* cells than in wild type (Figure 6B), indicating that neither Npl3 nor the insertion of the MYC coding sequence into the *EXO1* gene affects *EXO1* transcription.

If Npl3 promoted *EXO1* pre-mRNA processing, *npl3Δ* cells should accumulate aberrant RNA molecules. Thus, the same RNA extracts were analyzed by northern blot with a 1437 nt DNA probe complementary to the *EXO1* coding sequence (Figure 6A). The probe was specific for the *EXO1* RNA species, as no signal was detected in RNA prepared from *exo1Δ* cells (Figure 6C). In wild type RNA extracts this probe revealed a single band that migrated between the two ribosomal RNA (rRNA) species 25S (3392 nt) and 18S (1798 nt), as expected for the *EXO1* RNA, whose length should be approximately 2400 nt, considering that the average *S. cerevisiae* mRNA consists of the protein coding sequence (2109 nt for *EXO1*) plus 260 nt of 5′ and 3′ untranslated sequences (53). The same probe detected at least 3 additional longer bands in the *npl3Δ* RNA preparation (Figure 6C), indicating that the absence of Npl3 leads to the generation of longer than normal *EXO1* RNA molecules. Similarly, a single *EXO1* RNA species migrating just below the 3392 nt-long 25S rRNA was detected in cells carrying the *EXO1-MYC* construct, while at least an additional longer band was present in RNA extracts from *npl3Δ EXO1-MYC* cells (Figure 6D). Furthermore, longer than normal *EXO1* RNA molecules were produced also in *npl3-LSNK* cells, where both Npl3 RRM domains were inactivated (Figure 6E). Thus, extended *EXO1* RNA species are produced in the absence of Npl3 or of its RNA-binding capacity, suggesting that Npl3 might regulate initiation, termination or processing of the *EXO1* transcript.

In order to verify whether the abnormal *EXO1* transcripts in *npl3Δ* cells are extended at the 5′ end, we performed 5′ rapid amplification of cDNA ends (5′-RACE) on wild type and *npl3Δ* RNA extracts that were subjected to reverse transcription with an *EXO1* specific primer. A poly(A) tail was added to the resulting cDNA, which was then used as a template for two subsequent PCR reactions with primers annealing to the appended tail and to the *EXO1* coding sequence. A PCR with primers located at the 5′ tail and 248 bp downstream the *EXO1* initiation codon revealed a ∼400 bp abundant product and two weak smaller products in wild type extracts, while a single slightly bigger band was detected in *npl3Δ* (Figure 6F). Although this result suggests that Npl3 influences the use of different transcription start sites in *EXO1* promoter, the small difference in length at the 5′ of the *EXO1* transcripts does not likely account for the extended RNA species observed by northern blot in *npl3Δ* cells (Figure 6C and E).

We then evaluated whether these transcripts were extended at the 3′ end, as Npl3 was recently found to prevent transcriptional readthrough of both protein-coding and non-coding genes (23). We therefore performed qRT-PCR analyses with different primer pairs located either internally to the *EXO1* coding sequence (PP1 and PP2), or 100, 300, 850, 1000 bp (PP3–PP6, respectively) downstream to the stop codon (Figure 6A). The RNA levels estimated with the different primer pairs were normalized with respect to the RNA levels evaluated with the PP1 primer pair, which were set to 1.0 for each strain (Figure 6G). The RNA levels estimated with the primer pair located immediately be-

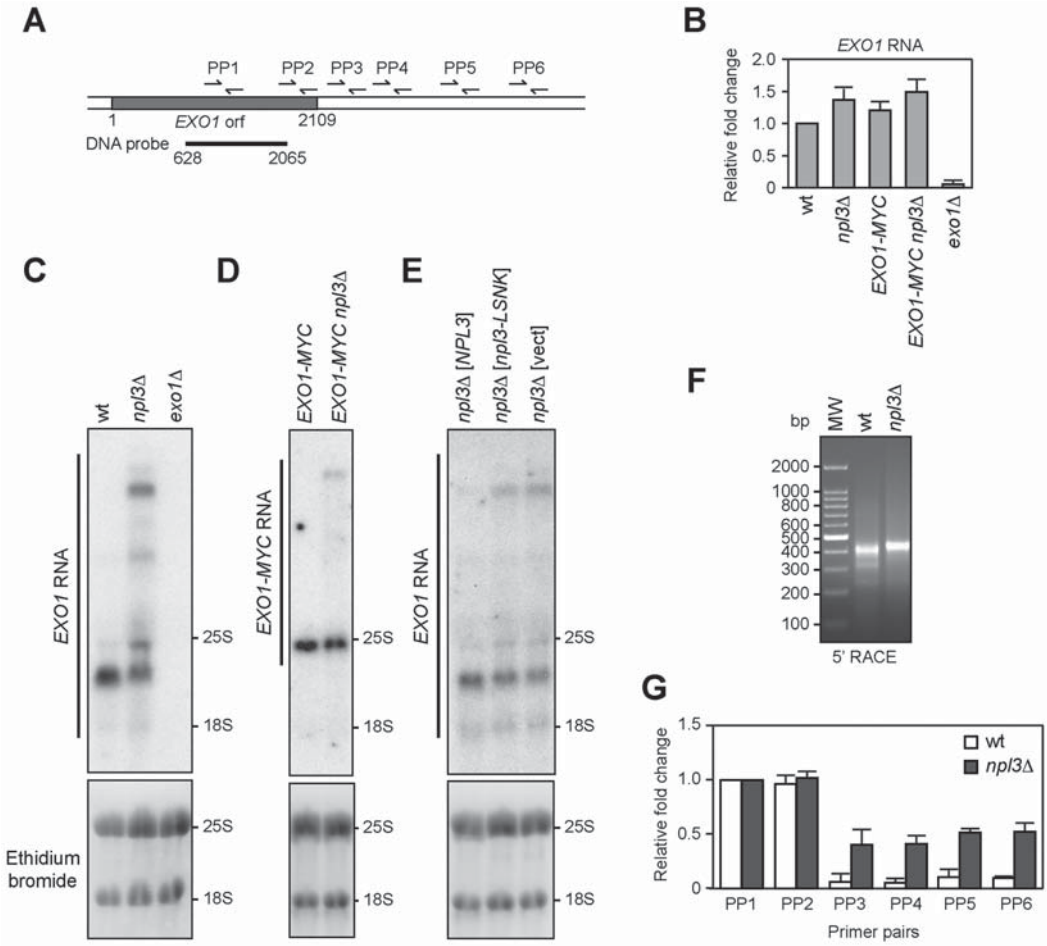

Figure 6. *EXO1* RNA in the absence of Npl3. (**A**) Schematic representation of the *EXO1* locus. Primer pairs (PP1-PP6) used for qRT-PCR are indicated by arrows. A bar indicates the 1437 bp-DNA probe internal to the *EXO1* coding sequence (+628 to + 2065 from the ATG initiation codon) used for northern blot. (**B**) Total RNA was extracted from exponentially growing YEPD cell cultures of the indicated strains and subjected to quantitative reverse transcriptase PCR (qRT-PCR) with primer pairs located into the *EXO1* (PP1 in (A)) and *ALG9* coding sequences. The *EXO1* RNA levels relative to wild type (set to 1.0) were calculated using ΔΔCt method after normalization to the *ALG9* RNA levels for each sample. The mean values are represented with error bars denoting SD ($n = 5$). (**C**–**E**) Total RNA extracted from the indicated cell cultures was subjected to northern blot and hybridized with the probe as in (A). The agarose gels were stained with ethidium bromide to detect 18S and 25S rRNAs (bottom). (**F**) Total RNA extracted from wild type and *npl3Δ* cells was subjected to 5′ RACE to visualize the *EXO1* 5′ partial cDNA ends. After reverse transcription with a *EXO1* specific primer and poly(A) tailing, two subsequent PCR reactions were performed with primers annealing to the appended tail and to the *EXO1* coding sequence 718 and 248 bp downstream the *EXO1* initiation codon. The final PCR products were separated on a 1.5% agarose gel and visualized with ethidium bromide. (**G**) Total RNA as in (F) was subjected to qRT-PCR with primer pairs depicted in (A), or located in the *ALG9* coding sequence. The amount of products obtained with different *EXO1* primer pairs was normalized to the *ALG9* product using ΔΔCt method. Then, the normalized RNA levels estimated with the different primer pairs in the *EXO1* locus were normalized to the RNA levels evaluated with the PP1 primer pair and set to 1.0 for each strain. The mean values are represented with error bars denoting SD ($n = 4$).

fore the stop codon (PP2) were almost identical to those evaluated with the primer pair internal to the *EXO1* coding sequence (PP1) in both wild type and *npl3Δ* extracts (Figure 6G). Strikingly, only *npl3Δ* extracts generated products with the primer pairs located downstream to the stop codon (PP3–PP6) (Figure 6G), although the amount of these products was lower (almost 40%) than that of the products obtained with primer pairs internal to the *EXO1* coding sequence (Figure 6G). These results indicate that a substantial fraction of *EXO1* RNA is not properly terminated in the absence of Npl3, thus generating RNA molecules with long 3′ tails that extend at least 1000 bp downstream to the *EXO1* stop codon.

Rrp6 controls the levels of the *EXO1* RNA

It is known that 3′-extended RNAs might be unstable and targeted to degradation by the RNA decay systems. In particular, defects in 3′-end processing result in nuclear retention and degradation of faulty transcripts mainly by the nuclear exosome (14). To test whether the nuclear exosome degrades the extended *EXO1* RNA molecules produced in the absence of Npl3, we checked if these abnormal *EXO1* RNAs further accumulate in *npl3Δ* cells lacking the exosome catalytic subunit Rrp6, whose lack was reported to impair viability of *npl3Δ* cells (54). In our genetic background, *npl3Δ rrp6Δ* spores generated by sporulation and tetrad dissection of a *NPL3/npl3Δ RRP6/rrp6Δ* diploid gave rise to very small colonies, which could be further propagated in YEPD, despite their growth defect (Figure 7A and E). We then subjected to both qRT-PCR and northern blot analysis the *EXO1* RNAs derived from exponentially growing wild type, *npl3Δ*, *rrp6Δ* and *npl3Δ rrp6Δ* cells. Both analyses revealed higher levels of *EXO1* RNA in *npl3Δ rrp6Δ* cells than in *npl3Δ* and *rrp6Δ* single mutants (Figure 7B and C). The intensity of the bands detected by the *EXO1* probe in the northern blot, and in particular that of the slowest migrating band, was higher in *npl3Δ rrp6Δ* RNA extracts than in *npl3Δ* (Figure 7C), suggesting that Rrp6 partially removes abnormal RNA intermediates that accumulate in the absence of Npl3.

As the amount of the 2400 nt-long *EXO1* RNA species was also higher in *npl3Δ rrp6Δ* cells compared to *npl3Δ* cells (Figure 7C), we asked whether the absence of Rrp6 also increased the levels of Exo1 protein in cells lacking Npl3. Indeed, the amount of the Exo1-MYC tagged variant was slightly higher in exponentially growing *npl3Δ rrp6Δ* cells than in *npl3Δ* cells (Figure 7D). This suggests that, in the presence of improperly processed transcripts, the exosome targets not only the faulty, but also some functional *EXO1* RNA molecules. Interestingly, although *npl3Δ rrp6Δ* cells grew poorly on YEPD plates (Figure 7A and E), they formed colonies in the presence of CPT more efficiently than *npl3Δ* cells (Figure 7E), similarly to what we observed with the overexpression of the *EXO1* gene (Figure 5D). Taken together, these results indicate that Npl3 promotes proper maturation of the *EXO1* RNA, thus preventing its degradation by the nuclear exosome.

DISCUSSION

Resection of DSB ends is a two-step process, which is initiated by MRX and Sae2 that induce an endonucleolytic cleavage of the 5′-terminated DNA strands. This cleavage promotes the access of the Exo1 and Dna2 nucleases, which allow the generation of long ssDNA tails (reviewed in (3,4)). Here, we show that the lack of the RBP Npl3 impairs the generation of long stretches of ssDNA at DSB ends and decreases the amount of the exonuclease Exo1. Furthermore, the lack of Exo1 does not exacerbate the resection defect of *npl3Δ* cells, while high Exo1 levels partially restore resection in these cells, indicating that Npl3 supports long-range resection by ensuring the production of a sufficient amount of Exo1.

We also found that Npl3 is required to activate a Mec1-dependent checkpoint in response to different kinds of DNA damage, but it is dispensable for checkpoint activation after phleomycin treatment in G2 (Figures 1 and 5). As Exo1 is required to generate long stretches of ssDNA (35,51,55), which are the signals that activate Mec1 at least in response to both DSBs and UV-induced DNA lesions (10,34,35,55,56), the reduced Exo1 amount in *npl3Δ* cells could account for the checkpoint defect of the same cells. However, *EXO1* overexpression does not alleviate the checkpoint defect of *npl3Δ* cells experiencing a single DSB. This result, together with the finding that the lack of Exo1 causes a very mild, if any, checkpoint defect in response to a single DSB (35,50), suggests that Npl3 regulates the functions of other proteins involved in checkpoint activation besides Exo1. Although genome-wide transcription analyses showed that most checkpoint genes are not significantly downregulated in the absence of Npl3 (20), a very mild decrease of *MEC1* gene expression was reported in *npl3Δ* cells (23), which also show a slight reduction in Mec1 protein abundance (Supplementary Figure S10E). Furthermore, *npl3Δ* cells show increased amounts of *SAE2* mRNA (23) that correlate with increased levels of the Sae2 protein (Supplementary Figure S5D). As high Sae2 levels have been shown to counteract Mec1-dependent checkpoint activation (50), the checkpoint defect of *npl3Δ* cells might be due to the high Sae2 levels. Thus, we speculate that the checkpoint defect of *npl3Δ* cells may result both from a defect in ssDNA generation due to low Exo1 levels and from a mild deregulation of factors involved in checkpoint signaling, such as Sae2 and Mec1. These Mec1 and Sae2 misregulations are likely not sufficient to impair checkpoint activation by themselves, as the checkpoint is strongly activated in *npl3Δ* cells treated with phleomycin. However, they might impair Mec1 recruitment/activation in response to DNA lesions that require extensive nucleolytic processing to be detected by Mec1, such as DSBs or UV-induced DNA lesions.

The idea that Npl3 regulates other DDR factors besides Exo1 is also supported by the observation that the lack of Npl3 causes hypersensitivity to DSB-inducing agents, whereas *EXO1* deletion does not (47,55). Accordingly, *EXO1* overexpression partially rescues the hypersensitivity to CPT of *npl3Δ* cells, while it does not affect the hypersensitivity of the same cells to MMS. This result also suggests that Exo1 is important to repair the damage induced by CPT, while other defects can contribute to the hy-

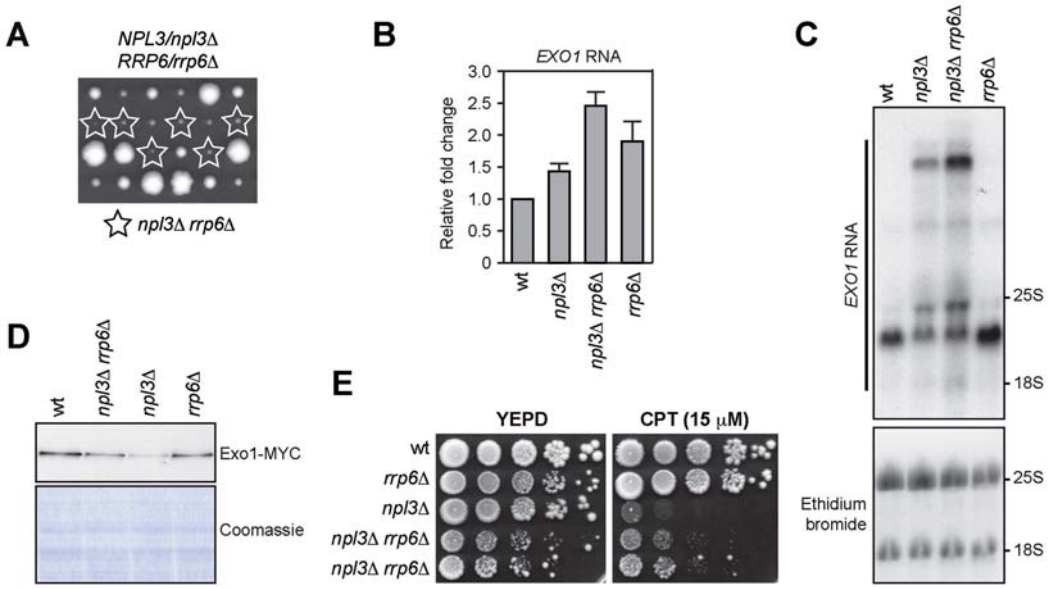

Figure 7. Rrp6 limits the accumulation of abnormal *EXO1* RNAs in the absence of Npl3. (**A**) Meiotic tetrads from diploid cells with the indicated genotype were dissected on YEPD plates that were incubated at 30°C for 3 days, followed by spore genotyping. (**B**, **C**) Total RNA was extracted from exponentially growing YEPD cultures of the indicated strains and subjected to both qRT-PCR as in Figure 6B and northern blot as in Figure 6C–E. (**D**) The same amounts of protein extracts prepared from exponentially growing cell cultures with the indicated genotypes and expressing the Exo1-MYC tagged protein were either stained with Coomassie or subjected to western blot with anti-MYC antibodies. (**E**) Exponentially growing cell cultures of the indicated strains were spotted out onto YEPD plates with or without CPT.

persensitivity to MMS of *npl3Δ* cells. One of these defects might be the replication stress caused by the accumulation of transcription-dependent DNA:RNA hybrids in the absence of Npl3. In fact, overproduction of RNaseH1, which removes these hybrids *in vivo* (20,27), suppresses the hypersensitivity to MMS (Figure 2A) and reduces the high levels of spontaneous mitotic recombination caused by the lack of Npl3 (20). On the contrary, *EXO1* overexpression does not reduce the recombination frequency in *npl3Δ* cells (Supplementary Figure S8).

How does Npl3 control the abundance of the Exo1 protein? As the low Exo1 amount in *npl3Δ* cells does not correlate with a decrease in total *EXO1* RNA levels (Figure 6) (20,23), we exclude that Npl3 promotes *EXO1* transcription. Rather, the extended *EXO1* RNA species detected in the absence of Npl3 may be due to termination defects and transcription readthrough. In fact, defects in transcription termination were seen for approximately 30% of protein-coding genes in *npl3Δ* cells (23), and we found that a region 1000 bp downstream to the *EXO1* stop codon was transcribed in *npl3Δ* cells but not in wild type, while we did not find a significant extension of the *EXO1* RNA 5′ end in the absence of Npl3. Furthermore, Npl3 was found to be co-transcriptionally recruited to DNA at highly transcribed genes (among which *EXO1*), where it distributes in a gradient that increases toward the 3′ end of the coding region (20), and to bind both the 5′ (23,52) and the 3′ ends of mRNAs (52). Npl3 inactivation is also known to impair mRNA export and to cause the accumulation of transcripts in the nucleus (57). Taken together, these results suggest that, in the absence of Npl3, some *EXO1* nascent transcripts are not appropriately packaged, thus possibly interfering with the transcription termination process and forming abnormal *EXO1* RNA species that are not exported to the cytoplasm and/or not efficiently translated.

These abnormal *EXO1* RNAs are likely degraded, at least in part, by the nuclear exosome, as the lack of Rrp6 in *npl3Δ* cells results in a further accumulation of extended *EXO1* RNA species. Accordingly, the exosome was found to degrade transcripts that are not co-transcriptionally packaged because of mutations in the THO complex, which, similarly to Npl3, is required for pre-mRNA processing and export (58). The lack of Rrp6 slightly increases Exo1 protein levels in *npl3Δ* cells, suggesting that in the presence of faulty transcripts Rrp6 can sequester and/or degrade also functional RNAs. Rrp6 was found to prevent chromatin release of aberrant transcripts when co-transcriptional pre-mRNA processing fails, thus eventually providing these transcripts with additional time to complete their maturation (59,60). Furthermore, Rrp6 was recently reported to participate in mRNA nuclear retention caused by Npl3 inactivation. In fact, while *npl3* temperature-sensitive mutant cells accumulate mRNAs in the nucleus at the restrictive temperature, mRNAs are partially released in the cytoplasm in *npl3 rrp6* double mutant cells (61). Interestingly, Rrp6 deletion also partially suppresses the temperature sensitivity of these *npl3*

mutant cells, suggesting that part of the improperly packaged mRNAs produced in the absence of Npl3 may be functional, although incompetent for export (61).

Exo1 is an evolutionarily conserved processive exonuclease that can degrade several kilobases of DNA (7,8) and is implicated in a variety of DNA metabolic processes including DNA repair as well as processing of both stalled replication forks and uncapped telomeres (2,5,62–64). Exo1 action is modulated by both positive and negative regulators, which control Exo1 access to DNA and limit excessive DNA degradation (3,4,6–8). Exo1 expression is also induced during yeast meiosis to promote meiotic DSB processing and crossing over (65). In mammals, splicing of *EXO1* transcripts is facilitated after DNA damage by a splicing complex that contains the DDR protein BRCA1 (66). The Npl3-mediated regulation of Exo1 amount that we show here represents another level of control of Exo1 activity that guarantees the availability of suitable amounts of Exo1 to respond to DNA damage and maintain genome integrity.

SUPPLEMENTARY DATA

Supplementary Data are available at NAR Online.

ACKNOWLEDGEMENTS

We thank J. Haber for yeast strains; A. Aguilera, E. Alani and J. Lee-Soety for plasmids and N. Lowndes and B. Stillman for antibodies. We are particularly grateful to M. Vai and I. Orlandi for technical advises, and to G. Lucchini for useful suggestions and critical reading of the manuscript.

FUNDING

Associazione Italiana per la Ricerca sul Cancro (AIRC) [IG15210]; Progetti di Ricerca di Interesse Nazionale (PRIN) 2015 (to M.P.L.). Funding for open access charge: Associazione Italiana per la Ricerca sul Cancro (AIRC) [IG15210 to M.P.L].
Conflict of interest statement. None declared.

REFERENCES

1. Ciccia,A. and Elledge,S.J. (2010) The DNA damage response: making it safe to play with knives. *Mol. Cell*, **40**, 179–204.
2. Symington,L.S., Rothstein,R. and Lisby,M. (2014) Mechanisms and regulation of mitotic recombination in Saccharomyces cerevisiae. *Genetics*, **198**, 795–835.
3. Daley,J.M., Niu,H., Miller,A.S. and Sung,P. (2015) Biochemical mechanism of DSB end resection and its regulation. *DNA Repair (Amst.)*, **32**, 66–74.
4. Villa,M., Cassani,C., Gobbini,E., Bonetti,D. and Longhese,M.P. (2016) Coupling end resection with the checkpoint response at DNA double-strand breaks. *Cell. Mol. Life Sci.*, **73**, 3655–3663.
5. Ferrari,M., Dibitetto,D., De Gregorio,G., Eapen,V.V., Rawal,C.C., Lazzaro,F., Tsabar,M., Marini,F., Haber,J.E. and Pellicioli,A. (2015) Functional interplay between the 53BP1-ortholog Rad9 and the Mre11 complex regulates resection, end-tethering and repair of a double-strand break. *PLoS Genet.*, **11**, e1004928.
6. Morin,I., Ngo,H.P., Greenall,A., Zubko,M.K., Morrice,N. and Lydall,D. (2008) Checkpoint-dependent phosphorylation of Exo1 modulates the DNA damage response. *EMBO J.*, **27**, 2400–2410.
7. Cannavo,E., Cejka,P. and Kowalczykowski,S.C. (2013) Relationship of DNA degradation by Saccharomyces cerevisiae Exonuclease 1 and its stimulation by RPA and Mre11-Rad50-Xrs2 to DNA end resection. *Proc. Natl. Acad. Sci. U.S.A.*, **110**, E1661–E1668.
8. Myler,L.R., Gallardo,I.F., Zhou,Y., Gong,F., Yang,S.H., Wold,M.S., Miller,K.M., Paull,T.T. and Finkelstein,I.J. (2016) Single-molecule imaging reveals the mechanism of Exo1 regulation by single-stranded DNA binding proteins. *Proc. Natl. Acad. Sci. U.S.A.*, **113**, E1170–E1179.
9. Nakada,D., Matsumoto,K. and Sugimoto,K. (2003) ATM-related Tel1 associates with double-strand breaks through an Xrs2-dependent mechanism. *Genes Dev.*, **17**, 1957–1962.
10. Zou,L. and Elledge,S.J. (2003) Sensing DNA damage through ATRIP recognition of RPA-ssDNA complexes. *Science*, **300**, 1542–1548.
11. Wickramasinghe,V.O. and Venkitaraman,A.R. (2016) RNA processing and genome stability: cause and consequence. *Mol. Cell*, **61**, 496–505.
12. Tutucci,E. and Stutz,F. (2011) Keeping mRNPs in check during assembly and nuclear export. *Nat. Rev. Mol. Cell Biol.*, **12**, 377–384.
13. Eberle,A.B. and Visa,N. (2014) Quality control of mRNP biogenesis: networking at the transcription site. *Semin. Cell Dev. Biol.*, **32**, 37–46.
14. Fox,M.J. and Mosley,A.L. (2016) Rrp6: Integrated roles in nuclear RNA metabolism and transcription termination. *Wiley Interdiscip. Rev. RNA*, **7**, 91–104.
15. García-Muse,T. and Aguilera,A. (2016) Transcription-replication conflicts: how they occur and how they are resolved. *Nat. Rev. Mol. Cell Biol.*, **17**, 553–563.
16. Janke,R., Kong,J., Braberg,H., Cantin,G., Yates,J.R., Krogan,N.J. and Heyer,W.D. (2016) Nonsense-mediated decay regulates key components of homologous recombination. *Nucleic Acids Res.*, **44**, 5218–5230.
17. Deka,P., Bucheli,M.E., Moore,C., Buratowski,S. and Varani,G. (2008) Structure of the yeast SR protein Npl3 and Interaction with mRNA 3′-end processing signals. *J. Mol. Biol.*, **375**, 136–150.
18. Dermody,J.L., Dreyfuss,J.M., Villén,J., Ogundipe,B., Gygi,S.P., Park,P.J., Ponticelli,A.S., Moore,C.L., Buratowski,S. and Bucheli,M.E. (2008) Unphosphorylated SR-like protein Npl3 stimulates RNA polymerase II elongation. *PLoS One*, **3**, e3273.
19. Lei,E.P., Krebber,H. and Silver,P.A. (2001) Messenger RNAs are recruited for nuclear export during transcription. *Genes Dev.*, **15**, 1771–1782.
20. Santos-Pereira,J.M., Herrero,A.B., García-Rubio,M.L., Marín,A., Moreno,S. and Aguilera,A. (2013) The Npl3 hnRNP prevents R-loop-mediated transcription-replication conflicts and genome instability. *Genes Dev.*, **27**, 2445–2458.
21. Bucheli,M.E., He,X., Kaplan,C.D., Moore,C.L. and Buratowski,S. (2007) Polyadenylation site choice in yeast is affected by competition between Npl3 and polyadenylation factor CFI. *RNA*, **13**, 1756–1764.
22. Wong,C.M., Tang,H.M., Kong,K.Y., Wong,G.W., Qiu,H., Jin,D.Y. and Hinnebusch,A.G. (2010) Yeast arginine methyltransferase Hmt1p regulates transcription elongation and termination by methylating Npl3p. *Nucleic Acids Res.*, **38**, 2217–2228.
23. Holmes,R.K., Tuck,A.C., Zhu,C., Dunn-Davies,H.R., Kudla,G., Clauder-Munster,S., Granneman,S., Steinmetz,L.M., Guthrie,C. and Tollervey,D. (2015) Loss of the yeast SR protein Npl3 alters gene expression due to transcription readthrough. *PLoS Genet.*, **11**, e1005735.
24. McKinney,J.S., Sethi,S., Tripp,J.D., Nguyen,T.N., Sanderson,B.A., Westmoreland,J.W., Resnick,M.A. and Lewis,L.K. (2013) A multistep genomic screen identifies new genes required for repair of DNA double-strand breaks in Saccharomyces cerevisiae. *BMC Genomics*, **14**, 251.
25. Pan,X., Ye,P., Yuan,D.S., Wang,X., Bader,J.S. and Boeke,J.D. (2006) A DNA integrity network in the yeast Saccharomyces cerevisiae. *Cell*, **124**, 1069–1081.
26. Smolka,M.B., Albuquerque,C.P., Chen,S.H. and Zhou,H. (2007) Proteome-wide identification of in vivo targets of DNA damage checkpoint kinases. *Proc. Natl. Acad. Sci. U.S.A.*, **104**, 10364–10369.
27. Castellano-Pozo,M., García-Muse,T. and Aguilera,A. (2012) R-loops cause replication impairment and genome instability during meiosis. *EMBO Rep.*, **13**, 923–929.
28. Sokolsky,T. and Alani,E. (2000) EXO1 and MSH6 are high-copy suppressors of conditional mutations in the MSH2 mismatch repair gene of Saccharomyces cerevisiae. *Genetics*, **155**, 589–599.

29. Lee-Soety,J.Y., Jones,J., MacGibeny,M.A., Remaly,E.C., Daniels,L., Ito,A., Jean,J., Radecki,H. and Spencer,S. (2012) Yeast hnRNP-related proteins contribute to the maintenance of telomeres. *Biochem. Biophys. Res. Commun.*, **426**, 12–17.
30. Trovesi,C., Falcettoni,M., Lucchini,G., Clerici,M. and Longhese,M.P. (2011) Distinct Cdk1 requirements during single-strand annealing, noncrossover, and crossover recombination. *PLoS Genet.*, **7**, e1002263.
31. Gietz,R.D. and Sugino,A. (1988) New yeast-Escherichia coli shuttle vectors constructed with in vitro mutagenized yeast genes lacking six-base pair restriction sites. *Gene*, **74**, 527–534.
32. Viscardi,V., Bonetti,D., Cartagena-Lirola,H., Lucchini,G. and Longhese,M.P. (2007) MRX-dependent DNA damage response to short telomeres. *Mol. Biol. Cell*, **18**, 3047–3058.
33. Lee,S.E., Moore,J.K., Holmes,A., Umezu,K., Kolodner,R.D. and Haber,J.E. (1998) Saccharomyces Ku70, Mre11/Rad50 and RPA proteins regulate adaptation to G2/M arrest after DNA damage. *Cell*, **94**, 399–409.
34. Pellicioli,A., Lee,S.E., Lucca,C., Foiani,M. and Haber,J.E. (2001) Regulation of Saccharomyces Rad53 checkpoint kinase during adaptation from DNA damage-induced G2/M arrest. *Mol. Cell*, **7**, 293–300.
35. Mantiero,D., Clerici,M., Lucchini,G. and Longhese,M.P. (2007) Dual role for Saccharomyces cerevisiae Tel1 in the checkpoint response to double-strand breaks. *EMBO Rep.*, **8**, 380–387.
36. Paciotti,V., Clerici,M., Lucchini,G. and Longhese,M.P. (2000) The checkpoint protein Ddc2, functionally related to S. pombe Rad26, interacts with Mec1 and is regulated by Mec1-dependent phosphorylation in budding yeast. *Genes Dev.*, **14**, 2046–2059.
37. Zhao,X., Muller,E.G. and Rothstein,R. (1998) A suppressor of two essential checkpoint genes identifies a novel protein that negatively affects dNTP pools. *Mol. Cell*, **2**, 329–340.
38. Redon,C., Pilch,D.R., Rogakou,E.P., Orr,A.H., Lowndes,N.F. and Bonner,W.M. (2003) Yeast histone 2A serine 129 is essential for the efficient repair of checkpoint-blind DNA damage. *EMBO Rep*, **4**, 678–684.
39. Nakada,D., Shimomura,T., Matsumoto,K. and Sugimoto,K. (2003). The ATM-related Tel1 protein of Saccharomyces cerevisiae controls a checkpoint response following phleomycin treatment. *Nucleic Acids Res.*, **31**, 1715–1724.
40. Ohle,C., Tesorero,R., Schermann,G., Dobrev,N., Sinning,I. and Fischer,T. (2016) Transient RNA-DNA hybrids are required for efficient double-strand break repair. *Cell*, **167**, 1001–1013.
41. Li,L., Germain,D.R., Poon,H.Y., Hildebrandt,M.R., Monckton,E.A., McDonald,D., Hendzel,M.J. and Godbout,R. (2016) DEAD Box 1 facilitates removal of RNA and homologous recombination at DNA double-strand breaks. *Mol. Cell. Biol.*, **36**, 2794–2810.
42. Hegnauer,A.M., Hustedt,N., Shimada,K., Pike,B.L., Vogel,M., Amsler,P., Rubin,S.M., van Leeuwen,F., Guénolé,A., van Attikum,H. *et al.* (2012) An N-terminal acidic region of Sgs1 interacts with Rpa70 and recruits Rad53 kinase to stalled forks. *EMBO J.*, **31**, 3768–3783.
43. Clerici,M., Mantiero,D., Lucchini,G. and Longhese,M.P. (2005) The Saccharomyces cerevisiae Sae2 protein promotes resection and bridging of double strand break ends. *J. Biol. Chem.*, **280**, 38631–38638.
44. Manfrini,N., Trovesi,C., Wery,M., Martina,M., Cesena,D., Descrimes,M., Morillon,A., d'Adda di Fagagna,F. and Longhese,M.P. (2015) RNA-processing proteins regulate Mec1/ATR activation by promoting generation of RPA-coated ssDNA. *EMBO Rep.*, **16**, 221–231.
45. Shima,H., Suzuki,M. and Shinohara,M. (2005) Isolation and characterization of novel xrs2 mutations in Saccharomyces cerevisiae. *Genetics*, **170**, 71–85.
46. Mimitou,E.P. and Symington,L.S. (2008) Sae2, Exo1 and Sgs1 collaborate in DNA double-strand break processing. *Nature*, **455**, 770–774.
47. Zhu,Z., Chung,W.H., Shim,E.Y., Lee,S.E. and Ira,G. (2008) Sgs1 helicase and two nucleases Dna2 and Exo1 resect DNA double-strand break ends. *Cell*, **134**, 981–994.
48. Gobbini,E., Villa,M., Gnugnoli,M., Menin,L., Clerici,M. and Longhese,M.P. (2015) Sae2 Function at DNA Double-Strand Breaks Is Bypassed by Dampening Tel1 or Rad53 Activity. *PLoS Genet*. **11**, e1005685.
49. Longhese,M.P., Plevani,P. and Lucchini,G. (1994) Replication factor A is required in vivo for DNA replication, repair, and recombination. *Mol Cell Biol*. **14**, 7884–7890.
50. Clerici,M., Mantiero,D., Lucchini,G. and Longhese,M.P. (2006) The Saccharomyces cerevisiae Sae2 protein negatively regulates DNA damage checkpoint signalling. *EMBO Rep.*, **7**, 212–218.
51. Giannattasio,M., Follonier,C., Tourrière,H., Puddu,F., Lazzaro,F., Pasero,P., Lopes,M., Plevani,P. and Muzi-Falconi,M. (2010) Exo1 competes with repair synthesis, converts NER intermediates to long ssDNA gaps, and promotes checkpoint activation. *Mol. Cell*, **40**, 50–62.
52. Baejen,C., Torkler,P., Gressel,S., Essig,K., Söding,J. and Cramer,P. (2014) Transcriptome maps of mRNP biogenesis factors define pre-mRNA recognition. *Mol. Cell*, **55**, 745–757.
53. Hurowitz,E.H. and Brown,P.O. (2003) Genome-wide analysis of mRNA lengths in Saccharomyces cerevisiae. *Genome Biol.*, **5**, R2.
54. Burkard,K.T. and Butler,J.S. (2000) A nuclear 3′-5′ exonuclease involved in mRNA degradation interacts with Poly(A) polymerase and the hnRNA protein Npl3p. *Mol. Cell. Biol.*, **20**, 604–616.
55. Nakada,D., Hirano,Y. and Sugimoto,K. (2004) Requirement of the Mre11 complex and exonuclease 1 for activation of the Mec1 signaling pathway. *Mol. Cell. Biol.*, **24**, 10016–10025.
56. Zierhut,C. and Diffley,J.F. (2008) Break dosage, cell cycle stage and DNA replication influence DNA double strand break response. *EMBO J.*, **27**, 1875–1885.
57. Lee,M.S., Henry,M. and Silver,P.A. (1996) A protein that shuttles between the nucleus and the cytoplasm is an important mediator of RNA export. *Genes Dev.*, **10**, 1233–1246.
58. Libri,D., Dower,K., Boulay,J., Thomsen,R., Rosbash,M. and Jensen,T.H. (2002) Interactions between mRNA export commitment, 3′-end quality control, and nuclear degradation. *Mol. Cell. Biol.*, **22**, 8254–8266.
59. Hilleren,P., McCarthy,T., Rosbash,M., Parker,R. and Jensen,T.H. (2001) Quality control of mRNA 3′-end processing is linked to the nuclear exosome. *Nature*, **413**, 538–542.
60. Kallehauge,T.B., Robert,M.C., Bertrand,E. and Jensen,T.H. (2012) Nuclear retention prevents premature cytoplasmic appearance of mRNA. *Mol. Cell*, **48**, 145–152.
61. Babour,A., Shen,Q., Dos-Santos,J., Murray,S., Gay,A., Challal,D., Fasken,M., Palancade,B., Corbett,A., Libri,D. *et al.* (2016) The Chromatin Remodeler ISW1 Is a Quality Control Factor that Surveys Nuclear mRNP Biogenesis. *Cell*, **167**, 1201–1214.
62. Tran,P.T., Erdeniz,N., Dudley,S. and Liskay,R.M. (2002) Characterization of nuclease-dependent functions of Exo1p in Saccharomyces cerevisiae. *DNA Repair (Amst)*, **1**, 895–912.
63. Cotta-Ramusino,C., Fachinetti,D., Lucca,C., Doksani,Y., Lopes,M., Sogo,J. and Foiani,M. (2005) Exo1 processes stalled replication forks and counteracts fork reversal in checkpoint-defective cells. *Mol. Cell*, **17**, 153–159.
64. Maringele,L. and Lydall,D. (2002) EXO1-dependent single-stranded DNA at telomeres activates subsets of DNA damage and spindle checkpoint pathways in budding yeast yku70Delta mutants. *Genes Dev.*, **16**, 1919–1933.
65. Tsubouchi,H. and Ogawa,H. (2000) Exo1 roles for repair of DNA double-strand breaks and meiotic crossing over in Saccharomyces cerevisiae. *Mol. Biol. Cell*, **11**, 2221–2233.
66. Savage,K.I., Gorski,J.J., Barros,E.M., Irwin,G.W., Manti,L., Powell,A.J., Pellagatti,A., Lukashchuk,N., McCance,D.J., McCluggage,W.G. *et al.* (2014) Identification of a BRCA1-mRNA splicing complex required for efficient DNA repair and maintenance of genomic stability. *Mol. Cell*, **54**, 445–459.

PLOS | GENETICS

RESEARCH ARTICLE

Sae2 Function at DNA Double-Strand Breaks Is Bypassed by Dampening Tel1 or Rad53 Activity

Elisa Gobbini☯, Matteo Villa☯, Marco Gnugnoli, Luca Menin, Michela Clerici, Maria Pia Longhese*

Dipartimento di Biotecnologie e Bioscienze, Università di Milano-Bicocca, Milano, Italy

☯ These authors contributed equally to this work.
* mariapia.longhese@unimib.it

OPEN ACCESS

Citation: Gobbini E, Villa M, Gnugnoli M, Menin L, Clerici M, Longhese MP (2015) Sae2 Function at DNA Double-Strand Breaks Is Bypassed by Dampening Tel1 or Rad53 Activity. PLoS Genet 11 (11): e1005685. doi:10.1371/journal.pgen.1005685

Editor: Sue Jinks-Robertson, Duke University, UNITED STATES

Received: June 17, 2015

Accepted: October 29, 2015

Published: November 19, 2015

Data Availability Statement: All relevant data are within the paper and its Supporting Information files.

Funding: This work was supported by grants from Associazione Italiana per la Ricerca sul Cancro (AIRC) (grant IG15210) and Cofinanziamento 2010-2011 Ministero dell'Istruzione, dell'Università e della Ricerca (MIUR)/Università di Milano-Bicocca to MPL. The funders had no role in study design, data collection and analysis, decision to publish, or preparation of the manuscript.

Competing Interests: The authors have declared that no competing interests exist.

Abstract

The MRX complex together with Sae2 initiates resection of DNA double-strand breaks (DSBs) to generate single-stranded DNA (ssDNA) that triggers homologous recombination. The absence of Sae2 not only impairs DSB resection, but also causes prolonged MRX binding at the DSBs that leads to persistent Tel1- and Rad53-dependent DNA damage checkpoint activation and cell cycle arrest. Whether this enhanced checkpoint signaling contributes to the DNA damage sensitivity and/or the resection defect of *sae2*Δ cells is not known. By performing a genetic screen, we identify *rad53* and *tel1* mutant alleles that suppress both the DNA damage hypersensitivity and the resection defect of *sae2*Δ cells through an Sgs1-Dna2-dependent mechanism. These suppression events do not involve escaping the checkpoint-mediated cell cycle arrest. Rather, defective Rad53 or Tel1 signaling bypasses Sae2 function at DSBs by decreasing the amount of Rad9 bound at DSBs. As a consequence, reduced Rad9 association to DNA ends relieves inhibition of Sgs1-Dna2 activity, which can then compensate for the lack of Sae2 in DSB resection and DNA damage resistance. We propose that persistent Tel1 and Rad53 checkpoint signaling in cells lacking Sae2 increases the association of Rad9 at DSBs, which in turn inhibits DSB resection by limiting the activity of the Sgs1-Dna2 resection machinery.

Author Summary

Genome instability is one of the most pervasive characteristics of cancer cells and can be due to DNA repair defects and failure to arrest the cell cycle. Among the many types of DNA damage, the DNA double strand break (DSB) is one of the most severe, because it can cause mutations and chromosomal rearrangements. Generation of DSBs triggers a highly conserved mechanism, known as DNA damage checkpoint, which arrests the cell cycle until DSBs are repaired. DSBs can be repaired by homologous recombination, which requires the DSB ends to be nucleolytically processed (resected) to generate single-stranded DNA. In *Saccharomyces cerevisiae*, DSB resection is initiated by the MRX

complex together with Sae2, whereas more extensive resection is catalyzed by both Exo1 and Dna2-Sgs1. The absence of Sae2 not only impairs DSB resection, but also leads to the hyperactivation of the checkpoint proteins Tel1/ATM and Rad53, leading to persistent cell cycle arrest. In this manuscript we show that persistent Tel1 and Rad53 signaling activities in *sae2*Δ cells cause DNA damage hypersensitivity and defective DSB resection by increasing the amount of Rad9 bound at the DSBs, which in turn inhibits the Sgs1-Dna2 resection machinery. As ATM inhibition has been proposed as a strategy for cancer treatment, the finding that defective Tel1 signaling activity restores DNA damage resistance in *sae2*Δ cells might have implications in cancer therapies that use ATM inhibitors for synthetic lethal approaches that are devised to kill tumor cells with defective DSB repair.

Introduction

Programmed DNA double-strand breaks (DSBs) are formed during meiotic recombination and rearrangement of the immunoglobulin genes in lymphocytes. Furthermore, potentially harmful DSBs can arise by exposure to environmental factors, such as ionizing radiations and radiomimetic chemicals, or by failures in DNA replication. DSB generation elicits a checkpoint response that depends on the mammalian protein kinases ATM and ATR, whose functional orthologs in *Saccharomyces cerevisiae* are Tel1 and Mec1, respectively [1]. Tel1/ATM is recruited to DSBs by the MRX (Mre11-Rad50-Xrs2)/MRN (Mre11-Rad50-Nbs1) complex, whereas Mec1/ATR recognizes single-stranded DNA (ssDNA) covered by Replication Protein A (RPA) [2]. Once activated, Tel1/ATM and Mec1/ATR propagate their checkpoint signals by phosphorylating the downstream checkpoint kinases Rad53 (Chk2 in mammals) and Chk1, to couple cell cycle progression with DNA repair [2].

Repair of DSBs can occur by either non-homologous end joining (NHEJ) or homologous recombination (HR). Whereas NHEJ directly joins the DNA ends, HR uses the sister chromatid or the homologous chromosome to repair DSBs. HR requires that the 5' ends of a DSB are nucleolytically processed (resected) to generate 3'-ended ssDNA that can invade an undamaged homologous DNA template [3,4]. In *Saccharomyces cerevisiae*, recent characterization of core resection proteins has revealed that DSB resection is initiated by the MRX complex, which catalyzes an endonucleolytic cleavage near a DSB [4], with the Sae2 protein (CtIP in mammals) promoting MRX endonucleolytic activity [5]. This MRX-Sae2-mediated DNA clipping generates 5' DNA ends that are optimal substrates for the nucleases Exo1 and Dna2, the latter working in concert with the helicase Sgs1 [6–9]. In addition, the MRX complex recruits Exo1, Sgs1 and Dna2 to DSBs independently of the Mre11 nuclease activity [10]. DSB resection is also negatively regulated by Ku and Rad9, which inhibit the access to DSBs of Exo1 and Sgs1-Dna2, respectively [11–14].

The MRX-Sae2-mediated endonucleolytic cleavage is particularly important to initiate resection at DNA ends that are not easily accessible to Exo1 and Dna2-Sgs1. For instance, both *sae2*Δ and *mre11* nuclease defective mutants are completely unable to resect meiotic DSBs, where the Spo11 topoisomerase-like protein remains covalently attached to the 5'-terminated strands [15,16]. Furthermore, the same mutants exhibit a marked sensitivity to camptothecin (CPT), which extends the half-life of DNA-topoisomerase I cleavable complexes [17,18], and to methyl methanesulfonate (MMS), which can generate chemically complex DNA termini. The lack of Rad9 or Ku suppresses both the hypersensitivity to DSB-inducing agents and the resection defect of *sae2*Δ cells [10–14]. These suppression events require Dna2-Sgs1 and Exo1, respectively, indicating that Rad9 increases the requirement for MRX-Sae2 activity in DSB

resection by inhibiting Sgs1-Dna2 [13,14], while Ku mainly limits the action of Exo1 [10–12]. By contrast, elimination of either Rad9 or Ku does not bypass Sae2/MRX function in resecting meiotic DSBs [11,13], likely because Sgs1-Dna2 and Exo1 cannot substitute for the Sae2/MRX-mediated endonucleolytic cleavage when this event is absolutely required to generate accessible 5'-terminated DNA strands.

Sae2 plays an important role also in modulating the checkpoint response. Checkpoint activation in response to DSBs depends primarily on Mec1, with Tel1 playing a minor role [19]. On the other hand, impaired Mre11 endonuclease activity caused by the lack of Sae2 leads to increased MRX persistence at the DSB ends. The enhanced MRX signaling in turn causes unscheduled Tel1-dependent checkpoint activation that is associated to prolonged Rad53 phosphorylation [20–22]. Mutant *mre11* alleles that reduce MRX binding to DSBs restore DNA damage resistance in *sae2*Δ cells and reduce their persistent checkpoint activation without restoring efficient DSB resection [23,24], suggesting that enhanced MRX association to DSBs contributes to the DNA damage hypersensitivity caused by the lack of Sae2. Persistently bound MRX might increase the sensitivity to DNA damaging agents of *sae2*Δ cells by hyperactivating the DNA damage checkpoint. If this were the case, then the DNA damage hypersensitivity of *sae2*Δ cells should be restored by the lack of Tel1 or of its downstream effector Rad53, as they are responsible for the *sae2*Δ enhanced checkpoint signaling [20,22]. However, while Rad53 inactivation has never been tested, *TEL1* deletion not only fails to restore DNA damage resistance in *sae2*Δ cells, but it exacerbates their sensitivity to DNA damaging agents [23,24]. Therefore, other studies are required to understand whether the Tel1- and Rad53-mediated checkpoint signaling has any role in determining the DNA damage sensitivity of *sae2*Δ cells.

By performing a genetic screen, we identified *rad53* and *tel1* mutant alleles that suppress both the hypersensitivity to DNA damaging agents and the resection defect of *sae2*Δ cells by reducing the amount of Rad9 at DSBs. Decreased Rad9 binding at DNA ends bypasses Sae2 function in DNA damage resistance and resection by relieving the inhibition of the Sgs1-Dna2 resection machinery. Altogether our data suggest that the primary cause of the resection defect of *sae2*Δ cells is Rad9 association to DSBs, which is promoted by persistent Tel1 and Rad53 signaling activities in these cells.

Results

The Rad53-H88Y and Tel1-N2021D variants suppress the DNA damage hypersensitivity of *sae2*Δ cells

We have previously described our search for extragenic mutations that suppress the CPT hypersensitivity of *sae2*Δ cells [13]. This genetic screen identified 15 single-gene suppressor mutants belonging to 11 distinct allelism groups. Analysis of genomic DNA by next-generation Illumina sequencing of 5 non allelic suppressor mutants revealed that the DNA damage resistance was due to single base pair substitutions in the genes encoding Sgs1, Top1, or the multidrug resistance proteins Pdr3, Pdr10 and Sap185 [13]. Subsequent genome sequencing and genetic analysis of 2 more non allelic suppressor mutants allowed to link suppression to either the *rad53-H88Y* mutant allele, causing the replacement of Rad53 amino acid residue His88 by Tyr, or the *tel1-N2021D* allele, resulting in the replacement of Tel1 amino acid residue Asn2021 by Asp. Both *rad53-H88Y* and *tel1-N2021D* alleles restored resistance of *sae2*Δ cells not only to CPT, but also to phleomycin (phleo) and MMS (Fig 1A). While both *rad53-H88Y* and *tel1-N2021D* fully rescued the hypersensitivity of *sae2*Δ cells to phleomycin and MMS, the CPT hypersensitivity of *sae2*Δ cells was only partially suppressed by the same alleles (Fig 1A), suggesting that they did not bypass all Sae2 functions.

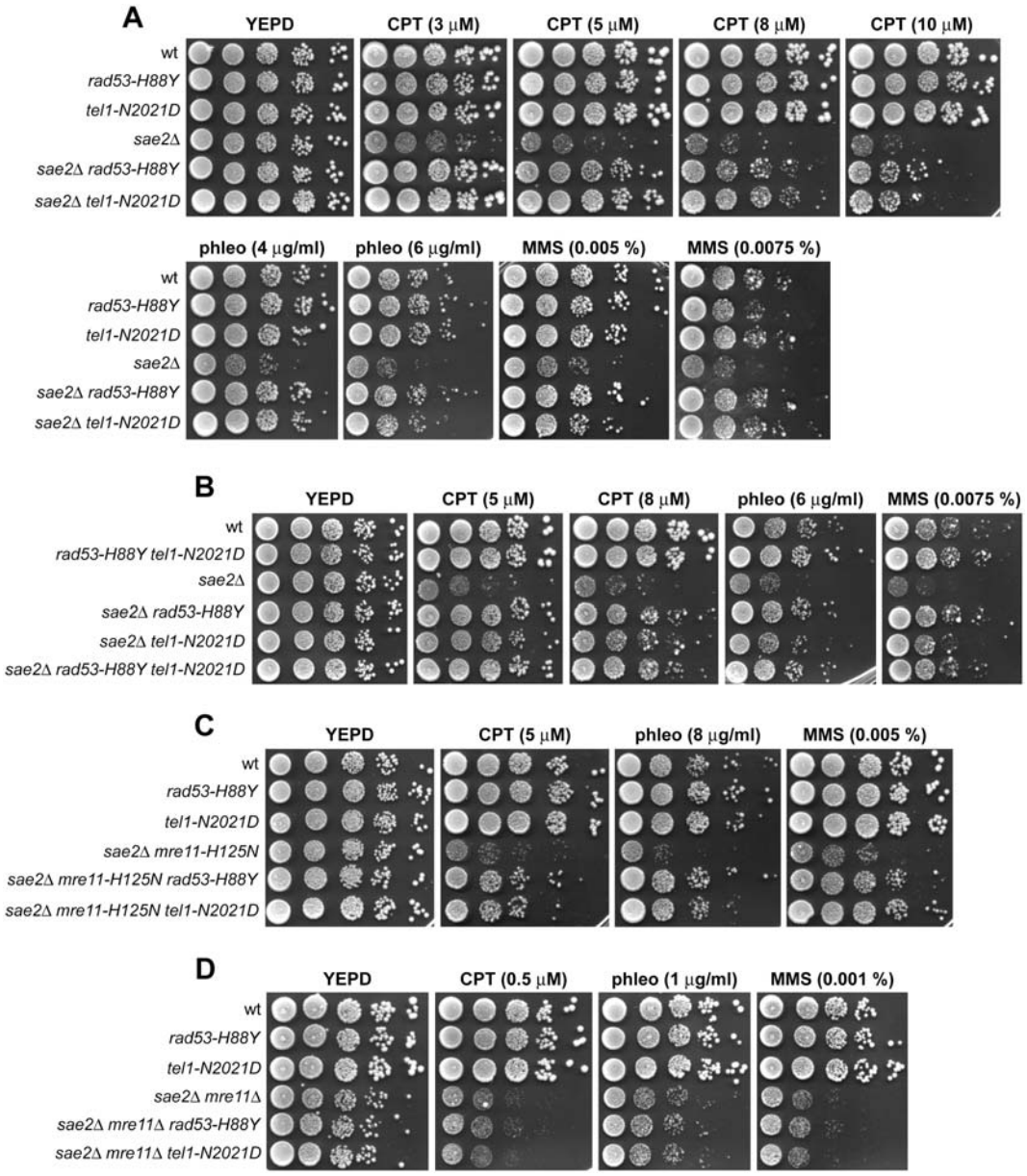

Fig 1. Rad53-H88Y and Tel1-N2021D suppress the hypersensitivity to genotoxic agents of *sae2*Δ cells. (A-D) Exponentially growing cells were serially diluted (1:10) and each dilution was spotted out onto YEPD plates with or without CPT, phleomycin or MMS.

doi:10.1371/journal.pgen.1005685.g001

Both *rad53-H88Y* and *tel1-N2021D* suppressor alleles were recessive, as the sensitivity to genotoxic agents of *sae2*Δ/*sae2*Δ *RAD53*/*rad53-H88Y* and *sae2*Δ/*sae2*Δ *TEL1*/*tel1-N2021D* diploid cells was similar to that of *sae2*Δ/*sae2*Δ *RAD53*/*RAD53 TEL1*/*TEL1* diploid cells (S1 Fig), suggesting that *rad53-H88Y* and *tel1-N2021D* alleles encode hypomorphic variants. Furthermore, both variants suppressed the hypersensitivity to DNA damaging agents of *sae2*Δ cells by altering the same mechanism, as *sae2*Δ *rad53-H88Y tel1-N2021D* triple mutant cells survived in the presence of DNA damaging agents to the same extent as *sae2*Δ *rad53-H88Y* and *sae2*Δ *tel1-N2021D* double mutant cells (Fig 1B).

The MRX complex not only provides the nuclease activity for initiation of DSB resection, but also it promotes the binding of Exo1, Sgs1 and Dna2 at the DSB ends [10]. These MRX multiple roles explain the severe DNA damage hypersensitivity and resection defect of cells lacking any of the MRX subunits compared to cells lacking either Sae2 or the Mre11 nuclease activity. As Sae2 has been proposed to activate Mre11 nuclease activity [5], we asked whether the suppression of *sae2*Δ DNA damage hypersensitivity by Rad53-H88Y and Tel1-N2021D requires Mre11 nuclease activity. Both *rad53-H88Y* and *tel1-N2021D* alleles suppressed the hypersensitivity to DNA damaging agents of *sae2*Δ cells carrying the nuclease defective *mre11-H125N* allele (Fig 1C). By contrast, *sae2*Δ *mre11*Δ *rad53-H88Y* and *sae2*Δ *mre11*Δ *tel1-N2021D* triple mutant cells were as sensitive to genotoxic agents as *sae2*Δ *mre11*Δ double mutant cells (Fig 1D), indicating that neither the *rad53-H88Y* nor the *tel1-N2021D* allele can suppress the hypersensitivity to DNA damaging agents of *sae2*Δ *mre11*Δ cells. Altogether, these findings indicate that both Rad53-H88Y and Tel1-N2021D require the physical presence of the MRX complex, but not its nuclease activity, to bypass Sae2 function in cell survival to genotoxic agents.

The Rad53-H88Y variant is defective in the interaction with Rad9 and bypasses the adaptation defect of *sae2*Δ cells by impairing checkpoint activation

A single unrepairable DSB induces a DNA damage checkpoint that depends primarily on Mec1, with Tel1 playing a minor role [19]. This checkpoint response can be eventually turned off, allowing cells to resume cell cycle progression through a process that is called adaptation [25–27]. In the absence of Sae2, cells display heightened checkpoint activation that prevents cells from adapting to an unrepaired DSB [20,22]. This persistent checkpoint activation is due to increased MRX amount/persistence at the DSB that in turn causes enhanced and prolonged Tel1 activation that is associated with persistent Rad53 phosphorylation [20–22,28].

If the *rad53-H88Y* mutation impaired Rad53 activity, then it is expected to suppress the adaptation defect of *sae2*Δ cells by lowering checkpoint activation. We addressed this point by using JKM139 derivative strains, where a single DSB at the *MAT* locus can be generated by expression of the HO endonuclease gene under the control of a galactose-dependent promoter. This DSB cannot be repaired by HR because of the deletion of the homologous donor loci *HML* and *HMR* [27]. We measured checkpoint activation by monitoring the ability of cells to arrest the cell cycle and to phosphorylate Rad53 after HO induction. Both *rad53-H88Y* and *sae2*Δ *rad53-H88Y* cells formed microcolonies of more than 2 cells with higher efficiency than either wild type or *sae2*Δ cells (Fig 2A). Furthermore, the Rad53-H88Y variant was poorly phosphorylated after HO induction both in the presence and in the absence of Sae2 (Fig 2B). Thus, the *rad53-H88Y* mutation suppresses the adaptation defect of *sae2*Δ cells by impairing Rad53 activation.

DNA damage-dependent activation of Rad53 requires its phospho-dependent interaction with Rad9, which acts as a scaffold to allow Rad53 intermolecular authophosphorylation and

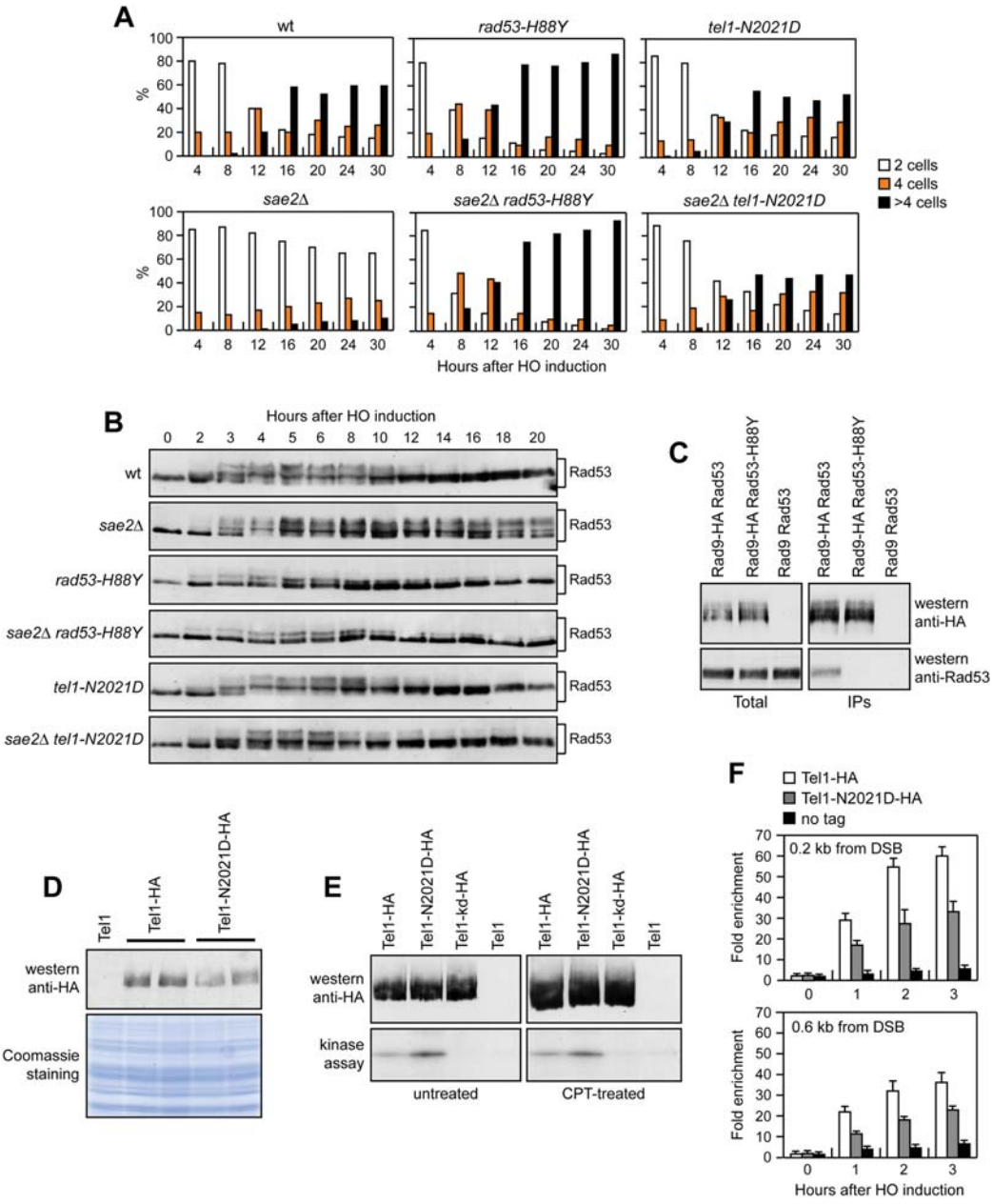

Fig 2. Rad53-H88Y and Tel1-N2021D suppress the checkpoint shut off defect of *sae2*Δ cells. (A) G1-arrested cell cultures of JKM139 derivative strains were plated on galactose-containing plates (time zero). At the indicated time points, 200 cells for each strain were analyzed to determine the frequency of large budded cells (2 cells) and of cells forming microcolonies of 4 or more than 4 cells. (B) Exponentially growing YEPR cultures of the strains in (A) were transferred to YEPRG (time zero), followed by western blot analysis with anti-Rad53 antibodies. (C) Protein extracts were analyzed by western blot with anti-HA or anti-Rad53 antibodies either directly (Total) or after Rad9-HA immunoprecipitation (IPs) with anti-HA antibodies. (D) Protein extracts from

exponentially growing cells were analyzed by western blotting with anti-HA antibodies. The same amounts of protein extracts were separated by SDS-PAGE and stained with Coomassie as loading control. (E) Kinase assay was performed on equal amounts of anti-HA immunoprecipitates of protein extracts from cells either exponentially growing in YEPD or after treatment with 50μM CPT for 1 hour. All the immunoprecipitates were also subjected to western blot analysis using anti-HA antibodies. (F) Relative fold enrichment of Tel1-HA and Tel1-N2021D-HA compared to untagged Tel1 (no tag) at the indicated distance from the HO cleavage site was evaluated after ChIP with anti-HA antibodies and qPCR analysis. In all diagrams, the ChIP signals were normalized for each time point to the amount of the corresponding immunoprecipitated protein and input signal. The mean values are represented with error bars denoting s.d. (n = 3).

doi:10.1371/journal.pgen.1005685.g002

activation [29–31]. Interestingly, the His88 residue, which is replaced by Tyr in the Rad53-H88Y variant, is localized in the forkhead-associated domain 1 of the protein and has been implicated in mediating Rad9-Rad53 interaction [32]. Thus, we asked whether the Rad53-H88Y variant was defective in the interaction with Rad9. When HA-tagged Rad9 was immunoprecipitated with anti-HA antibodies from wild type and *rad53-H88Y* cells grown for 4 hours in the presence of galactose to induce HO, wild type Rad53 could be detected in Rad9-HA immunoprecipitates, whereas Rad53-H88Y did not (Fig 2C). This defective interaction of Rad53-H88Y with Rad9 could explain the impaired checkpoint activation in *sae2*Δ *rad53-H88Y* double mutant cells.

The Tel1-N2021D variant binds poorly to DSBs and bypasses the adaptation defect of *sae2*Δ cells by reducing persistent Rad53 activation

Tel1 signaling activity is responsible for the prolonged Rad53 activation that prevents *sae2*Δ cells to adapt to the checkpoint triggered by an unrepairable DSB [20,22]. Although telomere length in *tel1-N2021D* mutant cells was unaffected both in the presence and in the absence of Sae2 (S2 Fig), the recessivity of *tel1-N2021D* suppressor effect on *sae2*Δ DNA damage hypersensitivity suggests that the N2021D substitution impairs Tel1 function. If this were the case, Tel1-N2021D might suppress the adaptation defect of *sae2*Δ cells by reducing the DSB-induced persistent Rad53 phosphorylation. When G1-arrested cell cultures were spotted on galactose-containing plates to induce HO, wild type, *sae2*Δ, *tel1-N2021D* and *sae2*Δ *tel1-N2021D* cells accumulated large budded cells within 4 hours (Fig 2A). This cell cycle arrest is due to checkpoint activation. In fact, when the same cells exponentially growing in raffinose were transferred to galactose, Rad53 phosphorylation was detectable about 2–3 hours after galactose addition (Fig 2B). However, while *sae2*Δ cells remained arrested as large budded cells for at least 30 hours (Fig 2A) and showed persistent Rad53 phosphorylation (Fig 2B), wild type, *tel1-N2021D* and *sae2*Δ *tel1-N2021D* cells formed microcolonies with more than 2 cells (Fig 2A) and decreased the amounts of phosphorylated Rad53 (Fig 2B) with similar kinetics 10–12 hours after HO induction. Therefore, the Tel1-N2021D variant impairs Tel1 signaling activity, as it rescues the *sae2*Δ adaptation defect by reducing the persistent Rad53 phosphorylation.

The N2021D substitution resides in the Tel1 FAT domain, a helical solenoid that encircles the kinase domain of all the phosphoinositide 3-kinase (PI3K)-related kinases (PIKKs) [33,34], suggesting that this amino acid change might reduce Tel1 kinase activity. Western blot analysis revealed that the amount of Tel1-N2021D was slightly lower than that of wild type Tel1 (Fig 2D). We then immunoprecipitated equivalent amounts of Tel1-HA and Tel1-N2021D-HA variants from both untreated and CPT-treated cells (Fig 2E, top), and we measured their kinase activity in vitro using the known artificial substrate of the PIKKs family PHAS-I (Phosphorylated Heat and Acid Stable protein) [35]. Both Tel1-HA and Tel1-N2021D-HA were capable to phosphorylate PHAS-I, with the amount of phosphorylated substrate being slighly higher in Tel1-N2021D-HA than in Tel1-HA immunoprecipitates (Fig 2E, bottom). This PHAS-I phosphorylation was dependent on Tel1 kinase activity, as it was not detectable when the immunoprecipitates were

prepared from strains expressing either kinase dead Tel1-kd-HA or untagged Tel1 (Fig 2E, bottom). Thus, the *tel1-N2021D* mutation does not affect Tel1 kinase activity.

Interestingly, the FAT domain is in close proximity to the FATC domain, which was shown to be important for Tel1 recruitment to DNA ends [36], suggesting that the Tel1-N2021D variant might be defective in recruitment/association to DSBs. Strikingly, when we analyzed Tel1 and Tel1-N2021D binding at the HO-induced DSB by chromatin immunoprecipitation (ChIP) and quantitative real time PCR (qPCR), the amount of Tel1-N2021D bound at the DSB turned out to be lower than that of wild type Tel1 (Fig 2F). This decreased Tel1-N2021D association was not due to lower Tel1-N2021D levels, as the ChIP signals were normalized for each time point to the amount of immunoprecipitated protein. Thus, the inability of *sae2*Δ *tel1-N2021D* cells to sustain persistent Rad53 phosphorylation after DSB generation can be explained by a decreased association of Tel1-N2021D to DSBs.

Checkpoint-mediated cell cycle arrest is not responsible for the DNA damage hypersensitivity of *sae2*Δ cells

As both Rad53-H88Y and Tel1-N2021D reduce checkpoint signaling in *sae2*Δ cells, we asked whether the increased DNA damage resistance of *sae2*Δ *rad53-H88Y* and *sae2*Δ *tel1-N2021D* cells was due to the elimination of the checkpoint-mediated cell cycle arrest. This hypothesis could not be tested by deleting the *MEC1*, *DDC1*, *RAD24*, *MEC3* or *RAD9* checkpoint genes, because they also regulate DSB resection [37–39]. On the other hand, an HO-induced DSB activates also the Chk1 checkpoint kinase [40], which contributes to arrest the cell cycle in response to DSBs by controlling a pathway that is independent of Rad53 [41]. Importantly, *chk1*Δ cells do not display DNA damage hypersensitivity and are not defective in resection of uncapped telomeres [38,41]. We therefore asked whether *CHK1* deletion restores DNA damage resistance in *sae2*Δ cells. Consistent with the finding that Chk1 contributes to arrest the cell cycle after DNA damage independently of Rad53 [41], Rad53 was phosphorylated with wild type kinetics after HO induction in both *chk1*Δ and *sae2*Δ *chk1*Δ cells (Fig 3A). Furthermore, *CHK1* deletion suppresses the adaptation defect of *sae2*Δ cells. In fact, both *chk1*Δ and *sae2*Δ *chk1*Δ cells spotted on galactose-containing plates formed microcolonies of more than 2 cells with higher efficiency than wild type and *sae2*Δ cells (Fig 3B), although they did it less efficiently than *mec1*Δ cells, where both Rad53 and Chk1 signaling were abrogated [41]. Strikingly, the lack of Chk1 did not suppress the hypersensitivity to DNA damaging agents of *sae2*Δ cells (Fig 3C), although it overrides the checkpoint-mediated cell cycle arrest.

To rule out the possibility that *CHK1* deletion failed to restore DNA damage resistance in *sae2*Δ cells because it impairs DSB resection, we used JKM139 derivative strains to monitor directly generation of ssDNA at the DSB ends in the absence of Chk1. As ssDNA is resistant to cleavage by restriction enzymes, we followed loss of SspI restriction sites as a measure of resection by Southern blot analysis under alkaline conditions, using a single-stranded probe that anneals to the 3' end at one side of the break. Consistent with previous indications that Chk1 is not involved in DNA-end resection [38], *chk1*Δ single mutant cells resected the DSB with wild type kinetics (Fig 3D). Furthermore, *CHK1* deletion did not exacerbate the resection defect of *sae2*Δ cells (Fig 3E). Altogether, these data indicate that the prolonged checkpoint-mediated cell cycle arrest of *sae2*Δ cells is not responsible for their hypersensitivity to DNA damaging agents.

The Rad53-H88Y and Tel1-N2021D variants restore resection and SSA in *sae2*Δ cells

As the checkpoint-mediated cell cycle arrest was not responsible for the DNA damage hypersensitivity of *sae2*Δ cells, we asked whether Rad53-H88Y and/or Tel1-N2021D suppressed the

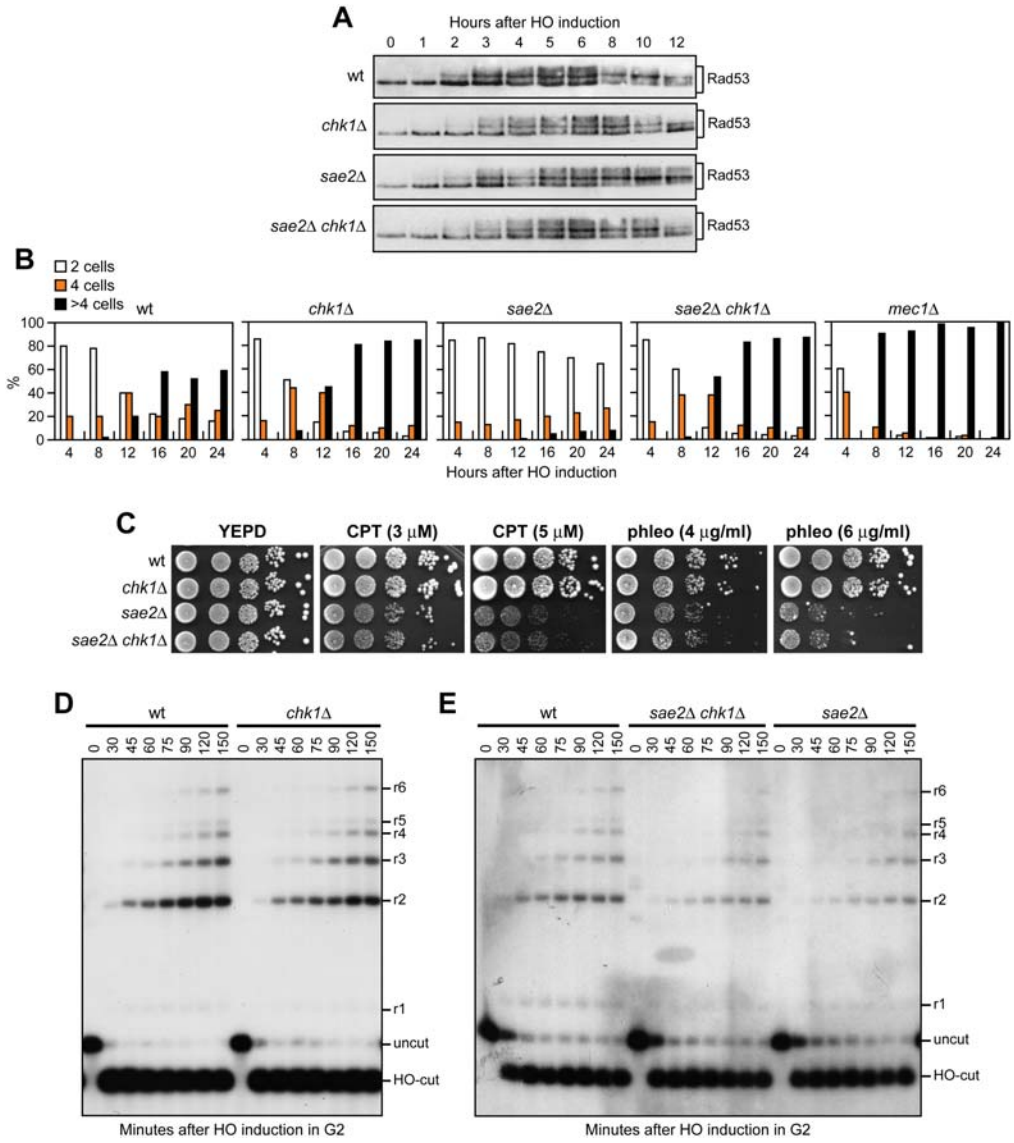

Fig 3. The lack of Chk1 does not suppress the hypersensitivity to DNA damaging agents of *sae2*Δ cells. (A) Exponentially growing YEPR cultures of JKM139 derivative strains were transferred to YEPRG (time zero), followed by western blot analysis with anti-Rad53 antibodies. (B) YEPR G1-arrested cell cultures of JKM139 derivative strains were plated on galactose-containing plates (time zero). At the indicated time points, 200 cells for each strain were analyzed to determine the frequency of large budded cells (2 cells) and of cells forming microcolonies of 4 or more than 4 cells. (C) Exponentially growing cells were serially diluted (1:10) and each dilution was spotted out onto YEPD plates with or without CPT and phleomycin. (D, E) DSB resection. YEPR exponentially growing cultures of JKM139 derivative cells were arrested in G2 with nocodazole and transferred to YEPRG in the presence of nocodazole at time zero. Gel blots of SspI-digested genomic DNA separated on alkaline agarose gel were hybridized with a single-stranded RNA probe that anneals to the unresected strand on one side of the break. 5'-3' resection progressively eliminates SspI sites, producing larger SspI fragments (r1 through r6) detected by the probe.

doi:10.1371/journal.pgen.1005685.g003

*sae2*Δ resection defect. We first measured the efficiency of single-strand annealing (SSA), a mechanism that repairs a DSB flanked by direct DNA repeats when sufficient resection exposes the complementary DNA sequences, which can then anneal to each other [3]. The *rad53-H88Y* and *tel1-N2021D* alleles were introduced in the YMV45 strain, which carries two tandem *leu2* gene repeats located 4.6 kb apart on chromosome III, with a HO recognition site adjacent to one of the repeats [42]. This strain also harbors a *GAL-HO* construct for galactose-inducible *HO* expression. Both Rad53-H88Y and Tel1-N2021D bypass Sae2 function in SSA-mediated DSB repair. In fact, accumulation of the SSA repair product after HO induction occurred more efficiently in both *sae2*Δ *rad53-H88Y* (Fig 4A and 4B) and *sae2*Δ *tel1-N2021D* (Fig 4C and 4D) than in *sae2*Δ cells, where it was delayed compared to wild type.

To confirm that Rad53-H88Y and Tel1-N2021D suppress the SSA defect of *sae2*Δ cells by restoring DSB resection, we used JKM139 derivative strains to monitor directly generation of ssDNA at the DSB ends. Indeed, *sae2*Δ *rad53-H88Y* (Fig 5A) and *sae2*Δ *tel1-N2021D* (Fig 5B) cells resected the HO-induced DSB more efficiently than *sae2*Δ cells, indicating that both Rad53-H88Y and Tel1-N2021D suppress the resection defect of *sae2*Δ cells.

The DSB resection defect of *sae2*Δ cells is thought to be responsible for the increased persistence of MRX at the DSB [43]. Because Rad53-H88Y and Tel1-N2021D restore DSB resection in *sae2*Δ cells, we expected that the same variants also reduce the amount of MRX bound at the DSB. The amount of Mre11 bound at the HO-induced DSB end turned out to be lower in both *sae2*Δ *rad53-H88Y* and *sae2*Δ *tel1-N2021D* than in *sae2*Δ cells (Fig 5C). Therefore, the Rad53-H88Y and Tel1-N2021D variants restore DSB resection in *sae2*Δ cells and reduce MRX association/persistence at the DSB.

Consistent with the finding that Rad53-H88Y and Tel1-N2021D do not fully restore CPT resistance in *sae2*Δ cells (Fig 1A), and therefore do not bypass completely all Sae2 functions, the *rad53-H88Y* and *tel1-N2021D* mutations were unable to suppress the sporulation defects of *sae2*Δ/*sae2*Δ diploid cells (Fig 5D), suggesting that they cannot bypass the requirement for Sae2/MRX endonucleolytic cleavage to remove Spo11 from meiotic DSBs.

Suppression of the DNA damage hypersensitivity of *sae2*Δ cells by Rad53-H88Y and Tel1-N2021D variants requires Sgs1-Dna2

The MRX complex not only provides the nuclease activity for initiation of DSB resection, but also allows extensive resection by promoting the binding at the DSB ends of the resection proteins Exo1 and Sgs1-Dna2 [6,7,10]. Suppression of the DNA damage hypersensitivity of *sae2*Δ cells by Rad53-H88Y and Tel1-N2021D requires the physical presence of the MRX complex but not its nuclease activity (Fig 1C and 1D). As the loading of Exo1, Sgs1-Dna2 at DSBs depends on the MRX complex independently of its nuclease activity [10], we asked whether the investigated suppression events require Exo1, Sgs1 and/or Dna2. This question was particularly interesting, as Rad53 was shown to inhibit resection at uncapped telomeres through phosphorylation and inhibition of Exo1 [38,44]. As shown in Fig 6A, *sae2*Δ suppression by Rad53-H88Y and Tel1-N2021D was Exo1-independent. In fact, although the lack of Exo1 exacerbated the sensitivity to DNA damaging agents of *sae2*Δ cells, both *sae2*Δ *exo1*Δ *rad53-H88Y* and *sae2*Δ *exo1*Δ *tel1-N2021D* triple mutants were more resistant to genotoxic agents than *sae2*Δ *exo1*Δ double mutant cells (Fig 6A).

By contrast, neither Rad53-H88Y nor Tel1-N2021D were able to suppress the sensitivity to DNA damaging agents of *sae2*Δ cells carrying the temperature sensitive *dna2-1* allele (Fig 6B), suggesting that Dna2 activity is required for their suppressor effect. Dna2, in concert with the helicase Sgs1, functions as a nuclease in DSB resection [7]. The *dna2-E675A* allele abolishes Dna2 nuclease activity, which is essential for cell viability and whose requirement is bypassed

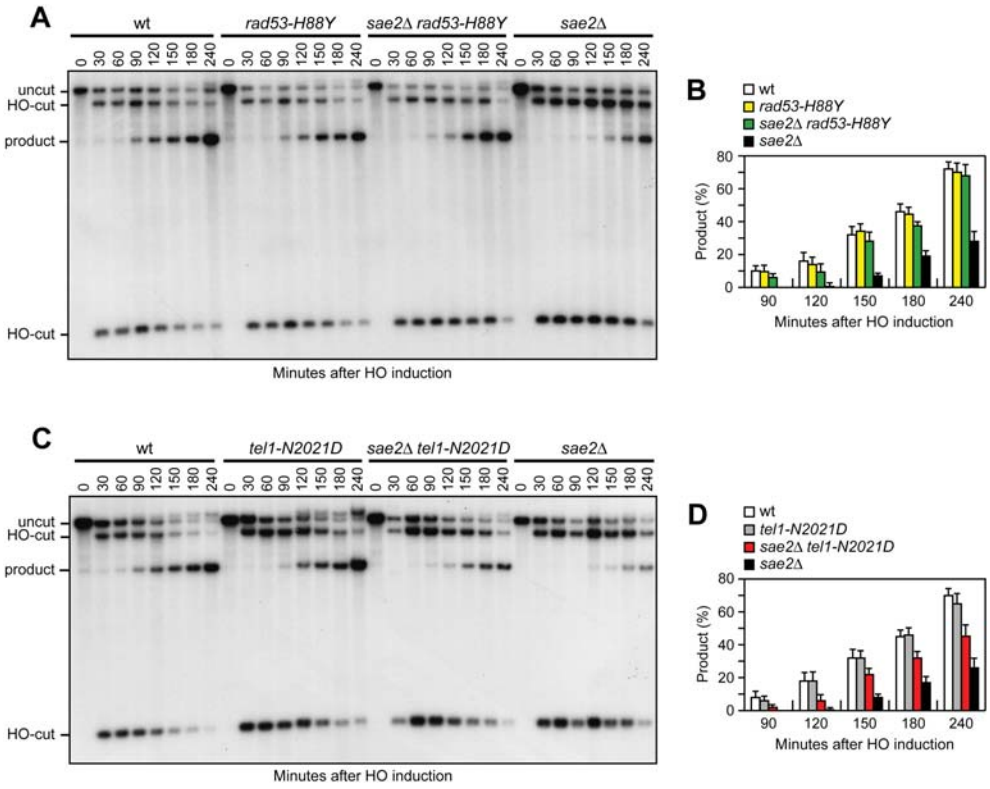

Fig 4. Rad53-H88Y and Tel1-N2021D suppress the SSA defect of *sae2*Δ cells. (A) DSB repair by SSA. YEPR exponentially growing cell cultures of YMV45 derivative strains, carrying the HO-cut site flanked by homologous *leu2* sequences that are 4.6 kb apart, were transferred to YEPRG at time zero. HO-induced DSB formation results in generation of 12 kb and 2.5 kb DNA fragments (HO-cut) that can be detected by Southern blot analysis with a *LEU2* probe of KpnI-digested genomic DNA. DSB repair by SSA generates an 8 kb fragment (product). (B) Densitometric analysis of the product band signals. The experiment as in (A) was independently repeated three times and the mean values are represented with error bars denoting s.d. (n = 3). (C) DSB repair by SSA was analyzed as in (A). (D) Densitometric analysis of the product band signals. The experiment as in (C) was independently repeated three times and the mean values are represented with error bars denoting s.d. (n = 3).

doi:10.1371/journal.pgen.1005685.g004

by the *pif1-M2* mutation that impairs the nuclear activity of the Pif1 helicase [45]. The lack of Sgs1 or expression of the Dna2-E675A variant in the presence of the *pif1-M2* allele impaired viability of *sae2*Δ cells even in the absence of genotoxic agents. The synthetic lethality of *sae2*Δ *sgs1*Δ cells, and possibly of *sae2*Δ *dna2-E675A pif1-M2*, is likely due to defects in DSB resection, as it is known to be suppressed by either *EXO1* overexpression or *KU* deletion [11]. Thus, we asked whether Rad53-H88Y and/or Tel1-N2021D could restore viability of *sae2*Δ *sgs1*Δ and/or *sae2*Δ *dna2-E675A pif1-M2* cells. Tetrad dissection of diploid cells did not allow to find viable spores with the *sae2*Δ *dna2-E675A pif1-M2 rad53-H88Y* (Fig 6C) or *sae2*Δ *dna2-E675A pif1-M2 tel1-N2021D* genotypes (Fig 6D), indicating that neither Rad53-H88Y nor Tel1-N2021D can restore the viability of *sae2*Δ *dna2-E675A pif1-M2* cells. Similarly, no viable *sae2*Δ *sgs1*Δ spores could be recovered, while *sae2*Δ *sgs1*Δ *rad53-H88Y* and *sae2*Δ *sgs1*Δ *tel1-N2021D* triple mutant spores formed very small colonies that could not be further propagated (Fig 6E and 6F). Finally, neither Rad53-H88Y nor Tel1-N2021D, which allowed DNA

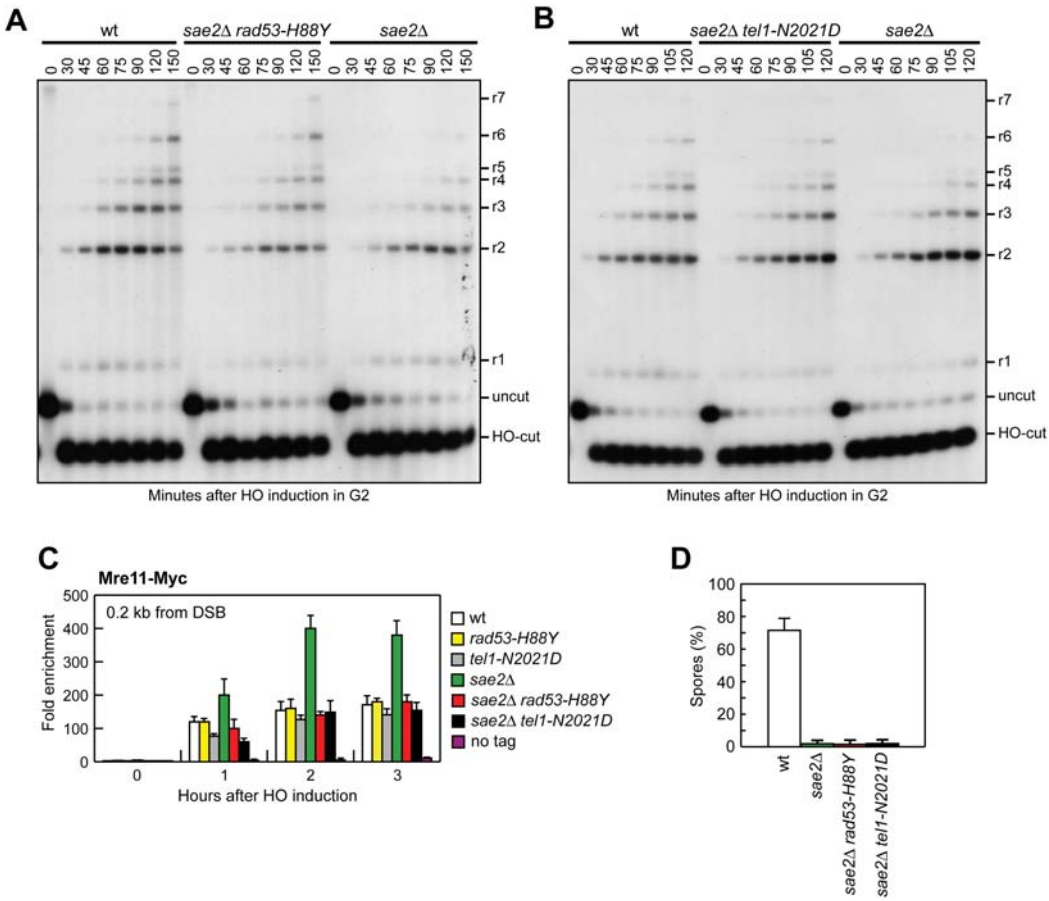

Fig 5. Rad53-H88Y and Tel1-N2021D suppress the resection defect of *sae2*Δ cells. (A, B) DSB resection. YEPR exponentially growing cultures of JKM139 derivative strains were arrested in G2 with nocodazole and transferred to YEPRG in the presence of nocodazole at time zero. Detection of ssDNA was carried out as described in Fig 3D. 5'-3' resection produces SspI fragments indicated as r1 to r7. (C) Exponentially growing YEPR cell cultures of JKM139 derivative strains were transferred to YEPRG. Relative fold enrichment of Mre11-Myc at 0.2 kb from the HO cleavage site was evaluated after ChIP with anti-Myc antibodies and qPCR analysis compared to untagged Mre11 (no tag). In all diagrams, the ChIP signals were normalized for each time point to the amount of the corresponding input signal. The mean values are represented with error bars denoting s.d. (n = 3). (D) Sporulation efficiency. Spores after 24h in sporulation medium of diploid cells homozygous for the indicated mutations.

doi:10.1371/journal.pgen.1005685.g005

damage resistance in *sae2*Δ *exo1*Δ cells (Fig 6A), were able to suppress the growth defect of *sgs1*Δ *exo1*Δ double mutant cells even in the absence of genotoxic agents (Fig 6G). Altogether, these findings indicate that suppression by Rad53-H88Y and Tel1-N2021D of the DNA damage hypersensitivity caused by the absence of Sae2 is dependent on Sgs1-Dna2.

The lack of Rad53 kinase activity suppresses the DNA damage hypersensitivity and the resection defect of *sae2*Δ cells

The Rad53-H88Y protein is defective in interaction with Rad9 (Fig 2C) and therefore fails to undergo autophosphorylation and activation, prompting us to test whether other mutations

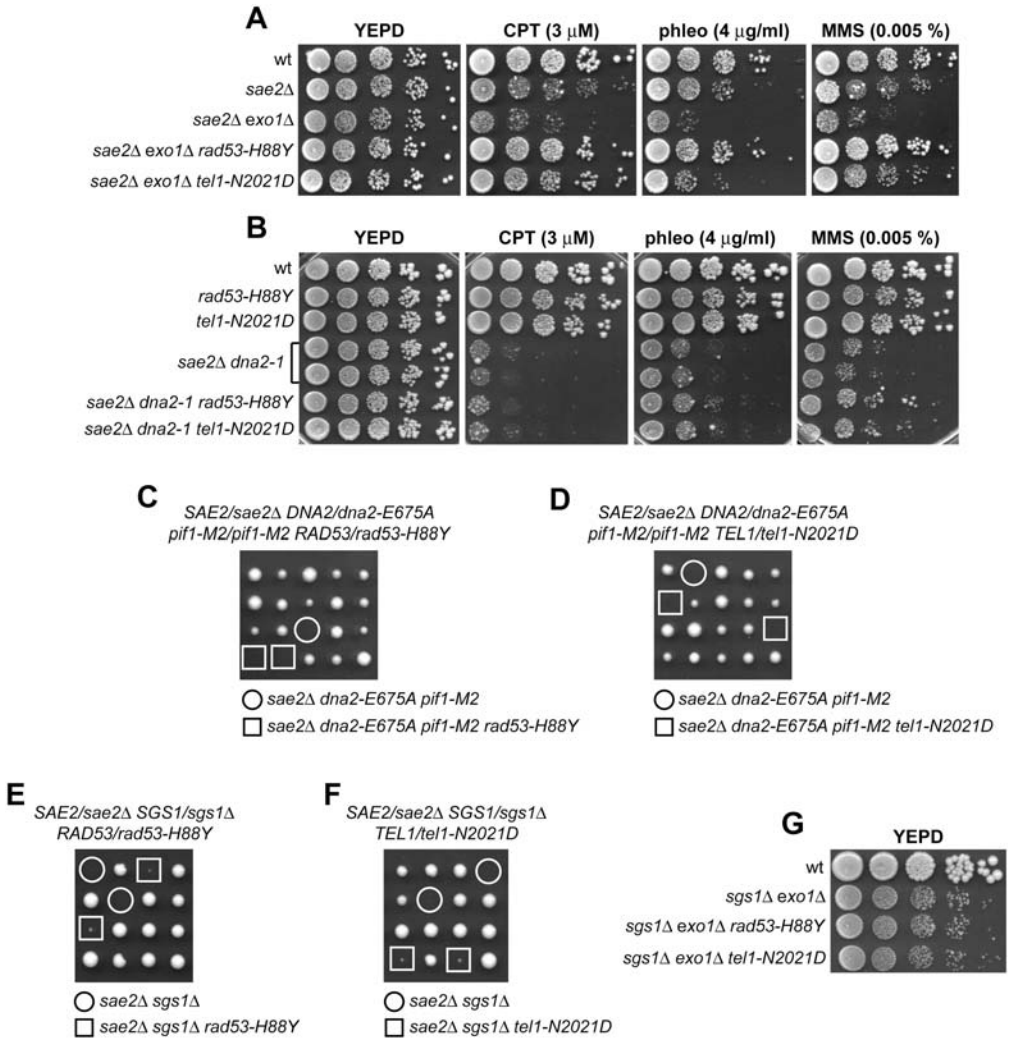

Fig 6. The Rad53-H88Y and Tel1-N2021D bypass of Sae2 function is Sgs1-Dna2-dependent. (A, B) Exponentially growing cells were serially diluted (1:10) and each dilution was spotted out onto YEPD plates with or without CPT, phleomycin or MMS. (C-F) Meiotic tetrads were dissected on YEPD plates that were incubated at 25°C, followed by spore genotyping. (G) Exponentially growing cells were serially diluted (1:10) and each dilution was spotted out onto YEPD plates.

doi:10.1371/journal.pgen.1005685.g006

affecting Rad53 activity can bypass Sae2 functions. To this end, we could not use *rad53*Δ cells because they show growth defects even when the lethal effect of *RAD53* deletion is suppressed by the lack of Sml1 [46]. We then substituted the chromosomal wild type *RAD53* allele with the kinase-defective *rad53-K227A* allele (*rad53-kd*), which does not impair cell viability in the absence of genotoxic agents but affects checkpoint activation [47]. The *rad53-kd* allele rescued the sensitivity of *sae2*Δ cells to CPT and MMS to an extent similar to Rad53-H88Y (Fig 7A).

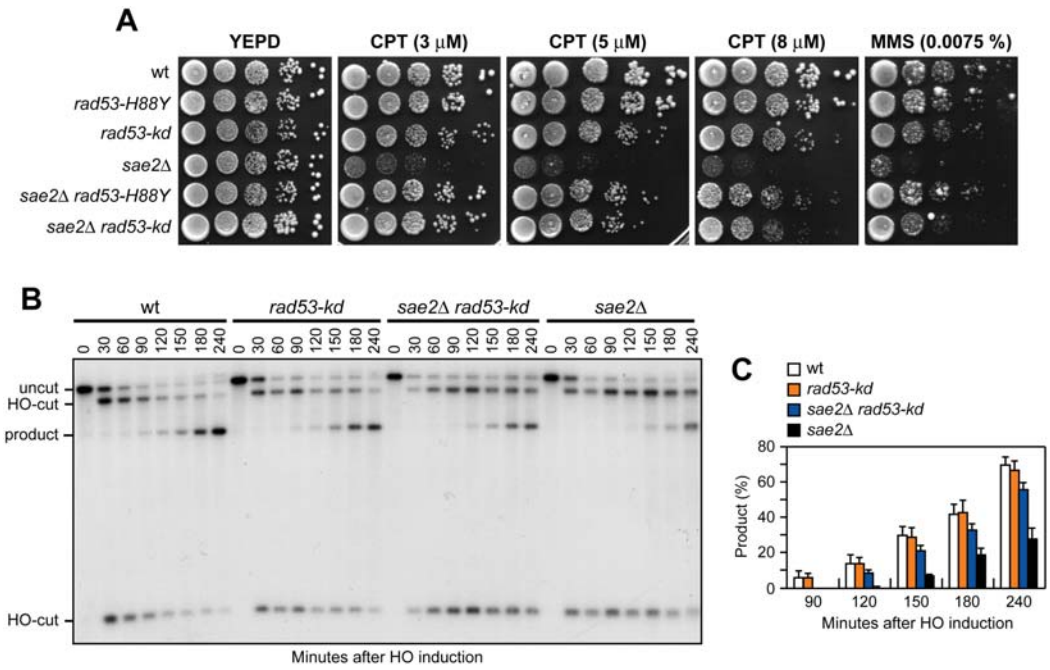

Fig 7. The Rad53-kd variant restores DNA damage resistance and SSA in *sae2*Δ cells. (A) Exponentially growing cells were serially diluted (1:10) and each dilution was spotted out onto YEPD plates with or without CPT or MMS. (B) DSB repair by SSA. The analysis was performed as described in Fig 4A. (C) Densitometric analysis of the product band signals. The experiment as in (B) was independently repeated three times and the mean values are represented with error bars denoting s.d. (n = 3).

doi:10.1371/journal.pgen.1005685.g007

Furthermore, accumulation of the SSA repair products occurred more efficiently in *sae2*Δ *rad53-kd* cells than in *sae2*Δ (Fig 7B and 7C), indicating that the lack of Rad53 kinase activity bypasses Sae2 function in SSA-mediated DSB repair.

The lack of Tel1 kinase activity bypasses Sae2 function at DSBs, whereas Tel1 hyperactivation increases Sae2 requirement

Suppression of *sae2*Δ may be peculiar to Tel1-N2021D, which is poorly recruited to DSBs (Fig 2F), or it might be performed also by *TEL1* deletion (*tel1*Δ) or by expression of a Tel1 kinase defective variant (Tel1-kd). Indeed, the Tel1-kd variant, carrying the G2611D, D2612A, N2616K, and D2631E amino acid substitutions that abolish Tel1 kinase activity in vitro (Fig 2E) [35], rescued the hypersensitivity of *sae2*Δ cells to genotoxic agents to an extent similar to Tel1-N2021D (Fig 8A). The lack of Tel1 kinase activity bypassed also Sae2 function in DSB resection, because *sae2*Δ *tel1-kd* cells repaired a DSB by SSA more efficiently than *sae2*Δ cells (Fig 8B and 8C). By contrast, and consistent with previous studies [23,24], *TEL1* deletion was not capable to suppress the hypersensitivity to DNA damaging agents of *sae2*Δ cells (Fig 8A). Rather, *tel1*Δ *sae2*Δ double mutant cells displayed higher sensitivity to CPT than *sae2*Δ cells (Fig 8A). Altogether, these data indicate that the lack of Tel1 kinase activity can bypass Sae2 function both in DNA damage resistance and DSB resection, but these suppression events require the physical presence of the Tel1 protein.

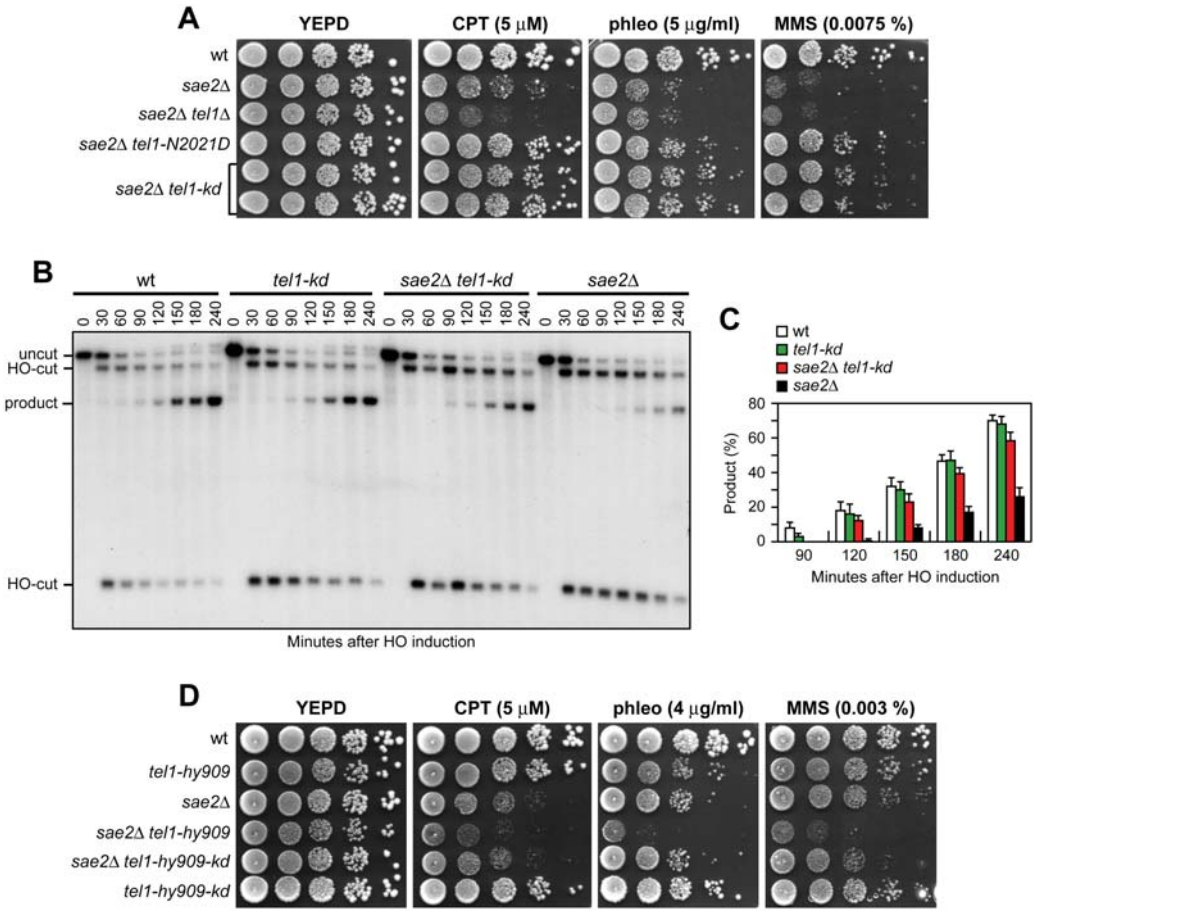

Fig 8. The Tel1-kd variant restores DNA damage resistance and SSA in *sae2*Δ cells. (A) Exponentially growing cells were serially diluted (1:10) and each dilution was spotted out onto YEPD plates with or without CPT, phleomycin or MMS. (B) DSB repair by SSA. The analysis was performed as described in Fig 4A. (C) Densitometric analysis of the product band signals. The experiment as in (B) was independently repeated three times and the mean values are represented with error bars denoting s.d. (n = 3). (D) Exponentially growing cells were serially diluted (1:10) and each dilution was spotted out onto YEPD plates with or without CPT, phleomycin or MMS.

doi:10.1371/journal.pgen.1005685.g008

As impairment of Tel1 function rescued the *sae2*Δ defects, we asked whether Tel1 hyperactivation exacerbates the DNA damage hypersensitivity of *sae2*Δ cells. We previously isolated the *TEL1-hy909* allele, which encodes a Tel1 mutant variant with enhanced kinase activity that causes an impressive telomere overelongation [48]. As shown in Fig 8D, *sae2*Δ *TEL1-hy909* double mutant cells were more sensitive to DNA damaging agents than *sae2*Δ single mutant cells. This enhanced DNA damage sensitivity was likely due to Tel1 kinase activity, as *sae2*Δ cells expressing a kinase defective Tel1-hy909-kd variant were as sensitive to DNA damaging agents as *sae2*Δ cells (Fig 8D). Thus, impairment of Tel1 activity bypasses Sae2 function at DSBs, whereas Tel1 hyperactivation increases the requirement for Sae2 in survival to genotoxic stress.

The absence of Tel1 failed not only to restore DNA damage resistance in *sae2*Δ cells (Fig 8A), but also to suppress their SSA defect (Fig 9A and 9B). The difference in the effects of *tel1*Δ and *tel1-kd* was not due to checkpoint signaling, as Rad53 phosphorylation decreased with similar kinetics in both *sae2*Δ *tel1-kd* and *sae2*Δ *tel1*Δ double mutant cells 10–12 hours after HO induction (Fig 9C). Interestingly, SSA-mediated DSB repair occurred with wild type kinetics in *tel1-kd* mutant cells (Fig 8B and 8C), while *tel1*Δ cells repaired a DSB by SSA less efficiently than wild type cells (Fig 9A and 9B), suggesting that Tel1 might have a function at DSBs that does not require its kinase activity. Indeed, *TEL1* deletion was shown to slight impair DSB resection [19]. Furthermore, it did not exacerbate the resection defect [19] and the hypersensitivity to DNA damaging agents of *mre11*Δ cells (Fig 9D), suggesting that the absence of Tel1 can impair MRX function. Tel1 was also shown to promote MRX association at DNA ends flanked by telomeric DNA repeats independently of its kinase activity [49], and we are showing that suppression of *sae2*Δ by Tel1-N2021D requires the physical presence of the MRX complex (Fig 1D). Thus, it is possible that the lack of Tel1 fails to bypass Sae2 function at DSBs because it reduces MRX association at DSBs to a level that is not sufficient to restore DNA damage resistance and DSB resection in *sae2*Δ cells. Indeed, the amount of Mre11 bound at the HO-induced DSB was decreased in *tel1*Δ, but not in *tel1-kd* cells, compared to wild type (Fig 9E). In agreement with a partial loss of Tel1 function, the Tel1-N2021D variant, whose association to DSBs is diminished compared to wild type Tel1 but not abolished (Fig 2F), only slightly decreased Mre11 association to the DSB (Fig 9E). As the rescue of *sae2*Δ by Tel1-N2021D requires the physical presence of the MRX complex, this Tel1 function in promoting MRX association to DSBs can explain the inability of *tel1*Δ to bypass Sae2 function in DNA damage resistance and resection.

Tel1 and Rad53 kinase activities promote Rad9 binding to the DSB ends

The suppression of the DNA damage hypersensitivity of *sae2*Δ cells by Rad53-H88Y and Tel1-N2021D requires Dna2-Sgs1 (Fig 6B–6G). Because Sgs1-Dna2 activity is counteracted by Rad9, whose lack restores DSB resection in *sae2*Δ cells [13,14], we asked whether suppression of the DSB resection defect of *sae2*Δ cells by Rad53 or Tel1 dysfunction might be due to decreased Rad9 association to the DSB ends. We have previously shown that wild type and *sae2*Δ cells have similar amounts of Rad9 bound at 1.8 kb from the DSB (Fig 10A) [43]. However, a robust increase in the amount of Rad9 bound at 0.2 kb and 0.6 kb from the DSB was detected in *sae2*Δ cells compared to wild type (Fig 10A) [14]. Strikingly, this enhanced Rad9 accumulation in *sae2*Δ cells was reduced in the presence of the Rad53-kd or Tel1-kd variant, which both decreased the amount of Rad9 bound at the DSB also in otherwise wild type cells (Fig 10A). Thus, Rad9 association close to the DSB depends on Rad53 and Tel1 kinase activity.

Rad9 inhibits DSB resection by counteracting Sgs1 recruitment to DSBs [13] and, as expected, Sgs1 binding to DSBs was lower in *sae2*Δ cells than in wild type (Fig 10B). By contrast, the presence of Rad53-kd or Tel1-kd variants increased the amount of Sgs1 at the DSB in both wild type and *sae2*Δ cells (Fig 10B). Together with the observation that the suppression of *sae2*Δ hypersensitivity to genotoxic agents by Rad53 and Tel1 dysfunctions requires Sgs1-Dna2, these findings indicate that the lack of Rad53 or Tel1 kinase activity restores DSB resection in *sae2*Δ cells by decreasing Rad9 association close to the DSB and therefore by relieving Sgs1-Dna2 inhibition. Although both *rad53-kd* and *tel1-kd* cells showed some lowering of Rad9 binding at DSBs compared to wild type cells (Fig 10A), they did not appear to accelerate SSA, suggesting that this extent of Rad9 binding is anyhow sufficient to limit resection in a wild type context.

Rad9 is known to be enriched at the sites of damage by interaction with histone H2A that has been phosphorylated on serine 129 (γH2A) by Mec1 and Tel1 [50–53]. As the lack of γH2A suppresses the SSA defect of *sae2*Δ cells [14], Tel1 activity might increase the amount of Rad9

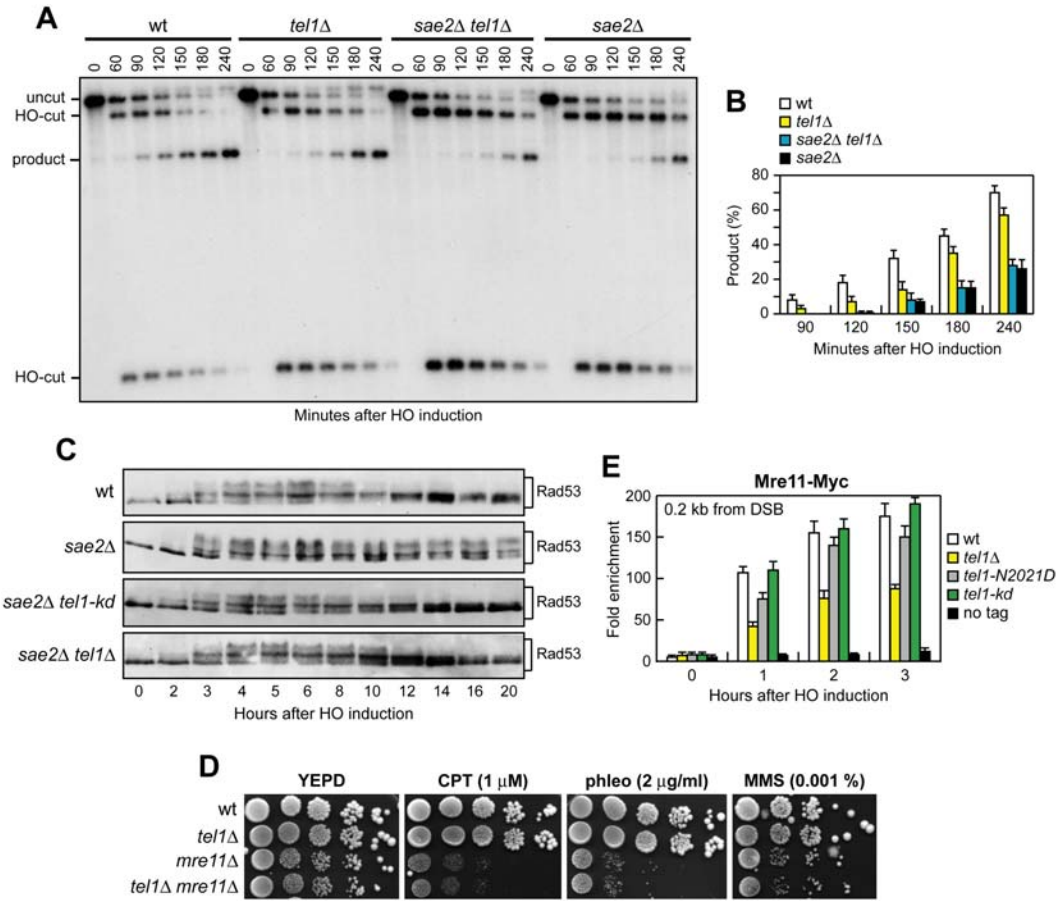

Fig 9. The lack of Tel1 does not restore DNA damage resistance and SSA in *sae2*Δ cells. (A) DSB repair by SSA. The analysis was performed as described in Fig 4A. (B) Densitometric analysis of the product band signals. The experiment as in (A) was independently repeated three times and the mean values are represented with error bars denoting s.d. (n = 3). (C) Exponentially growing YEPR cell cultures of JKM139 derivative strains were transferred to YEPRG (time zero), followed by western blot analysis with anti-Rad53 antibodies of protein extracts prepared at the indicated time points. (D) Exponentially growing cells were serially diluted (1:10) and each dilution was spotted out onto YEPD plates with or without CPT, phleomycin or MMS. (E) ChIP analysis. Exponentially growing YEPR cell cultures of JKM139 derivative strains were transferred to YEPRG. Recruitment of Mre11-Myc compared to untagged Mre11 (no tag) at 0.2 kb from the HO-cut was determined by ChIP analysis and qPCR. In all diagrams, the ChIP signals were normalized for each time point to the amount of the corresponding input signal. The mean values are represented with error bars denoting s.d. (n = 3).

doi:10.1371/journal.pgen.1005685.g009

bound at the DSB in *sae2*Δ cells by promoting generation of γH2A. Indeed, the *hta1-S129A* allele, which encodes a H2A variant where Ser129 is replaced by a non-phosphorylatable alanine residue, thus causing the lack of γH2A, suppressed the resection defect of *sae2*Δ cells (S3 Fig). Furthermore, γH2A formation turned out to be responsible for the enhanced Rad9 binding close to the break site, as *sae2*Δ *hta1-S129A* cells showed wild type levels of Rad9 bound at the DSB (Fig 10C). Finally, γH2A formation close to the DSB depends on Tel1 kinase activity, as γH2A at the DSB was not detectable in *sae2*Δ *tel1-kd* cells (Fig 10D). Altogether, these data indicate that Tel1 promotes Rad9 association to DSB in *sae2*Δ cells through γH2A generation.

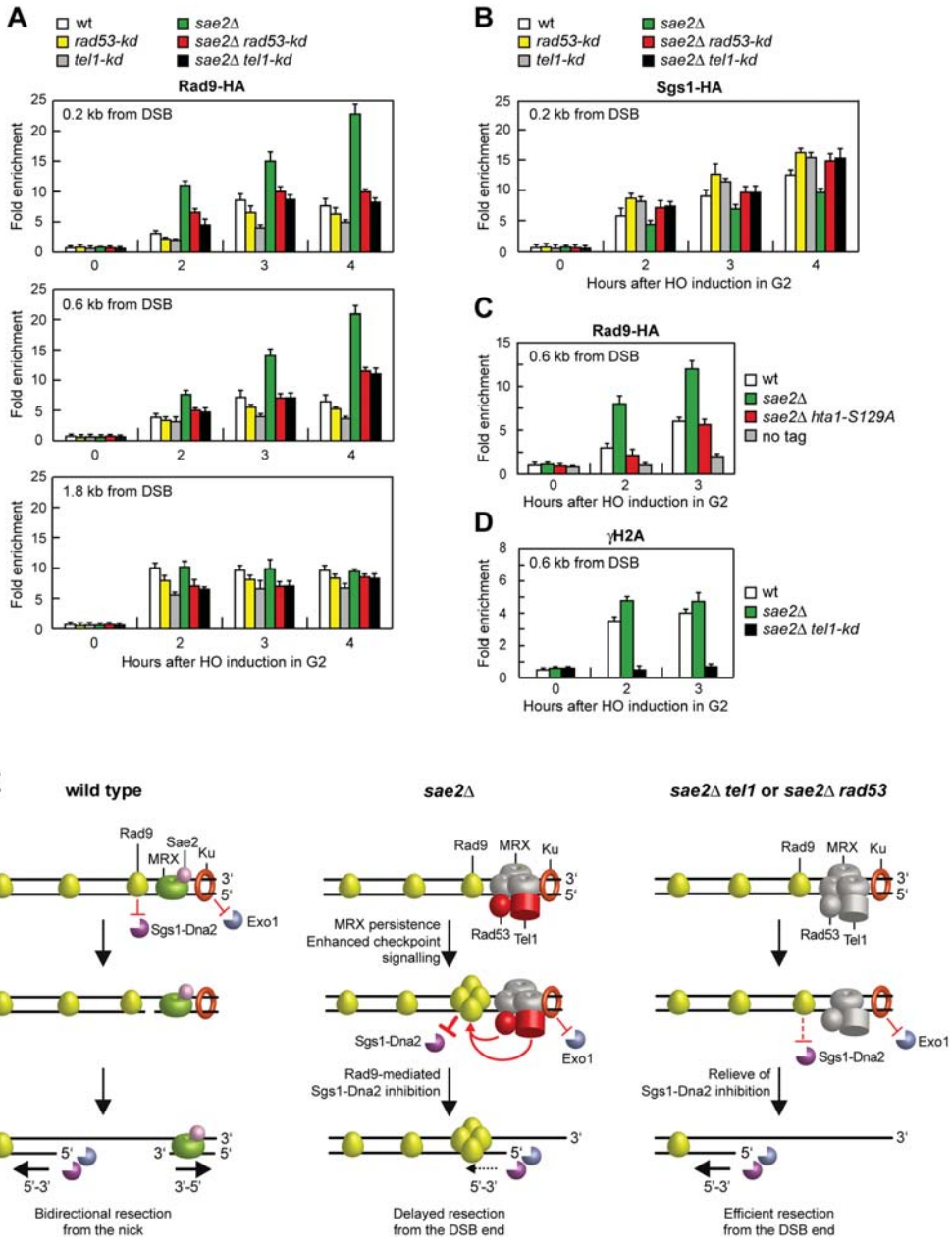

Fig 10. Rad53-kd and Tel1-kd prevent Rad9 association at DSBs. (A) Exponentially growing YEPR cell cultures of JKM139 derivative strains were arrested in G2 with nocodazole and transferred to YEPRG in the presence of nocodazole. Recruitment of Rad9-HA at the indicated distance from the HO-cut was determined by ChIP and qPCR. In all diagrams, the ChIP signals were normalized for each time point to the amount of the corresponding input signal. The mean values are represented with error bars denoting s.d. (n = 3). (B) As in (A), but showing Sgs1-HA binding. (C) As in (A). All strains carried also the deletion of *HTA2* gene. (D) As in (A), but showing γH2A binding. (E) Model for the role of Sae2 at DSBs. (Left) Sae2 activates the Mre11 endonuclease

activity to incise the 5' strand. Generation of the nick allows bidirectional processing by Exo1/Sgs1-Dna2 in the 5'-3' direction from the nick and MRX in the 3' to 5' direction toward the DSB ends. Ku and Rad9 inhibit DSB resection by limiting Exo1 and Sgs1-Dna2, respectively. (Middle) The absence of Sae2 impairs the MRX nuclease activity (non functional MRX nuclease is in grey). As a consequence, the endonucleolytic cleavage of the 5' strand does not occur and resection is carried out by Exo1 and Dna2-Sgs1 that degrade the 5' strands from the DSB ends. Impairment of Mre11 nuclease activity also causes increased MRX association at the DSB, which leads to enhanced Tel1-dependent Rad53 activation. Tel1 and Rad53 activities limit DSB resection from the DSB end (dashed arrow) by increasing the amount of DSB-bound Rad9, which inhibits Sgs1-Dna2 recruitment at DSBs. (Right) Impairments of Tel1 or Rad53 activity (non functional Tel1 and Rad53 are in grey) restore efficient resection in *sae2*Δ cells by relieving Rad9-mediated inhibition of Sgs1-Dna2. Restored DSB resection by Sgs1-Dna2 also reduces MRX persistence at the DSB.

doi:10.1371/journal.pgen.1005685.g010

Discussion

Cells lacking Sae2 not only are defective in DSB resection, but also show persistent DSB-induced checkpoint activation that causes a prolonged cell cycle arrest. This enhanced checkpoint signaling is due to persistent MRX binding at the DSBs, which activates a Tel1-dependent checkpoint that is accompanied by Rad53 phosphorylation [20,22]. While failure to remove MRX from the DSBs has been shown to sensitize *sae2*Δ cells to genotoxic agents [23,24], the possible contribution of the DNA damage checkpoint in determining the DNA damage hypersensitivity and the resection defect of *sae2*Δ cells has never been studied in detail.

We show that impairment of Rad53 activity either by affecting its interaction with Rad9 (Rad53-H88Y) or by abolishing its kinase activity (Rad53-kd) suppresses the sensitivity to DNA damaging agents of *sae2*Δ cells. A similar effect can be detected also when Tel1 function is compromised either by reducing its recruitment to DSBs (Tel1-N2021D) or by abrogating its kinase activity (Tel1-kd). These suppression effects are not due to the escape of the checkpoint-mediated cell cycle arrest, as *CHK1* deletion, which overrides the persistent cell cycle arrest of *sae2*Δ cells, does not suppress the hypersensitivity of the same cells to DNA damaging agents. Rather, we found that impairment of Rad53 or Tel1 signaling suppresses the resection defect of *sae2*Δ by decreasing the amount of Rad9 bound very close to the break site. As it is known that Rad9 inhibits Sgs1-Dna2 [13,14], this reduced Rad9 association at DSBs relieves inhibition of Sgs1-Dna2 activity that can then compensate for the lack of Sae2 function in DSB resection. In this view, active Rad53 and Tel1 increase the requirement for Sae2 in DSB resection by promoting Rad9 binding to DSBs and therefore by inhibiting Sgs1-Dna2. Consistent with a role of Sgs1 in removing MRX from the DSBs [54], the relieve of Sgs1-Dna2 inhibition by Rad53 or Tel1 dysfunction leads to a reduction of MRX association to DSBs in *sae2*Δ cells.

Our finding that Tel1 or Rad53 inactivation can restore both DNA damage resistance and DSB resection in *sae2*Δ cells is apparently at odds with previous findings that attenuation of the Rad53-dependent checkpoint signaling by decreasing MRX association to DSBs suppresses the DNA damage hypersensitivity of *sae2*Δ cells but not their resection defect [23,24]. Noteworthy, the bypass of Sae2 function by Rad53 or Tel1 dysfunction requires the physical presence of MRX bound at DSBs, which is known to promote stable association of Exo1, Sgs1 and Dna2 to DSBs [10]. Thus, we speculate that a reduced MRX association at DSBs allows *sae2*Δ cells to initiate DSB resection by relieving Rad9-mediated inhibition of Sgs1-Dna2 activity. As DSB repair by HR has been shown to require limited amount of ssDNA at DSB ends [55,56], the ssDNA generated by this initial DSB processing might be sufficient to restore DNA damage resistance in *sae2*Δ cells even when wild type levels of resection are not restored because DSB-bound MRX is not enough to ensure stable Sgs1 and Dna2 association.

Surprisingly, *TEL1* deletion, which relieves the persistent Tel1-dependent checkpoint activation caused by the lack of Sae2, did not restore DNA damage resistance and DSB resection in *sae2*Δ cells. We found that the lack of Tel1 protein affects the association of MRX to the DSB ends independently of its kinase activity. As the rescue of *sae2*Δ by Tel1-N2021D requires the physical presence of the MRX complex, this reduced MRX-DNA association can explain the

inability of *TEL1* deletion to restore DNA damage resistance and resection in *sae2*Δ cells. Therefore, while an enhanced Tel1 signaling activity in the absence of Sae2 leads to DNA damage hypersensitivity and resection defects, a sufficient amount of Tel1 needs to be present at DSBs to support MRX function at DSBs.

How do Rad53 and Tel1 control Rad9 association to DSB? Rad53-mediated phosphorylation of Rad9 does not appear to promote Rad9 binding to the DSB [57,58]. Because Rad53 and RPA compete for binding to Sgs1 [59], it is tempting to propose that impaired Rad53 signaling activity might shift Sgs1 binding preference from Rad53 to RPA, leading to increased Sgs1 association to RPA-coated DNA that can counteract Rad9 binding and inhibition of resection. In turn, Tel1 and Mec1 can phosphorylate Rad9 [60,61], and abrogation of these phosphorylation events rescues the sensitivity to DNA damaging agents of *sae2*Δ cells [14], suggesting that Tel1 might control Rad9 association to DSBs directly through phosphorylation. On the other hand, Tel1 promotes generation of γH2A [50–53], which counteracts DSB resection by favoring Rad9 association at the DSB [43]. We show that expression of a non-phosphorylatable H2A variant in *sae2*Δ cells suppresses their resection defect and prevents the accumulation of Rad9 at the DSB. Furthermore, γH2A generation close to the break site depends on Tel1 kinase activity. Thus, although we cannot exclude a direct control of Tel1 on Rad9 association to DNA ends, our findings indicate that Tel1 acts in this process mostly through γH2A generation.

Altogether, our results support a model whereby Tel1 and Rad53, once activated, limit DSB resection by promoting Rad9 binding to DSBs and therefore by inhibiting Sgs1-Dna2. Sae2 activates Mre11 endonucleolytic activity that clips the 5'-terminated DNA strand, thus generating 5' and 3' tailed substrates that can be processed by Exo1/Sgs1-Dna2 and Mre11 activity, respectively (Fig 10E, left). When Sae2 function fails, defective Mre11 nuclease activity causes increased MRX persistence at the DSB that leads to enhanced and prolonged Tel1-dependent Rad53 activation. As a consequence, Tel1- and Rad53-mediated phosphorylation events increase the amount of Rad9 bound at the DSB, which inhibits DSB resection by counteracting Sgs1-Dna2 activity (Fig 10E, middle). Dysfunction of Rad53 or Tel1 reduces Rad9 recruitment at the DSB ends and therefore relieves inhibition of Sgs1-Dna2, which can compensate for the lack of Sae2 in DNA damage resistance and resection (Fig 10E, right). Altogether, these findings indicate that the primary cause of the resection defect of *sae2*Δ cells is an enhanced Rad9 binding to DSBs that is promoted by the persistent MRX-dependent Tel1 and Rad53 signaling activities.

ATM inhibition has been proposed as a strategy for cancer treatment [62]. Therefore, the observation that dampening Tel1/ATM signaling activity restores DNA damage resistance in *sae2*Δ cells might have implications in cancer therapies that use ATM inhibitors for synthetic lethal approaches to threat tumors with deficiencies in the DNA damage response.

Materials and Methods

Yeast strains

The yeast strains used in this study are derivatives of W303, JKM139 and YMV45 strains and are listed in S1 Table. Cells were grown in YEP medium (1% yeast extract, 2% peptone) supplemented with 2% glucose (YEPD), 2% raffinose (YEPR) or 2% raffinose and 3% galactose (YEPRG).

Search for suppressors of *sae2*Δ sensitivity to CPT

To search for suppressor mutations of the CPT-sensitivity of *sae2*Δ mutant, $5x10^6$ *sae2*Δ cells were plated on YEPD in the presence of 30μM CPT. Survivors were crossed to wild type cells

to identify by tetrad analysis the suppression events that were due to single-gene mutations. Genomic DNA from two single-gene suppressors was analyzed by next-generation Illumina sequencing (IGA technology services) to identify mutations altering open reading frames within the reference *S. cerevisiae* genome. To confirm that *rad53-H88Y* and *tel1-N2021D* mutations were responsible for the suppression, either *URA3* or *HIS3* gene was integrated downstream of the *rad53-H88Y* and *tel1-N2021D* stop codon, respectively, and the resulting strain was crossed to wild type cells to verify by tetrad dissection that the suppression of the *sae2*Δ CPT sensitivity co-segregated with the *URA3* or *HIS3* allele.

DSB resection and repair by SSA

DSB end resection at the *MAT* locus in JKM139 derivative strains was analyzed on alkaline agarose gels as previously described [63]. DSB formation and repair in YMV45 strain were detected by Southern blot analysis using an *Asp*718-*Sal*I fragment containing part of the *LEU2* gene as a probe as previously described [63]. Quantitative analysis of the repair product was performed by calculating the ratio of band intensities for SSA product with respect to a loading control.

Other techniques

Protein extracts for western blot analysis were prepared by TCA precipitation. ChIP assays were performed as previously described [64]. Data are expressed as fold enrichment at the HO-induced DSB over that at the non-cleaved *ARO1* locus, after normalization of each ChIP signals to the corresponding amount of immunoprecipitated protein and input for each time point. Fold enrichment was then normalized to the efficiency of DSB induction. The kinase assay and coimmunoprecipitation were performed as previously described [48]. Rad53 was detected by using anti-Rad53 polyclonal antibodies (ab104232) from Abcam. γH2A was immunoprecipitated by using anti-γH2A antibodies (ab15083) from Abcam.

Supporting Information

S1 Fig. *rad53-H88Y* and *tel1-N2021D* suppressor alleles are recessive. Exponentially growing cells were serially diluted (1:10) and each dilution was spotted out onto YEPD plates with or without the indicated genotoxic agents.
(TIF)

S2 Fig. The Tel1-N2021D variant does not affect telomere length. Genomic DNA prepared from exponentially growing cells was digested with *Xho*I and hybridized with a poly(GT) telomere-specific probe.
(TIF)

S3 Fig. The lack of γH2A suppresses the resection defect of *sae2*Δ cells. DSB resection. YEPR exponentially growing cultures of JKM139 derivative cells with the indicated genotypes were arrested in G2 with nocodazole and transferred to YEPRG in the presence of nocodazole at time zero. All strains carried also the deletion of *HTA2* gene. Gel blots of SspI-digested genomic DNA separated on alkaline agarose gel were hybridized with a single-stranded RNA probe that anneals to the unresected strand on one side of the break. 5'-3' resection progressively eliminates SspI sites, producing larger SspI fragments (r1 through r7) detected by the probe.
(TIF)

S1 Table. List of yeast strains described in this work.
(DOC)

Acknowledgments

We thank J. Haber, T. Petes and L. Symington for strains. We are grateful to Marina Martina for preliminary results and to Giovanna Lucchini for critical reading of the manuscript.

Author Contributions

Conceived and designed the experiments: EG MV MC MPL. Performed the experiments: EG MV MG LM MC. Analyzed the data: EG MV MC MPL. Wrote the paper: MPL.

References

1. Gobbini E, Cesena D, Galbiati A, Lockhart A, Longhese MP (2013) Interplays between ATM/Tel1 and ATR/Mec1 in sensing and signaling DNA double-strand breaks. DNA Repair 12: 791–799. doi: 10.1016/j.dnarep.2013.07.009 PMID: 23953933
2. Ciccia A, Elledge SJ (2010) The DNA damage response: making it safe to play with knives. Mol Cell 40: 179–204. doi: 10.1016/j.molcel.2010.09.019 PMID: 20965415
3. Mehta A, Haber JE (2014) Sources of DNA double-strand breaks and models of recombinational DNA repair. Cold Spring Harb Perspect Biol 6: a016428. doi: 10.1101/cshperspect.a016428 PMID: 25104768
4. Symington LS, Gautier J (2011) Double-strand break end resection and repair pathway choice. Annu Rev Genet 45: 247–271. doi: 10.1146/annurev-genet-110410-132435 PMID: 21910633
5. Cannavo E, Cejka P (2014) Sae2 promotes dsDNA endonuclease activity within Mre11-Rad50-Xrs2 to resect DNA breaks. Nature 514: 122–125. doi: 10.1038/nature13771 PMID: 25231868
6. Mimitou EP, Symington LS (2008) Sae2, Exo1 and Sgs1 collaborate in DNA double-strand break processing. Nature 455: 770–774. doi: 10.1038/nature07312 PMID: 18806779
7. Zhu Z, Chung WH, Shim EY, Lee SE, Ira G (2008) Sgs1 helicase and two nucleases Dna2 and Exo1 resect DNA double-strand break ends. Cell 134: 981–994. doi: 10.1016/j.cell.2008.08.037 PMID: 18805091
8. Cejka P, Cannavo E, Polaczek P, Masuda-Sasa T, Pokharel S, Campbell JL, et al. (2010) DNA end resection by Dna2-Sgs1-RPA and its stimulation by Top3-Rmi1 and Mre11-Rad50-Xrs2. Nature 467: 112–116. doi: 10.1038/nature09355 PMID: 20811461
9. Niu H, Chung WH, Zhu Z, Kwon Y, Zhao W, Chi P, et al. (2010) Mechanism of the ATP-dependent DNA end-resection machinery from *Saccharomyces cerevisiae*. Nature 467: 108–111. doi: 10.1038/nature09318 PMID: 20811460
10. Shim EY, Chung WH, Nicolette ML, Zhang Y, Davis M, Zhu Z, et al. (2010) *Saccharomyces cerevisiae* Mre11/Rad50/Xrs2 and Ku proteins regulate association of Exo1 and Dna2 with DNA breaks. EMBO J 29: 3370–3380. doi: 10.1038/emboj.2010.219 PMID: 20834227
11. Mimitou EP, Symington LS (2010) Ku prevents Exo1 and Sgs1-dependent resection of DNA ends in the absence of a functional MRX complex or Sae2. EMBO J 29: 3358–3369. doi: 10.1038/emboj.2010.193 PMID: 20729809
12. Foster SS, Balestrini A, Petrini JH (2011) Functional interplay of the Mre11 nuclease and Ku in the response to replication-associated DNA damage. Mol Cell Biol 31: 4379–4389. doi: 10.1128/MCB.05854-11 PMID: 21876003
13. Bonetti D, Villa M, Gobbini E, Cassani C, Tedeschi G, Longhese MP (2015) Escape of Sgs1 from Rad9 inhibition reduces the requirement for Sae2 and functional MRX in DNA end resection. EMBO Rep 16: 351–361. doi: 10.15252/embr.201439764 PMID: 25637499
14. Ferrari M, Dibitetto D, De Gregorio G, Eapen VV, Rawal CC, Lazzaro F, et al. (2015) Functional interplay between the 53BP1-ortholog Rad9 and the Mre11 complex regulates resection, end-tethering and repair of a double-strand break. PLoS Genet 11: e1004928. doi: 10.1371/journal.pgen.1004928 PMID: 25569305
15. Keeney S, Kleckner N (1995) Covalent protein-DNA complexes at the 5' strand termini of meiosis-specific double-strand breaks in yeast. Proc Natl Acad Sci USA 92: 11274–11278. PMID: 7479978
16. Usui T, Ohta T, Oshiumi H, Tomizawa J, Ogawa H, Ogawa T (1998) Complex formation and functional versatility of Mre11 of budding yeast in recombination. Cell 95: 705–716. PMID: 9845372
17. Liu C, Pouliot JJ, Nash HA (2002) Repair of topoisomerase I covalent complexes in the absence of the tyrosyl-DNA phosphodiesterase Tdp1. Proc Natl Acad Sci USA 99: 14970–14975. PMID: 12397185
18. Deng C, Brown JA, You D, Brown JM (2005) Multiple endonucleases function to repair covalent topoisomerase I complexes in *Saccharomyces cerevisiae*. Genetics 170: 591–600. PMID: 15834151

19. Mantiero D, Clerici M, Lucchini G, Longhese MP (2007) Dual role for *Saccharomyces cerevisiae* Tel1 in the checkpoint response to double-strand breaks. EMBO Rep 8: 380–387. PMID: 17347674

20. Usui T, Ogawa H, Petrini JH (2001) A DNA damage response pathway controlled by Tel1 and the Mre11 complex. Mol Cell 7: 1255–1266. PMID: 11430828

21. Lisby M, Barlow JH, Burgess RC, Rothstein R (2004) Choreography of the DNA damage response: spatiotemporal relationships among checkpoint and repair proteins. Cell 118: 699–713. PMID: 15369670

22. Clerici M, Mantiero D, Lucchini G, Longhese MP (2006) The *Saccharomyces cerevisiae* Sae2 protein negatively regulates DNA damage checkpoint signalling. EMBO Rep 7: 212–218. PMID: 16374511

23. Chen H, Donnianni RA, Handa N, Deng SK, Oh J, Timashev LA, et al. (2015) Sae2 promotes DNA damage resistance by removing the Mre11-Rad50-Xrs2 complex from DNA and attenuating Rad53 signaling. Proc Natl Acad Sci USA 112: 1880–1887.

24. Puddu F, Oelschlaegel T, Guerini I, Geisler NJ, Niu H, Herzog M, et al. (2015) Synthetic viability genomic screening defines Sae2 function in DNA repair. EMBO J 34: 1509–1522. doi: 10.15252/embj.201590973 PMID: 25899817

25. Sandell LL, Zakian VA (1993) Loss of a yeast telomere: arrest, recovery, and chromosome loss. Cell 75: 729–739. PMID: 8242745

26. Toczyski DP, Galgoczy DJ, Hartwell LH (1997) CDC5 and CKII control adaptation to the yeast DNA damage checkpoint. Cell 90: 1097–1106. PMID: 9323137

27. Lee SE, Moore JK, Holmes A, Umezu K, Kolodner RD, Haber JE (1998) *Saccharomyces* Ku70, Mre11/Rad50 and RPA proteins regulate adaptation to G2/M arrest after DNA damage. Cell 94: 399–409. PMID: 9708741

28. Fukunaga K, Kwon Y, Sung P, Sugimoto K (2011) Activation of protein kinase Tel1 through recognition of protein-bound DNA ends. Mol Cell Biol 31: 1959–1971. doi: 10.1128/MCB.05157-11 PMID: 21402778

29. Sun Z, Hsiao J, Fay DS, Stern DF (1998) Rad53 FHA domain associated with phosphorylated Rad9 in the DNA damage checkpoint. Science 281: 272–274. PMID: 9657725

30. Gilbert CS, Green CM, Lowndes NF (2001) Budding yeast Rad9 is an ATP-dependent Rad53 activating machine. Mol Cell 8: 129–136. PMID: 11511366

31. Sweeney FD, Yang F, Chi A, Shabanowitz J, Hunt DF, Durocher D (2005) *Saccharomyces cerevisiae* Rad9 acts as a Mec1 adaptor to allow Rad53 activation. Curr Biol 15: 1364–1375. PMID: 16085488

32. Durocher D, Henckel J, Fersht AR, Jackson SP (1999) The FHA domain is a modular phosphopeptide recognition motif. Mol Cell 4: 387–394. PMID: 10518219

33. Bosotti R, Isacchi A, Sonnhammer EL (2000) FAT: a novel domain in PIK-related kinases. Trends Biochem Sci 25: 225–227. PMID: 10782091

34. Baretić D, Williams RL (2014) PIKKs—the solenoid nest where partners and kinases meet. Curr Opin Struct Biol 29: 134–142. doi: 10.1016/j.sbi.2014.11.003 PMID: 25460276

35. Mallory JC, Petes TD (2000) Protein kinase activity of Tel1p and Mec1p, two *Saccharomyces cerevisiae* proteins related to the human ATM protein kinase. Proc Natl Acad Sci USA 97: 13749–13754. PMID: 11095737

36. Ogi H, Goto GH, Ghosh A, Zencir S, Henry E, Sugimoto K (2015) Requirement of the FATC domain of protein kinase Tel1 for localization to DNA ends and target protein recognition. Mol Biol Cell 26: 3480–3488. doi: 10.1091/mbc.E15-05-0259 PMID: 26246601

37. Lydall D, Weinert T (1995) Yeast checkpoint genes in DNA damage processing: implications for repair and arrest. Science 270: 1488–1491. PMID: 7491494

38. Jia X, Weinert T, Lydall D (2004) Mec1 and Rad53 inhibit formation of single-stranded DNA at telomeres of *Saccharomyces cerevisiae cdc13-1* mutants. Genetics 166: 753–764. PMID: 15020465

39. Ngo GH, Lydall D (2015) The 9-1-1 checkpoint clamp coordinates resection at DNA double strand breaks. Nucleic Acids Res 43: 5017–5032. doi: 10.1093/nar/gkv409 PMID: 25925573

40. Pellicioli A, Lee SE, Lucca C, Foiani M, Haber JE (2001) Regulation of *Saccharomyces* Rad53 checkpoint kinase during adaptation from DNA damage-induced G2/M arrest. Mol Cell 7: 293–300. PMID: 11239458

41. Sanchez Y, Bachant J, Wang H, Hu F, Liu D, Tetzlaff M, et al. (1999) Control of the DNA damage checkpoint by Chk1 and Rad53 protein kinases through distinct mechanisms. Science 286: 1166–1171. PMID: 10550056

42. Vaze MB, Pellicioli A, Lee SE, Ira G, Liberi G, Arbel-Eden A, et al. (2002) Recovery from checkpoint-mediated arrest after repair of a double-strand break requires Srs2 helicase. Mol Cell 10: 373–385. PMID: 12191482

43. Clerici M, Trovesi C, Galbiati A, Lucchini G, Longhese MP (2014) Mec1/ATR regulates the generation of single-stranded DNA that attenuates Tel1/ATM signaling at DNA ends. EMBO J 33: 198–216. doi: 10.1002/embj.201386041 PMID: 24357557

44. Morin I, Ngo HP, Greenall A, Zubko MK, Morrice N, Lydall D (2008) Checkpoint-dependent phosphorylation of Exo1 modulates the DNA damage response. EMBO J 27: 2400–2410. doi: 10.1038/emboj.2008.171 PMID: 18756267

45. Budd ME, Choe Wc, Campbell JL (2000) The nuclease activity of the yeast *DNA2* protein, which is related to the RecB-like nucleases, is essential in vivo. J Biol Chem 275: 16518–16529. PMID: 10748138

46. Zhao X, Muller EG, Rothstein R (1998) A suppressor of two essential checkpoint genes identifies a novel protein that negatively affects dNTP pools. Mol Cell 2: 329–340. PMID: 9774971

47. Fay DS, Sun Z, Stern DF (1997) Mutations in *SPK1/RAD53* that specifically abolish checkpoint but not growth-related functions. Curr Genet 31: 97–105. PMID: 9021124

48. Baldo V, Testoni V, Lucchini G, Longhese MP (2008) Dominant *TEL1-hy* mutations compensate for Mec1 lack of functions in the DNA damage response. Mol Cell Biol 28: 358–375. PMID: 17954565

49. Hirano Y, Fukunaga K, Sugimoto K (2009) Rif1 and Rif2 inhibit localization of Tel1 to DNA ends. Mol Cell 33: 312–322. doi: 10.1016/j.molcel.2008.12.027 PMID: 19217405

50. Shroff R, Arbel-Eden A, Pilch D, Ira G, Bonner WM, Petrini JH, et al. (2004) Distribution and dynamics of chromatin modification induced by a defined DNA double-strand break. Curr Biol 14: 1703–1711. PMID: 15458641

51. Javaheri A, Wysocki R, Jobin-Robitaille O, Altaf M, Côté J, Kron SJ (2006) Yeast G1 DNA damage checkpoint regulation by H2A phosphorylation is independent of chromatin remodeling. Proc Natl Acad Sci USA 103: 13771–13776. PMID: 16940359

52. Toh GW, O'Shaughnessy AM, Jimeno S, Dobbie IM, Grenon M, Maffini S, et al. (2006) Histone H2A phosphorylation and H3 methylation are required for a novel Rad9 DSB repair function following checkpoint activation. DNA Repair 5: 693–703. PMID: 16650810

53. Hammet A, Magill C, Heierhorst J, Jackson SP (2007) Rad9 BRCT domain interaction with phosphorylated H2AX regulates the G1 checkpoint in budding yeast. EMBO Rep 8: 851–857. PMID: 17721446

54. Bernstein KA, Mimitou EP, Mihalevic MJ, Chen H, Sunjaveric I, Symington LS et al. (2013) Resection activity of the Sgs1 helicase alters the affinity of DNA ends for homologous recombination proteins in *Saccharomyces cerevisiae*. Genetics 195: 1241–1251. doi: 10.1534/genetics.113.157370 PMID: 24097410

55. Ira G, Haber JE (2002) Characterization of RAD51-independent break-induced replication that acts preferentially with short homologous sequences. Mol Cell Biol 22: 6384–6392. PMID: 12192038

56. Jinks-Robertson S, Michelitch M, Ramcharan S (1993) Substrate length requirements for efficient mitotic recombination in *Saccharomyces cerevisiae*. Mol Cell Biol 13: 3937–3950. PMID: 8321201

57. Naiki T, Wakayama T, Nakada D, Matsumoto K, Sugimoto K (2004) Association of Rad9 with double-strand breaks through a Mec1-dependent mechanism. Mol Cell Biol 24: 3277–3285. PMID: 15060150

58. Usui T, Foster SS, Petrini JH (2009) Maintenance of the DNA-damage checkpoint requires DNA-damage-induced mediator protein oligomerization. Mol Cell 33: 147–159. doi: 10.1016/j.molcel.2008.12.022 PMID: 19187758

59. Hegnauer AM, Hustedt N, Shimada K, Pike BL, Vogel M, Amsler P, et al. (2012) An N-terminal acidic region of Sgs1 interacts with Rpa70 and recruits Rad53 kinase to stalled forks. EMBO J 31: 3768–3783. doi: 10.1038/emboj.2012.195 PMID: 22820947

60. Emili A (1998) *MEC1*-dependent phosphorylation of Rad9p in response to DNA damage. Mol Cell 2: 183–189. PMID: 9734355

61. Vialard JE, Gilbert CS, Green CM, Lowndes NF (1998) The budding yeast Rad9 checkpoint protein is subjected to Mec1/Tel1-dependent hyperphosphorylation and interacts with Rad53 after DNA damage. EMBO J 17: 5679–5688. PMID: 9755168

62. Cremona CA, Behrens A (2014) ATM signalling and cancer. Oncogene 33: 3351–3360. doi: 10.1038/onc.2013.275 PMID: 23851492

63. Trovesi C, Falcettoni M, Lucchini G, Clerici M, Longhese MP (2011) Distinct Cdk1 requirements during single-strand annealing, noncrossover, and crossover recombination. PLoS Genet 7: e1002263. doi: 10.1371/journal.pgen.1002263 PMID: 21901114

64. Viscardi V, Bonetti D, Cartagena-Lirola H, Lucchini G, Longhese MP (2007) MRX-dependent DNA damage response to short telomeres. Mol Biol Cell 18: 3047–3058. PMID: 17538011